The Cytochrome P450 Family 4 Enzymes:

Focus on Inhibition by Formamidoximes and Metabolism of Vitamin K

Katheryne Zumberge Edson

A dissertation submitted in partial fulfillment of the requirements for the degree of

Doctor of Philosophy

University of Washington

2013

Program Authorized to Offer Degree:

Medicinal Chemistry

School of Pharmacy

Acknowledgements

I would like to express my sincere gratitude to my supervising professor, Dr. Allan Rettie, whose experience and erudition have profoundly contributed to my development as a scientist. His excellence in grant writing and funding procurement, balanced approach to scientific mentorship, and intriguing project proposals have made my Ph.D. pursuit productive and enjoyable. I am also grateful for the auxiliary support and guidance from my committee members, Dr. Kent Kunze, Dr. Rheem Totah, and Dr. Ken Thummel.

I would likely not have embarked down this road if not for my amazing parents, John and Debbe. My father's Ph.D. in geochemistry and my grandfather's Ph.D. in glaciology instilled in me a respect for higher learning at an early age. My mother's pride and encouragement is infinite, and I am grateful for their love and support.

Finally, I would like to thank my husband, Jed, for his love, friendship, patience, and understanding. He is the reason I still have my sanity and is a steady reminder of the importance of balance in life. He is also the reason I have our wonderful daughter, Marilyn, who has brought us immense joy and happiness.

Abstract

The studies presented in this dissertation explore Cytochrome P450 family 4 (CYP4) enzyme inhibition and metabolism. The structure-activity relationships between CYP4 enzymes and the potent formamidoxime inhibitor, HET0016, was defined, which led to the development of competitive inhibitors that are selective for CYP4F2 and CYP4F3B and do not inhibit CYP4A11. These CYP4 enzymes are principally responsible for biosynthesis of the signaling eicosanoid, 20-HETE. Additionally, HET0016 was established as a mechanism-based inhibitor of CYP4A11, but not of other CYP4 enzymes. Studies to characterize the kinetic properties of this mechanism based inhibitor and identify a reactive species have shown the inactivation is potent and efficient, does not result in metabolite intermediate complex formation or nitric oxide release, and does not destroy the heme cofactor. A carbodiimide or isocyanate reactive intermediate has been proposed that could result in apo-protein adduction. In the second portion of this thesis, it was established that CYP4F2 and CYP4F11 metabolize vitamin K1 and K2 to their respective ω-hydroxy metabolites, and that CYP4F2 sequentially metabolizes vitamin K to the ω-carboxy metabolites. Microsomal alcohol dehydrogenase/ fatty-aldehyde dehydrogenase (ADH/fALDH) or other P450 enzymes may also play a role in formation of ω-carboxy vitamin K after initial ω-hydroxylation by these CYP4 enzymes. For the first time, the amount of CYP4F11 protein in human liver was quantitated, using a new LC/MS-MS method and it was confirmed that the amount of CYP4F2 protein in human liver correlates with the presence of the common *CYP4F2*3* (V433M) allelic variant. Menaquinone-4 (MK4) is one form of Vitamin K2, and this work has shown that metabolism of MK4 is distinctly different from that of Vitamin K1 (phylloquinone). P450 enzymes other than those in the CYP4 family were shown to ω-hydroxylate MK4 *in vitro* and two new oxidized microsomal metabolites of MK4 were characterized. This work has laid groundwork for future studies that should establish the differences in the metabolic fate of the various forms of vitamin K *in vivo* and help clarify a genetic basis for the inter-individual variability in response to these supplements when used as pharmacotherapeutic agents.

Table of Contents

List of Figures and Tables

Chapter 4

Chapter 5

Introduction

CYP4 Enzymes: Drug Targets for 20-HETE and Fatty Acid Modulation and Role in Vitamin K Catabolism

1.1 Introduction

The Cytochrome P450 4 (CYP4) family of enzymes typically metabolizes fatty acids, including many important cellular signaling eicosanoids. Eicosanoids are the oxidation products of 20-carbon essential fatty acids, such as arachidonic acid, that constitute a complex network of molecular controls throughout the human body. 20-Hydroxyeicosatetraenoic acid (20-HETE), generated mainly by CYP4A and/or CYP4F enzymes, is a key arachidonic acid metabolite that exhibits a plethora of biological functions, such that pharmacological manipulation of tissue 20-HETE levels has promise for the treatment of hypertension, stroke, and some cancers. Induction of CYP4 activity and thus fatty acid ω-hydroxylase activity has been considered for treatment of Refsum Disease and X-ALD. Furthermore, some CYP4 enzymes metabolize vitamin K and vitamin E. Supplementation with these vitamins is currently used and holds promise for therapeutic benefit in several disease states. These therapeutic areas and their relationship to CYP4 enzyme catalysis are discussed below.

1.2 Overview of CYP4 Enzyme Catalysis, Expression, and Regulation

CYP4 enzymes are heme-containing monooxygenases with an unusual ability to catalyze hydroxylation of a terminal carbon atom on an unactivated alkyl chain. This is in contrast to most other human P450 enzymes, which also catalyze aliphatic chain oxidations, but favor internal hydroxylations (ω-1, ω-2, ω-3, etc.) due, in part, to the lower energetic cost of breaking a substituted C-H bond as opposed to a terminal C-H bond. The topology of the CYP4 active site and steric constraints imposed by the nearby amino acids are important factors dictating product regioselectivity. A likely additional important structural consideration is the unique covalent link to the heme cofactor that is present in numerous members of the CYP4 family of enzymes [1, 2]. This unusual covalent ester bond formed between a glutamate residue on the CYP4 I-helix and a methyl substituent on the B-type heme may rigidify the active site to enhance regio-control of substrate hydroxylation (Figure 1). It is important to note that this ω-regioselectivity is not absolute, and most CYP4 enzymes produce a mixture of end-chain hydroxylated

products. The ratios of ω: ω-1, ω-2, and ω-3 hydroxylated products can range from >20:1 to 0:1 and can vary widely for each enzyme/substrate pair. Two of the twelve human CYP4 enzymes, CYP4F8 and CYP4F12, have a glycine residue in place of the glutamic acid on the I-helix and do not possess a covalently bound heme. Perhaps as a result, these enzymes catalyze the hydroxylation of eicosanoids such as prostaglandin H2 and arachidonic acid at the ω-2 and ω-3 positions, and are thus not strictly ω-hydroxylases [3, 4]. CYP4X1 and CYP4Z1 also lack a glutamic acid in the I-helix and likely have no covalently bound heme cofactor, however the substrate specificity and product regio-selectivity of these enzymes are not yet well defined.

The twelve human CYP4 isoforms are distributed among six CYP4 subfamilies whose constituent enzymes are shown in Figure 1.1. The CYP4A, B, X, and Z genes are clustered on chromosome 1, while the CYP4F and CYP4V genes reside on chromosome 19 and 4, respectively. P450 enzymes are grouped into families and subfamilies based on their amino acid sequence similarity. Enzymes with >40% amino acid identity are classified into the same family, and enzymes with >55% identity are members of the same subfamily. The substrate selectivity, human protein expression levels, and regulation of expression for each CYP4 subfamily are described below.

The CYP4A subfamily

Within the human CYP4A subfamily, CYP4A11 is very efficient at ω-hydroxylation of medium-chain length (C10-C16) fatty acid substrates. CYP4A22 is the only other known human CYP4A enzyme. However, CYP4A22 is expressed at very low levels in few tissues and may not be a functional enzyme [5]. CYP4A22 does not hydroxylate lauric acid, the prototypical CYP4A substrate, although it shares 95% sequence homology with CYP4A11. CYP4A11 catalyzes lauric acid hydroxylation with a V_{max} of 38 ± 8 min^{-1}, K_m of 200 ± 50 μM, and a product ω: ω -1 ratio in excess of 10:1 [6]. As the chain length of the substrate increases beyond C12 this ratio decreases. For example, the ω: ω -1 ratio for arachidonic acid hydroxylation (producing 20- and 19-HETE) is only 4.7:1 [7]. CYP4A11 is expressed primarily in the liver and kidney. In human liver and renal cortex microsomes the specific contents of the enzyme have been reported to be as high as 48 ± 28 pmol/mg and 32 ± 18 pmol/mg (n=9), respectively, as determined by immunoquantitative Western blotting [8].

Amongst CYP4 enzymes, those of the CYP4A subfamily are the most studied in regard to regulation of hepatic expression. Most of this work has been performed in the rat and mouse, experimental animals that

possess multiple functionally important CYP4A enzymes (CYP4A1, 2, 3, and 8 in rats and CYP4a10, 12, and 14 in mice). It is well established that the nuclear receptor, PPARα, mediates marked induction of mouse and rat CYP4A mRNA, protein, and lauric acid hydroxylase activity in response to the fibrate class of hypolipidemic drugs, as well as in states of fasting and diabetic ketoacidosis [9, 10]. Under these conditions, PPARα is activated due to increased levels of free fatty acids resulting from adipocyte lipolysis and increased ketogenesis as the cells attempt to make energy from stored fatty acids to counteract glucose shortage. However, a number of studies have failed to demonstrate PPARα-mediated induction of peroxisome proliferation-associated genes by fibrates in human hepatocytes and HepG2 cells, although the orthologous genes were substantially up-regulated in rat hepatocytes [11, 12]. This led to speculation that PPARα does not mediate CYP4A11 induction in humans. However, human CYP4A11 transgenic mice exhibit a ~3-fold increase in CYP4A11 mRNA and protein expression in response to both fibrate agonists for PPARα and fasting states, and CYP4A11 was no longer inducible in PPARα deficient CYP4A11 transgenic mice [13]. Increased CYP4A11 mRNA and protein expression in response to fibrates and other more potent PPARα agonists in human hepatocytes (1.5- 4 fold) has since been shown, although induction is always modest when compared to rodent hepatocytes [11, 14, 15]. This may be due to the >ten-fold lower expression level of PPARα in human liver compared to rodent liver [10]. Thus, PPARα mediates CYP4A11 induction in humans, but exerts a more constrained effect than is observed in rodents.

The CYP4F subfamily

CYP4F2, CYP4F3A, CYP4F3B, CYP4F8, CYP4F11, CYP4F12, and CYP4F22 are the seven members of the human CYP4F subfamily. These enzymes ω-hydroxylate medium-chain (C10-C16), long-chain (C17-C21), and very long chain (C22-C26) fatty acids that are saturated, unsaturated, and/or branched. They also metabolize various eicosanoids, vitamin E, vitamin K, and a few xenobiotics [16-25]. The rat has four members of the CYP4F subfamily (CYP4F1, 4, 5, and 6) and the mouse possesses five CYP4F enzymes (CYP4F13, 14, 15, 16, and 18) [26].

Human CYP4F3A is expressed only in neutrophils and is involved in the inflammatory process. This enzyme ω-hydroxylates leukotriene-B4 (LTB4), a pro-inflammatory eicosanoid, to produce a less active compound, 20-hydroxy-LTB4. CYP4F3A and CYP4F3B enzymes are structurally identical except for residues 67-114. Alternative splicing of the *CYP4F3* gene leads to insertion of exon 4 into CYP4F3A RNA and exon 3

into CYP4F3B RNA to generate proteins with unique functional activities and tissue expression. CYP4F8 is expressed mainly in seminal vesicles, testis, and epidermis, where it metabolizes prostaglandins and eicosanoids [27]. CYP4F22 is expressed in epidermis and also metabolizes eicosanoids [28, 29]. CYP4F2, CYP4F3B, CYP4F11, and CYP4F12 are mainly expressed in liver and kidney [4, 7, 8, 30, 31]. These four enzymes share a high degree of sequence homology, making it difficult to determine the absolute amount of each enzyme in tissue using immunoquantitation with polyclonal antibodies. Hirani *et al*. developed a selective peptide antibody for CYP4F2 that reportedly did not have affinity for other CYP4F enzymes [32], and found that CYP4F2 enzyme content varied widely in human liver (ranging from 0-80 pmoles/mg microsomal protein) with an average of 18 ± 20 pmol/mg (*n*= 29). CYP4F2 content in kidney averaged 4 ± 4 pmol/mg and ranged from 0-11 pmol/mg *(n*= 10). McDonald *et al.* found CYP4F2 specific content to range from 3-11 pmoles/mg pooled liver microsomal protein and to vary according to the presence or absence of the common Val433Met polymorphism that is observed in ~30% of Caucasians [16]. The specific enzyme content of CYP4F3B, CYP4F11, and CYP4F12 in the liver is presently unknown, however, total CYP4F content in the liver is reported to range from 18-128 pmol/mg liver microsomal protein [33]. This represents a significant fraction of total hepatic P450 when compared to the major drug metabolizing P450 enzymes. Recently, tryptic digestion followed by mass spectrometry with target peptide selection has been used to provide absolute quantitation of P450 enzymes in pooled human liver microsomes. CYP3A4, CYP1A2, CYP2C9, and CYP2D6 specific content was 64, 18, 80, and 12 pmol/mg respectively [19]. This approach may be useful for absolute quantitation of CYP4 enzymes in the liver (and other tissues) as it does not depend on the availability of monospecific antibodies.

Figure 1.2 depicts the CYP4F gene cluster on chromosome 19. Regulation of CYP4F enzymes, unlike those in the CYP4A sub-family, is not controlled by the nuclear receptor PPARα. Instead, statin drugs such as lovastatin and mevastatin induce CYP4F2 mRNA and protein in both HepG2 cells and primary human hepatocytes [34]. In these studies, statins selectively increased CYP4F2 mRNA by 3-fold in HepG2 cells and 5-fold in hepatocytes, with no increase in CYP4F3B mRNA. Immunoquantitation with an antibody that recognized both CYP4F2 and CYP4F3B showed a 2-fold increase in protein in HepG2 cells and a 3-fold increase in hepatocytes. Induction was mediated by the DNA-binding protein, sterol regulatory element-binding protein (SREBP), which regulates transcription of genes involved in cholesterol and fatty acid synthesis. In the endoplasmic reticulum (ER) SREBP is bound to the SREBP cleavage-activating protein (SCAP). When cell

sterol levels are high, Insig (insulin-induced gene) protein binds to the SCAP-SREBP complex and retains it in the ER. Upon sterol depletion, which occurs after statin treatment, the SCAP-SREBP complex is transferred to the Golgi where SREBP is proteolysed and the active portion of the protein moves to the nucleus and regulates gene transcription [35]. Statin drugs have two main mechanisms for decreasing cholesterol from circulation; decreased biosynthesis of cholesterol by inhibiting the enzyme, HMG CoA reductase, and enhanced cholesterol uptake into the hepatocyte by increased expression of the low density lipoprotein (LDL) receptor. Thus, the *CYP4F2* gene may be transactivated by SREBP in order to clear the increased flux of triglycerides and other fatty acids resulting from increased LDL import into the liver cell. CYP4F2 expression is also induced in hepatocytes and HepG2 cells by AMP-activated protein kinase (AMPK) activators [36]. In these studies CYP4F2 mRNA was increased (2.5-13-fold) by three indirect AMPK activators: AICAR, genistein, and resveratrol. Inhibitors of AMPK were shown to potentiate this increase in expression. In contrast, CYP4F3, CYP4A11, and CYP4F11 mRNAs were not affected by any AMPK activator in HepG2 cells, and CYP4F12 mRNA was only modestly increased (2-fold) upon treatment with genistein. Immunoquantitation with an antibody recognizing CYP4F2 and CYP4F3B, but not CYP4F11 or CYP4F12, revealed 1.6-1.9-fold increases in protein in HepG2 cells upon treatment with the AMPK activators. The physiological reason for AMPK-mediated CYP4F2 induction is unclear; however, it may be a defensive response to high levels of fatty acids in the mitochondria that result in lipotoxicity and hindered ATP synthesis [37]. AMPK is activated when AMP/ATP ratios in the cell are high in order to increase ATP production and reduce its utilization. Upon activation, AMPK phosphorylating activity is increased 1000-fold, and phosphorylation of, yet to be defined, transcription factors may be responsible for transactivation of the *CYP4F2* gene. Induction of CYP4F2 could increase clearance of excess free fatty acids and increase mitochondrial efficiency. Regardless, AMPK activation occurs when cellular ATP levels fall. This can arise due to numerous cellular stress factors, which may contribute to the large inter-individual variation of CYP4F2 protein levels observed in human liver microsomes.

CYP4F3B mRNA is induced in HepaRG cells by prostaglandin A1 (PGA1) in a concentration-dependent manner (1.8-6-fold after 1-40 μM PGA1 treatment) [38]. In contrast, basal CYP4F3A mRNA is low in the cells and is not inducible by PGA1. Other prostaglandins and eicosanoids tested did not increase CYP4F3B mRNA. Western blotting with an antibody that recognized CYP4F3B, but not CYP4F3A, showed that protein levels were increased 3-fold in HepaRG cells after exposure to PGA1 (20 μM). The antibody used was raised against the

amino acids encoded by the CYP4F3B-specific exon of the *CYP4F3* gene. This amino acid sequence (residues 67-114) shares 27%, 83%, and 66% sequence identity with CYP4F3A, CYP4F2, and CYP4F11, respectively. Cross reactivity with CYP4F2 was not assessed and CYP4F2 mRNA was not measured, therefore it is unclear whether CYP4F3B alone or both CYP4F3B and CYP4F2 were induced by PGA1. PGA1 is a signaling eicosanoid that causes renal vasodilation, promotes sodium excretion in the kidney, and is an anti-hypertensive agent. PGA1 also has been shown to inhibit growth of some tumor cells. Therefore, regulation of CYP4F3B by PGA1 may be yet another factor in 20-HETE homeostasis and regulation of vascular tone.

Regulation of expression of CYP4F3A differs markedly from that of CYP4F3B. CYP4F3A mRNA and associated LTB-4 ω-hydroxylase activity is induced by all-trans retinoic acid (ATRA) in HL60 cells [39]. Benzene is toxic to bone marrow and since CYP4F3A is expressed selectively in myeloid tissue, regulation of this enzyme by benzene and its metabolites has been studied by several groups. CYP4F3A protein was induced *in vivo* in white blood cells of patients with occupational benzene exposure [40], and CYP4F3A mRNA and protein levels were markedly induced in HL-60 cells by phenol, a metabolite of benzene, and by ATRA. Benzene itself showed only modest induction of CYP4F3A in this cell line.

CYP4F11 is regulated by the nuclear receptor, RXR, in HaCaT cells and HepG2 cells. The RXR selective chemical agonist, LG268 (aka LG100268), induced CYP4F11 mRNA (12-fold) and protein in HaCaT cells, whereas the RAR selective chemical agonist, TTNBP, decreased mRNA (3-fold) and protein [41]. In the same cell line, the cytokines, TNFα and IL-1B, induced CYP4F11 *via* a JNK, AP-1, and RXR/RAR mediated signaling pathway. In HepG2 cells, TNFα also induced CYP4F11. Enzyme induction was greater when a NF-kB translocase inhibitor (IMD0354) was added to the TNFα treatment. Thus, NF-kB may negatively regulate CYP4F11 expression [42]. However, cross-reactivity of the antibody used for western blotting was not assessed in these studies; therefore, other CYP4F enzymes may also have been induced.

CYP4F12 expression appears to be controlled by the pregnane-X receptor (PXR) [43]. In a chromatin immunoprecipitation (ChIP) study, a PXR binding site was found on the *CYP4F12* gene. Furthermore, siRNA knockdown of PXR in human hepatocytes resulted in an ~80% decrease CYP4F12 basal mRNA. Thus, CYP4F12 protein would be expected to be induced by PXR agonists such as rifampicin. This is significant because CYP4F12 is involved in xenobiotic metabolism. Indeed, drugs such as ebastine and terfenadine are CYP4F12

substrates, and induction by PXR ligands might be expected to lead to drug-drug interactions. Regulation of CYP4F8 and CYP4F22 expression has not been investigated to date.

Other CYP4 subfamilies

CYP4B1, the only member of the CYP4B subfamily, is expressed at the RNA level at high levels in human lung, but is catalytically inactive due to a mutation (Pro427Ser) in the meander region of the protein [44]. However, CYP4B1 is functional in other mammals, many of which are used to model human disease. The potential species-difference in metabolism is important because animal forms of CYP4B1 metabolize some procarcinogens and xenobiotics, in addition to short (C7-C10) chain fatty acids [45, 46].

The remaining CYP4 subfamilies each have one member: CYP4V2, CYP4X1, and CYP4Z1. These enzymes have been classified as orphan P450s, as their substrates and functions *in vivo* are poorly defined. CYP4V2 is known to hydroxylate medium chain fatty acids *in vitro* [47]. The enzyme is expressed ubiquitously and mutations in the *CYP4V2* gene are associated with the rare eye disease; Bietti's crystalline dystrophy. CYP4Z1 is expressed solely in mammary tissue, and can be induced by dexamethasone in breast cancer cell lines [48]. CYP4X1 is expressed mostly in aorta and trachea, however it is also present in liver, kidney, and a few other extrahepatic tissues. In HepG2 cells, CYP4X1 was induced by the potent PPARα agonist, WY17643, although basal levels were undetectable by western blotting [48]. Known inducers of CYP4 enzymes are summarized in Table 1.

1.3 Inhibition of CYP4 enzymes and 20-hydroxyeicosatetraenoic acid (20-HETE) biosynthesis for therapeutic use

The oxidation of arachidonic acid by cyclooxygenases, lipoxygenases, and P450 enzymes generates eicosanoids that possess a wide spectrum of biological activities and regulate complex signaling processes such as inflammation, platelet aggregation, and vascular and bronchiolar tone. CYP4 enzymes catalyze the formation of the key signaling eicosanoid, 20-HETE, which is the ω-hydroxylated metabolite of arachidonic acid. As discussed in detail below, inhibition of CYP4 enzymes, and thus of 20-HETE biosynthesis, has been suggested as a therapeutic strategy for hypertension, stroke, and some cancers because 20-HETE may contribute to the pathogenesis of these conditions [49-52].

20-HETE can be produced from arachidonic acid by human CYP4A11, CYP4F2, CYP4F11, CYP4F3A and CYP4F3B [53-55]. Reported i*n vitro* catalytic efficiencies can vary widely for this reaction [5, 7, 8], which may reflect the degree of difficulty involved in measuring accurate kinetic constants for very lipophilic endogenous compounds residing mostly in biological membranes. 19-HETE is also a minor metabolite produced by these enzymes from arachidonic acid, but it is often ignored or misassigned as 20-HETE because it is difficult to distinguish 19- and 20-HETE with HPLC separation gradients shorter than 30 minutes [7, 8]. Therefore, when interpreting reports of 20-HETE levels in urine, tissue, or enzyme incubations, it is important to evaluate whether the assay achieved chromatographic separation because these two metabolites are typically monitored by the same mass spectral multiple-reaction monitoring (MRM) transition. Pharmacologically, this is critical because 19-HETE is an antagonist of 20-HETE and is the major arachidonic acid metabolite formed by other P450 enzymes such as CYP2E1 [56-58] .

Hypertension

20-HETE has pro- and anti-hypertensive effects in numerous studies conducted in rat and mouse models of hypertension. The extensive body of literature investigating the role of 20-HETE in animal models of hypertension has been thoroughly reviewed elsewhere [49, 59, 60]. It is clear from these studies that 20-HETE plays a complex role in blood pressure regulation, and the balance between pro- and anti-hypertensive effects is critically dependent on the extent and site of 20-HETE biosynthesis. Moreover, the mouse and rat possess many CYP4 enzymes that generate 20-HETE, each with expression patterns and modes of regulation that may differ from human CYP4 enzymes, making translation of results from *in vivo* animal studies to the human situation particularly difficult.

Generally speaking, 20-HETE is a potent vasoconstrictor in the vasculature, including arterioles in the kidney, brain, and heart, and so is considered to be pro-hypertensive in these tissues. 20-HETE activates a number of kinase pathways that contribute to vascular tone regulation and blocks calcium-dependent potassium (K_{Ca}) channels that lead to increased calcium entry through L-type Calcium channels in the vascular smooth muscle cell. Increased Ca^{2+} in these cells causes smooth muscle contraction and vasoconstriction. However, in the kidney 20-HETE has an *anti*-hypertensive effect. This appears to be due to inhibition of Na^{+} reabsorption in the proximal tubule of the nephron through activation of protein kinase C that phosphorylates renal

Na^+K^+ATPase, causing decreased sodium transport through this channel. In the thick ascending loop of Henle (TALH), 20-HETE blocks other ion channels, namely $Na^+K^+2Cl^-$ and 70pS K^+, leading to reduced passive reabsorption of Na^+ in this region of the nephron. Thus, in the nephron, 20-HETE has a natriuretic effect leading to less water reabsorption, thereby lowering blood pressure [49, 59, 61].

In humans, genetic association studies linking variants of CYP4A11 and CYP4F2 with elevated blood pressure have highlighted the complexity inherent in having multiple CYP4 enzymes contributing to the biosynthesis of 20-HETE. A T8590C single nucleotide polymorphism (SNP) in the *CYP4A11* gene (rs1126742) results in an F434S amino acid substitution that decreases V_{max} and catalytic efficiency for 20-HETE formation when compared to the wild type enzyme [5]. In two separate populations (n=512 and n=1538), individuals who were homozygous or heterozygous carriers of the 8590C allele had an increased risk of hypertension (odds ratio of 2.31 and 1.21 for each cohort, respectively) compared to 8590T homozygotes. The functional deficit of the variant enzyme should result in decreased 20-HETE production in tissue where CYP4A11 is expressed, suggesting that the natriuretic and anti-hypertensive effects of 20-HETE at the level of the nephron drive the genetic association. Correspondingly, in the *CYP4F2* gene a C1347T SNP (rs2108622) results in a V433M amino acid substitution and a T84G SNP (rs3093105) results in a W12G amino acid substitution. The V433M mutant, expressed in insect cells, exhibited a decreased kcat for 20-HETE formation from 0.08 min^{-1} to 0.03 min^{-1} at a concentration of 42 μM arachidonic acid [62], and there was no change in enzyme activity of the W12G mutant. Surprisingly, there are no published data on K_m, V_{max}, or catalytic efficiency for these CYP4F2 mutants and 20-HETE formation, so it cannot be conclusively stated that they are either gain or loss of function polymorphisms. A study (n=235) that measured the effects of both loss of function polymorphisms in *CYP4A11* (rs1126742) and *CYP4F2* (rs2108622) on blood pressure and urinary 20-HETE levels provide a less clear conclusion. In carriers of the *CYP4A11* 8590C SNP, there was a decrease in urinary 20-HETE, but no effect on blood pressure. In carriers of the CYP4F2 1347T SNP, there was an unexpected increase in urinary 20-HETE as well as an increase in blood pressure. However, a 50% increase in enzyme activity above wild-type levels for 20-HETE production by the CYP4F2 W12G mutant was later reported, suggesting a gain of function polymorphism that may have been overlooked in the earlier study. A different study looked at mutations in haplotypes in the regulatory regions of the *CYP4F2* gene and found an association between a common genetic variant of one haplotype (Hap I: rs3093098, rs3093100, rs3093103, and rs3093105) and increased risk of hypertension along with elevated urinary

20-HETE levels [63]. The authors propose that differences in NF-κB (nuclear factor kappa-light-chain-enhancer of activated B cells) binding to the regulatory region may be the cause for this association. Another study in Swedes (n=6002) found subjects with the CYP4A11 F434S mutation (rs1126742) had higher blood pressure and hypertension prevalence, corroborating earlier findings. However, the same study found increased blood pressure and a slight trend towards increased hypertension risk only in males with the CYP4F2 V433M mutation, with no effect in females [64]. Collectively, these genetic association studies suggest that both CYP4A11 and CYP4F2 contribute to 20-HETE biosynthesis and blood pressure regulation *in vivo* in humans, but the precise mechanisms are difficult to unravel. A further complication is that no studies have yet been reported in humans concerning the effect on blood pressure of polymorphisms in CYP4F3B and CYP4F11, two other potentially important 20-HETE synthases.

Clearly, the role of 20-HETE in the pathophysiology of hypertension is complex, since it is a natriuretic and anti-hypertensive factor in the nephron of the kidney and a vasoconstrictor and pro-hypertensive eicosanoid in the vascular smooth muscle cells. Additionally, other eicosanoids, such as EETs and diHETEs, contribute to vascular tone regulation and introduce additional complications [65]. Nevertheless, numerous animal studies have provided strong evidence overall that indicates that inhibition of CYP4 enzymes and 20-HETE formation is a promising route to hypertension therapy.

Hemorrhagic and Ischemic Stroke

There are a number of studies that have investigated the potential for CYP4 inhibition as a treatment after stroke to reduce brain damage. The rationale here is that 20-HETE is a vasoconstrictor in cerebral arteries *in vitro* and *in vivo* [66]. In the brain, oxygen deprivation to tissue occurs during both hemorrhagic stroke and ischemic stroke. During ischemic stroke caused by prolonged blockage of cerebral arteries, blood flow to tissue is restricted and neurons die, resulting in an infarct. The size of the resulting infarct reflects the extent of damage to brain tissue. During subarachnoid hemorrhage (SAH) caused by a ruptured aneurysm or head injury, there is an acute drop in cerebral blood flow resulting in ischemia. After SAH in rats, inhibitors of 20-HETE synthesis, such as HET0016 and 17-ODYA, decreased 20-HETE levels in cerebral spinal fluid (CSF) and prevented the acute fall in cerebral blood flow. However, the inhibitors used in this study were likely not CYP4 selective. As mentioned above, 17-ODYA inhibits EET and HETE formation at similar IC_{50} values *in vitro*, and the dose of HET0016

given to the rats (10 mg/kg) was rather large and perhaps sufficiently high to inhibit other P450 enzymes, such as isoforms from the CYP2C sub-family. However, a subsequent study found that TS-011 also prevented the drop in cerebral blood flow and rise in 20-HETE levels in the CSF after SAH, and the dose was more appropriately reflective (0.01-1 mg/kg) of a potent enzyme inhibitor [55]. After ischemic stroke in rats, CYP4 inhibition by TS-011 treatment decreased 20-HETE production and caused a 35% decrease in infarct size. Furthermore, in a different rat model of ischemic stroke (transient occlusion of the middle cerebral artery), there was a 55% and 65% decrease in infarct volume size after TS-011 and HET0016 administration, respectively [67]. This latter study measured HETE and EET levels in brain tissue and found an 80% decrease in 20-HETE after inhibitor dosing with no effect on EET levels. The HPLC/MS/MS method also enabled analytical discrimination of 19- and 20-HETE, although 19-HETE was not quantitated. Together, these studies indicate a potential for targeting CYP4 enzymes in the cerebral vasculature with the aim of reducing 20-HETE production, decreasing vasoconstriction, and thus increasing blood flow to ischemic regions of the brain after stroke. Additionally, inhibitors like TS-011 may cross the blood brain barrier and affect 20-HETE biosynthesis in the neuron, as well as the cerebral vasculature. Because 20-HETE is involved in numerous signal transduction pathways and affects ion transport across cell membranes, there may be additional mechanisms for the protective effects of CYP4 inhibitors after ischemia. However, it is not clear which CYP4 enzymes are expressed and produce 20-HETE in the neuron, and a non-CYP4 brain P450, CYP2U1, has been shown to form both 19- and 20-HETE [68]. It is also not known if HET0016 or TS-011 inhibit CYP2U1. Therefore, more work must be done to validate this alternative mechanism of action and clarify whether CYP4 inhibitors could be viable drugs for stroke victims.

Cancer

Angiogenesis is the growth of new blood vessels from vascular endothelial cells and is mediated by a number of peptide growth factors and cytokines. 20-HETE is a pro-angiogenic signaling eicosanoid and mediates neovascularization of various cancers through activation of vascular endothelial growth factor (VEGF) [69]. Additionally, CYP4 enzymes that biosynthesize 20-HETE are up-regulated in some cancers [52]. Remarkable decreases in tumor size after administration of HET0016 to animal models have been observed [70]. *In vitro*, HET0016 inhibited brain tumor cell proliferation (U251 glioma cells) in a dose dependent manner. In a rat model of a highly aggressive brain tumor, HET0016 dosed daily for 2 weeks (10 mg/kg/day) decreased the size of the

tumor by 80%, decreased neovascularization by ~50%, and increased mean survival time of the animal from 17 to 22 days [71, 72]. Thus, CYP4 appears to be a promising drug target for inhibition in rat solid brain tumors. Additionally, HET0016 inhibited growth of human renal adenocarcinoma cell lines (786-O and 769-P cell lines) *in vitro*. An adenocarcinoma is cancer of the epithelial cells originating in a glandular tissue. Cells were implanted in an ectopic mouse model of cancer and administration of a 20-HETE antagonist, 20–5(Z),14(Z)-hydroxyeicosadienoic acid (WIT002), decreased the tumor size by 84% [73]. The study did not report similar results with any CYP4 inhibitor, and so more work is needed before it can be concluded that 20-HETE reduction by CYP4 inhibition is a possible therapeutic modality for renal adenocarcinoma.

1.4 Induction of CYP4 enzymes for therapy in fatty acid clearance disorders

Fatty acid oxidation and clearance overview

Most fatty acids (FAs) are cleared by the well-characterized elimination pathway, mitochondrial or peroxisomal β-oxidation (Figure 1.3). Acyl CoA-esters of FAs are transferred into the mitochondria and undergo four transformations performed by four separate enzymes: dehydrogenation, hydration, a second dehydrogenation, and finally cleavage of the acyl-CoA group. This cascade yields a FA that is two carbons shorter than the original substrate. Generally, short, medium, and long chain FAs undergo β-oxidation in the mitochondria by enzymes with specificities for each chain length. Very long chained FAs (>C22) are β-oxidized in the peroxisomes and then transferred to the mitochondria where further rounds of β-oxidation occur. FAs that are branched or substituted at the β-carbon must first undergo α-oxidation, and this only occurs only in the peroxisome [74]. ω-Oxidation is a third route of FA degradation, accounting for only a small percentage of the total clearance pathway under normal conditions. As noted in earlier sections, CYP4 enzymes ω-hydroxylate FAs, and alcohol dehydrogenases (ADH), aldehyde dehydrogenases (ALDH), as well as other P450 enzymes, perform further oxidative steps to yield a dicarboxylic acid [75]. The dicarboxylic acid can then be esterified to an acyl CoA-ester and transferred to the peroxisome to be degraded *via* β-oxidation.

X-linked adrenoleukodystrophy (X-ALD)

X-ALD is an inherited disorder characterized by an increase in very long chain fatty acids (VLCFA) in plasma and tissue resulting in demyelination of neurons. The incidence of X-ALD is 1 in 20,000 males and

treatments are limited to bone marrow transplantation and gene therapy. Mutations in the *ABCD1* (ATP-binding cassette, subfamily D, member 1) gene on the X chromosome leads to a dysfunctional protein normally responsible for transporting VLCFAs into the peroxisome for degradation. Increasing ω-hydroxylation of excess VLCFAs to generate dicarboxylic acids via *CYP4F2* induction has been suggested as a therapeutic strategy for X-ALD patients [75, 76]. Very long chain dicarboxylic acids are transported into the peroxisome by a different transporter than their monocarboxylic acid counterparts. Thus, CYP4F2 induction might be an alternative pathway to clear VLCFAs from the liver cell and thus the systemic circulation. Lovastatin, a CYP4F2 inducer, was reported to lower VLCFAs in plasma of patients and has been used as an off-label therapy for this disease [77, 78]. However, a recent placebo-controlled trial showed no benefit of lovastatin treatment in X-ALD patients [79].

Refsum Disease

Adult Refsum disease is an autosomal recessive disorder characterized by an increase in phytanic acid in plasma and tissue resulting in neural defects. Loss of function mutations in either the Peroxin 7 (*PEX7)* gene or the phytanoyl-CoA 2-hydroxylase (*PAHX aka PHYH*) gene that lead to impaired α-oxidation of phytanic acid underlie adult Refsum. Phytanic acid has a methyl group in the β-position, necessitating α-oxidation in the peroxisome before it can undergo β-oxidation in the mitochondria. Phytanoyl-CoA 2-hydroxylase is responsible for the hydroxylation step of phytanoyl-CoA during α-oxidation. The *PEX7* gene codes for the PTS2 (peroxisomal targeting signal 2) receptor, which binds to some proteins synthesized in the cytoplasm and directs them to the peroxisome. A dysfunctional PTS2 receptor results in faulty transport of phytanoyl-CoA 2-hydroxylase from the cytoplasm to the peroxisome. In patients with Refsum disease, phytanic acid plasma concentrations have been reported to increase from <10 μM to as high as 1.3 mM [80]. CYP4 mediated ω-hydroxylation is responsible for only a small percentage of the clearance pathway under normal conditions, but may be an alternate route to phytanic acid clearance in the disease state. The catalytic efficiencies in human P450 Supersomes for ω-hydroxylation of phytanic acid are CYP4F3A> CYP4F3B> CYP4F2> CYP4A11 [81]. Consequently, induction of CYP4F/CYP4A enzymes has been proposed as a therapeutic route for Refsum disease [74, 82].

1.5 Therapeutic uses of Vitamin K

Vitamin K Overview

As noted above, CYP4F2 was recently identified as a key enzyme in initiating the catabolism of vitamin K1 [16]. Vitamin K is a collective term for a series of naphthoquinone derivatives with important biological activities. Vitamin K1, also known as phylloquinone (PK), and menaquinone-4 (MK4), a form of vitamin K2, have 20-carbon phytyl chains that differ only in their degree of unsaturation. Other menaquinones (MK5 - MK13) have longer unsaturated phytyl chains, whereas menadione (MN), also referred to as vitamin K3, possesses no phytyl side-chain (Figure 1.4). PK is biosynthesized by plants, and humans acquire it by eating green vegetables. MK4 is biosynthesized in humans from either PK or MN [83-85]. MK4 can also be acquired from eating animal products such as meat and liver. Longer-chain menaquinones are synthesized by bacteria in the human intestinal flora and by bacteria in fermented foods such as cheese and fermented soybeans [86, 87].

Vitamin K is the cofactor for the γ-glutamyl carboxylase (GGCX) enzyme that uses the reduced dihydroquinone form of vitamin K, along with molecular oxygen and carbon dioxide, to γ–carboxylate at least 17 human proteins [88]. These so called Gla proteins have domains rich in glutamic acid residues (ranging from 3-16) that upon γ–carboxylation are capable of chelating calcium ions. This induces a unique post-translational modification resulting in a significant conformational change of the Gla domain, which increases the proteins' ability to bind to membranes and adopt a favorable orientation with respect to the membrane-associated protein substrate [89, 90].

Seven of the 17 human vitamin K dependent Gla proteins are involved in blood clotting. GGCX carboxylates clotting factors II, VII, IX, and X and protein C, S, and Z in the liver. Subsequently the activated protein is exported out of the hepatocyte and into the blood, which is the site of clotting action. The activated clotting factors are serine proteases that cleave a peptide bond of their substrate protein in the coagulation cascade.

GGCX is a trans-membrane protein located in the endoplasmic reticulum and is expressed ubiquitously, however mRNA levels are approximately 10-fold higher in the liver compared to other tissues [91]. Mutations in this protein cause bleeding and calcium homeostasis disorders, and GGCX knock-out mice die from massive abdominal hemorrhage at birth [92]. Thus, vitamin K deficiency, as seen in patients treated with warfarin, results

in under-carboxylated Gla proteins and an anticoagulant effect ensues because active clotting factors are not produced.

The other ten known human vitamin K dependent Gla proteins are involved in a variety of physiological processes including inhibition of arterial calcification (Matrix-Gla protein), bone mineralization (osteocalcin), and cell growth regulation (Growth arrest sequence 6 protein, Gas6). The remaining 7 known Gla proteins have less well established physiological roles.

Vitamin K is also important in physiological processes apart from GGCX-driven activation of clotting factors. MK4 is an electron carrier in the electron transport chain in mitochondria of eukaryotic cells [93]. MK4 is also an established ligand for the steroid and xenobiotic receptor (SXR) [94]. SXR is a nuclear receptor controlling the expression of a large family of genes involved in transport and metabolism of endo- and xenobiotics. Thus vitamin K may regulate transcription levels of numerous genes.

It has been established that the major urinary metabolites of PK and MK4 are K acid 1 and K acid 2 (Figure 1.5a). This catabolic pathway presumably involves an initial ω-hydroxylation event followed by two additional oxidations to generate aldehyde and carboxylic acid products (Figure 1.5b). The carboxylic acids can then be esterified to their CoA derivatives and transferred from the ER to either the mitochondria or peroxisomes for β-oxidation to the chain shortened metabolites that have been found in the urine as glucuronide conjugates. Analogous pathways exist for the structurally similar compounds, vitamin E and coenzyme Q [95-97].

Warfarin Stabilization Therapy

The vitamin K cycle is shown in Figure 1.6. Vitamin K is reduced to the dihydroquinone, at which point it is used as the cofactor for GGCX to activate the clotting factor proteins. Meanwhile, vitamin K is converted to the vitamin K epoxide. The enzyme vitamin K epoxide (VKOR) reduces vitamin K epoxide back to vitamin K, thereby recycling the cofactor. Warfarin inhibits VKOR and thus decreases the vitamin K levels available to GGCX. This reduces the levels of activated clotting factors and hinders the clotting cascade, resulting in an anticoagulation effect. Warfarin has a very narrow therapeutic range. Patients are started at a specific dose, and their coagulation is monitored and the dose is adjusted accordingly until the adequate coagulation effect is achieved and is stable. Many patients receiving warfarin fail to stabilize within a target range of time, resulting in increased risk of adverse events such as thromboembolism, due to lack of efficacy, or bleeding, due to overdose.

Some studies have shown that patients with unstable anticoagulation response may benefit from vitamin K supplementation [98-100]. The rationale here is that supplementation would increase body stores of vitamin K, thereby reducing the effect of changes in dietary intake.

Cardiovascular Disease and Chronic Kidney Disease

Vascular calcification (VC) is a complex, highly regulated physiological process resembling that of bone mineralization. It is highly correlated with cardiovascular disease mortality and is a common comorbidity of chronic kidney disease (CKD), such that the most common cause of death in patients with CKD is cardiovascular disease. The vitamin K-dependent product, matrix-Gla protein (MGP), is a potent inhibitor of VC. Genetic mutations in the gene encoding MGP cause Keutal Syndrome, characterized by both vascular and skeletal abnormalities. MGP knockout mice die in the first 2 months of life from massive arterial calcification and blood vessel rupture. In a rat model of CKD, supplementation with high dietary phylloquinone blunts the development of VC [101]. In humans, a prospective population-based study showed dietary intake of all vitamin K2 forms, but not phylloquinone, was protective against VC and mortality [102].

Osteoporosis

Osteocalcin is a 5-6 kDa Gla-protein found in bone and secreted into the blood by osteoblast cells. It is used as a biomarker for bone formation. Generally, serum osteocalcin levels are correlated with bone mineral density (BMD), and under-carboxylated serum osteocalcin is indicative of vitamin K deficiency, as seen in prolonged warfarin therapy. Periostin is a 90 kDa Gla-protein involved in bone metabolism [103], among other physiological processes. It is secreted by fibroblasts, the predominate cell type in connective tissues, into the extracellular matrix. Periostin is involved in several intracellular and extracellular functions resulting in stimulation of bone formation during development or after bone fracture.

In Japan, MK4 has been prescribed since 1995 for the prevention and treatment of osteoporosis at a dose of 45 mg/day. MK7 is found at high levels in the common Japanese breakfast food, nattō, and has been associated with increased BMD in elderly men [104]. Across the many studies investigating vitamin K associations with osteoporosis, it is clear that vitamin K deficiency is associated with higher risk of bone fracture. However, supplementation with vitamin K either leads to increased BMD or no effect on BMD, providing a less

clear overall conclusion [88]. To further complicate the matter, many studies use either PK, MK4, or MK7 as the supplement at variable doses, and it is unclear if one form is more important or effective for bone formation than others.

Parkinson's Disease

Parkinson's disease (PD) is a neurodegenerative disorder of the central nervous system characterized by the death of dopamine generating cells. The cause of cell death is largely unknown, however decreased mitochondrial activity, α-synuclein aggregation, and proteosomal or lysosomal dysfunction have all been proposed. A genetic loss of function mutation in the *pink1* gene (PTEN-induced putative kinase 1) has been causally linked to less than 1% of early onset PD [105]. PINK1 is a mitochondrial protein kinase thought to protect cells from mitochondrial dysfunction. In fruit flies with reduced motor neuron capacity due to *Heix* mutations, a modifier of *pink1*, MK4 treatment restored motor neuron function [93]. This suggests that MK4, much like the structurally similar Coenzyme Q10, is an electron carrier in the electron transport chain of mitochondria of eukaryotes. MK4 was previously only known to be an electron carrier in membranes of bacteria. There have been a number of studies suggesting that CoQ10 supplementation may be beneficial for PD patients, and now MK4 is also being considered.

1.6 Conclusions and Scope of Dissertation Research

CYP4 enzymes are potential drug targets for treatment of hypertension, stroke, and some cancers by pharmacological manipulation of 20-HETE levels. HET0016 is a potent inhibitor of 20-HETE synthases in renal microsomes. However, the precise enzymes inhibited by HET0016 and the mechanisms involved have received little attention. Chapters 2 and 3 are devoted to filling this knowledge gap. The structure-activity relationships and mechanisms of CYP4 enzyme inhibition by HET0016 are critical to any further development of this compound as a therapeutic agent and to further understanding of CYP4 enzymology.

There are numerous biological functions now attributed to vitamin K, and there is substantial interest in its use as a therapeutic agent. Therefore it is important to understand how the body regulates tissue concentrations of the various vitamin K forms. Metabolic processes involving CYP4 enzymes can be expected to play an important role in vitamin K homeostasis. This will be investigated in Chapters 4 and 5. This work expands what

is known about vitamin K catabolism with the goal of understanding factors involved in inter-individual variability in vitamin K status that may affect supplementation for the aforementioned conditions.

Figure 1.1: The CYP4 enzyme partial I-helix sequence compared to CYP3A4, CYP1A2, and CYP2C9. The conserved glutamic acid residue that forms a covalent bond with the heme cofactor in several CYP4 enzymes is highlighted.

Enzyme	PARTIAL I-HELIX SEQUENCE (conserved xxGxxT MOTIF)
CYP4A11	DTFMF**E**GHDTTAS
CYP4B1	DTFMF**E**GHDTTTS
CYP4F2	DTFMF**E**GHDTTAS
CYP4F3	DTFMF**E**GHDTTAS
CYP4F8	DTFMF**G**GHDTTAS
CYP4F11	DTFMF**E**GHDTTAS
CYP4F12	DTFMF**G**GHDTTAS
CYP4F22	DTFMF**E**GHDTTSS
CYP4V2	DTFMF**E**GHDTTAA
CYP4X1	STFLL**A**GHDTLAA
CYP4Z1	KTFMF**A**GHDTTSS
CYP3A4	IIFIF**A**GYETTSS
CYP1A2	NDIFG**A**GFDTVTT
CYP2C9	VDLFG**A**GTETTST

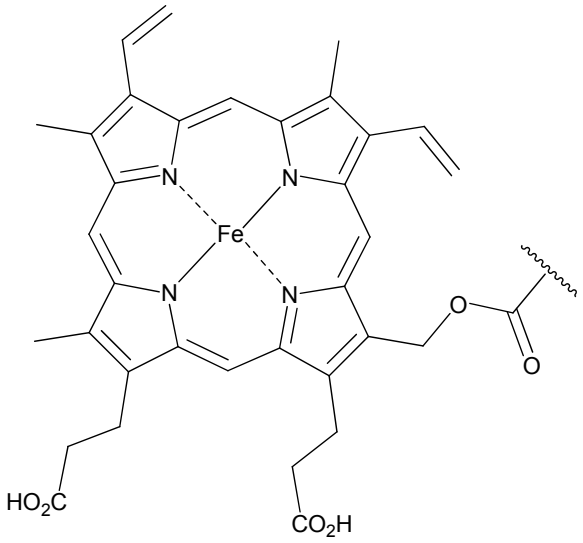

Figure 1.2: The CYP4F gene cluster on chromosome 19

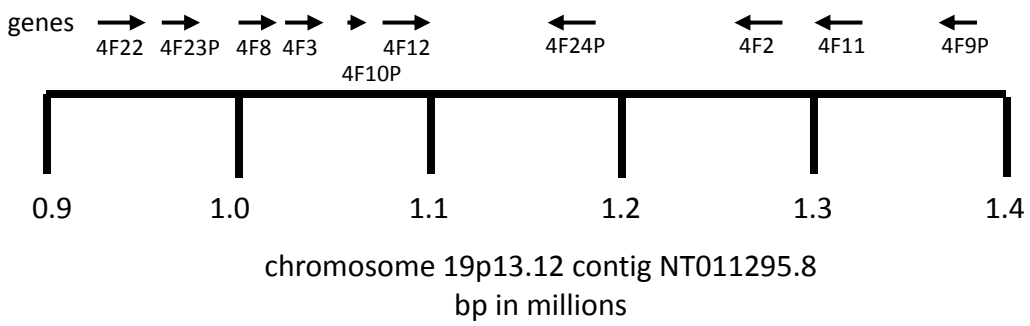

Figure 1.3: Fatty acid degradation pathways

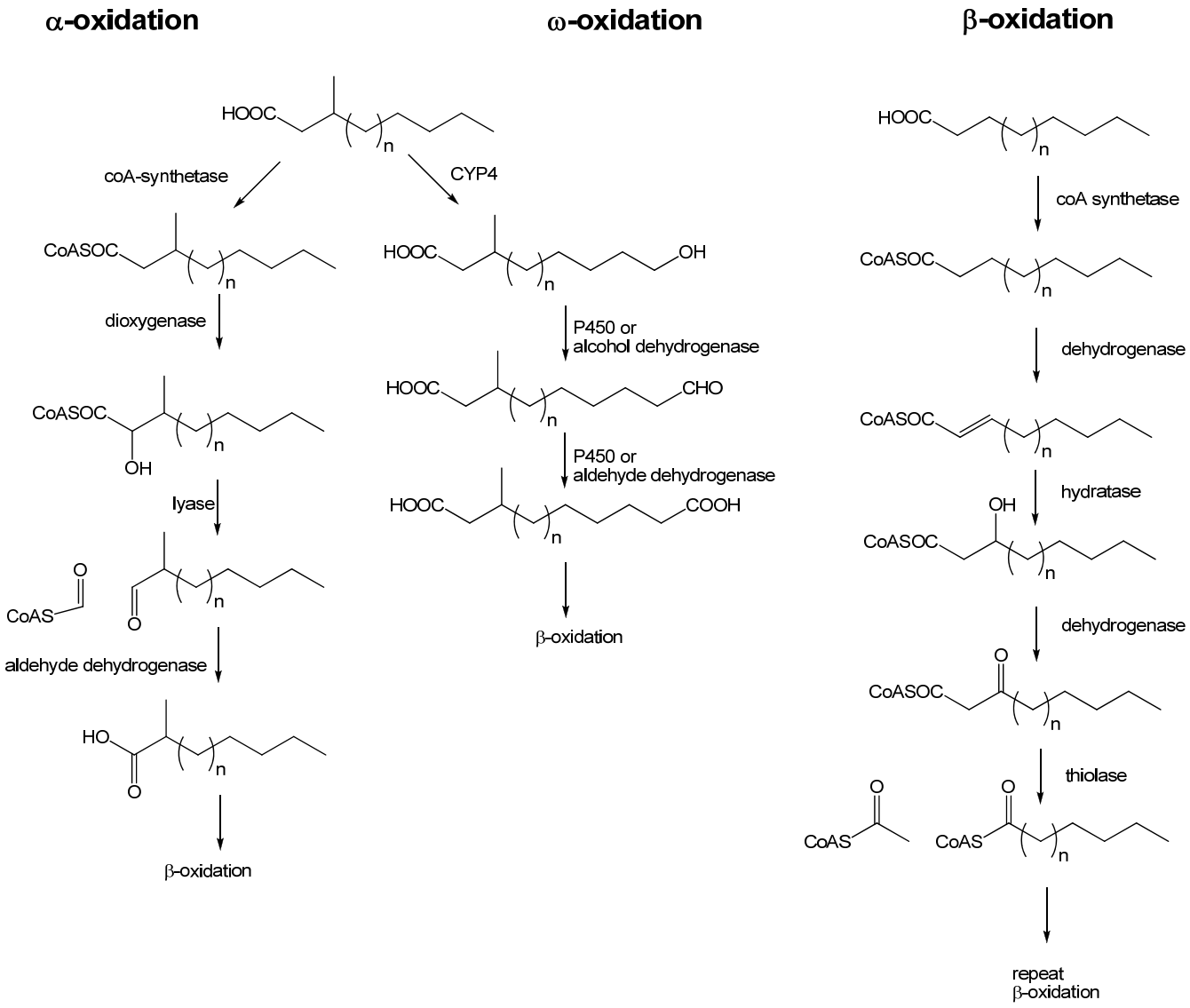

Figure 1.4: Vitamin K structures

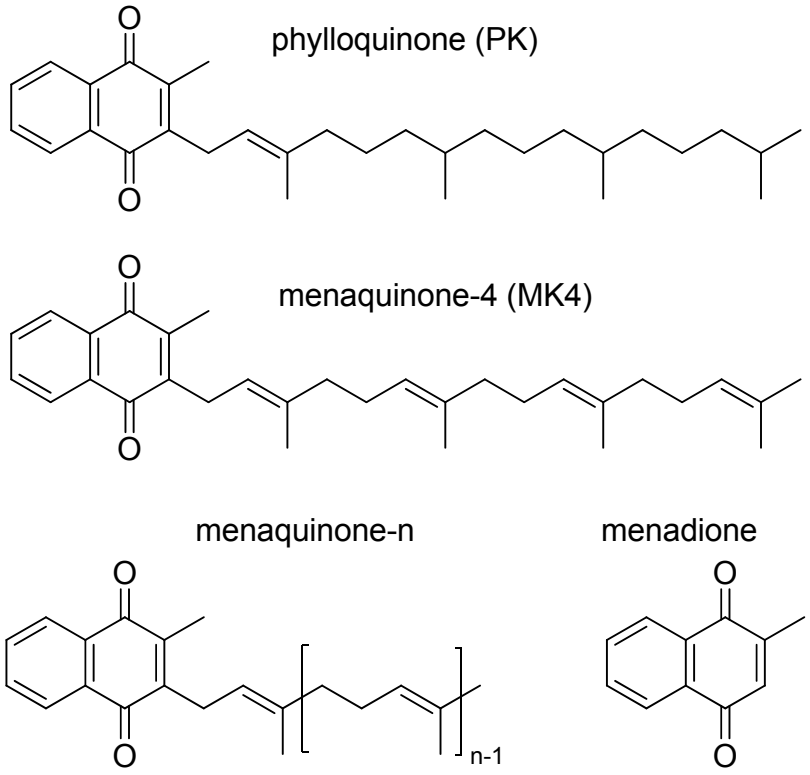

Figure 1.5 A) The elimination pathway of phylloquinone (PK) and menaquinone-4 (MK4). The major urinary metabolites are the β-oxidized, chain-shortened glucuronides of K acid 1 and K acid 2. B) Both PK and MK4 must undergo an initial ω-hydroxylation step before β-oxidation can commence.

A

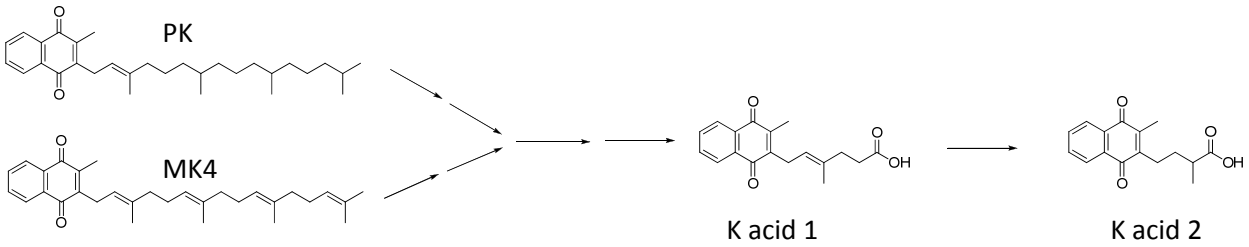

B

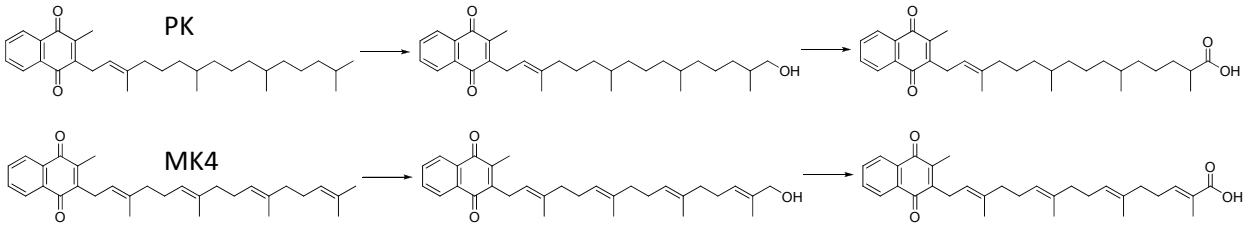

Figure 1.6: The vitamin K cycle

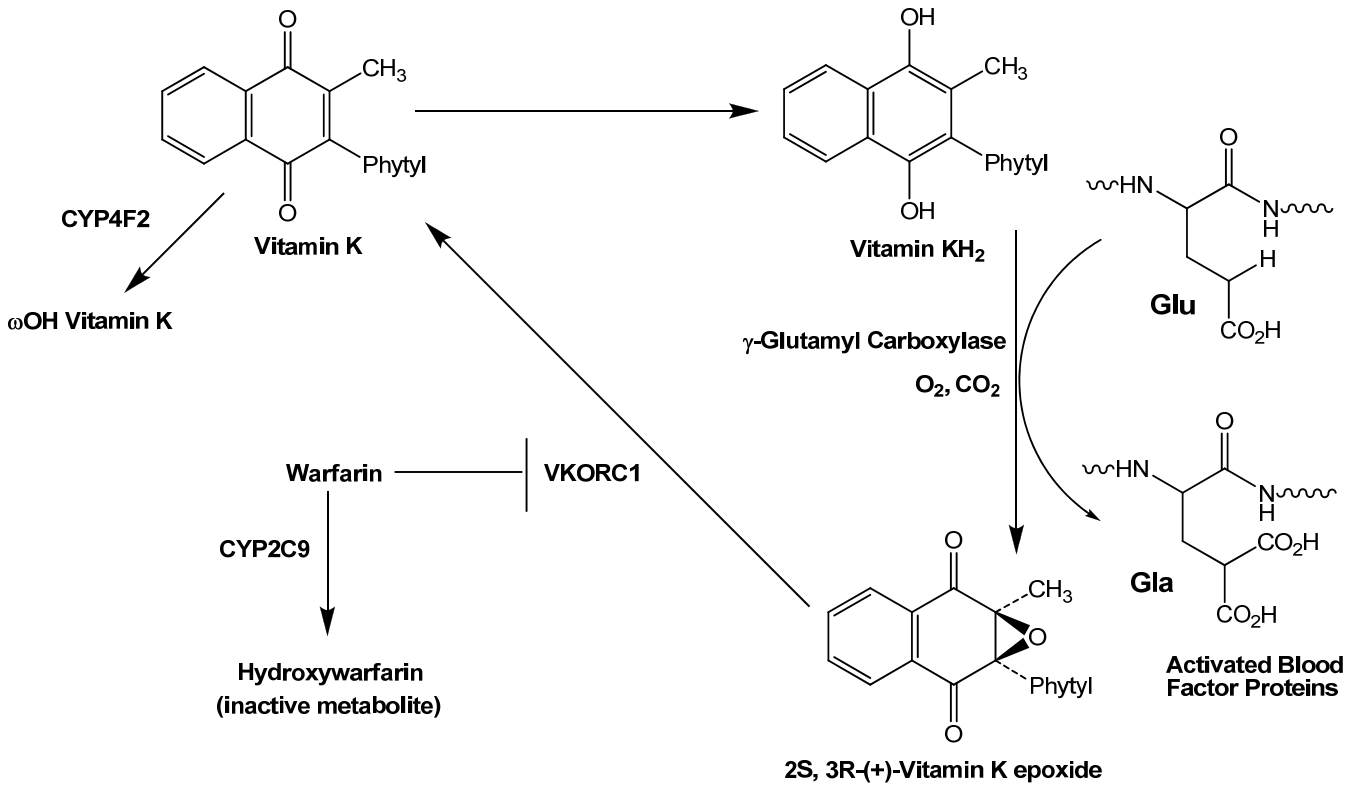

Table 1: Summary of CYP4 inducers

Enzyme	Cell System	Inducer	Regulator(s) and/or nuclear receptor(s)	Reference
CYP4F2	HepG2, primary HH	lovastatin, mevastatin	SREBP	[34]
CYP4F2	HepG2	genistein, AICAR, resveratrol	AMPK	[36]
CYP4F3B	HepaRG	PGA1	unknown	[38]
CYP4F11	HaCaT	LG268 (aka LG100268)	RXR	[41]
CYP4F11	HaCaT	TNFα, IL-1B	JNK, AP-1 (RXR, RAR)	[41]
CYP4F11	HepG2	TNFα, TNFa+IMD0354	JNK, AP-1 (RXR, RAR) (+ NF-κB)	[42]
CYP4A11	HepG2, primary HH	Fibrates	PPARα	[11, 14]
CYP4Z1	T47-D (breast tumor)	dexamethasone, progesterone	PXR	[48]
CYP4Z1	MCF-7 (breast cancer)	dexamethasone	PXR	[48]
CYP4X1	HepG2	WY17643	PPARα	[48]
CYP4F12	Primary HH	rifampicin	PXR	[43]

1.7 References

[1] Hoch, U.; Ortiz De Montellano, P.R., Covalently linked heme in cytochrome p4504a fatty acid hydroxylases. *J Biol Chem,* 2001, *276*(14), 11339-11346.
[2] Henne, K.R.; Kunze, K.L.; Zheng, Y.M.; Christmas, P.; Soberman, R.J.; Rettie, A.E., Covalent linkage of prosthetic heme to CYP4 family P450 enzymes. *Biochemistry,* 2001, *40*(43), 12925-12931.
[3] Bylund, J.; Hidestrand, M.; Ingelman-Sundberg, M.; Oliw, E.H., Identification of CYP4F8 in human seminal vesicles as a prominent 19-hydroxylase of prostaglandin endoperoxides. *J Biol Chem,* 2000, *275*(29), 21844-21849.
[4] Bylund, J.; Bylund, M.; Oliw, E.H., cDna cloning and expression of CYP4F12, a novel human cytochrome P450. *Biochem Biophys Res Commun,* 2001, *280*(3), 892-897.
[5] Gainer, J.V.; Bellamine, A.; Dawson, E.P.; Womble, K.E.; Grant, S.W.; Wang, Y.; Cupples, L.A.; Guo, C.Y.; Demissie, S.; O'Donnell, C.J.; Brown, N.J.; Waterman, M.R.; Capdevila, J.H., Functional variant of CYP4A11 20-hydroxyeicosatetraenoic acid synthase is associated with essential hypertension. *Circulation,* 2005, *111*(1), 63-69.
[6] Dierks, E.A.; Zhang, Z.; Johnson, E.F.; de Montellano, P.R., The catalytic site of cytochrome P4504A11 (CYP4A11) and its L131F mutant. *J Biol Chem,* 1998, *273*(36), 23055-23061.
[7] Powell, P.K.; Wolf, I.; Jin, R.; Lasker, J.M., Metabolism of arachidonic acid to 20-hydroxy-5,8,11, 14-eicosatetraenoic acid by P450 enzymes in human liver: involvement of CYP4F2 and CYP4A11. *J Pharmacol Exp Ther,* 1998, *285*(3), 1327-1336.
[8] Lasker, J.M.; Chen, W.B.; Wolf, I.; Bloswick, B.P.; Wilson, P.D.; Powell, P.K., Formation of 20-hydroxyeicosatetraenoic acid, a vasoactive and natriuretic eicosanoid, in human kidney. Role of Cyp4F2 and Cyp4A11. *J Biol Chem,* 2000, *275*(6), 4118-4126.
[9] Johnson, E.F.; Palmer, C.N.; Griffin, K.J.; Hsu, M.H., Role of the peroxisome proliferator-activated receptor in cytochrome P450 4A gene regulation. *FASEB J,* 1996, *10*(11), 1241-1248.
[10] Johnson, E.F.; Hsu, M.H.; Savas, U.; Griffin, K.J., Regulation of P450 4A expression by peroxisome proliferator activated receptors. *Toxicology,* 2002, *181-182*, 203-206.
[11] Lawrence, J.W.; Li, Y.; Chen, S.; DeLuca, J.G.; Berger, J.P.; Umbenhauer, D.R.; Moller, D.E.; Zhou, G., Differential gene regulation in human versus rodent hepatocytes by peroxisome proliferator-activated receptor (PPAR) alpha. PPAR alpha fails to induce peroxisome proliferation-associated genes in human cells independently of the level of receptor expresson. *J Biol Chem,* 2001, *276*(34), 31521-31527.
[12] Cattley, R.C.; DeLuca, J.; Elcombe, C.; Fenner-Crisp, P.; Lake, B.G.; Marsman, D.S.; Pastoor, T.A.; Popp, J.A.; Robinson, D.E.; Schwetz, B.; Tugwood, J.; Wahli, W., Do peroxisome proliferating compounds pose a hepatocarcinogenic hazard to humans? *Regul Toxicol Pharmacol,* 1998, *27*(1 Pt 1), 47-60.
[13] Savas, U.; Machemer, D.E.; Hsu, M.H.; Gaynor, P.; Lasker, J.M.; Tukey, R.H.; Johnson, E.F., Opposing roles of peroxisome proliferator-activated receptor alpha and growth hormone in the regulation of CYP4A11 expression in a transgenic mouse model. *J Biol Chem,* 2009, *284*(24), 16541-16552.
[14] Alvergnas, M.; Richert, L.; Blanchard, N.; Abadie, C.; Heyd, B.; Mantion, G.; Gallemann, D.; Martin, H., Regulation of CYP4A expression by bezafibrate in primary culture of rat and human hepatocytes: interspecies difference and influence of N-acetylcysteine. *Toxicol In Vitro,* 2009, *23*(7), 1259-1267.
[15] Raucy, J.L.; Lasker, J.; Ozaki, K.; Zoleta, V., Regulation of CYP2E1 by ethanol and palmitic acid and CYP4A11 by clofibrate in primary cultures of human hepatocytes. *Toxicol Sci,* 2004, *79*(2), 233-241.
[16] McDonald, M.G.; Rieder, M.J.; Nakano, M.; Hsia, C.K.; Rettie, A.E., CYP4F2 is a vitamin K1 oxidase: An explanation for altered warfarin dose in carriers of the V433M variant. *Mol Pharmacol,* 2009, *75*(6), 1337-1346.
[17] Tamraz, B.; Fukushima, H.; Wolfe, A.R.; Kaspera, R.; Totah, R.A.; Floyd, J.S.; Ma, B.; Chu, C.; Marciante, K.D.; Heckbert, S.R.; Psaty, B.M.; Kroetz, D.L.; Kwok, P.Y., OATP1B1-related drug-drug and drug-gene interactions as potential risk factors for cerivastatin-induced rhabdomyolysis. *Pharmacogenet Genomics,* 2013.
[18] Lee, C.A.; Jones, J.P., 3rd; Katayama, J.; Kaspera, R.; Jiang, Y.; Freiwald, S.; Smith, E.; Walker, G.S.; Totah, R.A., Identifying a selective substrate and inhibitor pair for the evaluation of CYP2J2 activity. *Drug Metab Dispos,* 2012, *40*(5), 943-951.
[19] Kawakami, H.; Ohtsuki, S.; Kamiie, J.; Suzuki, T.; Abe, T.; Terasaki, T., Simultaneous absolute quantification of 11 cytochrome P450 isoforms in human liver microsomes by liquid chromatography tandem mass spectrometry with in silico target peptide selection. *J Pharm Sci,* 2011, *100*(1), 341-352.

[20] Shea, M.K.; O'Donnell, C.J.; Hoffmann, U.; Dallal, G.E.; Dawson-Hughes, B.; Ordovas, J.M.; Price, P.A.; Williamson, M.K.; Booth, S.L., Vitamin K supplementation and progression of coronary artery calcium in older men and women. *Am J Clin Nutr,* 2009, *89*(6), 1799-1807.
[21] Fu, X.; Wang, X.D.; Mernitz, H.; Wallin, R.; Shea, M.K.; Booth, S.L., 9-Cis retinoic acid reduces 1alpha,25-dihydroxycholecalciferol-induced renal calcification by altering vitamin K-dependent gamma-carboxylation of matrix gamma-carboxyglutamic acid protein in A/J male mice. *J Nutr,* 2008, *138*(12), 2337-2341.
[22] Shea, M.K.; Booth, S.L., Update on the role of vitamin K in skeletal health. *Nutr Rev,* 2008, *66*(10), 549-557.
[23] Booth, S.L.; Dallal, G.; Shea, M.K.; Gundberg, C.; Peterson, J.W.; Dawson-Hughes, B., Effect of vitamin K supplementation on bone loss in elderly men and women. *J Clin Endocrinol Metab,* 2008, *93*(4), 1217-1223.
[24] Kruger, M.C.; Booth, C.L.; Coad, J.; Schollum, L.M.; Kuhn-Sherlock, B.; Shearer, M.J., Effect of calcium fortified milk supplementation with or without vitamin K on biochemical markers of bone turnover in premenopausal women. *Nutrition,* 2006, *22*(11-12), 1120-1128.
[25] Booth, S.L., Vitamin K: food composition and dietary intakes. *Food Nutr Res,* 2012, *56*.
[26] Cui, X.; Kawashima, H.; Barclay, T.B.; Peters, J.M.; Gonzalez, F.J.; Morgan, E.T.; Strobel, H.W., Molecular cloning and regulation of expression of two novel mouse CYP4F genes: expression in peroxisome proliferator-activated receptor alpha-deficient mice upon lipopolysaccharide and clofibrate challenges. *J Pharmacol Exp Ther,* 2001, *296*(2), 542-550.
[27] Stark, K.; Torma, H.; Cristea, M.; Oliw, E.H., Expression of CYP4F8 (prostaglandin H 19-hydroxylase) in human epithelia and prominent induction in epidermis of psoriatic lesions. *Arch Biochem Biophys,* 2003, *409*(1), 188-196.
[28] Nilsson, T.; Ivanov, I.V.; Oliw, E.H., LC-MS/MS analysis of epoxyalcohols and epoxides of arachidonic acid and their oxygenation by recombinant CYP4F8 and CYP4F22. *Arch Biochem Biophys,* 2010, *494*(1), 64-71.
[29] Kelly, E.J.; Nakano, M.; Rohatgi, P.; Yarov-Yarovoy, V.; Rettie, A.E., Finding homes for orphan cytochrome P450s: CYP4V2 and CYP4F22 in disease states. *Mol Interv,* 2011, *11*(2), 124-132.
[30] Cui, X.; Nelson, D.R.; Strobel, H.W., A novel human cytochrome P450 4F isoform (CYP4F11): cDNA cloning, expression, and genomic structural characterization. *Genomics,* 2000, *68*(2), 161-166.
[31] Christmas, P.; Jones, J.P.; Patten, C.J.; Rock, D.A.; Zheng, Y.; Cheng, S.M.; Weber, B.M.; Carlesso, N.; Scadden, D.T.; Rettie, A.E.; Soberman, R.J., Alternative splicing determines the function of CYP4F3 by switching substrate specificity. *J Biol Chem,* 2001, *276*(41), 38166-38172.
[32] Hirani, V.; Yarovoy, A.; Kozeska, A.; Magnusson, R.P.; Lasker, J.M., Expression of CYP4F2 in human liver and kidney: assessment using targeted peptide antibodies. *Arch Biochem Biophys,* 2008, *478*(1), 59-68.
[33] Jin, Y.; Zollinger, M.; Borell, H.; Zimmerlin, A.; Patten, C.J., CYP4F enzymes are responsible for the elimination of fingolimod (FTY720), a novel treatment of relapsing multiple sclerosis. *Drug Metab Dispos,* 2011, *39*(2), 191-198.
[34] Hsu, M.H.; Savas, U.; Griffin, K.J.; Johnson, E.F., Regulation of human cytochrome P450 4F2 expression by sterol regulatory element-binding protein and lovastatin. *J Biol Chem,* 2007, *282*(8), 5225-5236.
[35] Goldstein, J.L.; DeBose-Boyd, R.A.; Brown, M.S., Protein sensors for membrane sterols. *Cell,* 2006, *124*(1), 35-46.
[36] Hsu, M.H.; Savas, U.; Lasker, J.M.; Johnson, E.F., Genistein, resveratrol, and 5-aminoimidazole-4-carboxamide-1-beta-D-ribofuranoside induce cytochrome P450 4F2 expression through an AMP-activated protein kinase-dependent pathway. *J Pharmacol Exp Ther,* 2011, *337*(1), 125-136.
[37] Weinberg, J.M., Lipotoxicity. *Kidney Int,* 2006, *70*(9), 1560-1566.
[38] Antoun, J.; Goulitquer, S.; Amet, Y.; Dreano, Y.; Salaun, J.P.; Corcos, L.; Plee-Gautier, E., CYP4F3B is induced by PGA1 in human liver cells: a regulation of the 20-HETE synthesis. *J Lipid Res,* 2008, *49*(10), 2135-2141.
[39] Mizukami, Y.; Sumimoto, H.; Takeshige, K., Induction of cytochrome CYP4F3A in all-trans-retinoic acid-treated HL60 cells. *Biochem Biophys Res Commun,* 2004, *314*(1), 104-109.
[40] Zhao, Z.; He, X.; Bi, Y.; Xia, Y.; Tao, N.; Li, L.; Ma, Q., Induction of CYP4F3 by benzene metabolites in human white blood cells in vivo in human promyelocytic leukemic cell lines and ex vivo in human blood neutrophils. *Drug Metab Dispos,* 2009, *37*(2), 282-291.
[41] Wang, Y.; Bell, J.C.; Keeney, D.S.; Strobel, H.W., Gene regulation of CYP4F11 in human keratinocyte HaCaT cells. *Drug Metab Dispos,* 2010, *38*(1), 100-107.

[42] Bell, J.C.; Strobel, H.W., Regulation of cytochrome P450 4F11 by nuclear transcription factor-kappaB. *Drug Metab Dispos,* 2012, *40*(1), 205-211.
[43] Hariparsad, N.; Chu, X.; Yabut, J.; Labhart, P.; Hartley, D.P.; Dai, X.; Evers, R., Identification of pregnane-X receptor target genes and coactivator and corepressor binding to promoter elements in human hepatocytes. *Nucleic Acids Res,* 2009, *37*(4), 1160-1173.
[44] Zheng, Y.M.; Henne, K.R.; Charmley, P.; Kim, R.B.; McCarver, D.G.; Cabacungan, E.T.; Hines, R.N.; Rettie, A.E., Genotyping and site-directed mutagenesis of a cytochrome P450 meander Pro-X-Arg motif critical to CYP4B1 catalysis. *Toxicol Appl Pharmacol,* 2003, *186*(2), 119-126.
[45] Baer, B.R.; Rettie, A.E., CYP4B1: an enigmatic P450 at the interface between xenobiotic and endobiotic metabolism. *Drug Metab Rev,* 2006, *38*(3), 451-476.
[46] Fisher, M.B.; Zheng, Y.M.; Rettie, A.E., Positional specificity of rabbit CYP4B1 for omega-hydroxylation1 of short-medium chain fatty acids and hydrocarbons. *Biochem Biophys Res Commun,* 1998, *248*(2), 352-355.
[47] Nakano, M.; Kelly, E.J.; Rettie, A.E., Expression and characterization of CYP4V2 as a fatty acid omega-hydroxylase. *Drug Metab Dispos,* 2009, *37*(11), 2119-2122.
[48] Savas, U.; Hsu, M.H.; Griffin, K.J.; Bell, D.R.; Johnson, E.F., Conditional regulation of the human CYP4X1 and CYP4Z1 genes. *Arch Biochem Biophys,* 2005, *436*(2), 377-385.
[49] Williams, J.M.; Murphy, S.; Burke, M.; Roman, R.J., 20-hydroxyeicosatetraeonic acid: a new target for the treatment of hypertension. *J Cardiovasc Pharmacol,* 2010, *56*(4), 336-344.
[50] Dunn, K.M.; Renic, M.; Flasch, A.K.; Harder, D.R.; Falck, J.; Roman, R.J., Elevated production of 20-HETE in the cerebral vasculature contributes to severity of ischemic stroke and oxidative stress in spontaneously hypertensive rats. *Am J Physiol Heart Circ Physiol,* 2008, *295*(6), H2455-2465.
[51] Miyata, N.; Roman, R.J., Role of 20-hydroxyeicosatetraenoic acid (20-HETE) in vascular system. *J Smooth Muscle Res,* 2005, *41*(4), 175-193.
[52] Alexanian, A.; Miller, B.; Roman, R.J.; Sorokin, A., 20-HETE-producing Enzymes Are Up-regulated in Human Cancers. *Cancer Genomics Proteomics,* 2012, *9*(4), 163-169.
[53] Harmon, S.D.; Fang, X.; Kaduce, T.L.; Hu, S.; Raj Gopal, V.; Falck, J.R.; Spector, A.A., Oxygenation of omega-3 fatty acids by human cytochrome P450 4F3B: effect on 20-hydroxyeicosatetraenoic acid production. *Prostaglandins Leukot Essent Fatty Acids,* 2006, *75*(3), 169-177.
[54] Tang, Z.; Salamanca-Pinzon, S.G.; Wu, Z.L.; Xiao, Y.; Guengerich, F.P., Human cytochrome P450 4F11: heterologous expression in bacteria, purification, and characterization of catalytic function. *Arch Biochem Biophys,* 2010, *494*(1), 86-93.
[55] Miyata, N.; Seki, T.; Tanaka, Y.; Omura, T.; Taniguchi, K.; Doi, M.; Bandou, K.; Kametani, S.; Sato, M.; Okuyama, S.; Cambj-Sapunar, L.; Harder, D.R.; Roman, R.J., Beneficial effects of a new 20-hydroxyeicosatetraenoic acid synthesis inhibitor, TS-011 [N-(3-chloro-4-morpholin-4-yl) phenyl-N'-hydroxyimido formamide], on hemorrhagic and ischemic stroke. *J Pharmacol Exp Ther,* 2005, *314*(1), 77-85.
[56] Alonso-Galicia, M.; Falck, J.R.; Reddy, K.M.; Roman, R.J., 20-HETE agonists and antagonists in the renal circulation. *Am J Physiol,* 1999, *277*(5 Pt 2), F790-796.
[57] Cheng, J.; Ou, J.S.; Singh, H.; Falck, J.R.; Narsimhaswamy, D.; Pritchard, K.A., Jr.; Schwartzman, M.L., 20-hydroxyeicosatetraenoic acid causes endothelial dysfunction via eNOS uncoupling. *Am J Physiol Heart Circ Physiol,* 2008, *294*(2), H1018-1026.
[58] Kroetz, D.L.; Zeldin, D.C., Cytochrome P450 pathways of arachidonic acid metabolism. *Curr Opin Lipidol,* 2002, *13*(3), 273-283.
[59] Sarkis, A.; Lopez, B.; Roman, R.J., Role of 20-hydroxyeicosatetraenoic acid and epoxyeicosatrienoic acids in hypertension. *Curr Opin Nephrol Hypertens,* 2004, *13*(2), 205-214.
[60] Sarkis, A.; Roman, R.J., Role of cytochrome P450 metabolites of arachidonic acid in hypertension. *Curr Drug Metab,* 2004, *5*(3), 245-256.
[61] Pat Kunert, M.; Drenjancevic, I., 20-hydroxyeicosatetraenoic acid, endothelial dysfunction and hypertension. *Med Glas Ljek komore Zenicko-doboj kantona,* 2011, *8*(2), 170-180.
[62] Stec, D.E.; Roman, R.J.; Flasch, A.; Rieder, M.J., Functional polymorphism in human CYP4F2 decreases 20-HETE production. *Physiol Genomics,* 2007, *30*(1), 74-81.
[63] Liu, H.; Zhao, Y.; Nie, D.; Shi, J.; Fu, L.; Li, Y.; Yu, D.; Lu, J., Association of a functional cytochrome P450 4F2 haplotype with urinary 20-HETE and hypertension. *J Am Soc Nephrol,* 2008, *19*(4), 714-721.

[64] Fava, C.; Montagnana, M.; Almgren, P.; Rosberg, L.; Lippi, G.; Hedblad, B.; Engstrom, G.; Berglund, G.; Minuz, P.; Melander, O., The V433M variant of the CYP4F2 is associated with ischemic stroke in male Swedes beyond its effect on blood pressure. *Hypertension,* 2008, *52*(2), 373-380.
[65] Kaspera, R.; Totah, R.A., Epoxyeicosatrienoic acids: formation, metabolism and potential role in tissue physiology and pathophysiology. *Expert Opin Drug Metab Toxicol,* 2009, *5*(7), 757-771.
[66] Gebremedhin, D.; Lange, A.R.; Lowry, T.F.; Taheri, M.R.; Birks, E.K.; Hudetz, A.G.; Narayanan, J.; Falck, J.R.; Okamoto, H.; Roman, R.J.; Nithipatikom, K.; Campbell, W.B.; Harder, D.R., Production of 20-HETE and its role in autoregulation of cerebral blood flow. *Circ Res,* 2000, *87*(1), 60-65.
[67] Renic, M.; Klaus, J.A.; Omura, T.; Kawashima, N.; Onishi, M.; Miyata, N.; Koehler, R.C.; Harder, D.R.; Roman, R.J., Effect of 20-HETE inhibition on infarct volume and cerebral blood flow after transient middle cerebral artery occlusion. *J Cereb Blood Flow Metab,* 2009, *29*(3), 629-639.
[68] Chuang, S.S.; Helvig, C.; Taimi, M.; Ramshaw, H.A.; Collop, A.H.; Amad, M.; White, J.A.; Petkovich, M.; Jones, G.; Korczak, B., CYP2U1, a novel human thymus- and brain-specific cytochrome P450, catalyzes omega- and (omega-1)-hydroxylation of fatty acids. *J Biol Chem,* 2004, *279*(8), 6305-6314.
[69] Chen, P.; Guo, M.; Wygle, D.; Edwards, P.A.; Falck, J.R.; Roman, R.J.; Scicli, A.G., Inhibitors of cytochrome P450 4A suppress angiogenic responses. *Am J Pathol,* 2005, *166*(2), 615-624.
[70] Moreno, J.J., New aspects of the role of hydroxyeicosatetraenoic acids in cell growth and cancer development. *Biochem Pharmacol,* 2009, *77*(1), 1-10.
[71] Guo, M.; Roman, R.J.; Falck, J.R.; Edwards, P.A.; Scicli, A.G., Human U251 glioma cell proliferation is suppressed by HET0016 [N-hydroxy-N'-(4-butyl-2-methylphenyl)formamidine], a selective inhibitor of CYP4A. *J Pharmacol Exp Ther,* 2005, *315*(2), 526-533.
[72] Guo, M.; Roman, R.J.; Fenstermacher, J.D.; Brown, S.L.; Falck, J.R.; Arbab, A.S.; Edwards, P.A.; Scicli, A.G., 9L gliosarcoma cell proliferation and tumor growth in rats are suppressed by N-hydroxy-N'-(4-butyl-2-methylphenol) formamidine (HET0016), a selective inhibitor of CYP4A. *J Pharmacol Exp Ther,* 2006, *317*(1), 97-108.
[73] Alexanian, A.; Rufanova, V.A.; Miller, B.; Flasch, A.; Roman, R.J.; Sorokin, A., Down-regulation of 20-HETE synthesis and signaling inhibits renal adenocarcinoma cell proliferation and tumor growth. *Anticancer Res,* 2009, *29*(10), 3819-3824.
[74] Wanders, R.J.; Komen, J.; Kemp, S., Fatty acid omega-oxidation as a rescue pathway for fatty acid oxidation disorders in humans. *FEBS J,* 2011, *278*(2), 182-194.
[75] Sanders, R.J.; Ofman, R.; Dacremont, G.; Wanders, R.J.; Kemp, S., Characterization of the human omega-oxidation pathway for omega-hydroxy-very-long-chain fatty acids. *FASEB J,* 2008, *22*(6), 2064-2071.
[76] Sanders, R.J.; Ofman, R.; Duran, M.; Kemp, S.; Wanders, R.J., Omega-oxidation of very long-chain fatty acids in human liver microsomes. Implications for X-linked adrenoleukodystrophy. *J Biol Chem,* 2006, *281*(19), 13180-13187.
[77] Singh, I.; Khan, M.; Key, L.; Pai, S., Lovastatin for X-linked adrenoleukodystrophy. *N Engl J Med,* 1998, *339*(10), 702-703.
[78] Singh, I.; Pahan, K.; Khan, M., Lovastatin and sodium phenylacetate normalize the levels of very long chain fatty acids in skin fibroblasts of X- adrenoleukodystrophy. *FEBS Lett,* 1998, *426*(3), 342-346.
[79] Engelen, M.; Ofman, R.; Dijkgraaf, M.G.; Hijzen, M.; van der Wardt, L.A.; van Geel, B.M.; de Visser, M.; Wanders, R.J.; Poll-The, B.T.; Kemp, S., Lovastatin in X-linked adrenoleukodystrophy. *N Engl J Med,* 2010, *362*(3), 276-277.
[80] Verhoeven, N.M.; Jakobs, C., Human metabolism of phytanic acid and pristanic acid. *Prog Lipid Res,* 2001, *40*(6), 453-466.
[81] Komen, J.C.; Wanders, R.J., Identification of the cytochrome P450 enzymes responsible for the omega-hydroxylation of phytanic acid. *FEBS Lett,* 2006, *580*(16), 3794-3798.
[82] Wanders, R.J.; Komen, J.C., Peroxisomes, Refsum's disease and the alpha- and omega-oxidation of phytanic acid. *Biochem Soc Trans,* 2007, *35*(Pt 5), 865-869.
[83] Nakagawa, K.; Hirota, Y.; Sawada, N.; Yuge, N.; Watanabe, M.; Uchino, Y.; Okuda, N.; Shimomura, Y.; Suhara, Y.; Okano, T., Identification of UBIAD1 as a novel human menaquinone-4 biosynthetic enzyme. *Nature,* 2010, *468*(7320), 117-121.
[84] Okano, T.; Shimomura, Y.; Yamane, M.; Suhara, Y.; Kamao, M.; Sugiura, M.; Nakagawa, K., Conversion of phylloquinone (Vitamin K1) into menaquinone-4 (Vitamin K2) in mice: two possible routes for menaquinone-4 accumulation in cerebra of mice. *J Biol Chem,* 2008, *283*(17), 11270-11279.

[85] Thijssen, H.H.; Vervoort, L.M.; Schurgers, L.J.; Shearer, M.J., Menadione is a metabolite of oral vitamin K. *Br J Nutr,* 2006, *95*(2), 260-266.
[86] Elder, S.J.; Haytowitz, D.B.; Howe, J.; Peterson, J.W.; Booth, S.L., Vitamin k contents of meat, dairy, and fast food in the u.s. Diet. *J Agric Food Chem,* 2006, *54*(2), 463-467.
[87] Booth, S.L.; Suttie, J.W., Dietary intake and adequacy of vitamin K. *J Nutr,* 1998, *128*(5), 785-788.
[88] Vermeer, C., Vitamin K: the effect on health beyond coagulation - an overview. *Food Nutr Res,* 2012, *56*.
[89] Vadivel, K.; Bajaj, S.P., Structural biology of factor VIIa/tissue factor initiated coagulation. *Front Biosci,* 2012, *17*, 2476-2494.
[90] Banner, D.W.; D'Arcy, A.; Chene, C.; Winkler, F.K.; Guha, A.; Konigsberg, W.H.; Nemerson, Y.; Kirchhofer, D., The crystal structure of the complex of blood coagulation factor VIIa with soluble tissue factor. *Nature,* 1996, *380*(6569), 41-46.
[91] Shirakawa, H.; Ohsaki, Y.; Minegishi, Y.; Takumi, N.; Ohinata, K.; Furukawa, Y.; Mizutani, T.; Komai, M., Vitamin K deficiency reduces testosterone production in the testis through down-regulation of the Cyp11a a cholesterol side chain cleavage enzyme in rats. *Biochim Biophys Acta,* 2006, *1760*(10), 1482-1488.
[92] Zhu, A.; Sun, H.; Raymond, R.M., Jr.; Furie, B.C.; Furie, B.; Bronstein, M.; Kaufman, R.J.; Westrick, R.; Ginsburg, D., Fatal hemorrhage in mice lacking gamma-glutamyl carboxylase. *Blood,* 2007, *109*(12), 5270-5275.
[93] Vos, M.; Esposito, G.; Edirisinghe, J.N.; Vilain, S.; Haddad, D.M.; Slabbaert, J.R.; Van Meensel, S.; Schaap, O.; De Strooper, B.; Meganathan, R.; Morais, V.A.; Verstreken, P., Vitamin K2 is a mitochondrial electron carrier that rescues pink1 deficiency. *Science,* 2012, *336*(6086), 1306-1310.
[94] Suhara, Y.; Hanada, N.; Okitsu, T.; Sakai, M.; Watanabe, M.; Nakagawa, K.; Wada, A.; Takeda, K.; Takahashi, K.; Tokiwa, H.; Okano, T., Structure-activity relationship of novel menaquinone-4 analogues: modification of the side chain affects their biological activities. *J Med Chem,* 2012, *55*(4), 1553-1558.
[95] Kaspera, R.; Naraharisetti, S.B.; Evangelista, E.A.; Marciante, K.D.; Psaty, B.M.; Totah, R.A., Drug metabolism by CYP2C8.3 is determined by substrate dependent interactions with cytochrome P450 reductase and cytochrome b5. *Biochem Pharmacol,* 2011, *82*(6), 681-691.
[96] Bhagavan, H.N.; Chopra, R.K., Coenzyme Q10: absorption, tissue uptake, metabolism and pharmacokinetics. *Free Radic Res,* 2006, *40*(5), 445-453.
[97] Nakamura, T.; Ohno, T.; Hamamura, K.; Sato, T., Metabolism of coenzyme Q10: biliary and urinary excretion study in guinea pigs. *Biofactors,* 1999, *9*(2-4), 111-119.
[98] Suttie, J.W.; Booth, S.L., Vitamin K. *Adv Nutr,* 2011, *2*(5), 440-441.
[99] Crivello, N.A.; Casseus, S.L.; Peterson, J.W.; Smith, D.E.; Booth, S.L., Age- and brain region-specific effects of dietary vitamin K on myelin sulfatides. *J Nutr Biochem,* 2010, *21*(11), 1083-1088.
[100] Roosild, T.P.; Castronovo, S.; Miller, S.; Li, C.; Rasmussen, T.; Bartlett, W.; Gunasekera, B.; Choe, S.; Booth, I.R., KTN (RCK) domains regulate K+ channels and transporters by controlling the dimer-hinge conformation. *Structure,* 2009, *17*(6), 893-903.
[101] McCabe, K.M.; Booth, S.L.; Fu, X.; Shobeiri, N.; Pang, J.J.; Adams, M.A.; Holden, R.M., Dietary vitamin K and therapeutic warfarin alter the susceptibility to vascular calcification in experimental chronic kidney disease. *Kidney Int,* 2013.
[102] Geleijnse, J.M.; Vermeer, C.; Grobbee, D.E.; Schurgers, L.J.; Knapen, M.H.; van der Meer, I.M.; Hofman, A.; Witteman, J.C., Dietary intake of menaquinone is associated with a reduced risk of coronary heart disease: the Rotterdam Study. *J Nutr,* 2004, *134*(11), 3100-3105.
[103] Merle, B.; Garnero, P., The multiple facets of periostin in bone metabolism. *Osteoporos Int,* 2012, *23*(4), 1199-1212.
[104] Fujita, Y.; Iki, M.; Tamaki, J.; Kouda, K.; Yura, A.; Kadowaki, E.; Sato, Y.; Moon, J.S.; Tomioka, K.; Okamoto, N.; Kurumatani, N., Association between vitamin K intake from fermented soybeans, natto, and bone mineral density in elderly Japanese men: the Fujiwara-kyo Osteoporosis Risk in Men (FORMEN) study. *Osteoporos Int,* 2012, *23*(2), 705-714.
[105] Obeso, J.A.; Rodriguez-Oroz, M.C.; Goetz, C.G.; Marin, C.; Kordower, J.H.; Rodriguez, M.; Hirsch, E.C.; Farrer, M.; Schapira, A.H.; Halliday, G., Missing pieces in the Parkinson's disease puzzle. *Nat Med,* 2010, *16*(6), 653-661.

Chapter 2

Structure-Activity Relationships for Inhibition of CYP4 Enzyme Activity by HET0016

2.1 Introduction

Eicosanoids are oxidative products of arachidonic acid produced by cyclooxygenases, lipoxygenases, and cytochrome P450 enzymes. Selective chemical inhibition of these enzymes has been a useful strategy that has been extensively employed for studying eicosanoid bioactivity. One such eicosanoid, 20-hydroxyeicosatetraenoic acid (20-HETE), is a signaling compound produced by the ω-hydroxylation of arachidonic acid, a reaction that is generally dependent upon CYP4 enzymes [1]. The first CYP4-selective inhibitors used to study the biological effects of 20-HETE were designed as analogs of prototypical fatty acid substrates of the CYP4 enzymes. Fatty acid derivatives with terminal alkynes or halogenated terminal alkenes are mechanism based or reversible, competitive CYP4 inhibitors, respectively. From these studies, 17-octadecynoic acid (17-ODYA) emerged as the most widely used CYP4 inhibitor, with an IC_{50} for 20-HETE synthase activity in renal microsomes of 3 μM. However, it became clear that 17-ODYA, along with many of the other fatty acid analog inhibitors, were not specific for CYP4 enzymes. For instance, 17-ODYA inhibits epoxyeicosatrienoic acid (EET) and 20-HETE formation in renal microsomes to an equal extent, with an IC_{50} of 5 μM for the former processes. EETs are the epoxidized P450 metabolites of arachidonic acid, formed mostly by CYP2C and CYP2J enzymes, and they often result in physiological effects that oppose those of 20-HETE [2]. Sulfonated derivatives of these terminally functionalized fatty acids (e.g. 10-SUYS, DDMS, see Table 2.1) were developed with the aim of optimizing *in vivo* CYP4 inhibition because fatty acids in general are not useful as *in vivo* inhibitors due to rapid β-oxidation, resultant short half-lives, and esterification and storage in the liver. However, the sulfonated fatty acid inhibitors were generally even less potent inhibitors than their carboxylic acid analogues and similarly suffered from lack of selectivity [1]. Clearly, these observations highlight the need for better inhibitors to study the biosynthesis and physiological effects of lipid mediators generated by CYP4 enzyme catalysis.

HET0016 (N-hydroxy-N'-(4-n-butyl-2-methylphenyl)formamidine) emerged as a potent renal 20-HETE synthase inhibitor from Taisho Pharmaceutical Company's drug discovery program in the late 1990s on new hypertension therapeutics. HET0016 is a more potent and selective CYP4 inhibitor compared to 17-ODYA and

other fatty acid analogs, with IC_{50} values for 20-HETE and EET synthase activity in renal microsomes of 35 nM and 2.8 μM, respectively [3-5]. HET0016 appears to be a pan-CYP4 inhibitor, with low nanomolar IC_{50}s for CYP4A11, CYP4F2, CYP4F3B, and CYP4V2 of 42 nM, 125 nM, 100 nM, and 38 nM, respectively [6-8]. In contrast, IC_{50}s for recombinant CYP3A4, CYP2C9, CYP2D6, CYP2C19, and CYP1A2 are generally much higher (65.4 μM, 4.2 μM, 84.5 μM, 272 nM, and 461 nM, respectively) [5]. A number of HET0016 derivatives (e.g. TS-011) were synthesized by Taisho with the dual goals of increasing the selectivity of the drug even further with regards to inhibition of other P450 enzymes, and increasing water solubility and acid stability characteristics so that a 20-HETE inhibitor might be formulated as an injectable drug for treatment after cerebrovascular disease events [5, 9-11]. Table 2.1 summarizes the characteristics of several of the key CYP4 inhibitors that have been developed.

As reviewed in Chapter 1, 13 human CYP4 enzymes that perform many important endobiotic transformations are expressed in a variety of tissues. Seen in this light, any therapeutic strategy involving pan-CYP4 inhibition seems doomed to failure. However, modification of the chemical structure of HET0016 may be a rational approach to the discovery of CYP4 subfamily-selective chemical inhibitors. It is clear from studies with other cytochrome P450 enzymes that subfamily inhibitor discrimination is achievable. For instance, in the CYP2C family, CYP2C8, CYP2C9, and CYP2C19 are selectively inhibited by montelukast [12], sulfaphenazole [13], and (S)-benzylnirvanol [14], respectively, despite these enzymes' high degree of sequence homology (ranging from 78-92%). Therefore, major goals of work described in this Chapter were (i) to elucidate the mechanism of pan-CYP4 inhibition by HET0016 and the structural features of the compound that are necessary for high inhibitory potency, and (ii) to develop selective chemical inhibitors for specific CYP4 sub-families based on the HET0016 template.

2.2 Materials and Methods

Materials. CYP4A11, CYP4F3B, CYP4F2, and CYP4F12 Supersomes were purchased from BD Biosciences. Rabbit CYP4B1 was expressed in *Escherichia coli* and purified as previously described [15]. Human CYP4F2 was expressed in *Escherichia coli* as previously described [16]. Rat reductase and rat cytochrome b5 were expressed and purified as previously described [17, 18]. HET0016 was initially purchased from Cayman Chemical, and later synthesized in-house. BSTFA:TMCS was from Supelco. 6β-Hydroxy testosterone was a gift

from Dr. William Atkins (University of Washington, Seattle). Hydroxy-terfenadine was a gift from Dr. Rheem Totah (University of Washington, Seattle). All other chemicals were purchased from Sigma-Aldrich.

Synthesis of HET0016 Analogs. All formamidoxime derivatives (compounds 1-9) were prepared by the same general procedure (Figure 2.1 and 2.2). The corresponding para-alkyl aniline was refluxed in toluene for 6-18 hours with 1.2 molar equivalents of dimethylformamide dimethylacetal. Toluene was removed under vacuum. Dry methanol was added and stirred with 1.2 equivalents of hydroxylamine hydrochloride, at room temperature for 3-12 hours, until reaction was complete. For synthesis of compound 10, the same procedure was used except methoxylamine hydrochloride was used. The product was recrystallized from methanol or 1:1 methanol: water to afford a white solid. In some cases the product was purified on a silica column with 1:1 hexanes: ethyl acetate as mobile phase. Compound 11 was prepared by refluxing 4-butyl-2-methyl-aniline in toluene with 2 equivalents triethyl orthoacetate overnight. The toluene was removed by vacuum and 2 equivalents of hydroxylamine hydrochloride were added and stirred in methanol for 6 hours. The product was recrystallized from 1:1 methanol: water.

(1) HET0016 (N'-hydroxy-N-(4-n-butyl-2-methylphenyl)formamidine) Clear/pink solid crystals. 1H NMR(DMSO-d6, 500MHz): 9.930 (1H, s), 7.398 (1H, d, J=10.5), 7.241 (1H, d, J=10.5), 7.043 (1H, d, J=8), 6.964 (1H, s), 6.935 (1H, d, J=8.5), 2.466 (2H, t, J=8), 2.175 (3H, s), 1.499 (2H, qn, J=7.5), 1.278 (2H, sx, J=7.5), 0.880 (3H, t, J=7.5). 13C NMR(DMSO-d6, 500MHz): 139.169, 136.130, 135.171, 130.466, 126.453, 124.918, 114.947, 33.867, 33.160, 21.534, 16.936, 13.627. Found m/z (M+H) 207.1503, calculated monoisotopic mass 207.1497. ESI+ fragments (m/z): 190, 175, 147, 130.

(2) N'-hydroxy-N-phenylformamidine. White solid. 1H NMR(DMSO-d6, 500MHz): δ 9.802 (1H, s), 8.484 (1H, d, J=11), 7.418 (1H, d, J=10.5), 7.166 (2H, t, J=8.5 and 7), 7.109 (2H, d, J=8 Hz), 6.802 (1H, t, J=7). 13C NMR(DMSO-d6, 500MHz): 140.909, 137.838, 129.054, 120.244, 114.499. Found m/z (M+H) 137.0714, calculated monoisotopic mass 137.0715. ESI+ fragments (m/z): 119.

(3) N'-hydroxy-N-(4-ethylphenyl)formamidine. White solid. 1H NMR(DMSO-d6, 500MHz): δ 9.752 (1H, s), 8.397 (1H, d, J=9.5), 7.399 (1H, d, J=11), 7.054 (4H, s), 2.512 (2H, qr, J=7.5), 1.143 (3H, t, J=7.5). 13C NMR(DMSO-d6, 500MHz): 138.715, 138.126, 135.524, 128.246, 114.590, 27.242, 15.724. Found m/z (M+H) 165.1027, calculated monoisotopic mass 165.1028. ESI+ fragments (m/z): 143

(4) N'-hydroxy-N-(4-n-butylphenyl)formamidine. White solid. 1H NMR(DMSO-d6, 500MHz): δ 9.786 (1H, s), 8.450 (1H, d, J=11), 7.407 (1H, d, J=11), 7.027 (4H, dd, J=8.5 and 8.5), 2.464 (2H, t, J=7.5), 1.489 (2H, qn, J=7.5), 1.273 (2H, sx, J=7.5), 0.877 (3H, t, J=7.5). 13C NMR(DMSO-d6, 500MHz): 138.190, 137.719, 133.612, 128.320, 114.090, 33.439, 32.775, 21.100, 13.227. Found m/z (M+H) 193.1344, calculated monoisotopic mass 193.1341. ESI+ fragments (m/z): 175, 133.

(5) N'-hydroxy-N-(4-n-octylphenyl)formamidine. White solid. 1H NMR(DMSO-d6, 500MHz): δ 9.764 (1H, s), 8.421 (1H, d, J=10.5), 7.392 (1H, d, J=10.5), 7.020 (4H, dd, J=8.5 and 9.5), 2.453 (2H, t, J=7.5), 1.496 (2H, m), 1.240, (10H, m), 0.847 (3H, t, J=6.5). 13C NMR(DMSO-d6, 500MHz): 138.81, 138.21, 134.16, 128.89, 114.61, 34.34, 31.28, 31.17, 28.85, 28.69, 28.61, 22.09, 13.96. Found m/z (M+H) 249.1963, calculated monoisotopic mass 249.1967. ESI+ fragments (m/z): 231.2.

(6) N'-hydroxy-N-(4-n-dodecylphenyl)formamidine. Off-white solid. 1H NMR(DMSO-d6, 300MHz): δ 9.86 (1H, s), 8.55 (1H, m), 7.44 (1H, m), 7.03 (4H, dd, J=6 and 9), 2.45 (2H, t, J=7.5), 1.49 (2H, m), 1.23 (18H, m), 0.85 (3H, t J= 7.5). Found m/z (M+H) 305.2588, calculated monoisotopic mass 305.2593.

(7) N'-hydroxy-N-(4-n-hexadecylphenyl)formamidine. White solid. 1H NMR(DMSO-d6, 300MHz): Due to the insolubility of this compound, an NMR spectra was not attainable. Found m/z (M+H) 361, calculated monoisotopic mass 361.3219. ESI+ fragments (m/z) 343.

(8) N'-hydroxy-N-(4-t-butylphenyl)formamidine. White solid. 1H NMR(DMSO-d6, 300MHz): δ 9.76 (1H, s) 8.44, 8.41 (1H, d) 7.41, 7.37 (1H, d) 7.22, 7.19 (2H, d) 7.06, 7.03 (2H, d). Found m/z (M+H) 193, calculated monoisotopic mass 193.1341. ESI+ fragments (m/z) 175.

(9) N'-hydroxy-N-(naphthalen-2-yl)formamidine. White solid. 1H NMR(DMSO-d6, 300MHz): δ 9.96 (1H, s), 8.79 (1H, d, J=9), 7.76 (2H, d, J=6), 7.68 (1H, d, J=9), 7.63 (1H, d, J=12), 7.53 (1H, s), 7.47 (1H, d, J=9), 7.41 (1H, t, J=6), 7.27 (1H, t, J=6). Found m/z (M+H) 187.0872, calculated monoisotopic mass 187.0871. ESI+ fragments (m/z): 169, 147.

(10) N-(4-butyl-2-methylphenyl)-N'-methoxyformimidamide. White solid. ^{1}H NMR (500 MHz, Acetone-d_6) δ 7.40 (d, J = 10.8 Hz, 1H), 7.17 – 7.05 (m, 4H), 3.86 (s, 3H), 2.64 – 2.57 (m, 2H), 2.32 (s, 3H), 1.69 – 1.59 (m, 2H), 1.42 (h, J = 7.4 Hz, 2H), 1.00 (t, J = 7.4 Hz, 3H). ^{1}H NMR (500 MHz, Methanol-d_4) δ 7.27 (s, 1H), 6.99 (d, J = 3.4 Hz, 3H), 3.83 (d, J = 1.6 Hz, 3H), 2.53 (t, J = 7.7 Hz, 2H), 2.23 (s, 3H), 1.61 – 1.50 (m, 2H), 1.34 (h, J = 7.6 Hz, 2H), 0.93 (t, J = 7.3 Hz, 3H). Found m/z (M+H) 193. calculated monoisotopic mass 221.1654. ESI+ (m/z) 221.

(11) N-(4-butyl-2-methylphenyl)-N'-hydroxyacetimidamide. Off-white crystals. ^{1}H NMR (500 MHz, Acetone-d_6) δ 8.41 (s, 1H), 7.51 (d, J = 8.1 Hz, 1H), 7.03 – 6.94 (m, 2H), 2.79 (s, 1H), 2.54 (t, J = 7.8 Hz, 2H), 2.22 (s, 3H), 2.08 (s, 3H), 1.56 (p, J = 7.6 Hz, 2H), 1.34 (h, J = 7.4 Hz, 2H), 0.91 (t, J = 7.4 Hz, 3H). ^{1}H NMR (500 MHz, DMSO-d_6) δ 9.19 (s, 1H), 7.24 (d, J = 8.0 Hz, 1H), 7.00 (d, J = 2.2 Hz, 1H), 6.97 – 6.91 (m, 1H), 2.54 (t, J = 7.8 Hz, 2H), 2.15 (s, 3H), 2.02 (s, 3H), 1.57 – 1.47 (m, 2H), 1.29 (h, J = 7.4 Hz, 2H), 0.89 (t, J = 7.3 Hz, 3H). Found m/z (M+H) 193, calculated monoisotopic mass 221.1654. ESI+ (m/z) 221.

CYP4A11 expression and purification. A CYP4A11 pCWori expression vector was a gift from Dr. Eric Johnson (Scripps Institute, San Diego). The His-tagged protein was expressed in DH5α-F'1Q *Escherichia coli* cells (InVitrogen) similar to previously described methods [19, 20]. Protein was purified on a Ni-NTA column (Qiagen, Germantown, MD) followed by a hydroxyapatite column (Bio-Rad, Hercules, CA). The final yield of P450 after purification was approximately 20 nmoles/L of culture. Cytochrome P450 concentration was determined from the Fe^{2+}-CO - Fe^{2+}difference spectrum [21], protein purity was assessed by sodium dodecyl sulfate polyacrylamide gel electrophoresis (SDS-PAGE) with Coomassie brilliant blue staining, and total protein concentration was determined by the Lowry method [22].

Ligand binding spectra. Expressed and purified CYP4A11, CYP4F2, and CYP4B1 enzyme concentrations were quantified from the Fe^{2+}-CO- Fe^{2+} difference spectrum [21, 23, 24]. Ligand binding spectra were collected at 25°C on a dual-beam OLIS/Aminco DW2a spectrophotometer. Proteins were diluted to 1 μM with 100 mM KPi and dilauroyl-α-phosphatidylcholine (DLPC) was added at a concentration of 160 μM. HET0016 dissolved in DMSO was titrated into the sample, and DMSO was added to the reference cuvette. The final DMSO concentration did not exceed 1% of the total volume. Sigmaplot software was used to fit data to the tight-binding equation and to calculate K_d.

Assay of lauric acid metabolism catalyzed by CYP4A11, CYP4B1, CYP4F2 and CYP4F3B. Incubations were performed in 100 μM potassium phosphate buffer, pH 7.4, (KPi) in a final volume of 500 μL. Supersomes containing CYP4A11, CYP4F2, or CYP4F3B or reconstituted rabbit CYP4B1 (1:2:1:160 CYP4B1: P450 reductase: cytochrome b5: dilauroylphosphatidylcholine (DLPC) molar ratio) were mixed with the indicated concentrations of lauric acid (added in DMSO) and KPi. To this mixture was added inhibitor dissolved DMSO (2 μL) in a silanized glass test tube. Final DMSO concentrations did not exceed 0.5% v/v. Typical final enzyme concentrations were 2 nM CYP4A11, 12 nM CYP4F3B, 30 nM CYP4F2, and 10 nM CYP4B1. Reactions were initiated with 1 mM NADPH, allowed to proceed at 37°C for 15 minutes and quenched with 50 μL cold 10% HCl. The internal standard, 0.25 ug of 15-OH pentadecanoic acid (15-OH PDA) was added in 50 μL KPi. Samples were extracted with ethyl acetate (2 x 1 mL), dried under N_2, and dissolved in 100 μL 1:1 mixture of ethyl acetate and BSTFA+1%TMCS. Extracts were transferred to an autosampler vial with insert, capped, and incubated in an 80°C sand bath overnight (12-16 hours). Derivatized 12-hydroxy lauric acid and the internal standard were quantified using a Shimadzu GC/MS (Shimadzu Scientific Instruments, Inc., Columbia, MD). The gas chromatograph (GC-17A) was equipped with a 15 m capillary methyl silicone column. The carrier gas was helium with a constant flow rate of 2.4 mL/min. The injection port temperature was 250 °C and was set in splitless mode. The temperature gradient started at 100°C and was held for 2 minutes. Temperature increased to 160°C at a rate of 30°/min, then to 177°C at a rate of 4°/minute and finally to 300°C at a rate of 100°/minute before holding at this temperature for 2 minutes. The column was connected to a Shimadzu mass spectrometer (GCMS-QP5050). The interface temperature was 300°C. The following analytes were confirmed with authentic

chemical standards: 12-hydroxy lauric acid (5.92 min, *m/z* 345 (M-15)) and 15-Hydroxypentadecanoic (8.74 min, *m/z* 387 (M-15)). Ions were monitored in selected-ion monitoring mode with an interval time of 50 Ms. Data was analyzed using GC/MS solution version 1.20 software (Shimadzu Scientific Instruments, Inc., Columbia, MD).

Assay of CYP4F12 and CYP3A4 enzyme activities. CYP4F12 and CYP3A4 activities were monitored using the substrates, terfenadine and testosterone, respectively. CYP4F12 incubations contained 0.1 pmoles CYP4F12 Supersomes and 1 μM or 10 μM terfenadine in KPi buffer in a 96-well polymerase chain reaction (PCR) plate (100 μL final volume). A 1 mM stock of HET0016 in DMSO was diluted into KPi (1:1000) and 10 μL were added to the incubation. Metabolic reactions were initiated with NADPH (1 mM), incubated at 37°C for 10 minutes, and quenched with 100 μL IPA containing 2 μM 4-(3-phenylproyl)pyrimidine as internal standard. Samples were transferred to an autosampler 96 well plate, centrifuged at 1500 x g (4000 rpm) for 10 minutes, transferred to a new plate, and 20 μL was analyzed by LC/MS. LC/ESI+MS/MS multiple reaction monitoring (MRM) analyses were conducted on an API 4000 Triple Quadrupole Mass Spectrometer (Applied Biosystems, Foster City, CA) connected to a Shimadzu HPLC system. The capillary voltage was set to 5500 V. Separation was achieved on a Luna (50 mm x 2 mm x 5 micron) C8 column with 100 Å pore size (Phenomenex). Mobile phases were, A) water with 5 mM ammonium acetate and, B) acetonitrile. The elution gradient increased from 30%-100% B over 5 minutes, was held at 100% B for 2 minutes, and equilibrated back to 30% B over 1 minute. The flow rate was 0.3 mL/min. The following parent to daughter ion mass transitions were monitored with stated optimized conditions: Hydroxy-terfenadine metabolite (*m/z* 488.3 to 452.2, declustering potential (DP)= 90, Collision energy (CE)= 40); terfenadine substrate (*m/z* 472.2 to 436.1, DP= 80, CE= 37); 4-(3-phenylprop)pyrimidine internal standard (*m/z* 204.5 to 91.0, DP= 80, CE= 50).

CYP3A4 incubations contained 38 nM CYP3A4 Supersomes in 200 μL final volume of KPi. buffer. Testosterone and HET0016 were diluted from methanol and DMSO stock solutions, respectively. Organic solvent was less than 0.5% v/v. Reactions were initiated with NADPH (1mM) and run at 37°C for 15 minutes. Reactions were quenched with 50 μl cold methanol containing 20 μM progesterone (1 nmole added) as internal standard. Samples were centrifuged at 13,800 x g (13000 rpm) for 5 minutes and 5 μL was injected for analysis. LC/ESI+MS/MS multiple reaction monitoring (MRM) analyses were conducted on a Quattro II Tandem Quadrupole Mass Spectrometer (Micromass, Ltd., Manchester, UK) connected to a Shimadzu HPLC system. A

source block temperature of 120°C and a desolvation temperature of 330°C were used. Separation was achieved on a Nucleosil C18 column (100 mm x 4.6 mm x 5 microns) (Machery-Nagel, Bethlehem, PA). Mobile phases were, A) 10 mM ammonium acetate 0.05% formic acid in water and, B) methanol. The elution gradient increased linearly from 60-100% B over 5 minutes and was then held at 100% B for 3 minutes. B was then decreased to 60% and equilibration occurred over 2 minutes. The following (parent to daughter ion) mass transitions were monitored with optimized conditions: 6β-Hydroxy testosterone (*m/z* 305.0 to 269.0, cone voltage (CV) = 35, CE= 18) and progesterone internal standard (*m/z* 315.0 to 109.2, CV=30, CE=22).

Assay for CYP4F2-dependent 20-HETE formation from arachidonic acid. 20-HETE formation was measured in a final reaction volume of 150 µL KPi buffer containing 5 pmoles of CYP4F2 Supersomes and 24 µM arachidonic acid. The arachidonic acid stock solution was prepared in ethanol. Chemical inhibitors were added in DMSO, and the combined amount of organic solvent did not exceed 2 µL. Reactions were initiated with NADPH and allowed to proceed for 20 minutes at 37°C. Reactions were quenched by the addition of 30 µL cold acetonitrile containing 5 pmoles of d6-20-HETE as the internal standard. An Agilent 1290 G4220A UPLC was coupled to an API4000 triple quadruple mass spectrometer (Applied Biosciences). Metabolites were separated on a C18 BEH 50 x 2.1 mm column (Waters) with mobile phases A (0.5 mM ammonium formate pH=3.3) and B (0.5 mM ammonium formate in acetonitrile). Flow rate was 0.25 mL/min and the gradient was as follows: 0-10 minutes (10-78% B), 10-10.1 (78-100% B), 10.1-12 (hold at 100% B), 12-12.1 (100-10% B), 12.1-14 (hold at 10% B). The mass spectrometer was operated in ESI negative ion mode at the following settings: source temperature 550°C, curtain gas (CUR) 25 psi, ion source gas 1 (GS1) 45 psi, ion source gas 2 (GS2) 45 psi, collision gas (CAD) 7 psi, entrance potential (EP) 10 V, collision cell exit potential (CXP) 15 V, declustering potential (DP) 100 V, and collision energy (CE) 22 V. The MRM transition monitored 20-HETE at 319.0>301.0 and d6-20-HETE at 325.0>307.0, using a 500 ms dwell time.

2.3 Results

Structural studies of HET0016 by 1H and 13C NMR. Previous studies suggested that HET0016 may adopt a ring-closed conformation [5, 25]. Oxime compounds can also exist as *E* and *Z* isomers. To evaluate the *E/Z* ratio and ring open/closed state of HET0016 in solution, we performed ^{1}H and ^{13}C NMR experiments in both protic and

non-protic solvents. Methanol and DMSO were chosen because HET0016 was most soluble in these solvents. When HET0016 was dissolved in *d*6-DMSO, very sharp signals at 9.930 ppm (singlet) and 7.408 ppm (doublet) were observed that likely correspond to the exchangeable hydrogen atoms (A and C) in Figure 2.3A. No attempt was made to occlude air from the sample in these experiments, and there is an obvious residual water peak. This shows that in DMSO these exchangeable hydrogen atoms do not exchange with water, but are locked into place possibly in the ring-closed conformations shown in Figure 2.4A. In deuterated methanol (CD3OD), however, these NMR signals completely disappear due to rapid exchange with the methanol deuterium. A ^{13}C NMR of HET0016 in d6-DMSO showed only one signal for the formamidoxime carbon at 139.169 ppm (Figure 2.3B). This suggests that only one form of the oxime, either *E* or *Z*, is present [26]. In order to generate the putative ring-closed conformer that is observed when the compound is dissolved in DMSO, the conformation would need to be *E* (Figure 2.4 A and B). Collectively, these data suggest that in DMSO, or a non-protic environment, HET0016 hydrogen bonds to itself and exists as a ring-closed species. However, in a protic solvent, it is more likely to hydrogen bond with the solvent and exist in a ring-opened state.

HET0016 inhibition of CYP4 Enzymes. In a preliminary experiment, using formation of 12-hydroxy lauric acid as marker for CYP4 activity we confirmed that HET0016 (100 nM) is a potent inhibitor of CYP4F2, CYP4F3B, CYP4A11, and a much weaker inhibitor of CYP3A4 (Figure 2.5). Reporting the same experiment, we found for the first time that HET0016 is also a potent inhibitor of rabbit CYP4B1 and human CYP4F12. Human CYP4B1 is an inactive enzyme due to a critical mutation in the meander region of the P450 [27], therefore, rabbit CYP4B1 was used to assess inhibition of this CYP4 subfamily by HET0016. CYP4F2-, CYP4F3B-, and CYP4B1-dependent lauric acid hydroxylase activities were decreased by >95% at saturating substrate concentrations (10x K_m). In contrast, CYP4A11-dependent lauric acid hydroxylase activity and CYP4F12-mediated terfenadine hydroxylase activities were inhibited by <50% (46% and 31%, respectively). CYP3A4 testosterone hydroxylase activity was only modestly inhibited (10%) under these conditions.

Next, IC_{50} values for inhibition by HET0016 of CYP4A11, CYP4F3B, CYP4B1, CYP4F12, and CYP3A4 were measured at the K_m of each substrate in order to approximate the K_i (Figure 2.7). According to equations 1, for a non-competitive inhibitor, the IC_{50} should be equal to the K_i at substrate concentrations equal to the K_m. For a competitive inhibitor, the IC_{50} should be twice the K_i at the substrate K_m. The K_m values for lauric acid ω-

hydroxylation catalyzed by CYP4A11 and CYP4F3B were determined (Figure 2.6), and the K_m values for CYP4B1 (with lauric acid as substrate) [28], CYP4F12 (with terfenadine as substrate) [29], and CYP3A4 (with testosterone as substrate) [30, 31] were taken from literature values. As expected, the IC_{50} for CYP4F3B, CYP4B1, and CYP4A11 were all less than 30 nM. The IC_{50} for CYP4F12 was 516 +/- 1.1 nM, which is about 10-fold higher than the IC_{50} values for other CYP4 enzymes. As reported elsewhere, the IC_{50} for CYP3A4 inhibition by HET0016 was >20 μM [4].

Equations 1:

Competitive inhibitor $K_i = IC_{50} / (1+(S) / K_m)$

Noncompetitive Inhibitor $K_i = IC_{50} / ((S) / K_m)$

Mechanism of CYP4 enzyme inhibition by HET0016. HET0016 displayed type-II binding spectra with CYP4A11, CYP4B1 and CYP4F2 (Figure 2.8a). For each enzyme, the maximal difference in absorbance was reached at a HET0016 concentration equal to or near the enzyme concentration, suggesting that HET0016 is a stoichiometric, tight-binding ligand for each of these CYP4 enzymes. The data were fit to the tight-binding quadratic equation, as shown in Figure 2.8b for HET0016 binding to CYP4A11, which resulted in a Kd < 5 nM. Type-II binding was also observed with CYP102 and CYP3A4 (data not shown). This suggests that HET0016 binds in the active site of these CYP4 enzymes with a nitrogen-iron coordinate bond and implies a competitive mode of inhibition. However, reversible inhibition kinetics experiments for HET0016 inhibition of CYP4A11 resulted in an atypical Dixon plot, and the data could not be adequately fit to a competitive model (data not shown, see Chapter 3).

Development of CYP4 Selective FAO Inhibitors. Formamidoxime (FAO) derivatives with alkyl chains attached to the central phenyl ring that ranged from 0-16 carbon atoms were synthesized (see Figures 2.1 and 2.2), to test the hypothesis that HET0016 derivatives with varying alkyl chain lengths may differentially bind to enzymes within the CYP4A, CYP4B and CYP4F sub-families [32]. Additionally, the FAO moiety of HET0016 was methylated in two different positions (resulting in compounds 10 and 11) to explore potential effects on CYP4 enzyme inhibition due to this portion of the molecule.

Initially, we examined the ability of FAO derivatives to inhibit lauric acid hydroxylase activities of CYP4B1, CYP4F2, CYP4F3B, and CYP4A11 at a saturating substrate concentration of 300 μM and an inhibitor concentration of 100 nM (Figure 2.9). Under these conditions, many of the FAO derivatives exhibited pronounced inhibition of CYP4F2, CYP4F3B, and CYP4B1, but no inhibition of CYP4A11 was observed. However, when substrate concentrations were decreased to the K_m (1.2 μM) for incubations with CYP4A11, HET00016 and several FAO derivatives were then able to inhibit the enzyme at 100 nM concentrations.

CYP4A11 and CYP4F3B were chosen for the subsequent detailed FAO inhibition studies aimed at identifying selective inhibitors for each sub-family. CYP4F2 was not a convenient enzyme for these studies because it exhibited a very low lauric acid hydroxylase activity relative to the other two enzymes. However, since CYP4F3B and CYP4F2 appeared to be inhibited in a similar manner by this series of HET0016 derivatives (at least at saturating substrate concentrations) it seemed that CYP4F3B was a good proxy for studying inhibition of important hepatic CYP4F enzymes. At the measured K_m values for CYP4A11 and CYP4F3B (1.2 and 38 μM, respectively), HET0016 inhibited both enzymes by >80%. Removing the methyl group from HET0016 (compound 4) did not affect inhibitor potency towards either enzyme. For CYP4A11, the optimal chain length for inhibition by FAO derivatives was 4-8 carbon atoms. CYP4F3B tolerated a wider range, but was still inhibited >80% by FAO derivatives with a chain length of 2-12 carbons. Compounds 2, 6, and 7 were the only FAO derivatives that failed to inhibit CYP4A11, but these analogs were able to inhibit CYP4F3B, at least some extent, at an inhibitor concentration of 100 nM. Compound 7 was very insoluble, and it may have partially precipitated out of the DMSO stock solution. Therefore, compounds 2 and 6 were chosen for final study to determine the degree of inhibitor selectivity between CYP4A11, CYP4F3B and CYP4F2.

CYP4F2 enzyme activity was monitored using arachidonic acid as a substrate instead of lauric acid because the kcat was much higher and thus a lower enzyme concentration could be used in metabolic incubations with inhibitors. Additionally, the LC-MS/MS assay for 20-HETE is more sensitive than the EI-GC/MS assay for 12-hydroxy lauric acid. Finally, there was added value to using arachidonic acid since it is a physiologically relevant substrate for CYP4F enzymes.

IC_{50} values for inhibition by compounds 2 and 6 of human hepatic CYP4A and CYP4F enzyme activities are shown in Figure 2.11. Again, substrate concentrations were at the K_m, which is 24 μM for ω-hydroxylation of arachidonic acid by CYP4F2 [33]. Compound 6, with an n-dodecyl alkyl chain at the para position, was about

66-fold more potent towards CYP4F3B and CYP4F2 than CYP4A11 (top panel). Compound 2, with no alkyl group at the para position of the phenyl ring, was the most discriminatory inhibitor between CYP4A and CYP4F enzymes. The IC_{50} value for compound 2 was >1000x higher for inhibition of CYP4A11 than for inhibition of CYP4F3B or CYP4F2 (bottom panel).

2.4 Discussion

CYP4F enzymes are typically efficient ω-hydroxylases for fatty acid substrates with long alkyl chains (C16 - C26), while CYP4A11 metabolizes medium-chain fatty acids (C12-C16) very efficiently and CYP4B1 preferentially hydroxylates even smaller substrates such as the C8 compounds, octanoic acid and valproic acid [34]. We used this trend in substrate selectivity within the CYP4 family to design inhibitors that might discriminate between CYP4A, CYP4F, and CYP4B enzymes. We achieved partial success in this regard through synthesis of compounds 2 and 6, which are ~ 65 – 1000 x more potent inhibitors of human CYP4F2 and CYP4F3B compared to CYP4A11.

In terms of the factors underlying the pan-CYP4 inhibitor specificity of HET0016, it is notable that the IC_{50} value for HET0016 inhibition of CYP4F12 was 516 nM, which is about >10-fold higher than IC_{50}s for other CYP4F enzymes. This is a new finding that further sets CYP4F12 apart from other CYP4 enzymes. CYP4F12 is not technically an ω-hydroxylase enzyme. Its major arachidonic acid metabolites are 18- and 19-HETE (the ω-2 and ω-1 metabolites), while most other CYP4 enzymes produce the ω -hydroxy product, 20-HETE. CYP4F12 also generates ω-1 and ω-2 metabolites of prostaglandin E2 [35]. Interestingly, CYP4F12 lacks a glutamic acid in the I-helix position that binds covalently to the heme cofactor in other CYP4 enzymes [36]. This active site structural difference may contribute to the lack of ω-hydroxylase activity, despite the >85% sequence similarity of CYP4F12 to CYP4F2 and CYP4F3B.

The structure-activity relationships evident here for FAO-mediated inhibition of CYP4 enzyme activities suggests that HET0016 derives its inhibitory potency towards CYP4A and CYP4F inhibition from different regions of the molecule. The FAO moiety may be the “warhead” for potent CYP4F inhibition, because altering or completely removing the alkyl chain minimally affects the magnitude of enzyme inhibition. Moreover, adding methyl groups to the FAO moiety (compounds 10 and 11), attenuates inhibition of CYP4F3B more so than CYP4A11 inhibition (Figure 2.10). In contrast, the n-alkyl chain appears to be more important for potent

inhibition of CYP4A11 because removal of the chain entirely eliminates enzyme inhibition. The striking IC_{50} difference observed among these enzymes upon removal of the n-butyl chain (from <30 nM to >100 μM), highlights the significance of alkyl chain binding interactions in the CYP4A11 active site.

This work highlights that interpreting inhibitor constants, such as IC_{50} and K_i, for tight binding inhibitors of P450 enzymes should be done with caution. P450 enzymes are relatively slow, with k_{cat} rates on the order of a few min^{-1}, as opposed to many sec^{-1}, necessitating higher enzyme concentrations in a metabolic incubation in order to produce enough product to detect by current analytical methods. With this in mind, we note that the lowest possible IC_{50} that can be measured for a stoichiometric binding inhibitor is a value half that of the enzyme concentration. For example, a metabolic incubation with 100 nM enzyme and a 1:1 tight-binding inhibitor cannot report an IC_{50} lower than 50 nM, assuming that one inhibitor binds to a single enzyme. Herein, we measured an IC_{50} value of 7.9 ± 1.2 nM for HET0016 inhibition of CYP4F3B lauric acid hydroxylase activity. At the K_m of the substrate (38 μM), the metabolic incubation necessitated 12 nM CYP4F3B concentration. With a more sensitive assay, we might have lowered the enzyme concentration and likely reported a lower IC_{50}. Thus, with inhibitor concentrations close to the enzyme concentration, both the enzyme and substrate concentration will affect the IC_{50} reported. Obviously, the Michaelis-Menton assumption that unbound inhibitor concentration is constant cannot be made, which should also be kept in mind when interpreting IC_{50}s of very tight-binding ligands under turnover conditions.

CYP4A11, CYP4F2, CYP4F3B, CYP4F11 and CYP4F12 are all ω-hydroxylase enzymes present in human liver, but CYP4A11, CYP4F2 and CYP4F3B are arguably the three major forms responsible for 20-HETE formation. In support of this statement, total CYP4F content in the liver is reported to range from 18-128 pmol/mg [37], while CYP4A11 content has been reported to be 48 +/- 28 pmol/mg protein [38]. Therefore, CYP4A and CYP4F enzymes constitute a significant portion of total liver P450 (344 +/- 167 pmol/mg protein) [39]. Prior to the work described in this Chapter, no chemical inhibitors were available that could be used to probe these enzymes' contributions to metabolism of endogenous fatty acids, eicosanoids, vitamins or xenobiotics. Additionally, specific inhibition with antibodies is difficult due to a high degree of sequence similarity and antibody cross-reactivity. This work has shown that formamidoxime compounds 2 and 6 can discriminate readily between catalysis by CYP4A and CYP4F enzymes, and compound 6 in particular is expected to be of value in elucidating the enzymatic origin of bioactive eicosanoid metabolites generated by the action of

CYP4 enzymes in extrahepatic human tissues. However, more work is required to develop inhibitors with high selectivity for individual members of the human CYP4F subfamily.

In conclusion these studies demonstrate, (i) HET0016 displays its greatest inhibitory (nanomolar) potency towards CYP4 enzymes that display a high degree of selectivity for ω-hydroxylation, (ii) HET0016 binding to CYP4A11, CYP4B1 and CYP4F2 occurs by nitrogen coordination to the heme, resulting in Type II binding spectra, (iii) HET0116 is a tight-binding inhibitor of CYP4A11, (iv) inhibition of CYP4A11, but not CYP4F2 or CYP4F3B, by HET0016 analogs is greatly reduced by removal of n-alkyl groups from the HET0016 nucleus, resulting in the development of novel CYP4F-selective inhibitors.

Figure 2.1: Structure of HET0016 and all formamidoxime (FAO) derivatives synthesized. Compound 10 is referred to as a methoxyformimidamide (MFIA) and compound 11 is referred to as an acetamidoxime (AAO).

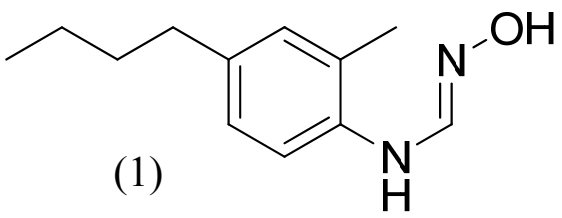

(1)

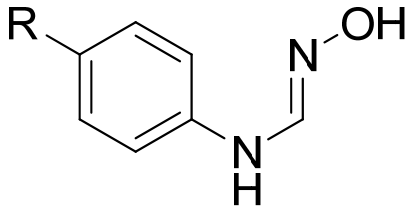

R= H (2)

ethyl (3)

n-butyl (4)

n-octyl (5)

n-dodecyl (6)

n-hexadecyl (7)

tert-butyl (8)

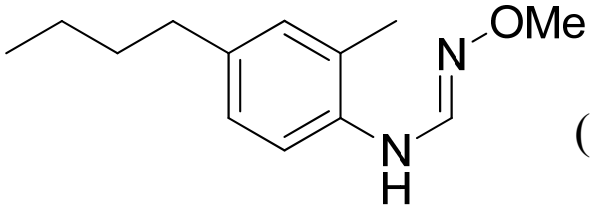

(10)

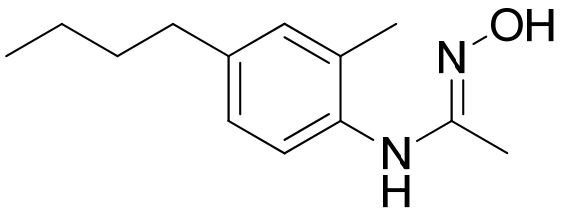

(11)

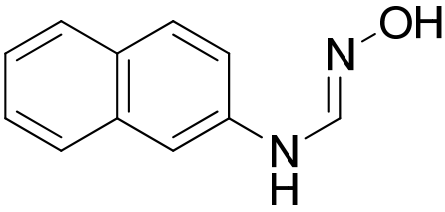

(9)

Figure 2.2: Synthesis of formamidoxime derivatives. See Figure 2.1 for structures of all derivatives synthesized by this general method.

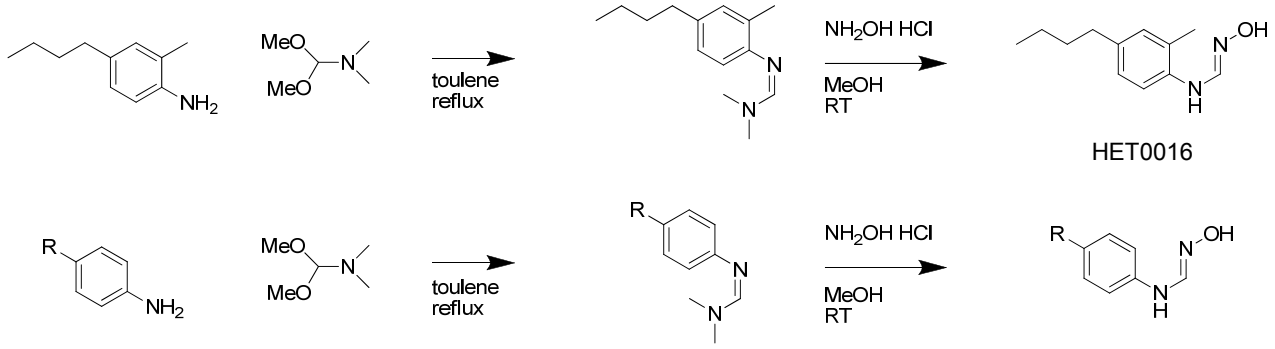

Figure 2.3: Representative ^{1}H (top) and ^{13}C (bottom) NMR of HET0016 synthesized in-house

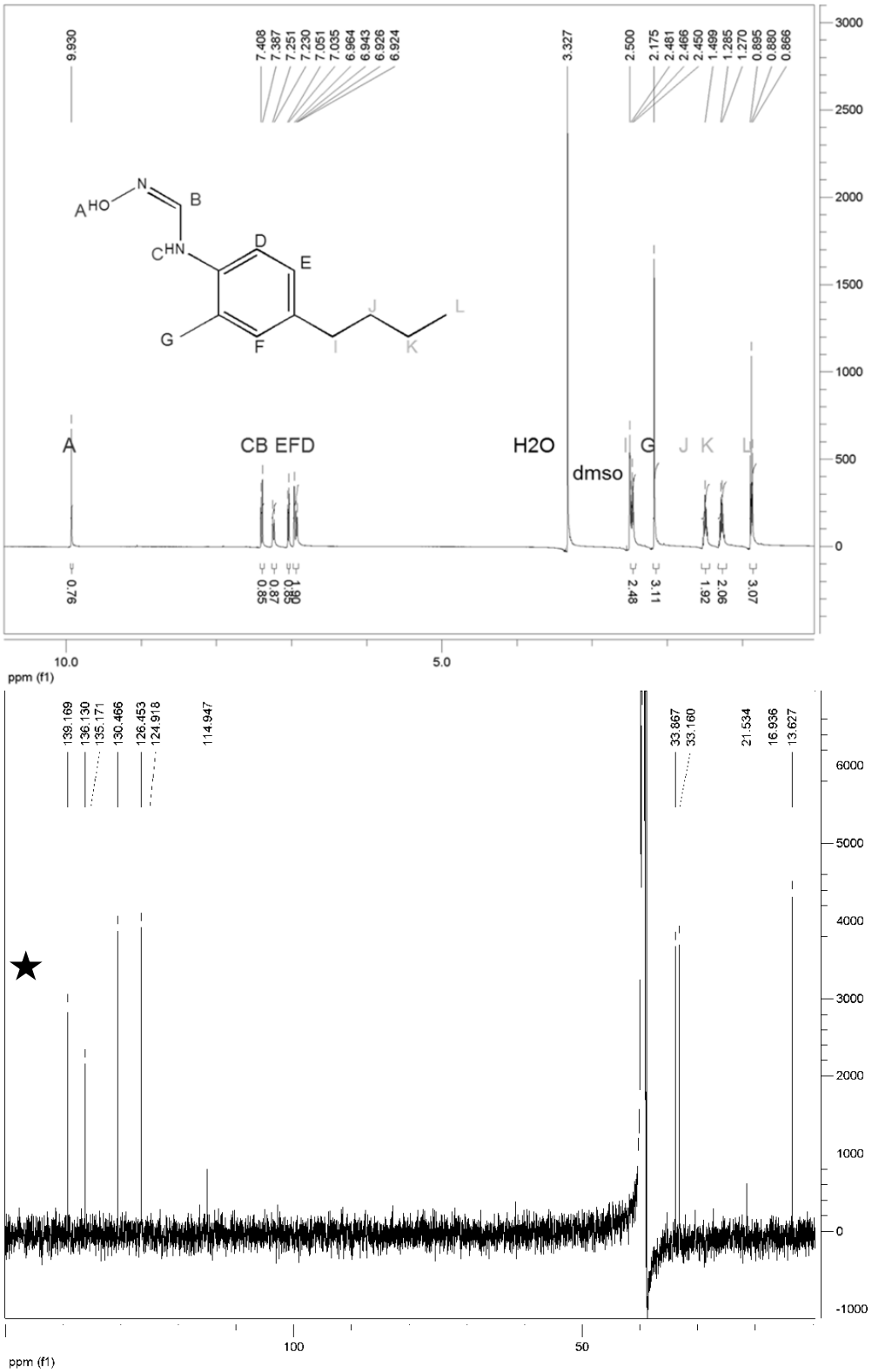

Figure 2.4: Different potential conformers of HET0016. A) Structures of ring-closed, cis conformers of HET0016. B) Structure of trans HET0016. C) Possible tautomer of HET0016

A)

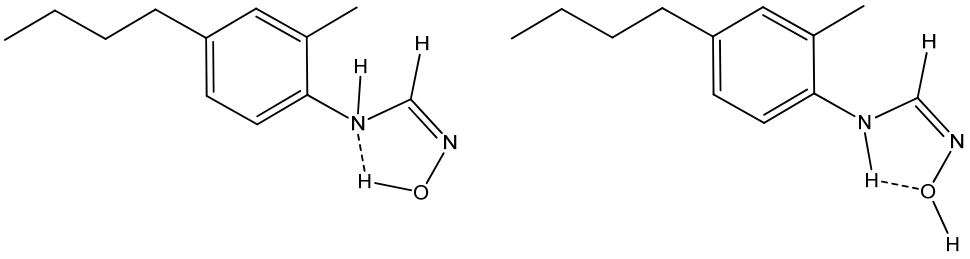

B)

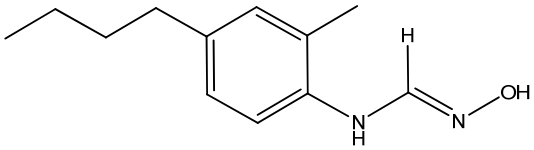

C)

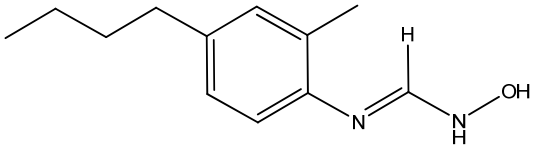

Figure 2.5: Inhibition of CYP4 enzymes and CYP3A4 by HET0016 (100 nM). Substrate concentrations were 10x K_m for each enzyme/substrate pair. CYP4F2, CYP4F3B, CYP4A11, and CYP4B1 activities were measured as the formation rates 12-hydroxy lauric acid. Control reaction rates in the absence of HET0016 (100% remaining activity) were 3.3, 15.2, 67.1 and 6.2 min^{-1}, respectively. CYP3A4 activity was measured as 6β-hydroxy testosterone formation, control activity was 60.9 min^{-1}. CYP4F12 activity was measured as hydroxy terfenadine formation, control activity was 2.8 min^{-1}.

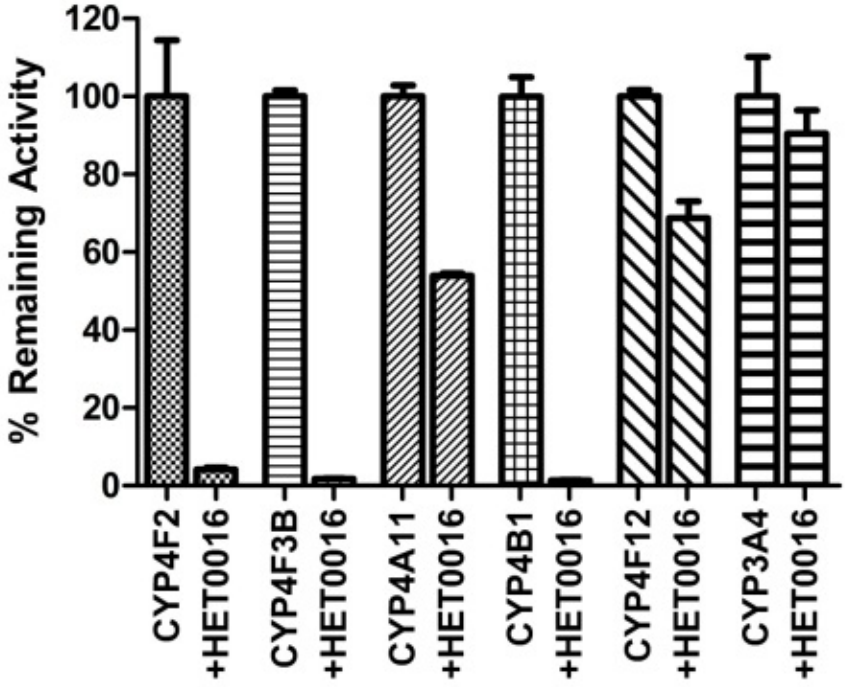

Figure 2.6: Direct kinetic plots of 12-hydroxy lauric acid formation by CYP4A11 (top) and CYP4F3B (bottom) Supersomes. TOP: K_m = 1.3 ± 0.17 μM, V_{max} = 24 ± 0.52 min^{-1}, V_{max} / K_m = 18.5 $\mu M^{-1}min^{-1}$. BOTTOM: K_m = 38 ± 5.8 μM, V_{max} = 7.4 ± 0.33, V_{max} / K_m = 0.19 $\mu M^{-1}min^{-1}$. At concentrations above 300 μM, substrate inhibition kinetics were observed for CYP4F3B.

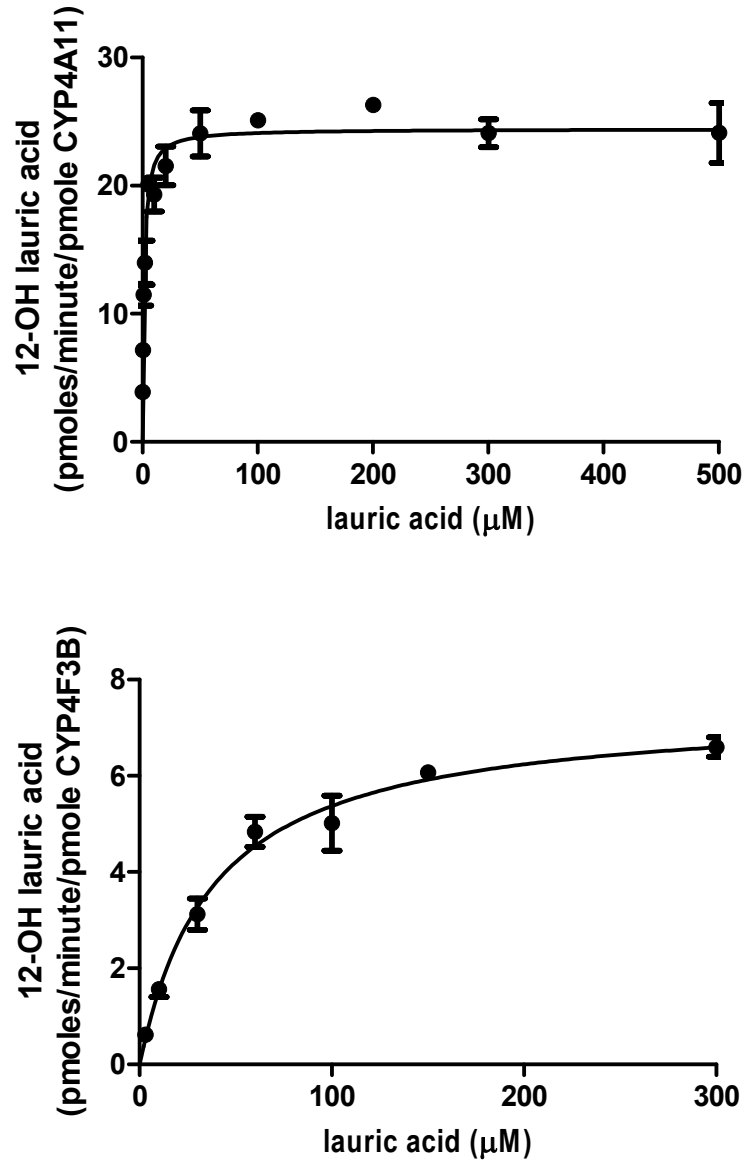

Figure 2.7: Comparative IC_{50} values for inhibition by HET0016 of CYP4 and CYP3A4 enzyme activities at the K_m of the substrate for each enzyme: CYP4F3B (K_m = 38 μM, lauric acid), CYP4A11 (K_m = 1.3 μM, lauric acid), CYP4B1 (K_m = 30 μM, lauric acid), CYP4F12 (K_m = 1 μM, terfenadine), CYP3A4 (K_m = 51 μM, testosterone). IC_{50} values and control reaction rates were as follows: CYP4F3B (7.9 ± 1.2 nM, 6.1 ± 0.4 min^{-1}), CYP4A11 (14.6 ± 1.1 nM, 18.1 ± 0.8 min^{-1}), CYP4B1 (24.4 ± 1.2 nM, 4.8 ± 0.4 min^{-1}), CYP4F12 (516 ± 1.1 nM, 2.1 ± 0.2 min^{-1}), CYP3A4 (>20 μM, 27.6 ± 0.7 min^{-1}). 50 μM is approximately the upper limit of HET0016 solubility under these conditions. Rank order of enzyme inhibition by HET0016: CYP4F3B>CYP4A11>CYP4B1 >>CYP4F12>>CYP3A4. Lauric acid hydroxyation rates with CYP4F2 were too low to obtain a good estimate of IC_{50} with this substrate.

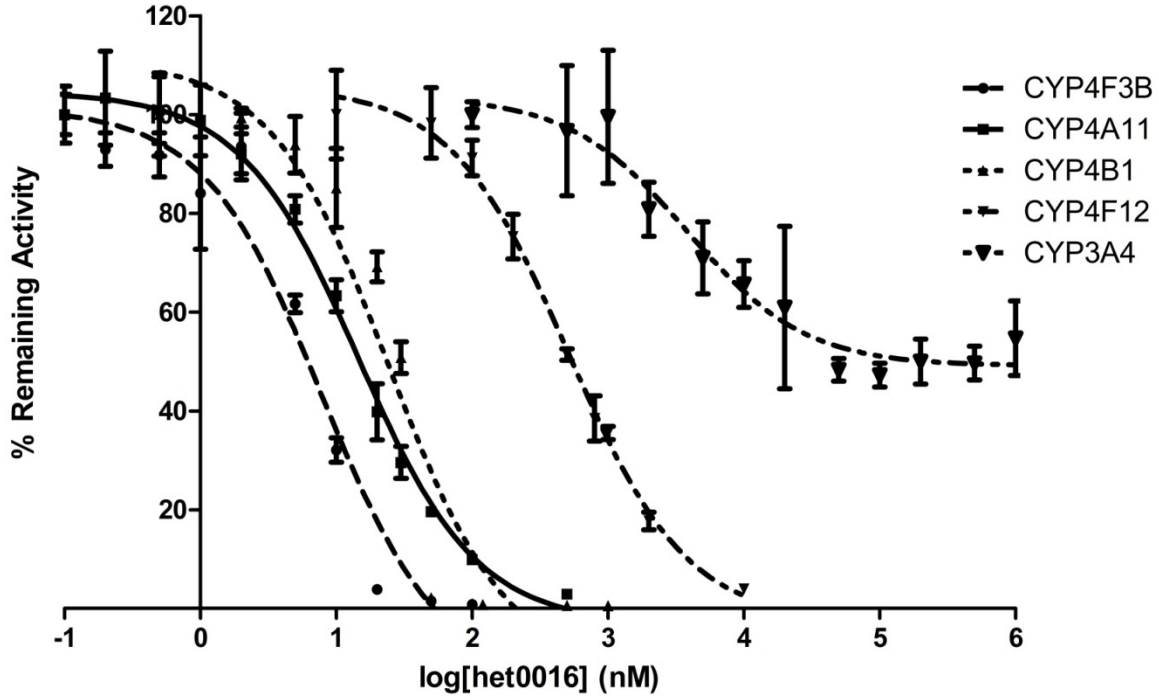

Figure 2.8: A) Difference spectra for HET0016 binding to purified CYP4A11, CYP4F2, and CYP4B1. P450 concentrations were 1 μM and HET0016 concentrations were saturating (1.25 μM, 0.9 μM, and 6 μM, respectively) B) Tight-binding kinetics of HET0016 to CYP4A11. The maximal absorbance difference is reached at a ligand concentration close to the enzyme concentration (1 μM).

A)

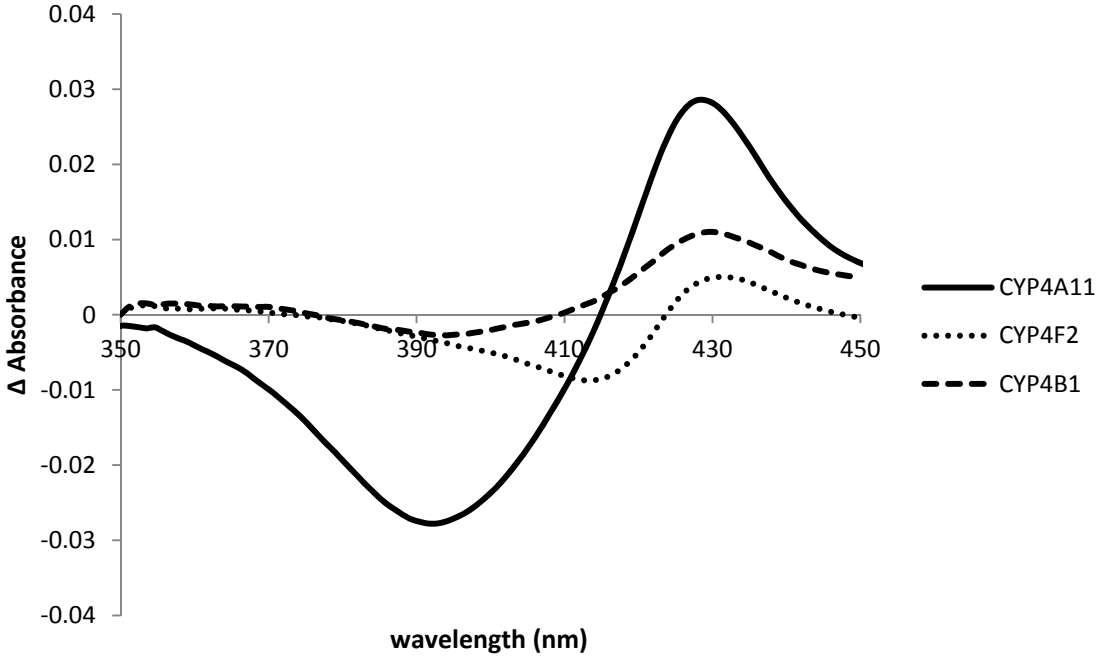

B)

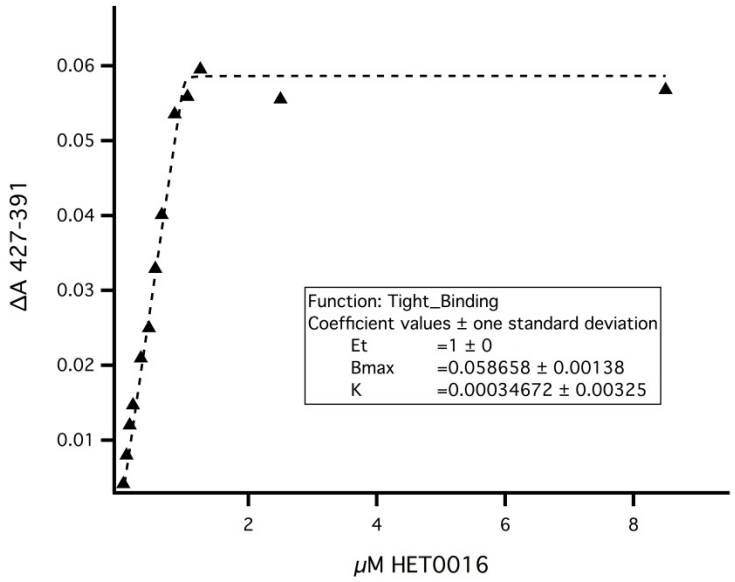

Figure 2.9: Inhibition of CYP4B1, CYP4F2, CYP4F3B, and CYP4A11 by formamidoxime derivatives. Numbers refer to compounds in Figure 2.1. Lauric acid substrate concentration was 300 μM for CYP4B1, CYP4F2, and CYP4F3B incubations. For CYP4A11, there was no apparent inhibition by HET0016 and FAO derivatives at 300 μM lauric acid concentrations. Thus, substrate concentration was decreased to the K_m for CYP4A11 (1.2 μM) for the inhibitor screen shown. Inhibitor concentrations were 100 nM in all cases.

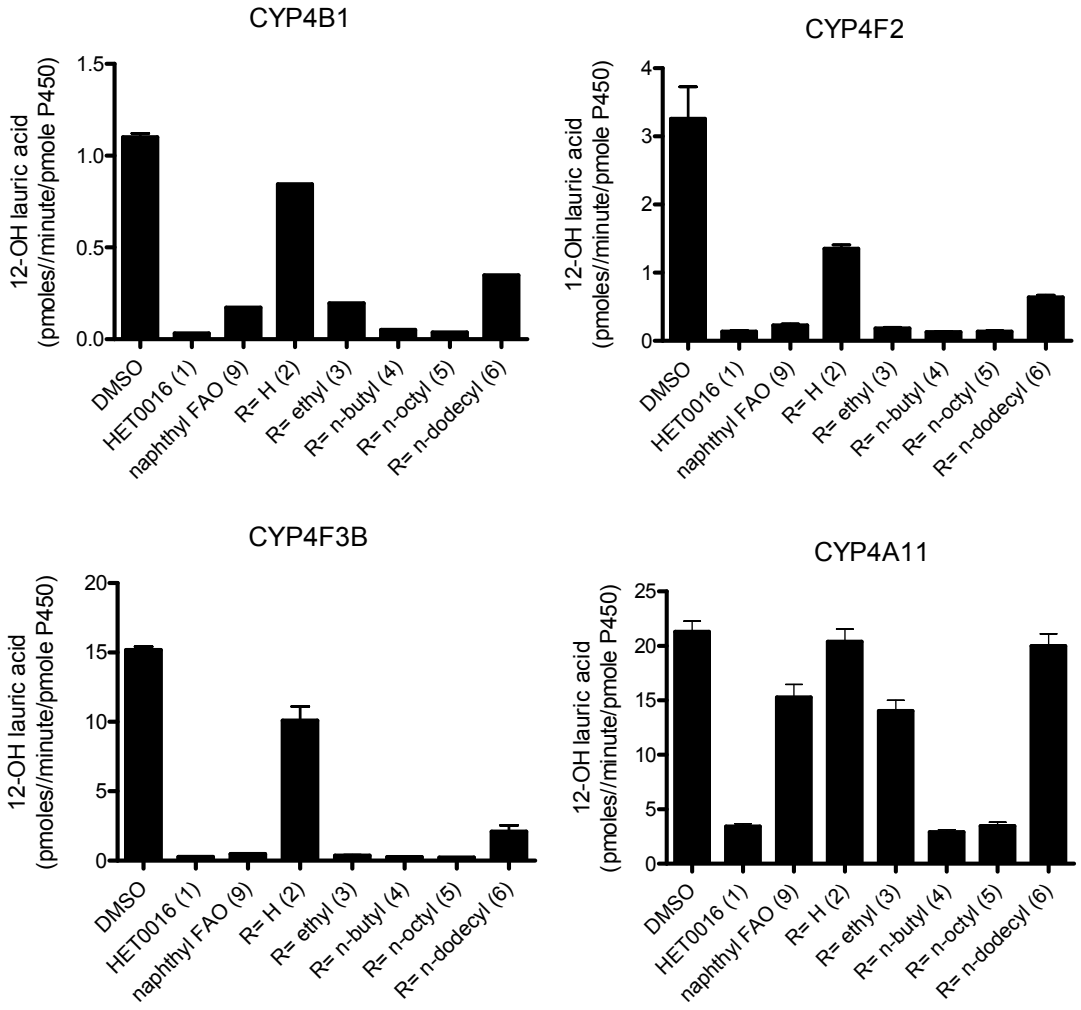

Figure 2.10: Inhibition of CYP4A11 and CYP4F3B by eleven FAO derivatives at the K_m of lauric acid for each enzyme (1.3 μM and 38 μM, respectively).

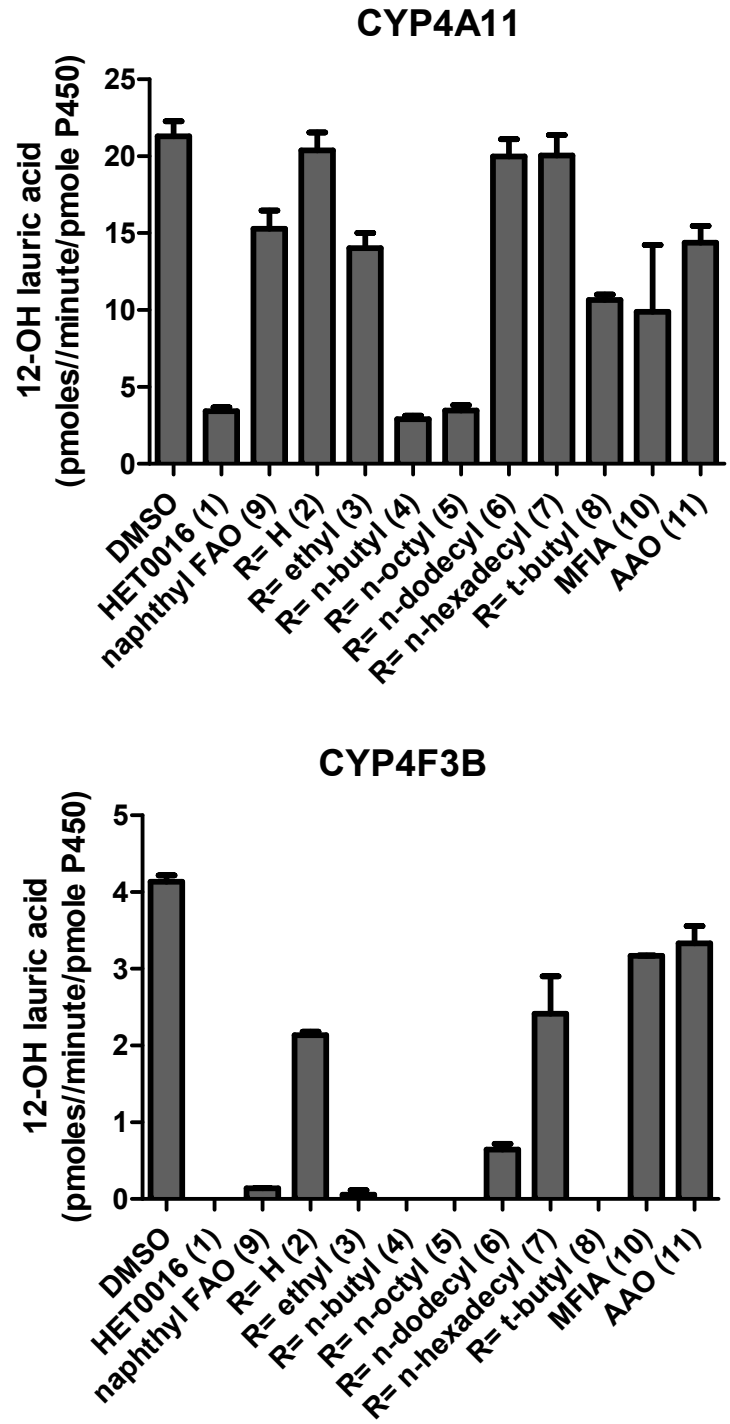

Figure 2.11: IC_{50} curves for the inhibition of CYP4A11, CYP4F3B, and CYP4F2 by phenyl FAO and phenyldodecyl FAO.
TOP: IC_{50} curves for n-dodecylphenyl FAO (6) inhibition of CYP4F3B- and CYP4A11-mediated lauric acid hydroxylation and CYP4F2-mediated 20-HETE formation. IC_{50} values were 22.5 ± 1.1 nM, 1.45 ± 1.3 μM, and 21.9 ± 1.1 nM respectively. Control reaction rates in the absence of inhibitor were 4.5 ± 0.1 min^{-1}, 11.5 ± 0.7 min^{-1} and 9.6 ± 0.3 min^{-1}, respectively. The n-dodecylphenyl FAO was 66x more potent against CYP4F3B and CYP4F2 when compared to CYP4A11, although the IC_{50} for CYP4A11 may be slightly underestimated because the limit of solubility is reached before activity is lowered to less than 10%.
BOTTOM: IC_{50} curves for inhibition by phenyl FAO (2) of CYP4F3B- and CYP4A11-mediated lauric acid hydroxylation and CYP4F2-mediated 20-HETE formation. IC_{50} values were 106.7 ± 1.1 nM, >100 μM, and 49.8 nM +/- 1.2 respectively. Control reaction rates in the absence of inhibitor were 4.7 ± 0.1 min^{-1} and 14.8 ± 0.1 min^{-1} and 8.3 ± 3.0 min^{-1} respectively. The phenyl formamidoxime was at least 1000X more potent against CYP4F3B and CYP4F2 when compared to CYP4A11.

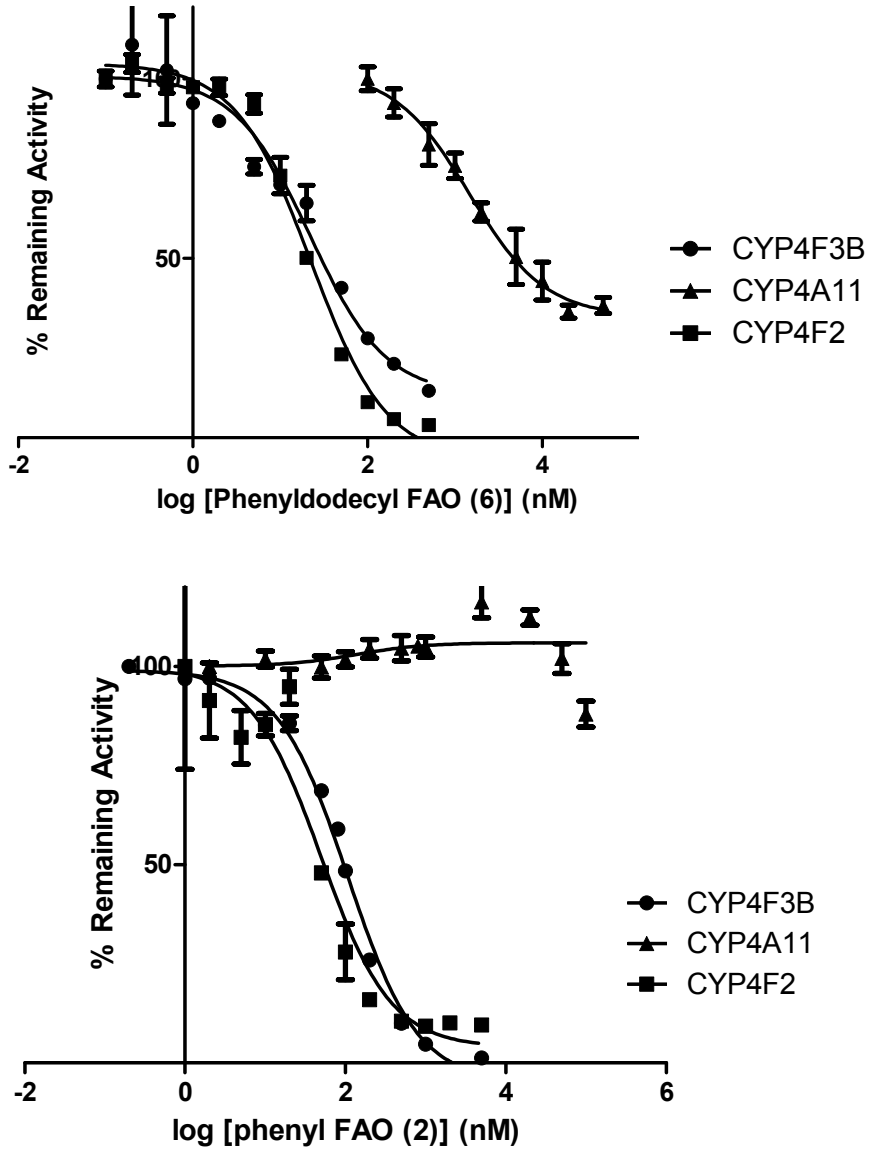

Table 2.1: 20-HETE synthase inhibitors

Inhibitor	Structure	IC_{50} for 20-HETE formation in renal microsomes	Type of Inhibitor	Reference
Terminal acetylenic fatty acids (17-ODYA)	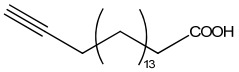	>5 μM	mechanism-based	[40]
Terminal di-bromo fatty acids (DBDD)	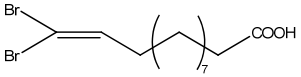	2 μM	reversible, competitive	[1]
Sulfonated fatty acids (10-SUYS)	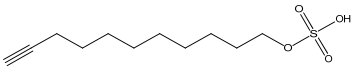	10 μM	mechanism-based	[41, 42]
(DDMS)	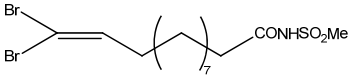	2 μM	reversible, competitive	
HET0016	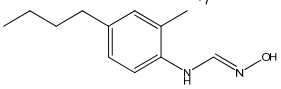	35 nM	unknown	[3, 4]
TS-011	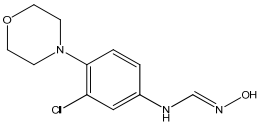	8 nM	unknown	[11]

2.5 References

[1] Kroetz, D.L.; Xu, F., Regulation and inhibition of arachidonic acid omega-hydroxylases and 20-HETE formation. *Annu Rev Pharmacol Toxicol,* 2005, *45*, 413-438.
[2] Kaspera, R.; Totah, R.A., Epoxyeicosatrienoic acids: formation, metabolism and potential role in tissue physiology and pathophysiology. *Expert Opin Drug Metab Toxicol,* 2009, *5*(7), 757-771.
[3] Sato, M.; Ishii, T.; Kobayashi-Matsunaga, Y.; Amada, H.; Taniguchi, K.; Miyata, N.; Kameo, K., Discovery of a N'-hydroxyphenylformamidine derivative HET0016 as a potent and selective 20-HETE synthase inhibitor. *Bioorg Med Chem Lett,* 2001, *11*(23), 2993-2995.
[4] Miyata, N.; Taniguchi, K.; Seki, T.; Ishimoto, T.; Sato-Watanabe, M.; Yasuda, Y.; Doi, M.; Kametani, S.; Tomishima, Y.; Ueki, T.; Sato, M.; Kameo, K., HET0016, a potent and selective inhibitor of 20-HETE synthesizing enzyme. *Br J Pharmacol,* 2001, *133*(3), 325-329.
[5] Nakamura, T.; Sato, M.; Kakinuma, H.; Miyata, N.; Taniguchi, K.; Bando, K.; Koda, A.; Kameo, K., Pyrazole and isoxazole derivatives as new, potent, and selective 20-hydroxy-5,8,11,14-eicosatetraenoic acid synthase inhibitors. *J Med Chem,* 2003, *46*(25), 5416-5427.
[6] Kehl, F.; Cambj-Sapunar, L.; Maier, K.G.; Miyata, N.; Kametani, S.; Okamoto, H.; Hudetz, A.G.; Schulte, M.L.; Zagorac, D.; Harder, D.R.; Roman, R.J., 20-HETE contributes to the acute fall in cerebral blood flow after subarachnoid hemorrhage in the rat. *Am J Physiol Heart Circ Physiol,* 2002, *282*(4), H1556-1565.
[7] Nakano, M.; Kelly, E.J.; Rettie, A.E., Expression and characterization of CYP4V2 as a fatty acid omega-hydroxylase. *Drug Metab Dispos,* 2009, *37*(11), 2119-2122.
[8] Parkinson, O.T.; Kelly, E.J.; Bezabih, E.; Whittington, D.; Rettie, A.E., Bioactivation of 4-Ipomeanol by a CYP4B enzyme in bovine lung and inhibition by HET0016. *J Vet Pharmacol Ther,* 2012, *35*(4), 402-405.
[9] Nakamura, T.; Ishii, T.; Miyata, N.; Taniguchi, K.; Tomishima, Y.; Ueki, T.; Sato, M., Design and synthesis of 1-(4-benzoylphenyl)imidazole derivatives as new potent 20-HETE synthase inhibitors. *Bioorg Med Chem Lett,* 2004, *14*(21), 5305-5308.
[10] Nakamura, T.; Kakinuma, H.; Umemiya, H.; Amada, H.; Miyata, N.; Taniguchi, K.; Bando, K.; Sato, M., Imidazole derivatives as new potent and selective 20-HETE synthase inhibitors. *Bioorg Med Chem Lett,* 2004, *14*(2), 333-336.
[11] Miyata, N.; Seki, T.; Tanaka, Y.; Omura, T.; Taniguchi, K.; Doi, M.; Bandou, K.; Kametani, S.; Sato, M.; Okuyama, S.; Cambj-Sapunar, L.; Harder, D.R.; Roman, R.J., Beneficial effects of a new 20-hydroxyeicosatetraenoic acid synthesis inhibitor, TS-011 [N-(3-chloro-4-morpholin-4-yl) phenyl-N'-hydroxyimido formamide], on hemorrhagic and ischemic stroke. *J Pharmacol Exp Ther,* 2005, *314*(1), 77-85.
[12] Walsky, R.L.; Obach, R.S.; Gaman, E.A.; Gleeson, J.P.; Proctor, W.R., Selective inhibition of human cytochrome P4502C8 by montelukast. *Drug Metab Dispos,* 2005, *33*(3), 413-418.
[13] Baldwin, S.J.; Bloomer, J.C.; Smith, G.J.; Ayrton, A.D.; Clarke, S.E.; Chenery, R.J., Ketoconazole and sulphaphenazole as the respective selective inhibitors of P4503A and 2C9. *Xenobiotica,* 1995, *25*(3), 261-270.
[14] Suzuki, H.; Kneller, M.B.; Haining, R.L.; Trager, W.F.; Rettie, A.E., (+)-N-3-Benzyl-nirvanol and (-)-N-3-benzyl-phenobarbital: new potent and selective in vitro inhibitors of CYP2C19. *Drug Metab Dispos,* 2002, *30*(3), 235-239.
[15] Cheesman, M.J.; Baer, B.R.; Zheng, Y.M.; Gillam, E.M.; Rettie, A.E., Rabbit CYP4B1 engineered for high-level expression in Escherichia coli: ligand stabilization and processing of the N-terminus and heme prosthetic group. *Arch Biochem Biophys,* 2003, *416*(1), 17-24.
[16] Nakano, M.; Kelly, E.J.; Wiek, C.; Hanenberg, H.; Rettie, A.E., CYP4V2 in Bietti's crystalline dystrophy: ocular localization, metabolism of omega-3-polyunsaturated fatty acids, and functional deficit of the p.H331P variant. *Mol Pharmacol,* 2012, *82*(4), 679-686.
[17] Mulrooney, S.B.; Waskell, L., High-level expression in Escherichia coli and purification of the membrane-bound form of cytochrome b(5). *Protein Expr Purif,* 2000, *19*(1), 173-178.
[18] Shen, A.L.; Porter, T.D.; Wilson, T.E.; Kasper, C.B., Structural analysis of the FMN binding domain of NADPH-cytochrome P-450 oxidoreductase by site-directed mutagenesis. *J Biol Chem,* 1989, *264*(13), 7584-7589.
[19] Kawashima, H.; Naganuma, T.; Kusunose, E.; Kono, T.; Yasumoto, R.; Sugimura, K.; Kishimoto, T., Human fatty acid omega-hydroxylase, CYP4A11: determination of complete genomic sequence and characterization of purified recombinant protein. *Arch Biochem Biophys,* 2000, *378*(2), 333-339.
[20] Dierks, E.A.; Zhang, Z.; Johnson, E.F.; de Montellano, P.R., The catalytic site of cytochrome P4504A11 (CYP4A11) and its L131F mutant. *J Biol Chem,* 1998, *273*(36), 23055-23061.
[21] Omura, T.; Sato, R., The Carbon Monoxide-Binding Pigment of Liver Microsomes. I. Evidence for Its Hemoprotein Nature. *J Biol Chem,* 1964, *239*, 2370-2378.

[22] Lowry, O.H.; Rosebrough, N.J.; Farr, A.L.; Randall, R.J., Protein measurement with the Folin phenol reagent. *J Biol Chem,* 1951, *193*(1), 265-275.
[23] Omura, T.; Sato, R., The Carbon Monoxide-Binding Pigment of Liver Microsomes. Ii. Solubilization, Purification, and Properties. *J Biol Chem,* 1964, *239*, 2379-2385.
[24] Guengerich, F.P.; Martin, M.V.; Sohl, C.D.; Cheng, Q., Measurement of cytochrome P450 and NADPH-cytochrome P450 reductase. *Nat Protoc,* 2009, *4*(9), 1245-1251.
[25] Olmstead, M.M.; Sahbari, J.J., Acetamidoxime. *Acta Crystallogr C,* 2003, *59*(Pt 12), o719-720.
[26] Hawkes, G.E.; Herwig, K.; Roberts, J.D., Nuclear Magnetic-Resonance Spectroscopy - Use of C-13 Spectra to Establish Configurations of Oximes. *Journal of Organic Chemistry,* 1974, *39*(8), 1017-1028.
[27] Zheng, Y.M.; Henne, K.R.; Charmley, P.; Kim, R.B.; McCarver, D.G.; Cabacungan, E.T.; Hines, R.N.; Rettie, A.E., Genotyping and site-directed mutagenesis of a cytochrome P450 meander Pro-X-Arg motif critical to CYP4B1 catalysis. *Toxicol Appl Pharmacol,* 2003, *186*(2), 119-126.
[28] Baer, B.R. Autocatalytic Mechanisms and Functional Consequences of Covalent Heme Attachment in CYP4B1. University of Washington, 2005.
[29] Parikh, S.; Gagne, P.; Miller, V.; Crespi, C.; Thummel, K.; Patten, C.
[30] Williams, J.A.; Ring, B.J.; Cantrell, V.E.; Jones, D.R.; Eckstein, J.; Ruterbories, K.; Hamman, M.A.; Hall, S.D.; Wrighton, S.A., Comparative metabolic capabilities of CYP3A4, CYP3A5, and CYP3A7. *Drug Metab Dispos,* 2002, *30*(8), 883-891.
[31] Kenworthy, K.E.; Clarke, S.E.; Andrews, J.; Houston, J.B., Multisite kinetic models for CYP3A4: simultaneous activation and inhibition of diazepam and testosterone metabolism. *Drug Metab Dispos,* 2001, *29*(12), 1644-1651.
[32] Hardwick, J.P., Cytochrome P450 omega hydroxylase (CYP4) function in fatty acid metabolism and metabolic diseases. *Biochem Pharmacol,* 2008, *75*(12), 2263-2275.
[33] Powell, P.K.; Wolf, I.; Jin, R.; Lasker, J.M., Metabolism of arachidonic acid to 20-hydroxy-5,8,11, 14-eicosatetraenoic acid by P450 enzymes in human liver: involvement of CYP4F2 and CYP4A11. *J Pharmacol Exp Ther,* 1998, *285*(3), 1327-1336.
[34] Fisher, M.B.; Zheng, Y.M.; Rettie, A.E., Positional specificity of rabbit CYP4B1 for omega-hydroxylation1 of short-medium chain fatty acids and hydrocarbons. *Biochem Biophys Res Commun,* 1998, *248*(2), 352-355.
[35] Stark, K.; Wongsud, B.; Burman, R.; Oliw, E.H., Oxygenation of polyunsaturated long chain fatty acids by recombinant CYP4F8 and CYP4F12 and catalytic importance of Tyr-125 and Gly-328 of CYP4F8. *Arch Biochem Biophys,* 2005, *441*(2), 174-181.
[36] Johnston, J.B.; Ouellet, H.; Podust, L.M.; Ortiz de Montellano, P.R., Structural control of cytochrome P450-catalyzed omega-hydroxylation. *Arch Biochem Biophys,* 2011, *507*(1), 86-94.
[37] Jin, Y.; Zollinger, M.; Borell, H.; Zimmerlin, A.; Patten, C.J., CYP4F enzymes are responsible for the elimination of fingolimod (FTY720), a novel treatment of relapsing multiple sclerosis. *Drug Metab Dispos,* 2011, *39*(2), 191-198.
[38] Lasker, J.M.; Chen, W.B.; Wolf, I.; Bloswick, B.P.; Wilson, P.D.; Powell, P.K., Formation of 20-hydroxyeicosatetraenoic acid, a vasoactive and natriuretic eicosanoid, in human kidney. Role of Cyp4F2 and Cyp4A11. *J Biol Chem,* 2000, *275*(6), 4118-4126.
[39] Shimada, T.; Yamazaki, H.; Mimura, M.; Inui, Y.; Guengerich, F.P., Interindividual variations in human liver cytochrome P-450 enzymes involved in the oxidation of drugs, carcinogens and toxic chemicals: studies with liver microsomes of 30 Japanese and 30 Caucasians. *J Pharmacol Exp Ther,* 1994, *270*(1), 414-423.
[40] Shak, S.; Reich, N.O.; Goldstein, I.M.; Ortiz de Montellano, P.R., Leukotriene B4 omega-hydroxylase in human polymorphonuclear leukocytes. Suicidal inactivation by acetylenic fatty acids. *J Biol Chem,* 1985, *260*(24), 13023-13028.
[41] Xu, F.; Straub, W.O.; Pak, W.; Su, P.; Maier, K.G.; Yu, M.; Roman, R.J.; Ortiz De Montellano, P.R.; Kroetz, D.L., Antihypertensive effect of mechanism-based inhibition of renal arachidonic acid omega-hydroxylase activity. *Am J Physiol Regul Integr Comp Physiol,* 2002, *283*(3), R710-720.
[42] Alonso-Galicia, M.; Drummond, H.A.; Reddy, K.K.; Falck, J.R.; Roman, R.J., Inhibition of 20-HETE production contributes to the vascular responses to nitric oxide. *Hypertension,* 1997, *29*(1 Pt 2), 320-325.

Chapter 3

Irreversible Inhibition of CYP4A11 by HET0016

3.1 Introduction

Mechanism-based inhibition of Cytochrome P450 enzymes is an important consideration during drug development. A mechanism based inhibitor (MBI) is any compound that is catalytically transformed to yield a reactive intermediate that irreversibly binds to the enzyme and renders it inactive. Drugs that inactivate P450 enzymes can lead to drug-drug interactions and/or the release of reactive metabolites that might bind cellular proteins or nucleic acids and result in toxicity. Therefore, it is important to identify structural moieties within drugs that may lead to reactive metabolites so that they might be avoided during drug development. However, these structural alerts are not always avoidable [1]. Figure 3.1 depicts some marketed drugs that are MBIs of P450 enzymes where the reactive intermediates have been well characterized. Typically, MBIs inactivate P450 enzymes by three different routes. Oftentimes, the reactive intermediate covalently binds to apo-protein, rendering the enzyme inactive. Alternatively, it can bind to or cause the chemical destruction of the heme cofactor; or it may form a quasi-irreversible coordinate-covalent bond with the heme iron, termed a metabolite-intermediate complex (MIC). Some MBIs result in multiple reactive intermediates that may inactivate a protein by combinations of these mechanisms.

There are several experimental criteria that a drug must display in order to be classified as an MBI [2]. Loss of enzyme activity is time-, NADPH-, and drug concentration-dependent. The rate of enzyme inactivation will exhibit saturation kinetics, and the k_{inact}, or maximum rate of inactivation, will be slower in the presence of a competing substrate for the enzyme. Additionally, enzyme activity does not return upon dialysis or gel filtration, and a 1:1 stoichiometry of radioactively labeled inhibitor: enzyme active site should be observed after inactivation followed by dialysis or gel filtration. Finally, reactive intermediate scavengers and trapping nucleophiles should have no effect on k_{inact}.

In this chapter, we have characterized the irreversible inhibition of CYP4A11 by HET0016. CYP4A11 is a principal 20-HETE synthase and a drug target of this compound when used experimentally as an anti-

hypertensive agent. Both mechanism-based inhibition and tight-binding inhibition of CYP4A11 by HET0016 were observed. Additionally, we probed the chemical mechanism of inhibition and the nature of the reactive intermediate that leads to CYP4A11 inactivation.

3.2 Materials and Methods

Materials. Peroxynitrite and DEANONOate were purchased from Cayman Chemical (Ann Arbor, MI). Nitrotyrosine monoclonal antibody, raised in mouse against peroxynitrite-treated KLH. was purchased from Cayman Chemical. 4-Butyl-2-methylphenyl aniline was purchased from Wako Chemicals (Osaka, Japan). N-Propylphenyl aniline was purchased from Alfa Aesar (Ward Hill, MA). Tritiated 4-n-propylaniline (5 mCi, 1 mCi/mL in ethanol) was purchased from ViTrax Company (Placentia, CA). The specific activity was >20 mCi/mmol. BSTFA +TMCS was from Supelco (Bellefonte, PA). 15-Hydroxypentadecanoic acid, lauric acid, 1-aminobenzotriazole (1-ABT), glutathione, N-acetyl lysine, N-acetyl cysteine, superoxide dismutase, or catalase were from Sigma-Aldrich. CYP4 Supersomes were purchased from BD Biosciences (San Jose, CA) Float-A-Lyzer dialysis tubes with 3.5-5 kD molecular weight cut-off cellulose ester membranes were obtained from Spectrum Labs, Inc., (Rancho Dominguez, CA). CYP4A11, P450 oxidoreductase, and cytochrome b5 were expressed and purified as described in Chapter 2 of this thesis. Dilaurylphosphatidylcholine (DLPC) was purchased from Avanti Polar Lipids (Alabaster, AL).

Irreversibility of Inhibition. Primary inhibition incubations were prepared with 50 nM CYP4A11 Supersomes in a total volume of 1 mL of 100 mM potassium phosphate buffer, pH 7.4 (KPi). Incubations were performed at 37 °C with 1 μM HET0016 and 1 mM NADPH for 12 minutes with a 2 minute pre-incubation. Three control incubations contained: 1) 1 mM NADPH without HET0016, 2) 1 μM HET0016 without NADPH, and 3) 10 mM 1-ABT with 1 mM NADPH. Each reaction was performed in duplicate. Samples were quenched on ice and transferred to 1 mL dialysis tubes. Tubes were capped and immediately dialyzed at 4°C with the following buffers: 1) KPi containing 50 μM fatty-acid free bovine serum albumin (BSA), pH = 7.4, 300 mL for 3 hours; 2) KPi containing 5 μM fatty-acid free BSA, pH = 7.4, 300 mL for 16 hours; 3) KPi, 300 mL for 3 hours. After dialysis, a 150 μL aliquot was taken to measure residual enzyme activity using lauric acid (100 μM) as a general

CYP4 enzyme activity probe. Final incubation volume was 0.5 mL and reaction in triplicated were initiated by the addition of 1 mM NADPH. After 15 minutes (with a 2 minute preincubation) at 37°C the reaction was quenched with 50 μL of 10% HCl, internal standard was added (15-hydroxy pentadecanoic acid (0.25 μg)). Samples were extracted with ethyl acetate (2 x 1 mL), dried under N_2, derivatized with BSTFA and analyzed by GC-MS as described in Chapter 2 of this thesis.

Time-dependent inactivation of CYP4A11 by HET0016. In a 96-well plate with 1.2 mL capacity, a primary incubation (500 μL total volume) in KPi buffer contained reconstituted CYP4A11 (50 pmoles purified P450, 100 pmoles P450 reductase, 50 pmoles cytochrome b5, and 8 nmoles DLPC) or 10 pmoles CYP4A11 Supersomes. HET0016 concentration was either 100 nM or 200 nM. Reactions were initiated with 1 mM NADPH and agitated in a water bath at 37°C. Control incubations lacking either NADPH or HET0016 were included. At four to five time points between 0 and 15 minutes, a 50 μL aliquot was transferred to a secondary incubation to measure remaining lauric acid hydroxyladse activity as described above. 12-Hydroxy lauric acid formation was quantitated and the rate was converted to ln % remaining activity, with each 0.25 minute time point re-set to 100%.

Determination of K_I and k_{inact} for HET0016 inactivation of CYP4A11. This experiment was also run in a 96-well plate with the primary incubation (400 μL total volume) in KPi buffer containing 2 pmoles CYP4A11 Supersomes (5 nM P450) and HET0016 dissolved in DMSO (0, 15, 30, 50, 80, 110 nM). The total DMSO concentration was always <0.5 % v/v. Reactions were initiated at 37°C with a final concentration of 1 mM NADPH. Control incubations lacking NADPH were included and reactions were performed in triplicate (with respect to HET0016 concentration). At 0.25, 1, 2, 3, and 4 minutes a 50 μL aliquot was diluted into a secondary incubation containing 100 μM lauric acid, 1 mM NADPH in a final volume of 500 μL KPi (1:10 dilution). After 20 minutes at 37°C, reactions were quenched with 50 μL cold 10% HCl, and residual lauric acid hydroxylase activity measured as described above. Pre-incubation time was plotted versus ln % remaining activity (RA). The slopes of each line were calculated to obtain the lambda value and HET0016 concentrations were plotted versus lambda with errors propagated. Prism GraphPad 5.0 was used to determine K_I and k_{inact} by nonlinear regression analysis.

Partition ratio. Primary metabolic incubations in a total volume of 200 µL KPi buffer contained 4 pmoles CYP4A11 (20 nM P450) and variable concentrations of HET0016 (0-2000 nM). A -NADPH and -HET0016 Control incubations lacking NADPH or HET0016 were included. Reactions were initiated with a final concentration of 1 mM NADPH and incubated at 37°C for 30 minutes. At 0.25 and 30 minutes, a 50 µL aliquot was diluted (1:10) into a secondary incubation to measure residual lauric acid hydroxylase activity as described above. The ratio of HET0016 to CYP4A11 concentrations in the primary incubation was plotted against % remaining activity for each HET0016 concentration.

Synthesis.

HET0016 formamide. This HET0016 metabolite (M5) was obtained by refluxing 4-butyl-2-methyl aniline with acetic anhydride and formic acid in THF, as according to previously published procedures[3]. 1H NMR (500 MHz, DMSO-d6) δ 9.46 (s, 1H), 8.25 (s, 1H), 7.58 (d, J = 8.1 Hz, 1H) , 7.15 – 6.94 (m, 2H), 2.25 – 2.16 (m, 2H), 1.91 (s, 3H), 1.60 – 1.45 (m, 2H), 1.29 (h, J = 7.4 Hz, 2H), 0.88 (t, J = 7.4 Hz, 3H). ESI+ (m/z) 192.1, 163.3, 136.0.

n-Propylphenyl formamidoxime. 2.4 mg of 4-n-propylaniline (17.8 µmoles) was dissolved in 1 mL toluene, and 7.1 µL (53.4 µmoles) of dimethylformamide dimethylacetal was added. The solution was refluxed for 3 hours and toluene was removed by vacuum. 1 mL of methanol and ~3.8 mg (54 µmoles) of hydroxylamine hydrochloride were added and stirred at room temperature overnight. The product was purified on a silica gel mini column (packed in a glass Pasteur pipette) with 1:1 hexanes:ethyl acetate as the mobile phase. 1H NMR: 1H NMR (500 MHz, DMSO-d6) δ 9.85 (s, 1H), 8.54 (broad s, 1H), 7.45 (d, J = 10.7 Hz, 1H), 7.02 (q, J = 8.6 Hz, 4H), 2.43 (t, J = 7.6 Hz, 2H), 1.51 (q, J = 7.4 Hz, 2H), 0.84 (t, J = 7.3 Hz, 3H). ESI+ (m/z) 179.0, 160.8.

^{3}H n-Propylphenyl formamidoxime. 2.4 mg of cold 4-n-propylaniline was added to the 24 µg of tritiated starting material. The ethanol was evaporated and 1 mL of toluene was added. The remainder of the synthesis proceeded exactly as described above. The yield was 0.844 mg (4.7 µmoles), and the specific activity was 11,132

dpm/pmole. Structure was confirmed with 1H-NMR, and was identical to the spectrum of the cold material with small amounts of water and ethyl acetate impurities.

HET0016 metabolite and glutathione adduct identification. Metabolic incubations were performed with 100 nM CYP4A11, CYP3A4, or CYP4F3B Supersomes or 2 mg/mL pooled human liver microsomes and 20 μM HET0016 in a total volume of 200 μL KPi buffer. .In some reactions glutathione or n-acetyl lysine were included at a concentrations of 5 mM. Reactions were initiated with NADPH (1 mM) and heated in a water bath at 37°C for 20 minutes. Reactions were quenched with 50 μL methanol and centrifuged at 13,000 rpm for 5 minutes in a table top centrifuge to precipitate protein. An Acquity C18 BEH 2.1 x 50 mm (Waters) column was used to separate metabolites on either a Waters or Agilent UPLC chromatography system. The mobile phases were: A) water and B) methanol and the flow rate was 0.3 ml/min. The mobile phase gradient was as follows: 0-1 min, hold at 10% B; 1-8 minutes, 10-100 % B; 8-10 minutes, hold at 100 % B; 10-10.1 minutes, 100-10 % B; 10.1-13 minutes, hold at 10 % B. Initially, a Waters accurate mass UPLC-TOF-MS instrument was used. The instrument, set in ESI+ ionization mode, simultaneously scanned from 50-1000 Da at high (30 V) and low (4 V) collision energies. After identification of the NADPH-dependent products by accurate mass, the spectra at both high and low collision energies were used to develop an MRM method to further analyze these metabolites using the same chromatographic conditions and ESI+ ionization mode. MRM channels and settings (DP, CE, CXP) monitored for each metabolite were: M1 and M2, 223.0>163.0 (40, 30, 15); M3, 191.0>164.0 (80, 30, 15); M5, 164.1>107.9 (46, 25, 10); M4, 192.1>135.8 (56, 21, 12), and HET0016, 207.0>147.0 (40, 30, 15).

Measurement of MI Complex formation. P450 enzyme was diluted into KPi buffer to a total volume of 900 μL and split evenly into 2 quartz cuvettes. The P450 concentration was 0.13 μM when using Supersomes. If using pure enzyme, 0.5 μM P450, 1 μM P450 reductase, and 80 μM DLPC were the final concentrations. An OLIS UV/Vis spectrophotometer was set to scan continuously from 430 nm to 495 nm (13 increments, 100 scans, 10 reads per datum, 0.1 s per scan). Cuvettes were pre-incubated at 37°C in the spectrophotometer for 3 minutes before scans were initiated. Between scans 2 and 3, NADPH was added to sample cuvette (1 mM), and KPi was added to reference cuvette. Between scans 9 and 10, HET0016 (10 μM) was added to both cuvettes. The final

DMSO concentration did not exceed 1% v/v. Scans 10-100 were collected over about 30 minutes. The average of scans 7-9 were subtracted as baseline and data were normalized to 490 nm.

Heme adduct detection by HPLC-UV/vis. Purified CYP4A11 (1 μM) was reconstituted in 100 mM KPi buffer with 2 μM P450 reductase, 1 μM cytochrome b5, and 160 μM DLPC on ice. In some cases, 8 units/μL catalase and superoxide dismutase were included. After a 3 minute incubation with HET0016 (10 μM) and NADPH (1 mM), 50 μL of the incubation was injected onto a Thermo Biobasic HPLC column (Thermo Scientific). Solvent A was water (0.05% formic acid) and solvent B was acetonitrile with 0.05% formic acid. Solvent B was linearly increased at a flow rate of 0.3 mL/min from 30 to 70% over 20 minutes, at which point it was held at 100% until 28 minutes. B was then decreased to 30% and held there from 28-31 minutes. A Shimadzu HPLC with a diode array UV/Vis detector was used to monitor heme at 400 nm and P450 apo-protein at 280 nm.

CO-binding to CYP4A11 after enzyme inactivation. In a total volume of 1 mL, 0.25 μM CYP4A11, 0.5 μM P450 reductase, and 40 μM DLPC were reconstituted on ice for 5 minutes. HET0016 (10 μM) was added in DMSO and the reaction was initiated by 1 mM NADPH. The samples were incubated at 37°C for 10 minutes after a 5 minute pre-incubation, and then quenched on ice. Sodium dithionite was added to the sample which was divided between two quartz cuvettes. Baseline readings were collected (400-500 nm) and CO was gently bubbled into the sample cuvette for 30 seconds.

Heme measurement using the hemochromogen assay. In a total volume of 700 μL KPi buffer, 0.5 μM CYP4A11, 1 μM P450 reductase, and 80 μM DLPC were reconstituted on ice for 5 minutes in KPi buffer. HET0016 (21 μM) was added in DMSO and the reaction was initiated with 1 mM NADPH. +/- NADPH and +/- HET0016 controls were included. The samples were incubated at 37°C for 15 minutes, and quenched with 200 μL of 100% re-distilled pyridine and 100 μL of 2M NaOH. The reaction was split between two quartz cuvettes and a baseline was collected from 500-600 nm. The sample cuvette was reduced with a few crystals of sodium dithionite and the peak absorbance at 557 nm was referenced to the absorbance at 575 nm to calculate heme concentration by Beer's law (ε= 32.4 $mM^{-1}cm^{-1}$).

Anaerobic spectral binding to CYP4A11 and CYP3A4. Storage buffer (20% glycerol, 100 mM EDTA, and 100 mM potassium phosphate, pH 7.4) was added to two 1 mL quartz cuvettes and an OLIS double beam UV/Vis spectrophotometer was set up to scan from 350 nm to 650 nm at 25 °C. A baseline scan was recorded. Purified CYP3A4 (1.5 μM) or CYP4A11 (1.5 μM) was added to the sample cuvette. A scan for the ferric protein was recorded and the cuvette was capped with a disposable rubber stopper. A needle was inserted into the rubber stopper with argon flowing into it, and another needle was inserted to allow gas to escape the system. The enzyme solution was not allowed to bubble, but argon flowed over the solution for 30 minutes on ice. Sodium dithionite was added as a saturated slurry in argon bubbled water with a gas tight syringe that punctured the rubber stopper. A spectrum for the ferrous enzyme was recorded. Ritonavir (30 μM) or HET0016 (100 μM) was added to sample and reference cuvettes in ethanol and DMSO, respectively. Spectra were recorded and scans were taken continuously for 15 minutes, or until there was no change in the spectral signal. CO was then bubbled into the sample cuvette gently for 3 minutes and a spectrum was recorded. The difference spectrum of CYP4A11 was calculated by subtracting the ferrous CYP4A11 scan from the ferrous CYP4A11+HET0016 scan.

HPLC and SDS-PAGE of CYP4A11 after inactivation by ^{3}H-n-propylphenyl formamidoxime. CYP4A11 (1.6 μM) was reconstituted in 100 mM KPi buffer with 3.2 μM P450 reductase, 1.6 μM cytochrome b5, and 256 μM DLPC on ice. After a 20 minute incubation at 37°C with ^{3}H-n-propylphenyl formamidoxime (118 μM, 59 μCi/ 100 μL) and NADPH (1 mM), 50 μL of the incubation was injected onto an R2 Poros HPLC column. The total volume of the incubation was 100 μL. The chromatography gradient increased linearly from 45-60% acetonitrile with 0.05% trifluoroacetic acid. A Shimadzu HPLC with a diode array UV/vis detector was used to monitor heme at 400 nm and apo-protein at 280 nm. Fractions were collected in scintillation vials over 1 minute time increments as the incubation eluted off of the column. EcoScint XR (5 mL) was added to the vial and radioactivity was counted on a liquid scintillation counting instrument (Packard 2200CA Tricarb liquid scintillation counter, Downers Grove, IL). Alternatively, 22 μL of the incubation was loaded onto a 1.5 mm polyacrylamide gel (4-12% Bis Tris) (Invitrogen) after addition of 8 μL sample buffer and 3 minutes of boiling. Reducing agent was omitted. The gel was stained with Coomasie brilliant blue (Biorad) and 1 cm bands were cut out of the gel and

placed in scintillation vials. The gel slice was covered in 1 M hyamine hydroxide solution in methanol and heated at 60°C for 3 hours. EcoScint XR (10 mL) was then added and radioactivity was counted by liquid scintillation counting.

Detection of nitrotyrosine modification by Western blot. Metabolic incubations were performed with CYP4A11, +/- HET0016 (40 μM), and +/- NADPH (1 mM) at 37°C in a total volume of 200 μL KPi buffer for 12 minutes. CYP4A11 (1 μM) was reconstituted with P450 reductase (2 μM), cytochrome b5 (1 μM), and DLPC (80 μM) in KPi buffer prior to addition of HET0016 and NADPH. For the positive control, 0.54 mg of DEANONOate was dissolved in 1 mL DMSO that had been purged with nitrogen gas (2.6 mM stock solution). The DEANONOate stock solution (0.2 μL) was added to the incubation every 2 minutes, in order to keep a constant supply of NO present throughout the incubation. In a pure 1 μM solution of CYP4A11, 0.5 μL peroxynitrite (PN) solution was added. The stock PN concentration (63.5 mM) was quantitated by measuring its absorbance in 0.3 M NaOH solution at the λmax of 302 nm (ε= 1670 $M^{-1}cm^{-1}$) [4]. The final concentration of PN in the CYP4A11 enzyme preparation was 160 μM. NuPAGE precast Bis-Tris polyacrylamide gels (Life technologies) were used (4-12%, 1.0 mm). An aliquot (13 μL) of each metabolic incubation was mixed with 2 μL reducing agent (DTT) and 5 μL NuPAGE LDS sample buffer, and samples were boiled for 3 minutes. A 20 μL aliquot was loaded into each lane, equivalent to 13 pmoles of CYP4A11 per lane. Two identical gels were run side by side with samples from the same incubations at 190 V for 35 minutes. One gel was stained with Coomassie brilliant blue dye. The second gel was prepared for Western blotting with the IBlot® dry blotting transfer system (Life Technologies). The gel was transferred to a nitrocellulose membrane over 7 minutes using the program setting, P0, which applies a step gradient from 20-25 V. The nitrocellulose was washed (PBS, pH 7.4 with 0.1% Tween) and blocked with Odyssey® blocking solution, then soaked in primary anti-nitrotyrosine antibody overnight at 4°C (1:200 dilution into Odyssey® block solution). The membrane was repeatedly washed in PBS/0.1% Tween and soaked at room temperature in fluorescent Odyssey® Licor secondary antibody (goat anti-mouse, 800 nm). The gel was again washed repeatedly and imaged using the Odyssey® fluorescent imaging instrument.

3.3 Results

Irreversible inhibition of CYP4A11. HET0016 inhibited CYP4A11-catalyzed lauric acid hydroxylation in an NADPH-dependent manner that was not recoverable by extensive dialysis (Figure 3.2). Activity was only recovered when either HET0016 or NADPH was omitted. When bovine serum albumin was omitted from the dialysis buffer, activity was not recovered from the control sample containing HET0016 only and no NADPH (data not shown). 1-Aminobenzotriazole (1-ABT), a pan-cytochrome P450 MBI, also irreversibly inactivated CYP4A11, although very high concentrations (10 mM) were necessary.

Time-and NADPH- dependent Inhibition of CYP4A11 by HET0016. HET0016 inhibited CYP4A11 in an NADPH-dependent manner and time-dependent manner (Figure 3.3). This occurred with CYP4A11 Supersomes, which lack cytochrome b5, as well as with purified CYP4A11 protein that had been reconstituted with cytochrome P450 reductase, cytochrome b5, and DLPC. Additionally, when glutathione, N-acetyl lysine, N-acetyl cysteine, superoxide dismutase or catalase was added to the pre-incubation mixture the rate of inactivation was not significantly altered (Figure 3.4). There was no time-dependent or NADPH-dependent inhibition of CYP4F12, CYP4B1 or CYP4F3B (Figure 3.5). On the contrary, HET0016 rescued the decrease in CYP4F3B activity over time that was likely due to auto-inactivation, which is typical behavior for a tightly-bound, reversible P450 inhibitor [5]. Likewise, HET0016 did not exhibit time-dependent or NADPH-dependent inhibition towards CYP4F2, CYP102 or CYP3A4 (data not shown). These experiments together suggest HET0016 is an MBI of CYP4A11, but a reversible, competitive inhibitor of other P450s including several CYP4 enzymes.

Mechanism based inhibition kinetics were measured for HET0016 with CYP4A11 Supersomes (Figure 3.6). A K_I= 38 nM and a k_{inact}= 0.4 min^{-1} were obtained. Enzyme inhibition deviated from linearity after 3 minutes, so reaction rates were measured at 1, 2 and 3 minutes only. The K_I and k_{inact} are calculated from equation 2, where λ is the inactivation rate. This equation assumes there is negligible change in inhibitor concentration during the incubation period and that the system is at rapid equilibrium. However, inhibitor depletion was most likely occurring under the experimental conditions that were used, because the lowest concentration of inhibitor contained 15 nM HET0016 in the inactivation step, while the CYP4A11 enzyme concentration was 5 nM; only a 3-fold difference in inhibitor compared to enzyme concentrations. After diluting out the inhibitor tenfold, the P450 concentration was 0.5 nM, which is near the lower limit of enzyme required to

obtain quantifiable turnover of substrate using this assay. Thus, HET0016 was likely depleted at lower inhibitor concentrations and the inactivation rates at those points are therefore underestimated. This would result in an even lower K_I measurement. Furthermore, tight binding inhibitors of P450 enzymes are often not in rapid equilibrium and display Briggs-Haldane behavior, where k_{off} is much slower than k_{cat} [6]. These are caveats of mechanism based inhibition kinetics that should be noted for very potent P450 mechanism based inhibitors.

Equation 2 $\lambda = (k_{inact} \times I)/(K_I + I)$

A partition ratio (*r*) is defined as the number of inhibitors metabolized and released from the active site per enzyme inactivation event and is a measure of MBI efficiency [7-9]. For a perfectly efficient MBI, $r = 0$. The reactivity of the reactive intermediate and its rate of diffusion out of the active site can influence the magnitude of the partition ratio. A substrate depletion-based partition ratio was measured for HET0016 inactivation of CYP4A11-dependent lauric acid hydroxylase activity ($r = 2.2$). As the I/Enzyme ratio ranged from 0.25-100, the % remaining activity was measured. The initial linear portion of the curve is projected to the x-axis to determine the turnover number. The partition ratio is equal to the turnover number minus 1. The very low partition ratio of 2.2 illustrates the high efficiency of CYP4A11 inactivation by HET0016.

HET0016 metabolites and glutathione adducts. To gain insight into the identity of the reactive chemical species that might be inactivating CYP4A11, we attempted to identify any metabolites of HET0016 formed during reaction with CYP4A11. LC-TOF-MS was first used to identify metabolites from metabolic incubations containing CYP4A11, CYP4F3B, CYP3A4, or human liver microsomes with HET0016 substrate (1 μM). The instrument, set in ESI+ ionization mode, simultaneously scanned from *m/z* 50-1000 at high and low collision energies. HET0016 fragmented to ions with *m/z* of 147 and 164, shown in Figure 3.7. Searching for the parent ion (*m/z* 207*),* the major fragments (*m/z* 147 and 164), and other expected fragments (i.e. *m/z* 163 in Figure 3.7) in both high and low collision energy scans led us to identify a number of metabolites. Other possible metabolites, such as the dehydrated nitrile product of HET0016 with a M+H of *m/z* 189, corresponding to *m/z* 207-18, were also searched for, but not found. Using these data, an MRM method with the same chromatographic conditions was developed on a triple quadrupole mass spectrometer. The structures of the putative metabolites (M1-M6) are shown in Figure 3.8, and the chromatograms from this assay are shown in Figure 3.9. M1, M2, M3, and M6 were

tentatively identified based on their mass spectrometry fragmentation. The synthetic standard of M4 was commercially available. M5 was synthesized and purified as described in methods. Accurate masses of M1-M5 were (*m/z*): M1= 223.1445, calculated= 223.1447; M2= 223.1455, calculated=223.1447; M3= 192.1394, calculated= 192.1388; M3=164.1448, calculated= 164.1439; M4= 191.1551, calculated= 191.1548; HET0016= 207.1509, calculated= 207.1497. Human liver microsomes produced a small amount of M4 and M5 in the absence of NADPH. CYP3A4 Supersomes produced metabolites M2-M5 in an NADPH dependent manner. CYP4A11 and CYP4F3B only made small amounts of M3 in an NADPH dependent manner. An NADPH dependent metabolite was evident in human liver microsomes in the *m/z* 207>147 *m/z* MRM channel (M6) whose mass fragmentation and retention time is consistent with its assignment as the HET0016 urea. This metabolite was not formed by CYP4A11 Supersomes.

In a similar fashion, covalent adducts to the reactive species with glutathione (GSH), cyanide, or N-acetyl-lysine (NAL) were sought when these compounds were included in the incubation. In addition to the mass and fragment masses of HET0016, fragments of glutathione and N-acetyl lysine were searched for in the high and low collision energy scans. Glutathione adducts commonly fragment to yield a *m/z* 308 fragment ion [10, 11]. NAL adducts and cyanide adducts exhibit a neutral loss of *m/z* 171 and 27, respectively [2, 12]. Numerous fragment masses were sought that corresponded to masses of expected adducts and their fragment ions in both high and low collision energy scans. However, no evidence for GSH, cyanide, or NAL adducts in incubations with CYP4A11 or human liver microsomes was obtained.

MI-complex formation. MIC formation was evaluated with CYP4A11 Supersomes and CYP4A11 reconstituted enzyme (Figure 3.10). Due to the lack of any known chemical that can generate an MIC with CYP4A11, formation of a CYP3A4 MIC with N-hydroxy fluoxetine was used as a positive control. There was no apparent MIC formation using CYP4A11 Supersomes at an enzyme concentration of 0.13 μM, as well as pure enzyme at a higher concentration (0.5 μM).

Determination of heme condition after HET0016 inhibition. Several methods are available for analyzing the heme cofactor of P450 after reaction with an MBI. The classic method is to measure reduced, CO-binding

difference spectra of the P450 enzyme after inactivation [13-15]. If the MBI has caused destruction of the heme, or is bound to the heme in a way the occludes CO from binding to it, an incubation containing inhibitor and NADPH should show decreased CO-binding spectra as compared to a control incubation with NADPH or inhibitor alone. This experiment was performed with HET0016 (10 μM) and CYP4A11 (Figure 3.11). When nothing or NADPH alone were added to the incubation, the Fe^{2+}-CO concentration was 0.14 μM. When HET0016 alone or HET0016 + NADPH were added, both CO-binding spectra were significantly decreased. This experiment indicates that HET0016 prevents CO from binding to reduced heme in an NADPH-*independent* way. However, these results were not consistent with the time dependent inhibition data which indicated that inhibition was both time- and NADPH-dependent. Thus, we further examined the ability of HET0016 to bind tightly to the reduced state of CYP4A11, which had previously been shown to occur with benzaldoxime [16].

Ritonavir also binds to reduced CYP3A4 and displays a peak at 442 nm in the absolute spectrum under anaerobic conditions (Figure 3.12A). This is a unique characteristic of a few P450 ligands, however most ligands do not bind to the reduced enzyme. Upon addition of carbon monoxide, the 442 nm peak can be shifted to 450 nm, indicating CO has displaced ritonavir from coordination with the heme. To determine if HET0016 was able to bind tightly to reduced CYP4A11 in a similar fashion, an identical experiment was performed with this ligand and enzyme (Figure 3.12B). A transient shoulder peak around 440 nm was observed after HET0016 addition to the reduced CYP4A11 that disappeared quickly after the first scan was collected. Time dependent loss of a Fe^{+2}-ligand 442 nm peak in rat liver microsomes has been previously observed with benzaldoxime [16]. The most prominent peak after HET0016 addition was at 424 nm. After bubbling CO, there was no peak observed at 450 nm. If HET0016 was not included, bubbling of CO resulted in a 452 nm peak. When the 452 nm peak was formed first and HET0016 was added afterwards, the 452 nm peak decreased but was not completely abolished (data not shown). As a control experiment, HET0016 was diluted into water that had been bubbled with argon and directly injected onto the mass spectrometer in ESI+ ionization mode. The expected signal at *m/z* 207 for the protonated molecular ion (M+H) was observed. When a small amount of sodium dithionite was added to the vial and after 1 minute the sample again injected the *m/z* 207 signal was no longer detectable (data not shown). This is a crude indication that HET0016 is not stable when sodium dithionite is present. These experiments showed that CO was unable to bind to the reduced enzyme after exposure to HET0016, and explain why the

classic method of assessing heme state by reduced-CO binding after enzyme inactivation is not appropriate for this tight binding ligand.

Another useful method of determining the state of the heme cofactor after inactivation by MBIs is HPLC/UV-Vis of the whole protein and of the heme after inactivation [17-19]. P450 reductase chromatographs as two distinct peaks by this assay, which has been previously observed [20]. The earlier eluting peak is termed "clipped" reductase. (Figure 3.13). Cytochrome b5, which also contains a heme cofactor, was also present. It would have been ideal to leave out cytochrome b5 so additional heme that would likely not form an adduct would not complicate the experiment. However when cytochrome b5 was excluded, after a 3 minute incubation with NADPH and no inhibitor, the heme peak disappeared completely. Figure 3.13 shows a chromatogram of an incubation mixture of CYP3A4, P450 reductase, cytochrome b5, and 1-aminobenzotriazole (1-ABT), a known CYP3A4 inactivator that forms heme adducts [21]. There are multiple heme adducts (panel A) that are NADPH dependent (panel B) at the retention time range from 14.5-15.5 minutes. Figure 3.14 shows the same experiment performed with CYP4A11 and HET0016. The small peak at 23-24 minutes in both the 280 nm channel and the 400 nm channel is CYP4A11 protein. Peak shape of the protein is markedly improved upon addition of DTT, however it was omitted to avoid any reduction of a possible heme adduct. When DTT is included and CYP4A11 recombinant protein is directly injected and analyzed by this method (without incubation) about 50% of the heme signal elutes with the protein (at 24 minutes) and 50% of the heme elutes at 12 minutes, indicating that half of the heme in this recombinant protein preparation is covalently bound to the I-helix [22]. There is one small, but discernible peak at 12 minutes that was both NADPH and HET0016 dependent; however, it was much less intense than the 1-ABT peaks in the CYP3A4 experiments. Due to the extensive heme bleaching and the addition of cytochrome b5 in these incubations, it was difficult to assess the percent of heme remaining after inactivation by this method.

A third way to analyze the state of the heme cofactor after inactivation by an MBI is with the pyridine hemochromogen assay [23]. This involves inactivation of the protein, followed by denaturing the protein with pyridine and NaOH and reduction with sodium dithionite. In CYP4 proteins it has been shown that the ester bond covalently linking the heme to the I-helix is hydrolyzed under basic conditions [24, 25], thus it was assumed that under these quenching conditions none of the heme was still covalently bound to the protein. Under basic

conditions, the ferrous heme binds two pyridine molecules and has a unique absorbance at 557 nm (Figure 3.15). The same concentration of heme was measured when HET0016 alone or nothing was added to the incubation (0.3 μM). Similar concentrations were measured when NADPH or NADPH and HET0016 were included in the incubation step. This suggests NADPH, rather than HET0016, is responsible for some heme destruction of CYP4A11 over the 15 minute incubation period. Adding HET0016 did not appear to add further decrease in the amount of measurable heme by this assay.

Exploring protein adduction of HET0016 to CYP4A11. The gold standard of experimental evidence to prove that a compound is an apo-protein-bound MBI is showing covalent binding of the molecule to the enzyme. This can be done with a radioactively labeled MBI, or the MBI might have a chromophore that is distinct from that of the heme or protein, as is the case with the MBI, raloxifene [18]. With a radioactive compound in hand, either SDS-PAGE or HPLC is commonly used to separate the inactivated protein from the incubation mixture and demonstrate that one molecule is still bound to the denatured protein. A derivative of HET0016, 4-propylphenyl FAO, was synthesized with a tritium label in the phenyl ring, as shown in Figure 3.16. This compound was also synthesized without any radioactive label, and shown to exhibit NADPH- and time-dependent inhibition of CYP4A11 (data not shown). In order to improve the chromatography of the CYP4A11 protein, an R2 Poros column (as opposed to the Thermo Biobasic column used in Figure 3.13 and 3.14) was used. The chromatographic conditions were adjusted so that immediately before the protein eluted, the organic phase increased sharply to elute the protein from the column. Chromatography under these experiments was particularly challenging because the radioactive ligand exhibited a broad peak that did not completely elute until ~10 minutes. Unbound heme, P450 reductase, and cytochrome b5 eluted rather early under these conditions. Perhaps extensive washing and concentrating cycles or dialysis would have been helpful to remove the residual radioactive ligand before injection onto the HPLC. The specific activity of the synthesized FAO derivative was 11,132 dpm/pmole, and 80 pmoles were typically injected onto the HPLC. Thus, the expected peak area if one radioactive molecule eluted with one protein molecule would be 890,560 dpm. The peak height observed was only 800 dpm, resulting in a much smaller peak area than would be consistent with significant metabolism-based inactivation. Importantly, the incubation without NADPH showed a similar result. Therefore, small radioactivity

peak that co-elutes with the protein is likely due to partial unfolding of the protein on column and tight binding of the formamidoxime to the protein. In summary, this experiment showed that the tritium labeled portion of HET0016 was not covalently bound to CYP4A11 or the covalently bound heme cofactor after incubation with NADPH.

Exploring the mechanism of inactivation with HET0016 Analogs - Compounds 2, 4, and 8 (Figure 2.1) were synthesized in Chapter 2. Time dependent inhibition (TDI) of CYP4A11 by these derivatives was assessed to determine what structural features of the molecule were necessary to inactivate the enzyme. The derivatives with an n-butyl phenyl ring or t-butyl phenyl ring, with no methyl group at the 2 position, inhibited CYP4A11 in a similar manner as HET0016 (Figure 3.17). The formamidoxime derivative with no alkyl groups on the phenyl ring was not a time dependent inhibitor of CYP4A11 at a concentration of 20 μM. However, it became evident that this concentration was likely too low to display TDI, as the IC_{50} was greater than 100 μM.

Compounds 10 and 11 (Figure 2.1) were also synthesized in Chapter 2 and tested for TDI of CYP4A11. These compounds are methylated at two different positions on the formamidoxime moiety of HET0016. At 100 nM concentrations, these compounds inhibited CYP4A11 activity by ~50% in a co-incubation experiment with lauric acid as a reporter substrate (Figure 2.10). In a TDI experiment at a concentration of 1 μM, the samples with NADPH and inhibitor displayed no more TDI than the control sample without NADPH (Figure 3.18). Competitive inhibition in the secondary incubation, as previously observed with HET0016, was not observed in these experiments (left panel), indicating that the tight- or slow- binding may have been eliminated by adding these methyl groups to the formamidoxime moiety.

Investigation of nitric oxide release by HET0016 upon incubation with CYP4A11. Peroxynitrite has been shown to inactivate some P450 enzymes by nitration of tyrosine residues [26-28]. Thus, we tested the hypothesis that upon incubation with CYP4A11, HET0016 was metabolized to release nitric oxide radical ($NO^{\cdot}$), which might further react with superoxide to produce peroxynitrite, ultimately causing CYP4A11 inactivation *via* tyrosine nitration. Figure 3.19 shows a Coomasie stained and western blotted gel of a CYP4A11 incubation with HET0016 and NADPH. Lane 1 is a purified protein standard of CYP4A11 that has been treated with

peroxynitrite. Lane 2 and 3 show untreated, un-incubated CYP4A11 and P450 reductase, respectively. Lane 4 is CYP4A11 and P450 reductase after incubation with HET0016 and NADPH, and lane 5 and 6 are the control incubations without either NADPH or HET0016. The peroxynitrite treated CYP4A11 immunoreacted with the nitrotyrosine antibody; however, there was no nitrotyrosinated CYP4A11 enzyme that could be detected after incubation with HET0016. Lane 7 consisted of a reaction mixture of CYP4A11, P450 reductase, and an $NO^{\cdot}$ releasing compound, DEANONOate, which also did not immunoreact with the antibody. DEANONOate is a small molecule that spontaneously dissociates in a pH-dependent, first-order process with a half-life of 2 minutes at 37°C (pH 7.4) to liberate 1.5 moles of $NO^{\cdot}$ per mole of parent compound [29, 30]. This experiment suggests that the reactive species that inactivates CYP4A11 is not nitric oxide. Additionally, our collaborator, Dr. Osawa at the University of Michigan, found that HET0016 did not release $NO^{\cdot}$ when incubated with recombinant endothelial NOS, as compared to N-hydroxy arginine (NOHA), the endogenous eNOS substrate, using an analytical method that measures oxyhemoglobin to methemoglobin conversion [31]. Nor was $NO^{\cdot}$ detected during incubations with recombinant CYP3A4 or CYP4A11 (data not shown).

3.4 Discussion

The main conclusion from these studies is that HET0016 is a tight-binding ligand to CYP4A11, however, it was demonstrated that irreversibility and TDI were both NADPH dependent processes. This suggests a mechanism-based process by which the inhibitor is metabolized to a reactive species that then inactivates the enzyme. We have yet to prove the identity of the reactive species; however herein we discuss a number of possibilities that are supported by data reported in this chapter.

In dialysis experiments to test irreversibility (Figure 3.2), the addition of bovine serum albumin to dialysis buffer was necessary to recover activity from samples incubated with HET0016 alone (omitting NADPH). This result is consistent with tight-binding irreversible inhibition of a very water insoluble inhibitor. HET0016 is only soluble in water to 34 μg/mL water [32] and has a calculated logP value of ~ 3.5. The fraction of HET0016 unbound in plasma is unknown, but these results indicated that BSA binds HET0016 because it was able to provide a sink for the non-covalently bound inhibitor.

A very low partition ratio (r = 2.2) was measured for HET0016 inactivation of CYP4A11 Supersomes, indicating the reactive metabolite is a very efficient inactivator of CYP4A11. This may account for our inability to detect glutathione, cyanide, or N-acetyl lysine adducts of HET0016 after incubations with CYP4A11, because the amount of adduct formed might be below the limit of detection, even at higher enzyme concentrations. We attempted to gain further insight into the reactive intermediate of HET0016 by identifying metabolites of the inhibitor formed by various P450s. This approach has been successful with terminal acetylene MBIs. These MBIs produce carboxylic acid metabolites from the reaction of water with the reactive ketene intermediate [33-35]. If the intermediate is extremely reactive, it might react with water before it has a chance to diffuse out of the active site and contact a trapping nucleophile like glutathione. CYP4A11 only produced small amounts of M3 in an NADPH dependent manner, however CYP3A4 and CY4F3B also formed this metabolite, and neither of these enzymes exhibited TDI. It may be worth considering whether this putative reductive metabolite of HET0016 can be formed with P450 reductase alone, or if it is actually P450 dependent. Previous studies on P450 inhibition by amidoximes, ketoximes, and N-hydroxy guanidines in human liver microsomes have had mechanisms proposed that involve formation of various ureas, NO·, and nitriles [36]. However, HET0016 is structurally different from all of these compounds, having an phenyl group on the amide nitrogen and a hydrogen on the oxime carbon. Perhaps the oxidation of N-methyl formamidoxime to form an isocyanate reactive species is an equally relevant P450 substrate to compare with HET0016 because of the presence of the formyl hydrogen atom and the amide N-hydrogen atom [37]. Following this line of reasoning, M5 might be reduced to an isocyanate, a potent electrophile, and inactivate CYP4A11 *via* this route, as depicted in Figure 3.20D.

Several potential mechanisms by which HET0016 inactivates CYP4A11 in an NADPH-dependent manner were considered. Firstly, dehydrogenation of the oxime moiety of HET0016 would result in a nitroso compound (Figure 3.20C), which is a functional group known to form MICs [38]. However, in both reconstituted enzyme preparations and Supersomes HET0016 did not form an MIC with CYP4A11 or CYP3A4.

Second, the nature of the heme after inactivation was assessed. Upon extensive binding studies with HET0016 and CYP4A11 under aerobic and anaerobic conditions, it was clear that HET0016 could compete with CO for binding to the reduced enzyme, making it impossible to draw meaningful conclusions about the heme state from the data in Figure 3.11. Therefore, the condition of the heme was assessed by HPLC-UV/vis spectroscopy.

Unfortunately, extensive heme bleaching (>90%) was observed after only a 3 minute incubation with both CYP4A11 and CYP3A4. This is evident for CYP3A4 in Figure 3.13 by comparing the magnitude of the heme peak in panel B (without NADPH) and panel A (with NADPH). The remaining free heme in panel A comes entirely from cytochrome b5, while in panel B the heme peak is from both cytochrome b5 and CYP3A4. This was determined from injections of equivalent amounts of the pure enzyme standards and from injections of incubation mixtures without NADPH. Heme destruction and bleaching in reconstituted enzyme preparations has been previously documented [39], however it is difficult to assess the percent remaining heme after inactivation by an MBI. Column chromatography required 0.1% formic acid to be present in the mobile phase, therefore if a heme adduct was unstable at low pH, it would not have been detected. Additionally, it is conceivable that a heme or protein adduct (if formed) is stable when the protein is folded, but becomes unstable or is cleaved when the protein unfolds and the active site becomes solvent accessible. Regardless, this method of assessing the state of the heme is useful to detect a prominent heme adduct, as demonstrated by the control experiment with 1-ABT, but it is not very useful for assessing how much of the original heme remains after a P450 reaction involving HET0016 and NADPH.

Thirdly, the hemochromogen assay was used to assess the heme after inactivation.. This seemed to be most useful for evaluating the effect of HET0016 on the heme cofactor of CYP4A11. HET0016 plus NADPH in the enzyme incubation did not decrease the amount of heme measured by this assay any more than NADPH alone, and, since the heme was completely extracted from the protein, the tight-binding complications encountered when using the reduced-CO binding assay did not exist here. From these data, we concluded that HET0016 does not destroy the heme cofactor.

Next, we explored the possibility that the inhibitor was bound to the apo-protein after inactivation. A derivative of HET0016, n-propylphenyl formamidoxime, was synthesized was confirmed to be a time-and NADPH- dependent inhibitor of CYP4A11. This compound was then synthesized with a tritium radiolabel on the two hydrogen atoms on the phenyl ring *ortho* to the formamidoxime moiety. This derivative was chosen for ease and cost effectiveness of the radiolabel synthesis. The tritiated HET0016 derivative did not show that it was bound to CYP4A11 in an NADPH dependent way on an HPLC column or an SDS-PAGE gel. From these experiments it was concluded that either the protein adduct did not contain the phenyl ring (i.e. the radiolabel was

released), the protein adduct was unstable and hydrolyzed or otherwise cleaved once the protein unfolds, or there was no protein adduct. Because about half of the heme cofactor is covalently bound to the protein in this enzyme preparation of CYP4A11, it can be concluded that the same is true for a potential adduct to the heme cofactor.

Another conceivable mechanism of inactivation is formation of peroxynitrite and tyrosine nitration. This hypothetical mechanism would be consistent with inactivation that did not incorporated a tritium label when this HET0016 derivative was bound to heme or protein. The formamidoxime moiety of HET0016 is similar in structure to the nitric oxide releasing moiety of the nitric oxide synthase (NOS) enzyme substrate, N-hydroxy-arginine (NOHA). P450 enzymes can perform similar chemistry to NOS with some substrates [36], therefore we hypothesized that HET0016 may be releasing nitric oxide. $NO^{\cdot}$ reacts with superoxide to form peroxynitrite:

$NO + O_2^{-} \rightarrow ONOO^{-}$

An antibody developed to recognize proteins with nitrosotyrosine residues did immunoreact with peroxynitrite treated CYP4A11, however there was no evidence that HET0016 incubated with NADPH resulted in any nitrated tyrosines on the enzyme. $NO^{\cdot}$ was introduced chemically into the incubation mixture with DEANONOate as a positive control (Figure 3.19, lane 7). Thus, if the CYP4A11 reaction cycle was uncoupled and producing any significant amount of superoxide, there would be $NO^{\cdot}$ present to react with it and subsequently nitrate tyrosine residues. However, the antibody did not detect nitrotyrosines under these conditions, suggesting that CYP4A11 is perhaps not sufficiently uncoupled to make the amount of superoxide necessary to form peroxynitrite, or that the necessary tyrosine residue is not accessible to peroxynitrite in this situation. These conjectures would of course need to be further explored.

HET0016 derivatives 4, 8, 10 and 11 were tested for TDI of CYP4A11 and provided some insight into the inactivation mechanism of CYP4A11 by HET0016. Figure 3.20 depicts possible reaction pathways that could lead to the observed time- and NADPH-dependent inhibition of CYP4A11 by HET0016. Pathway A leads to formation of an imine-methide, a reaction previously been shown to occur with some P450 MBIs [40]. Pathway B leads to the formation of a benzyl radical, which has been shown to cause heme adduct formation with gemfibrozil [41]. Compounds 4 and 8 both displayed TDI of CYP4A11, thus pathways A and B in Figure 3.20 were deemed unlikely. However, a reactive aldehyde metabolite on the alkyl chain has not been ruled out, although it seems improbable. Both compounds 10 and 11 did not display TDI of CYP4A11. That is to say,

methylation of HET0016 on either the formamidoxime carbon or the formamidoxime oxygen atoms rescues TDI of CYP4A11. These data do not support pathways D and E because a carbodiimide or an isocyanate could not be formed if the formamidoxime carbon is methylated. However, it must be noted that these methylated derivatives of HET0016 may alter the conformation/binding mode of the molecule in the enzyme active site; thus no firm conclusions can be made. Pathway E would require dehydration of HET0016, which is a non-oxidative process previously reported to occur with some P450 enzymes and benzaldoxime substrates [16]. Alternatively, pathway E' could form M3, followed by a dehydrogenation reaction that could lead to a carbodiimide reactive species. The putative M3 metabolite was the only one formed in an NADPH dependent fashion by CYP4A11 Supersomes. Carbodiimides are potent electrophiles and known amino acid crosslinking reagents. EDC (1-Ethyl-3-(3-dimethylaminopropyl)carbodiimide) is commonly used to activate carboxylic acids towards reactions with amines to form amide bonds [42] between glutamic acid residues and lysine residues. Thus, the reactive metabolite might inactivate CYP4A11 by this putative "hit-and-run" mechanism, leaving two active site residues cross-linked. One might also expect this pathway to result in a urea metabolite, which was not observed in incubations with CYP4A11, but is the putative M6 metabolite formed by human liver microsomes. A similar P450 dependent pathway resulting in an amide metabolite from the cyano guanidine compound, pinacidil, has been previously reported [43]. The very low partition ratio and efficient binding of any reactive species to CYP4A11 could be the reason it was undetected in CYP4A11 incubations and was not trapped by glutathione. It may be worthwhile to look for this metabolite in a purified, reconstituted preparation of CYP4A11 such that there is a smaller chance that the metabolite reacts with other nucleophiles in the reaction, such as other protein residues present in Supersomes. Alternatively, pathway D may lead to the formation of an electrophilic isocyanate species, which is equally well supported by these data.

In summary, the tight-binding aspect of HET0016 inhibition of CYP4A11 complicated much of the classic experiments one would perform to determine how an MBI inactivates a P450 enzyme and identify the reactive intermediate involved. Heme adducts, heme destruction, MIC formation, and apo-protein adduction of CYP4A11 were not observed upon metabolic incubation with HET0016 and NADPH. However, studies with HET0016 analogs and metabolite identification experiments lead us to speculate that either a carbodiimide or isocyanate is the reactive intermediate causing mechanism based inhibition of CYP4A11 by HET0016, resulting

in either an unstable, hydrolyzable heme or protein adduct or amino acid crosslinking in the CYP4A11 active site. Additional studies are needed to confirm these speculative scenarios.

Figure 3.1: Examples of marketed drugs that are mechanism-based inhibitors of P450 enzymes with well characterized reactive intermediates that illustrate the three main mechanisms of enzyme inactivation.

A) Metabolite-intermediate complex (MIC) formation

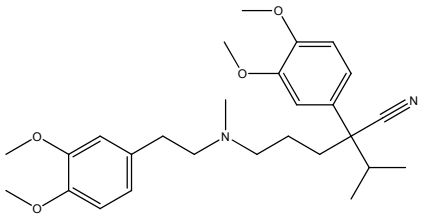

verapamil

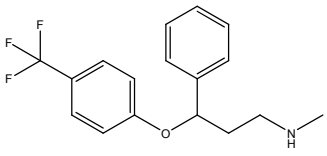

fluoxetine

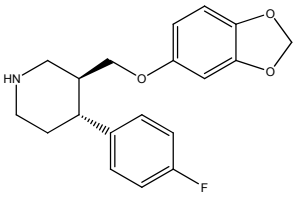

paroxetine

B) Protein adduct formation

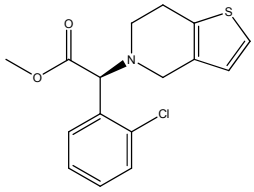

clopidogrel

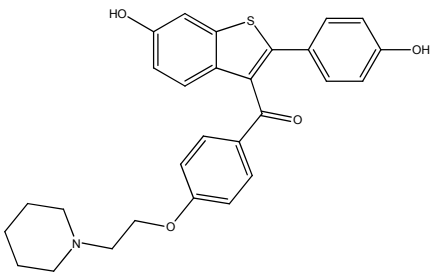

raloxifene

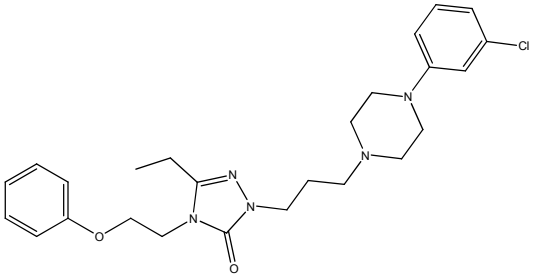

nefazadone

C) Heme adduct formation

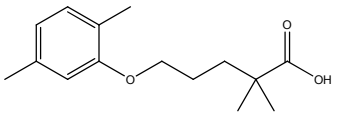

gemfibrozil

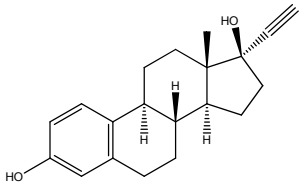

17-ethinyl estradiol

Figure 3.2: NADPH-dependent irreversibility of CYP4A11 inhibition by HET0016. Activity was not recovered after a preincubation with HET0016 (1 μM) + NADPH and subsequent dialysis to remove the non-covalently bound inhibitor. However, activity was recoverable when NADPH was omitted from the pre-incubation. The ABT reaction was included as a positive control for mechanism-based inhibition.

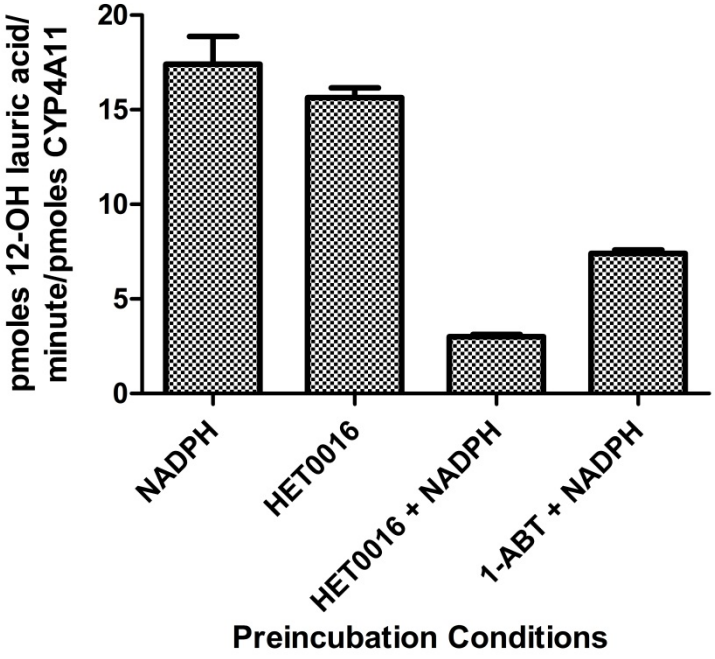

Figure 3.3: (A) Time-dependent and NADPH-dependent inhibition of CYP4A11 Supersomes by HET0016. CYP4A11 Supersomes do not contain cytochrome b5. Each curve is normalized to its own zero minute time point to account for any residual competitive inhibition in the secondary incubation. Rates at 100% remaining activity (ln=4.6) for NADPH only, HET0016 (100 nM) only, and HET0016 (100 nM) +NADPH curves are 25.0 ± 1.9 min^{-1}, 17.9 ± 2.4 min^{-1}, and 14.8 ± 1.9 min^{-1}, respectively. (B) Time and NADPH-dependent inhibition of reconstituted CYP4A11 by HET0016 (200 nM). The P450:reductase:b5 molar ratio is 1:2:1. Rates ate 100% remaining activity (ln=4.6) for NADPH only, HET0016 only (1 μM), and HET0016 (200 nM) +NADPH curves are 30.1 ± 3.1 min^{-1}, 8.4 ± 1.4 min^{-1}, and 16.1 ± 1.5 min^{-1}, respectively.

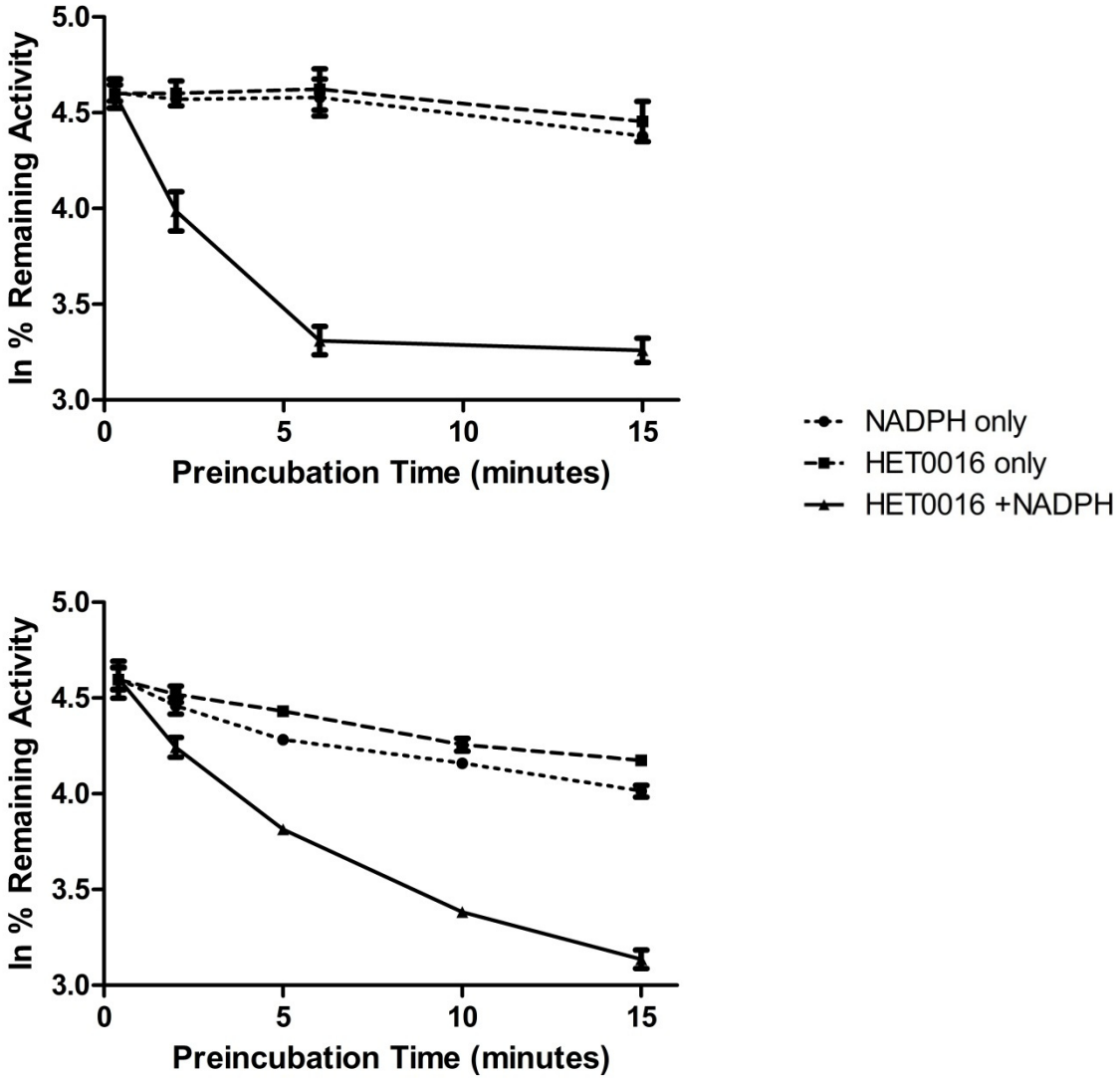

Figure 3.4: Effect of trapping agents, superoxide dismutase, and catalase on the time-dependent inhibition of CYP4A11 by HET0016. Exogenous nucleophiles and radical scavenging enzymes do not appear to affect the inactivation rate.

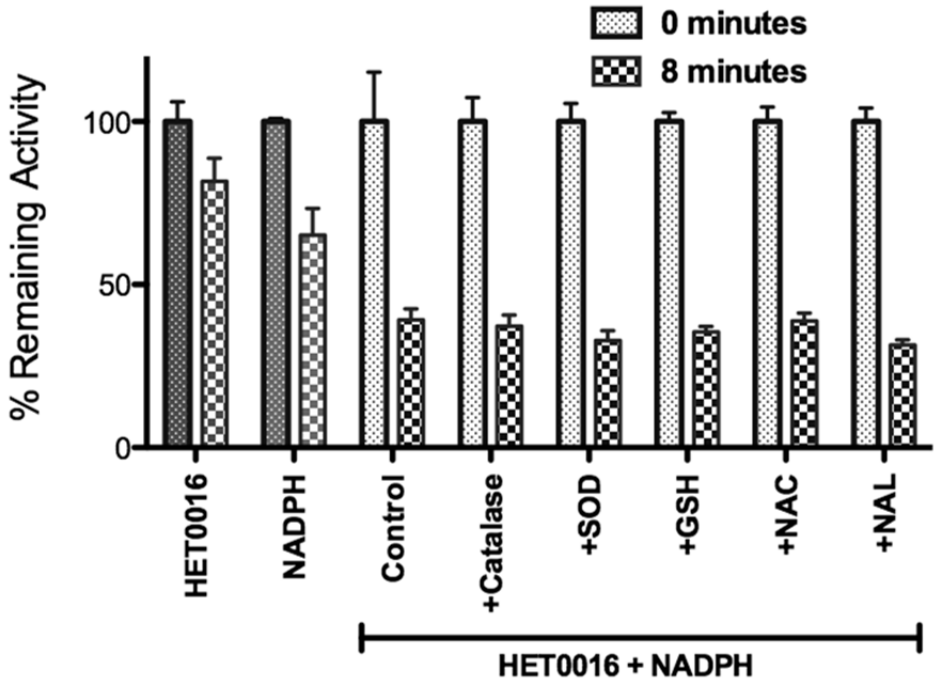

Figure 3.5: Lack of time-dependent or NADPH-dependent inhibition of: A) CYP4F3B, B) CYP4F12 and C) CYP4B1 by HET0016. Black, HET0016 + NADPH included in pre-incubation; Dark grey, NADPH only included in pre-incubation; Light grey, HET0016 only included in pre-incubation. HET0016 concentration was 120 nM for CYP4F3B and CYP4B1 and 750 nM for CYP4F12. Each curve is normalized to its own zero minute time point to account for residual competitive inhibition in the secondary incubation. Rates at 100% remaining activity are as follows: CYP4F3B, 8.3 ± 0.9 min^{-1} (Dark grey), 1.6 ± 0.2 min^{-1} (Light grey), and 2.4 ± 0.4 min^{-1} (Black); CYP4F12, 5.4 ± 0.2 min^{-1} (Dark grey), 4.7 ± 0.2 min^{-1} (Light grey), and 4.4 ± 0.5 min^{-1} (Black); CYP4B1, 24.9 ± 0.3 min^{-1} (Dark grey), 11.8 ± 1.1 min^{-1} (Light grey), and 12.7 ± 1.0 min^{-1} (Black).

A) CYP4F3B

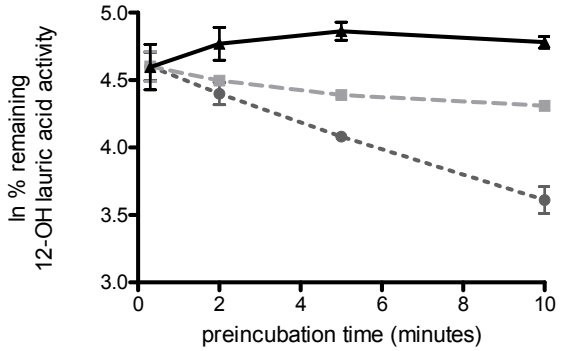

B) CYP4F12

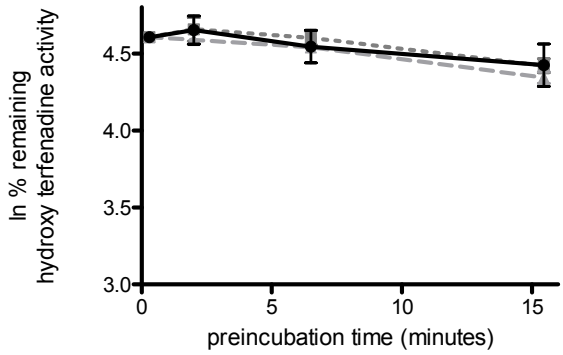

C) CYP4B1

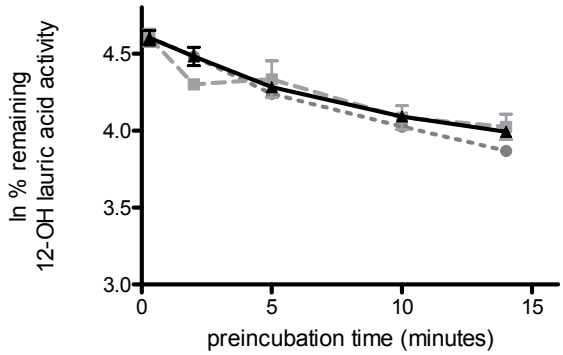

Figure 3.6: KI, kinact, and partition ratio for HET0016 inactivation of CYP4A11. K_I= 38 nM and a k_{inact}= 0.4 min^{-1}, partion ratio= 2.2.

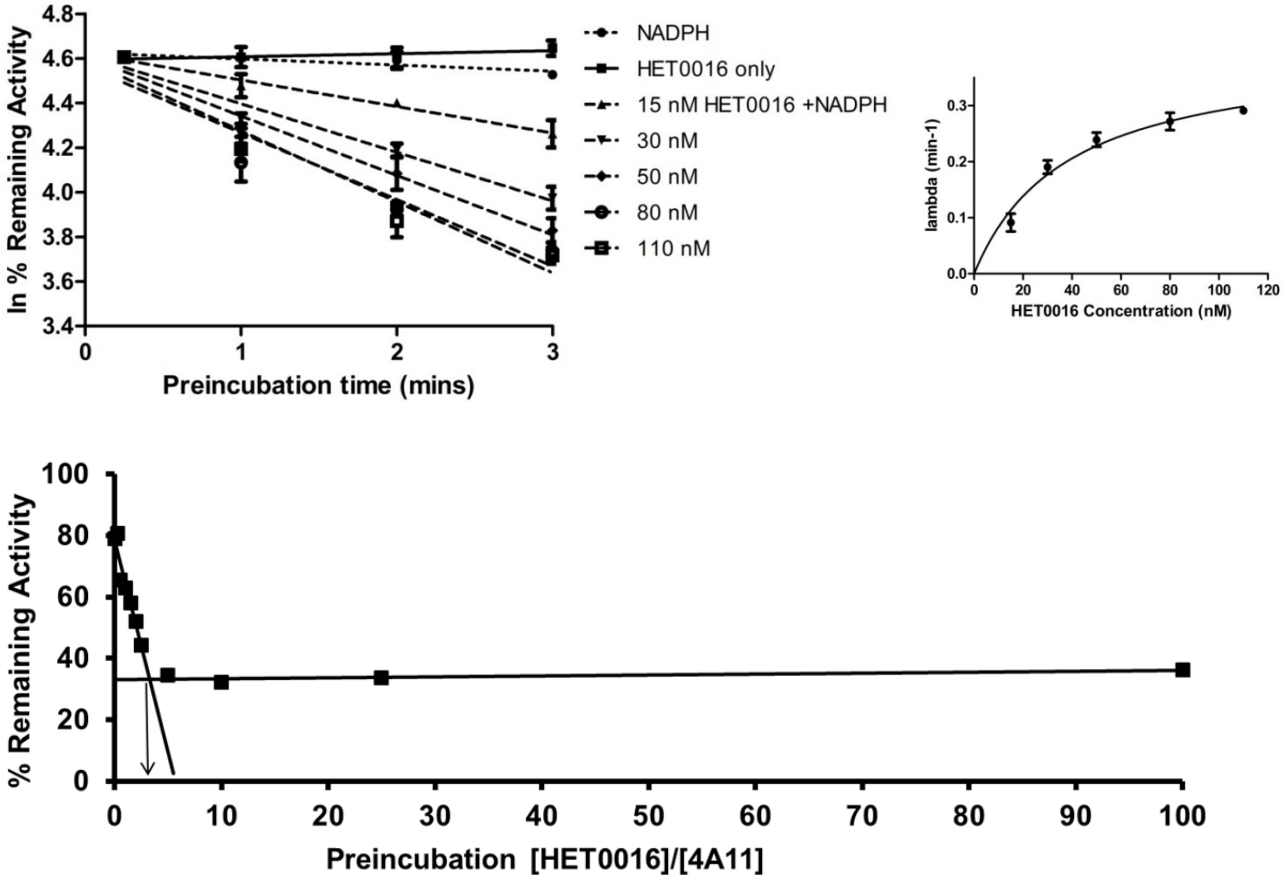

Figure 3.7: Common fragment ions of HET0016 and its metabolites

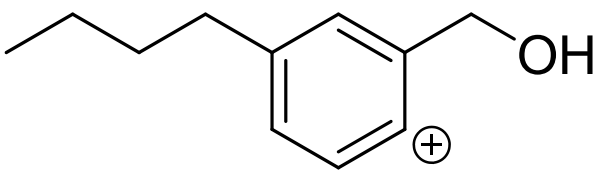

Exact Mass: 163.11

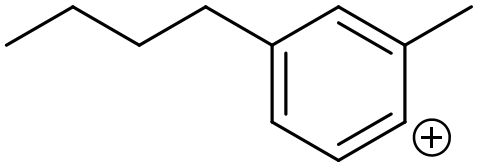

Exact Mass: 147.12

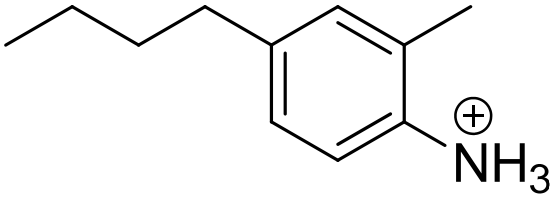

Exact Mass: 164.14

Figure 3.8: Putative HET0016 NADPH dependent metabolites produced in human liver microsomes

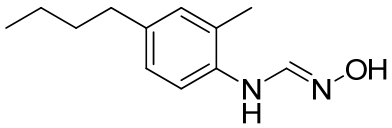

HET0016
m/z = 207
RT= 6.8 minutes

M1
m/z 223
RT= 4.4 minutes

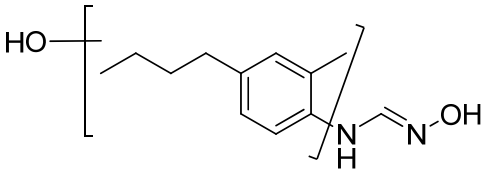

M2
m/z 223
RT= 4.9 minutes

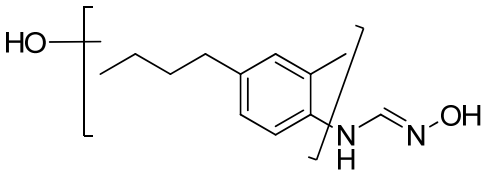

M3
m/z 191
RT= 5.2 minutes

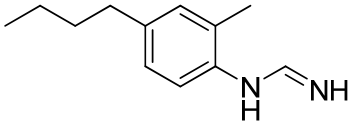

M4
m/z 164
RT= 5.7 minutes

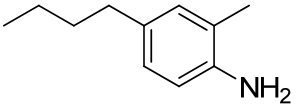

M5
m/z 192
RT= 6.5 minutes

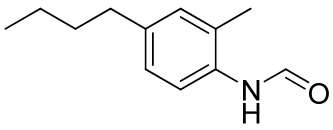

M6
m/z 207
RT= 2.7 minutes

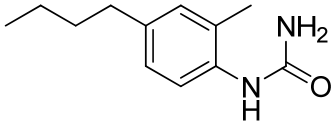

Figure 3.9: Chromatograms from HET0016 metabolic incubations with HLMs, CYP3A4, CYP4A11, and CYP4F3B Supersomes. Peaks marked with a star are not NADPH dependent. MRM channels: Red 223.0>163.0; Green 191.0>164.0; Light blue 164.1>107.9; Grey 192.1>135.8; Royal blue 207.0>147.0. All chromatograms are equally scaled.

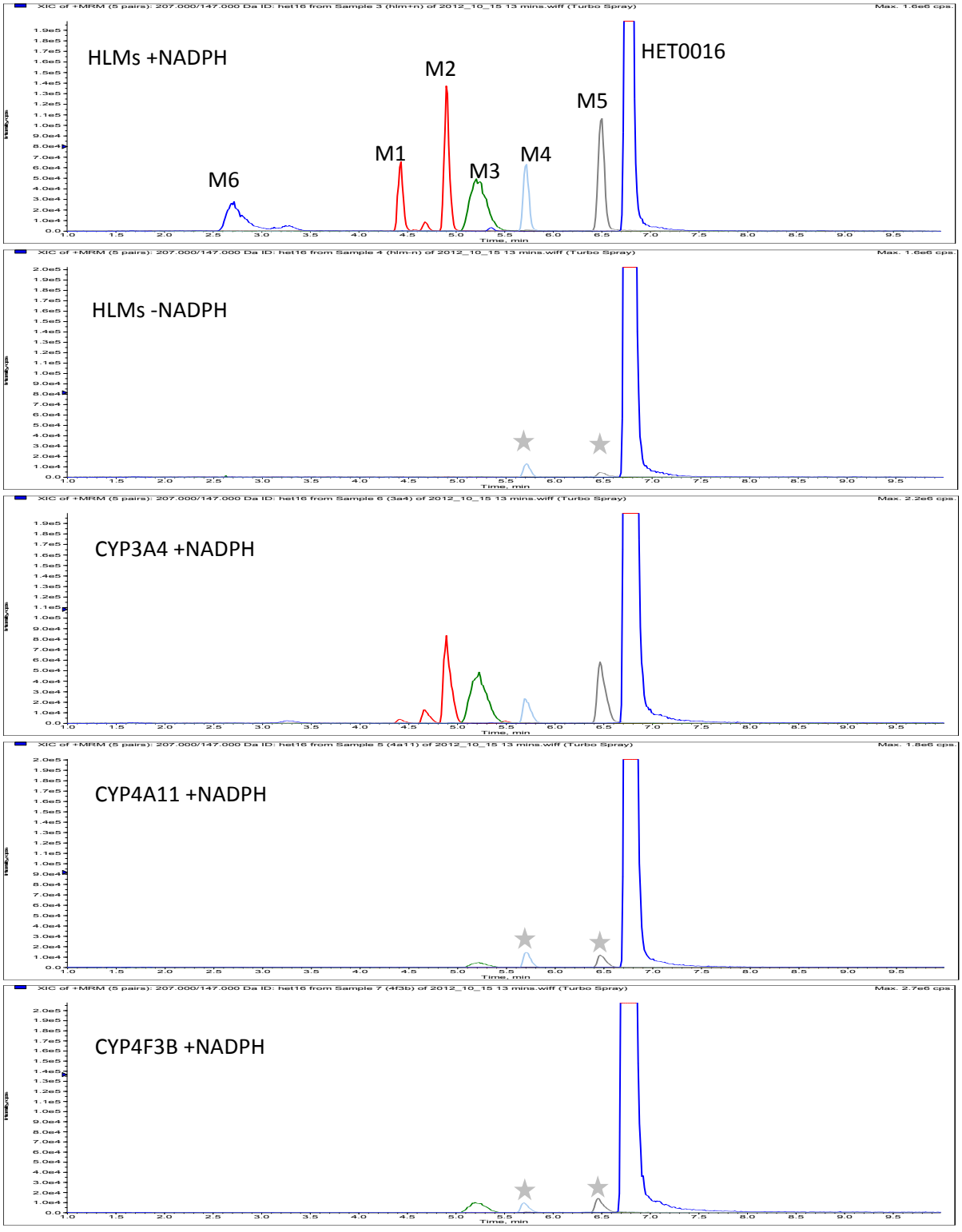

Figure 3.10: A) Lack of MI-complex formation with HET0016 and CYP4A11 Supersomes. B) Lack of MI-complex with HET0016 and reconstituted CYP4A11. C) Positive control MI-complex formation with N-hydroxy fluoxetine and CYP3A4 Supersomes.

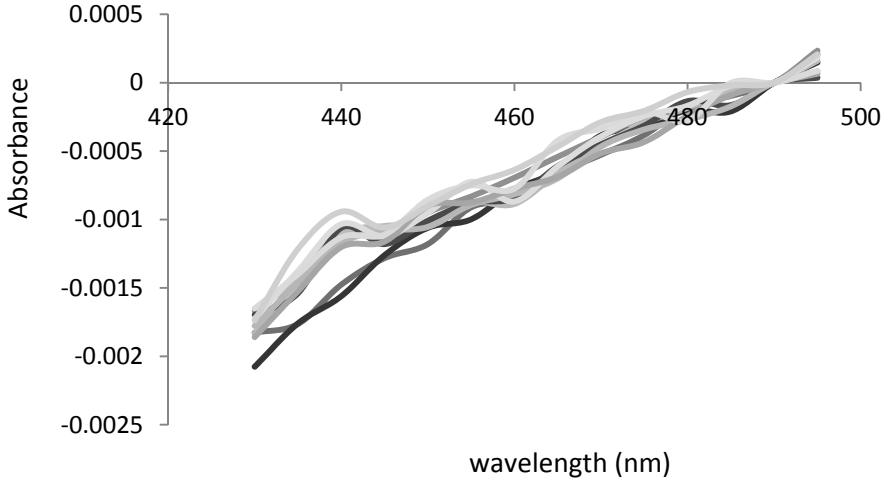

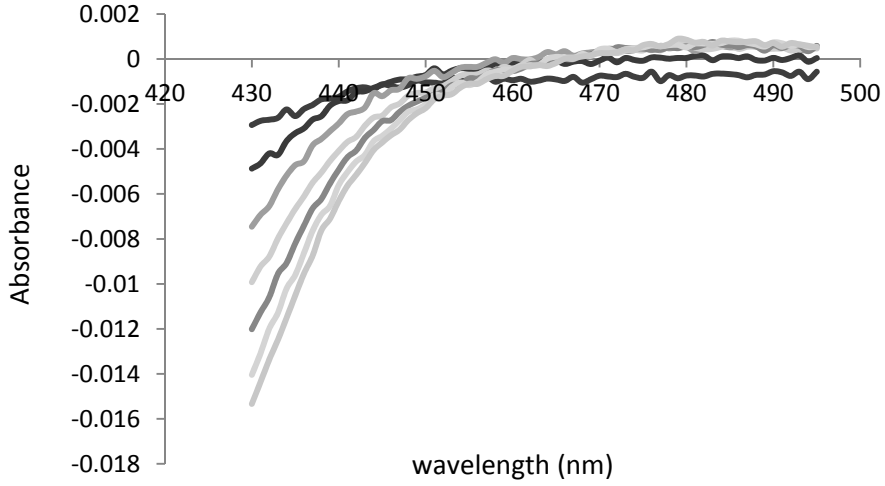

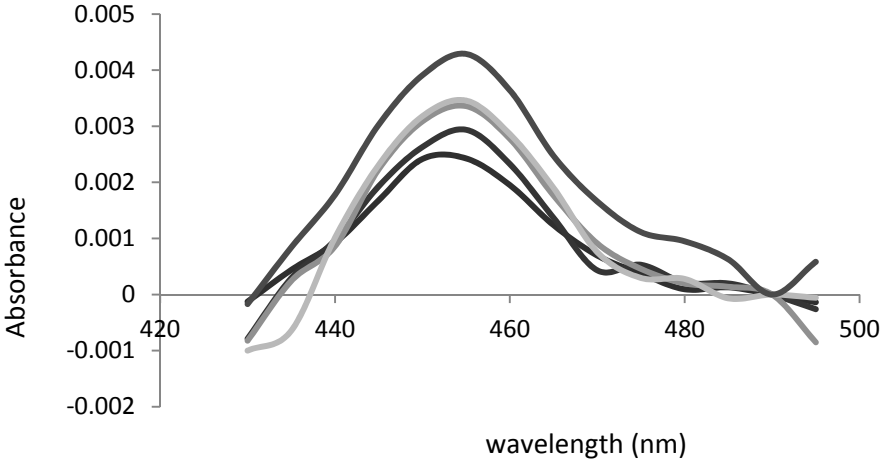

Figure 3.11: Reduced-CO binding spectra of CYP4A11 after inactivation by HET0016. Fe^{+2}-CO concentrations were: black (0.14 μM), dotted (0.14 μM), dark grey (0.05 μM), light grey (< 0.01 μM).

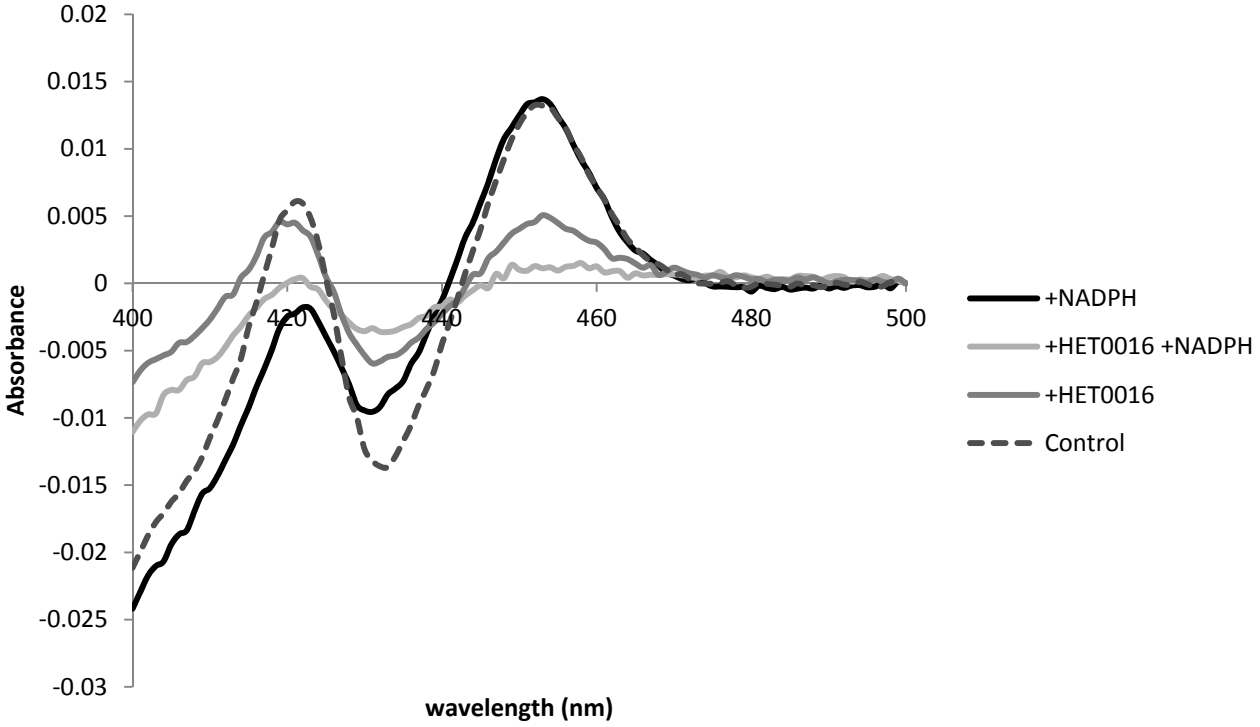

Figure 3.12: Absolute spectra of: A) CYP3A4 bound to ritonavir, B) CYP4A11 bound to HET0016. Black trace, ferric (Fe+3) protein; green trace, ferrous (Fe^{+2}) protein; purple trace, addition of ligand; red trace, addition of carbon monoxide. C) Difference spectra of reduced CYP4A11 bound to HET0016 immediately after HET0016 is added (purple) and after 1 minute has passed after HET0016 is added.

A)

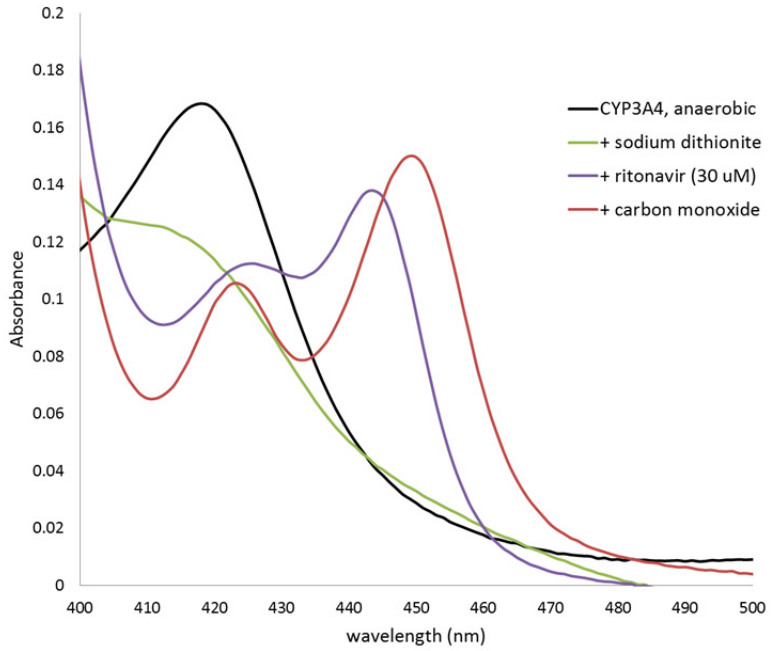

B)

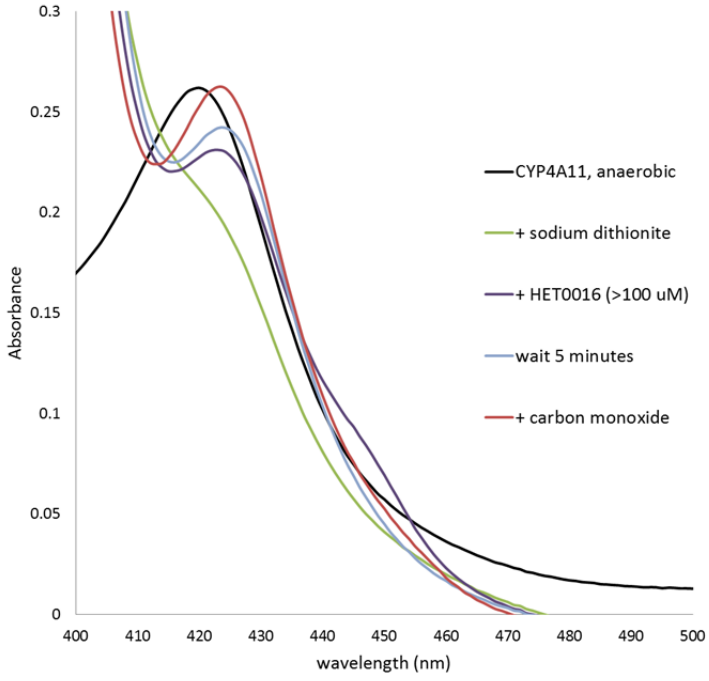

C)

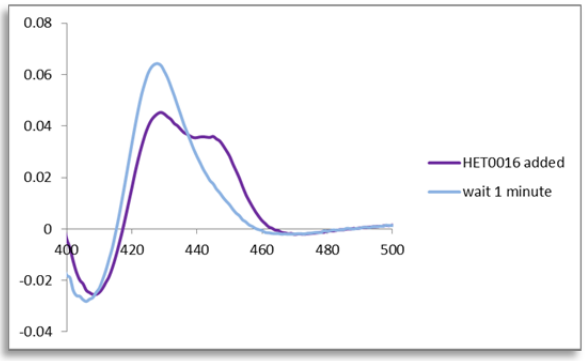

Figure 3.13: Heme adducts of CYP3A4 after incubation with 1-aminobenzotriazole (ABT) and chromatographic separation of incubation components on a R2 Poros HPLC column. Blue trace, 400 nm; Purple trace, 280 nm. A) +NADPH, B) –NADPH. Labels indicate P450 oxidoreductase (POR), Cytochrome b5 (B5), and CYP3A4 (3A4).

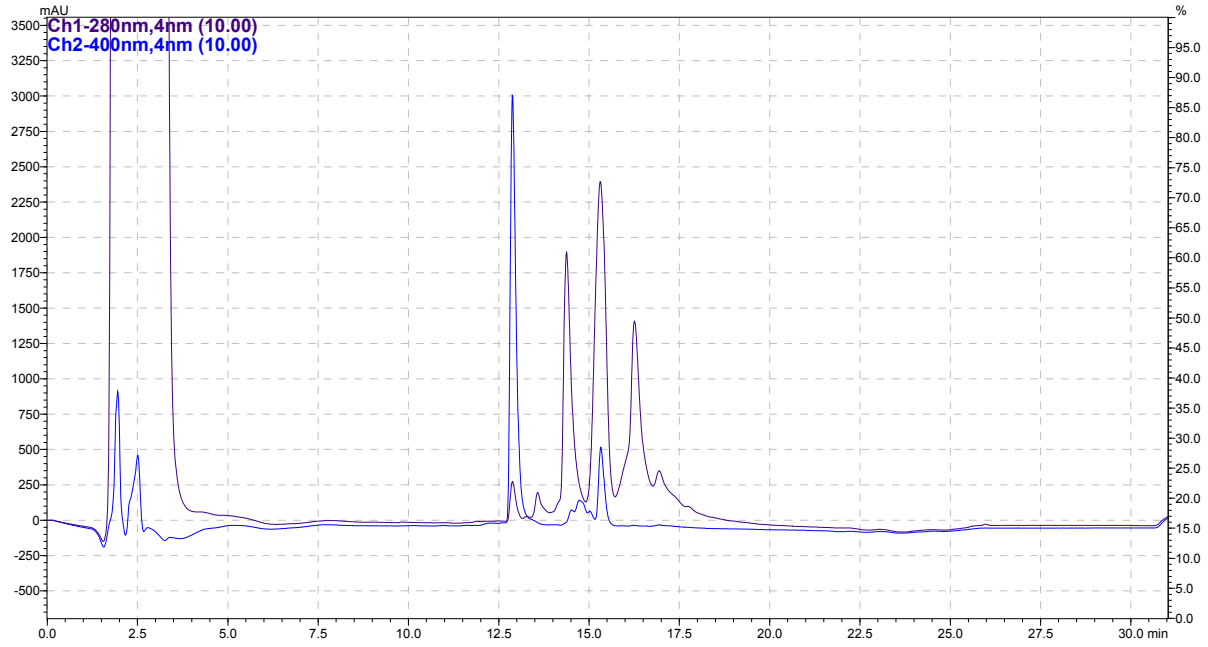

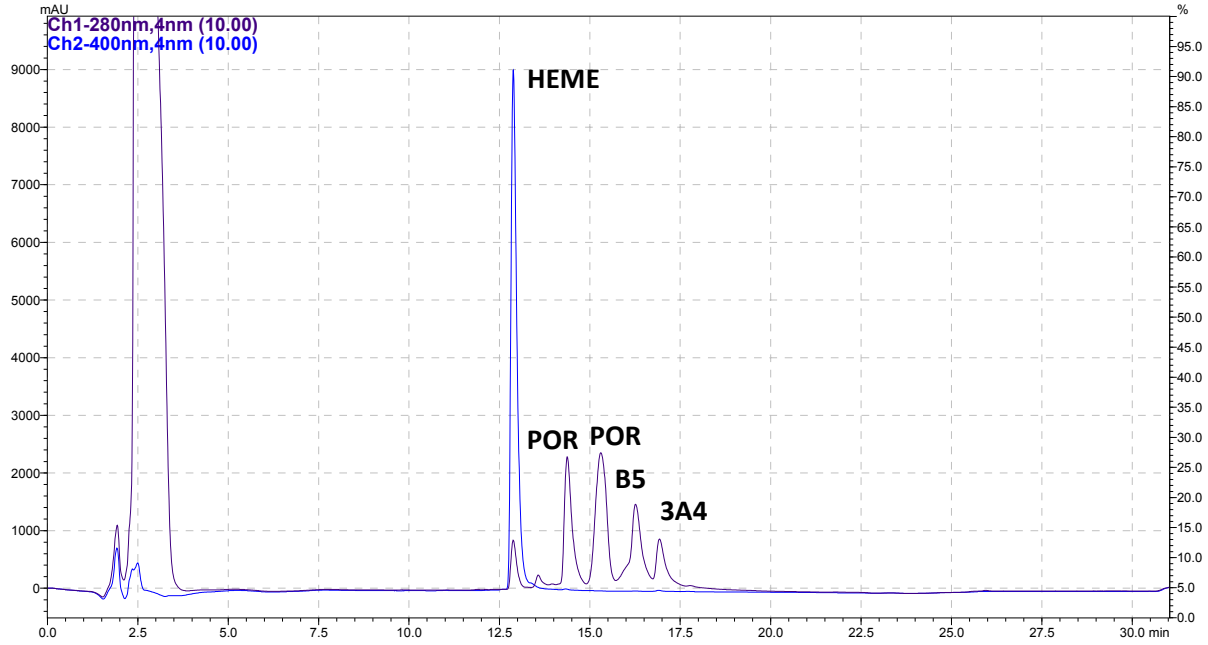

Figure 3.14 Lack of heme adducts of CYP4A11 after incubation with HET0016 and chromatographic separation of incubation components on a R2 Poros HPLC column. Blue trace, 400 nm; Purple trace, 280 nm. A) – HET0016, +NADPH B) +HET0016 +NADPH C) +HET0016 -NADPH.

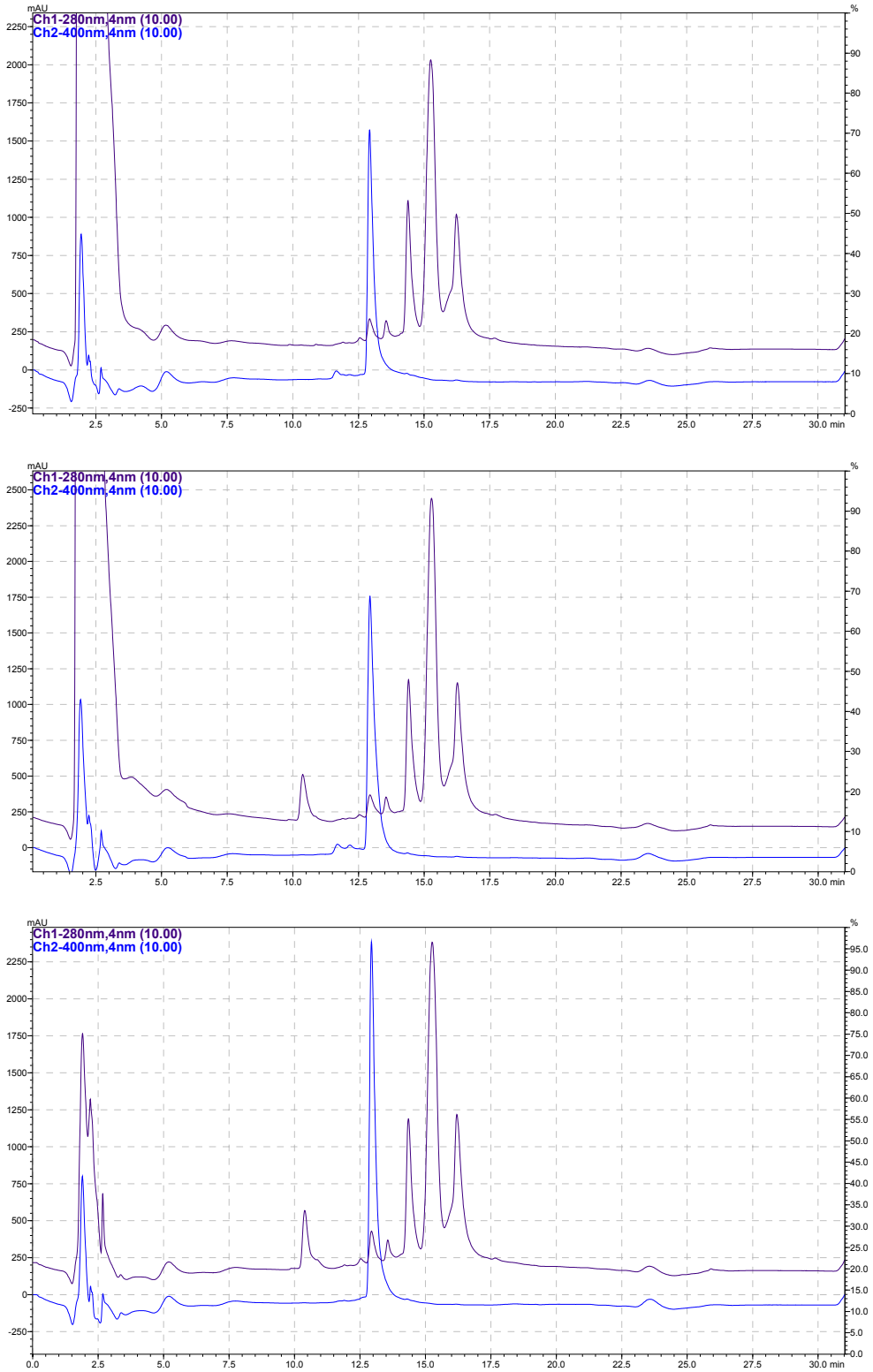

Figure 3.15: Heme content of CYP4A11 after inactivation by HET0016, as measured by the hemochromogen assay.

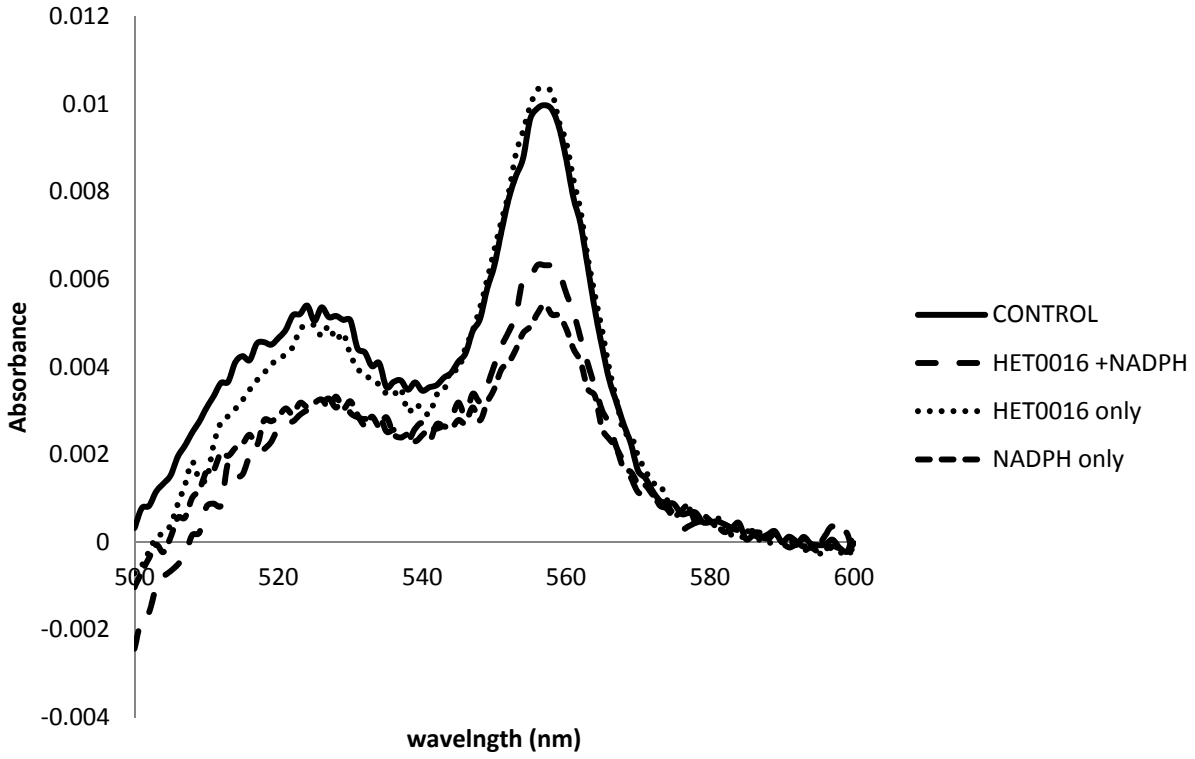

Incubation Conditions	Heme (μM)
CONTROL	0.31
HET0016 + NADPH	0.20
HET0016 only	0.32
NADPH only	0.17

Figure 3.16: Lack of ^{3}H-phenylpropyl FAO binding to CYP4A11 after inactivation by this HET0016 derivative. A) Synthetic scheme of tritiated (*H) n-propylphenyl formamidoxime. B) HPLC chromatogram of CYP4A11 after inactivation by tritiated n-propylphenyl formamidoxime monitoring protein at 280 nm and heme at 400 nm. C) Radioactivity of fractions collected from B. The small peak at 23 minutes was the same intensity for the –NADPH and +NADPH incubations.

A)

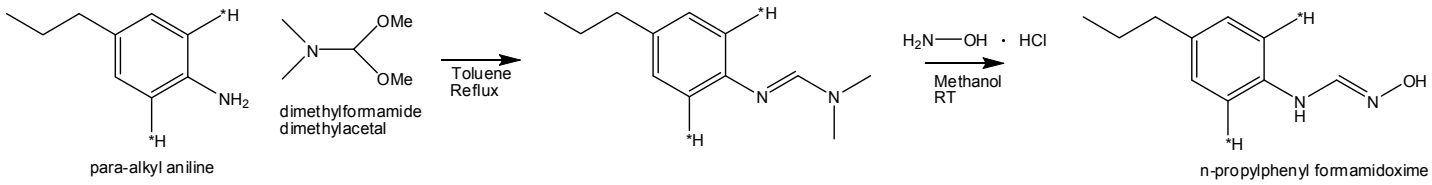

B)

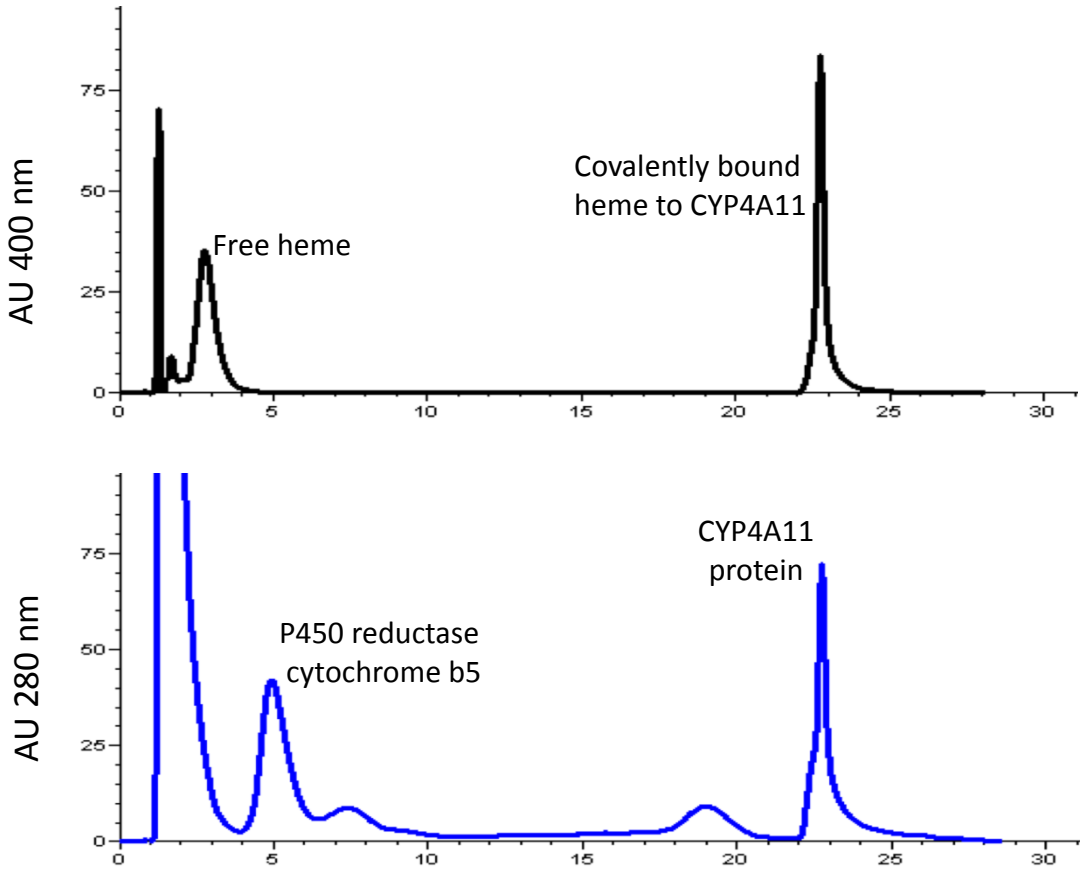

C)

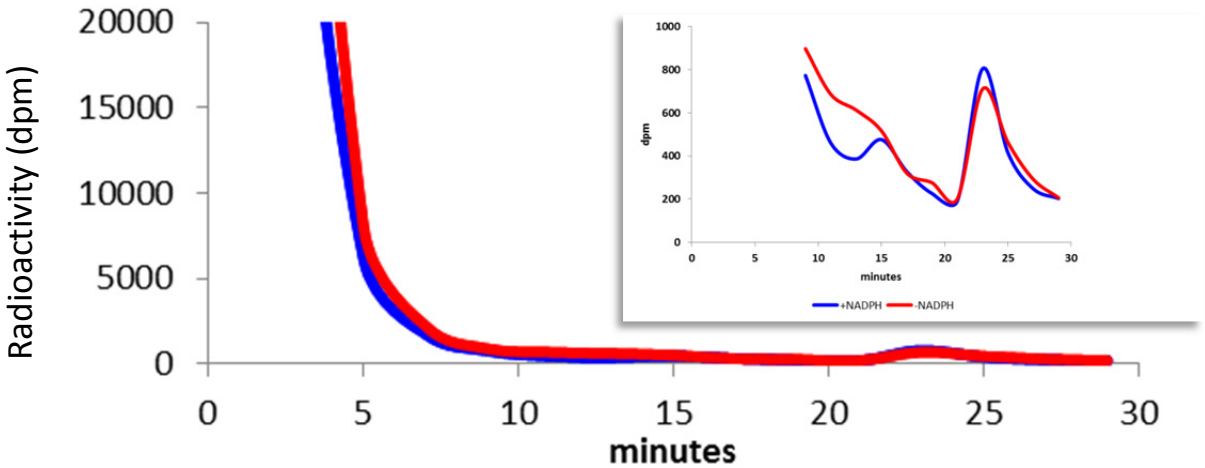

Figure 3.17: Time dependent inhibition curves of CYP4A11 by formamidoxime derivatives derivatives. Light gray curves are the –NADPH controls.

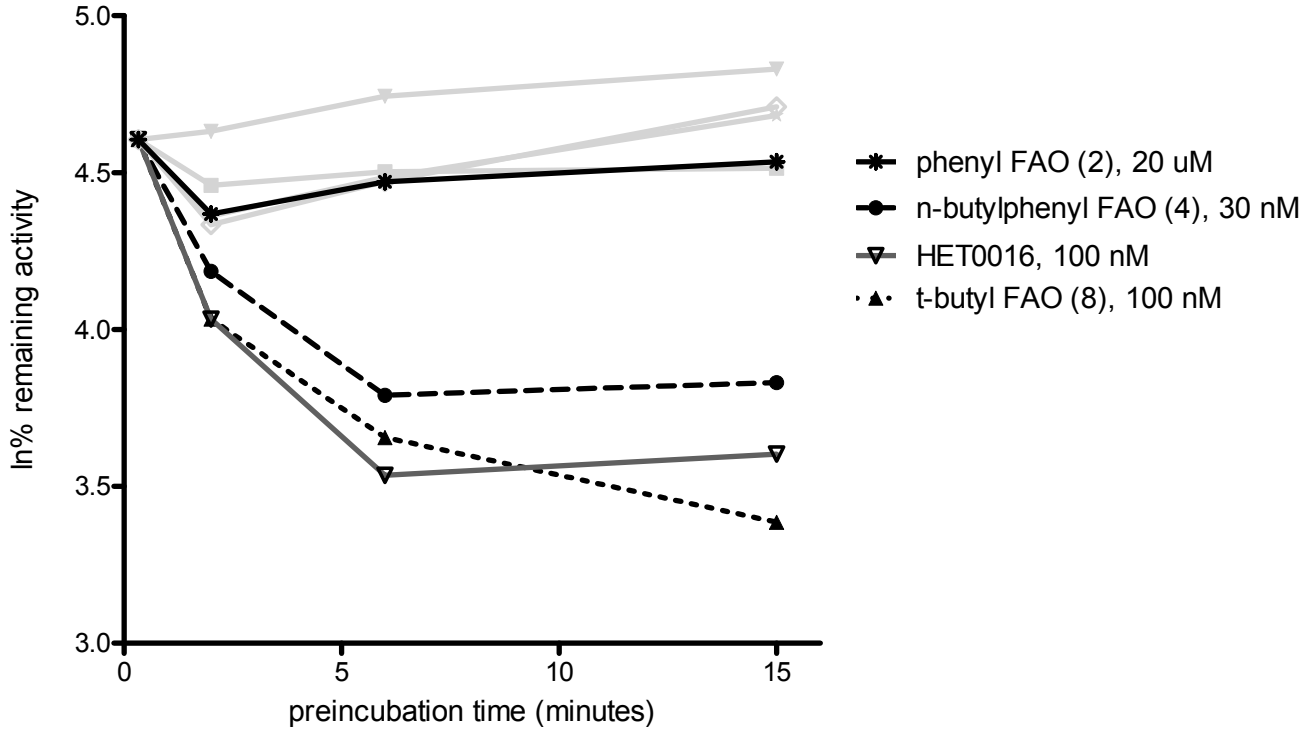

Figure 3.18: Time dependent inhibition curves for: A) compound 10, a methoxyformimidamide (MFIA) derivative, and B) compound 11, an acetamidoxime (AAO) derivative.

A)

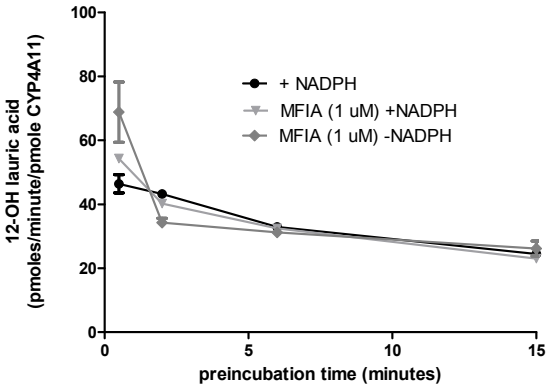

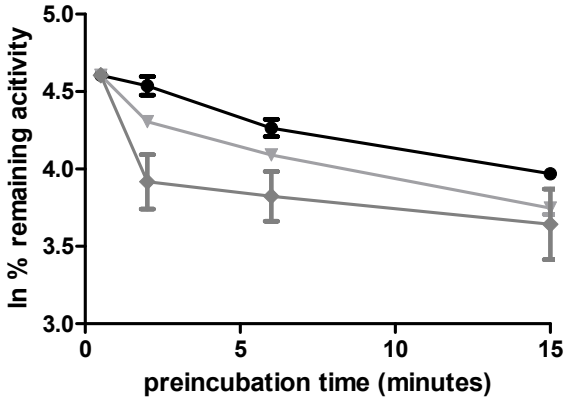

B)

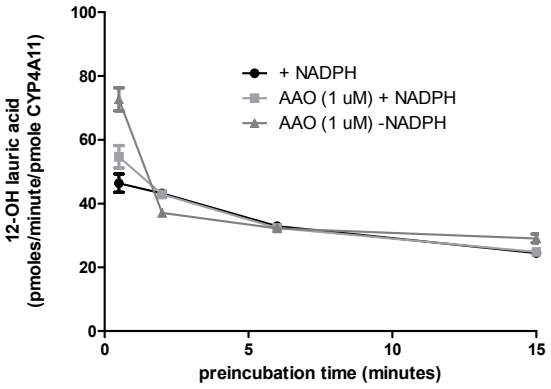

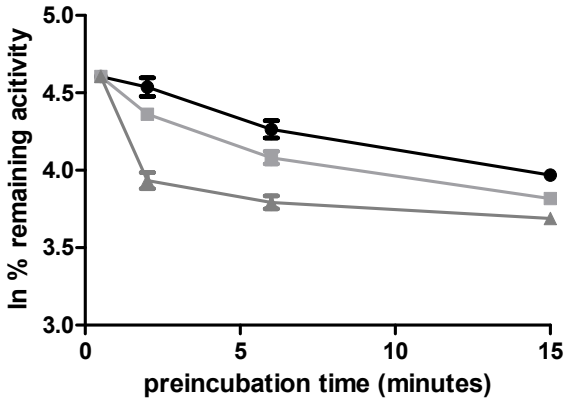

Figure 3.19: Lack of nitrated tyrosine residues on CYP4A11 after inactivation by HET0016. A) Coomasie stained gel of CYP4A11 incubation after inactivation by HET0016. B) Western blot of CYP4A11 incubation after inactivation by HET0016 with primary 3-Nitrotyrosine LSH Antibody. Peroxynitrite was 160 μM

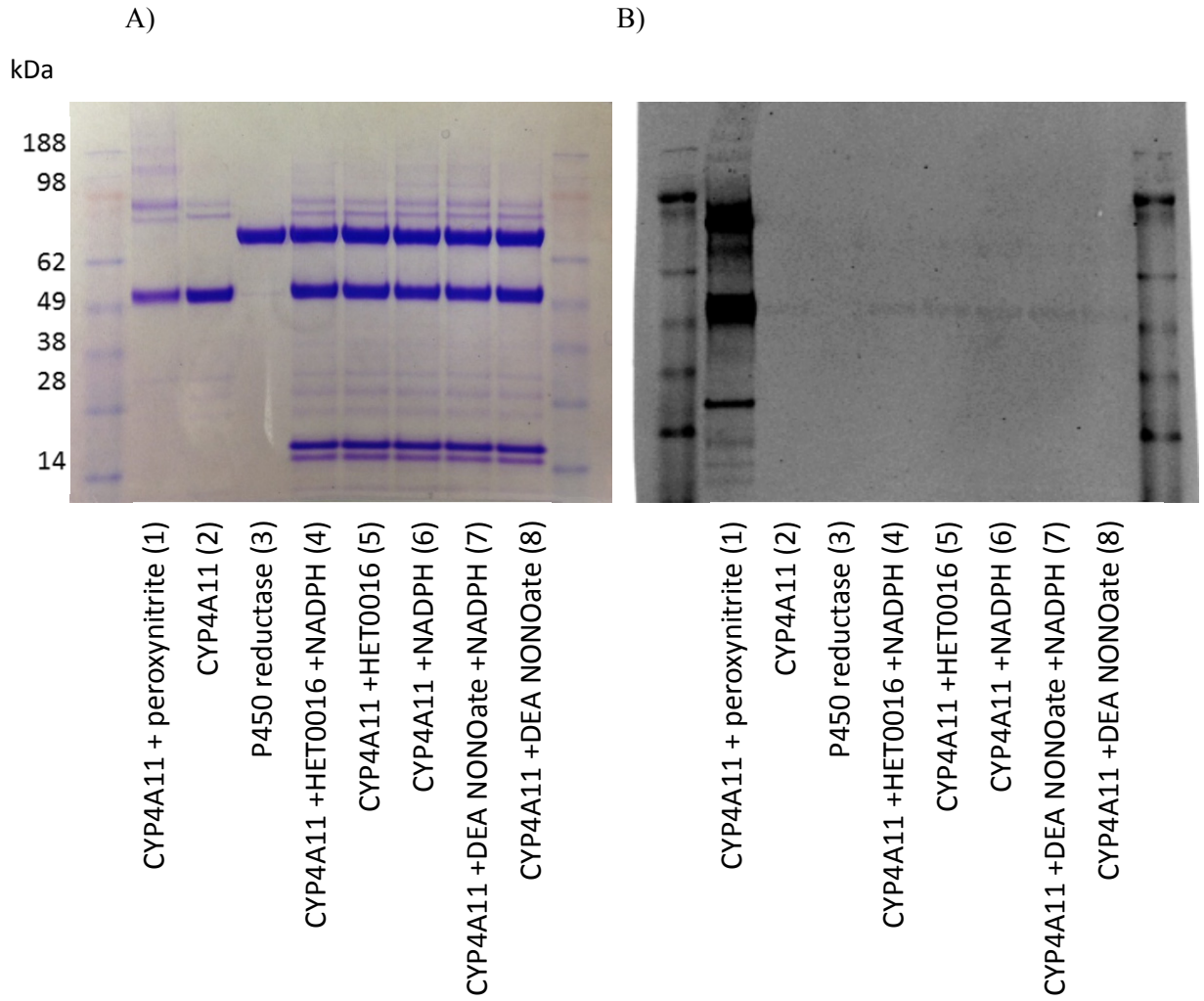

Figure 3.20: Potential reaction pathways leading to a reactive species responsible for CYP4A11 inactivation.

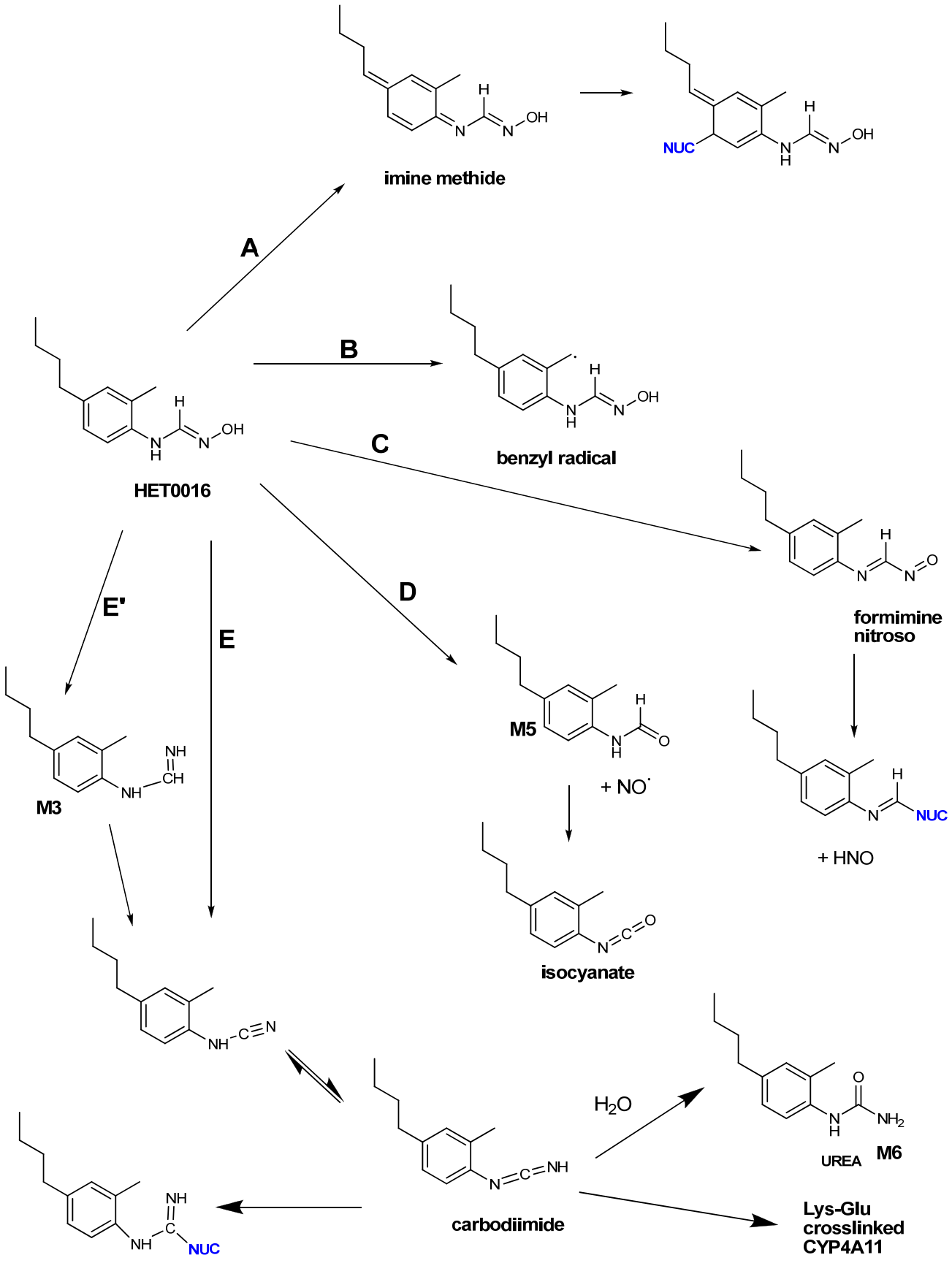

3.5 References

[1] VandenBrink, B.M.; Isoherranen, N., The role of metabolites in predicting drug-drug interactions: focus on irreversible cytochrome P450 inhibition. *Curr Opin Drug Discov Devel,* 2010, *13*(1), 66-77.
[2] Hollenberg, P.F.; Kent, U.M.; Bumpus, N.N., Mechanism-based inactivation of human cytochromes p450s: experimental characterization, reactive intermediates, and clinical implications. *Chem Res Toxicol,* 2008, *21*(1), 189-205.
[3] C.W., H., Formylation of Amines. *Journal of Organic Chemistry,* 1958, *23*, 727.
[4] Koppenol, W.H.; Moreno, J.J.; Pryor, W.A.; Ischiropoulos, H.; Beckman, J.S., Peroxynitrite, a cloaked oxidant formed by nitric oxide and superoxide. *Chem Res Toxicol,* 1992, *5*(6), 834-842.
[5] Venkatakrishnan, K.; Obach, R.S.; Rostami-Hodjegan, A., Mechanism-based inactivation of human cytochrome P450 enzymes: strategies for diagnosis and drug-drug interaction risk assessment. *Xenobiotica,* 2007, *37*(10-11), 1225-1256.
[6] Briggs, G.E.; Haldane, J.B., A Note on the Kinetics of Enzyme Action. *Biochem J,* 1925, *19*(2), 338-339.
[7] Grimm, S.W.; Einolf, H.J.; Hall, S.D.; He, K.; Lim, H.K.; Ling, K.H.; Lu, C.; Nomeir, A.A.; Seibert, E.; Skordos, K.W.; Tonn, G.R.; Van Horn, R.; Wang, R.W.; Wong, Y.N.; Yang, T.J.; Obach, R.S., The conduct of in vitro studies to address time-dependent inhibition of drug-metabolizing enzymes: a perspective of the pharmaceutical research and manufacturers of America. *Drug Metab Dispos,* 2009, *37*(7), 1355-1370.
[8] Silverman, R.B., Mechanism-based enzyme inactivators. *Methods Enzymol,* 1995, *249*, 240-283.
[9] Kunze, K.L.; Trager, W.F., Isoform-selective mechanism-based inhibition of human cytochrome P450 1A2 by furafylline. *Chem Res Toxicol,* 1993, *6*(5), 649-656.
[10] Kassahun, K.; Davis, M.; Hu, P.; Martin, B.; Baillie, T., Biotransformation of the naturally occurring isothiocyanate sulforaphane in the rat: identification of phase I metabolites and glutathione conjugates. *Chem Res Toxicol,* 1997, *10*(11), 1228-1233.
[11] Baillie, T.A.; Davis, M.R., Mass spectrometry in the analysis of glutathione conjugates. *Biol Mass Spectrom,* 1993, *22*(6), 319-325.
[12] Kellert, M.; Wagner, S.; Lutz, U.; Lutz, W.K., Biomarkers of furan exposure by metabolic profiling of rat urine with liquid chromatography-tandem mass spectrometry and principal component analysis. *Chem Res Toxicol,* 2008, *21*(3), 761-768.
[13] Lin, H.L.; Kent, U.M.; Hollenberg, P.F., Mechanism-based inactivation of cytochrome P450 3A4 by 17 alpha-ethynylestradiol: evidence for heme destruction and covalent binding to protein. *J Pharmacol Exp Ther,* 2002, *301*(1), 160-167.
[14] Lin, H.L.; Kent, U.M.; Hollenberg, P.F., The grapefruit juice effect is not limited to cytochrome P450 (P450) 3A4: evidence for bergamottin-dependent inactivation, heme destruction, and covalent binding to protein in P450s 2B6 and 3A5. *J Pharmacol Exp Ther,* 2005, *313*(1), 154-164.
[15] Koenigs, L.L.; Peter, R.M.; Hunter, A.P.; Haining, R.L.; Rettie, A.E.; Friedberg, T.; Pritchard, M.P.; Shou, M.; Rushmore, T.H.; Trager, W.F., Electrospray ionization mass spectrometric analysis of intact cytochrome P450: identification of tienilic acid adducts to P450 2C9. *Biochemistry,* 1999, *38*(8), 2312-2319.
[16] Boucher, J.L.; Delaforge, M.; Mansuy, D., Dehydration of alkyl- and arylaldoximes as a new cytochrome P450-catalyzed reaction: mechanism and stereochemical characteristics. *Biochemistry,* 1994, *33*(25), 7811-7818.
[17] Ortiz de Montellano, P.R.; Mathews, J.M., Autocatalytic alkylation of the cytochrome P-450 prosthetic haem group by 1-aminobenzotriazole. Isolation of an NN-bridged benzyne-protoporphyrin IX adduct. *Biochem J,* 1981, *195*(3), 761-764.
[18] Baer, B.R.; Wienkers, L.C.; Rock, D.A., Time-dependent inactivation of P450 3A4 by raloxifene: identification of Cys239 as the site of apoprotein alkylation. *Chem Res Toxicol,* 2007, *20*(6), 954-964.
[19] Hutzler, J.M.; Steenwyk, R.C.; Smith, E.B.; Walker, G.S.; Wienkers, L.C., Mechanism-based inactivation of cytochrome P450 2D6 by 1-[(2-ethyl-4-methyl-1H-imidazol-5-yl)methyl]- 4-[4-(trifluoromethyl)-2-pyridinyl]piperazine: kinetic characterization and evidence for apoprotein adduction. *Chem Res Toxicol,* 2004, *17*(2), 174-184.
[20] Regal, K.A.; Schrag, M.L.; Kent, U.M.; Wienkers, L.C.; Hollenberg, P.F., Mechanism-based inactivation of cytochrome P450 2B1 by 7-ethynylcoumarin: verification of apo-P450 adduction by electrospray ion trap mass spectrometry. *Chem Res Toxicol,* 2000, *13*(4), 262-270.
[21] PR Ortiz de Montellano, J.M., KC Langry, Autocatalytic inactivation of cytochrome p-450 and chloroperoxidase by 1-aminobenzotriazole and other aryne precursors. *Tetrahedron,* 1984, *40*(3), 511-519.

[22] Henne, K.R.; Kunze, K.L.; Zheng, Y.M.; Christmas, P.; Soberman, R.J.; Rettie, A.E., Covalent linkage of prosthetic heme to CYP4 family P450 enzymes. *Biochemistry,* 2001, *40*(43), 12925-12931.
[23] Halpert, J.; Neal, R.A., Inactivation of purified rat liver cytochrome P-450 by chloramphenicol. *Mol Pharmacol,* 1980, *17*(3), 427-431.
[24] Baer, B.R.; Schuman, J.T.; Campbell, A.P.; Cheesman, M.J.; Nakano, M.; Moguilevsky, N.; Kunze, K.L.; Rettie, A.E., Sites of covalent attachment of CYP4 enzymes to heme: evidence for microheterogeneity of P450 heme orientation. *Biochemistry,* 2005, *44*(42), 13914-13920.
[25] Zheng, Y.M.; Baer, B.R.; Kneller, M.B.; Henne, K.R.; Kunze, K.L.; Rettie, A.E., Covalent heme binding to CYP4B1 via Glu310 and a carbocation porphyrin intermediate. *Biochemistry,* 2003, *42*(15), 4601-4606.
[26] Lin, H.L.; Myshkin, E.; Waskell, L.; Hollenberg, P.F., Peroxynitrite inactivation of human cytochrome P450s 2B6 and 2E1: heme modification and site-specific nitrotyrosine formation. *Chem Res Toxicol,* 2007, *20*(11), 1612-1622.
[27] Lin, H.L.; Zhang, H.; Waskell, L.; Hollenberg, P.F., The highly conserved Glu149 and Tyr190 residues contribute to peroxynitrite-mediated nitrotyrosine formation and the catalytic activity of cytochrome P450 2B1. *Chem Res Toxicol,* 2005, *18*(8), 1203-1210.
[28] Lin, H.L.; Kent, U.M.; Zhang, H.; Waskell, L.; Hollenberg, P.F., Mutation of tyrosine 190 to alanine eliminates the inactivation of cytochrome P450 2B1 by peroxynitrite. *Chem Res Toxicol,* 2003, *16*(2), 129-136.
[29] Keefer, L.K.; Nims, R.W.; Davies, K.M.; Wink, D.A., "NONOates" (1-substituted diazen-1-ium-1,2-diolates) as nitric oxide donors: convenient nitric oxide dosage forms. *Methods Enzymol,* 1996, *268*, 281-293.
[30] Maragos, C.M.; Morley, D.; Wink, D.A.; Dunams, T.M.; Saavedra, J.E.; Hoffman, A.; Bove, A.A.; Isaac, L.; Hrabie, J.A.; Keefer, L.K., Complexes of .NO with nucleophiles as agents for the controlled biological release of nitric oxide. Vasorelaxant effects. *J Med Chem,* 1991, *34*(11), 3242-3247.
[31] Peng, H.M.; Morishima, Y.; Clapp, K.M.; Lau, M.; Pratt, W.B.; Osawa, Y., Dynamic cycling with Hsp90 stabilizes neuronal nitric oxide synthase through calmodulin-dependent inhibition of ubiquitination. *Biochemistry,* 2009, *48*(35), 8483-8490.
[32] Mu, Y.; Klamerus, M.M.; Miller, T.M.; Rohan, L.C.; Graham, S.H.; Poloyac, S.M., Intravenous formulation of N-hydroxy-N'-(4-n-butyl-2-methylphenyl)formamidine (HET0016) for inhibition of rat brain 20-hydroxyeicosatetraenoic acid formation. *Drug Metab Dispos,* 2008, *36*(11), 2324-2330.
[33] Kunze, K.L.; Mangold, B.L.; Wheeler, C.; Beilan, H.S.; Ortiz de Montellano, P.R., The cytochrome P-450 active site. Regiospecificity of prosthetic heme alkylation by olefins and acetylenes. *J Biol Chem,* 1983, *258*(7), 4202-4207.
[34] Ortiz de Montellano, P.R.; Kunze, K.L.; Mico, B.A., Destruction of cytochrome P-450 by olefins: N-alkylation of prosthetic heme. *Mol Pharmacol,* 1980, *18*(3), 602-605.
[35] Chan, W.K.; Sui, Z.; Ortiz de Montellano, P.R., Determinants of protein modification versus heme alkylation: inactivation of cytochrome P450 1A1 by 1-ethynylpyrene and phenylacetylene. *Chem Res Toxicol,* 1993, *6*(1), 38-45.
[36] Jousserandot, A.; Boucher, J.L.; Henry, Y.; Niklaus, B.; Clement, B.; Mansuy, D., Microsomal cytochrome P450 dependent oxidation of N-hydroxyguanidines, amidoximes, and ketoximes: mechanism of the oxidative cleavage of their C=N(OH) bond with formation of nitrogen oxides. *Biochemistry,* 1998, *37*(49), 17179-17191.
[37] Hyland, R.; Gescher, A.; Thummel, K.; Schiller, C.; Jheeta, P.; Mynett, K.; Smith, A.W.; Mraz, J., Metabolic oxidation and toxification of N-methylformamide catalyzed by the cytochrome P450 isoenzyme CYP2E1. *Mol Pharmacol,* 1992, *41*(2), 259-266.
[38] Hanson, K.L.; VandenBrink, B.M.; Babu, K.N.; Allen, K.E.; Nelson, W.L.; Kunze, K.L., Sequential metabolism of secondary alkyl amines to metabolic-intermediate complexes: opposing roles for the secondary hydroxylamine and primary amine metabolites of desipramine, (s)-fluoxetine, and N-desmethyldiltiazem. *Drug Metab Dispos,* 2010, *38*(6), 963-972.
[39] Karuzina, II; Zgoda, V.G.; Kuznetsova, G.P.; Samenkova, N.F.; Archakov, A.I., Heme and apoprotein modification of cytochrome P450 2B4 during its oxidative inactivation in monooxygenase reconstituted system. *Free Radic Biol Med,* 1999, *26*(5-6), 620-632.
[40] Leung, L.; Kalgutkar, A.S.; Obach, R.S., Metabolic activation in drug-induced liver injury. *Drug Metab Rev,* 2012, *44*(1), 18-33.
[41] Baer, B.R.; DeLisle, R.K.; Allen, A., Benzylic oxidation of gemfibrozil-1-O-beta-glucuronide by P450 2C8 leads to heme alkylation and irreversible inhibition. *Chem Res Toxicol,* 2009, *22*(7), 1298-1309.

[42] Grabarek, Z.; Gergely, J., Zero-length crosslinking procedure with the use of active esters. *Anal Biochem,* 1990, *185*(1), 131-135.
[43] Zhang, Z.; Li, Y.; Stearns, R.A.; Ortiz De Montellano, P.R.; Baillie, T.A.; Tang, W., Cytochrome P450 3A4-mediated oxidative conversion of a cyano to an amide group in the metabolism of pinacidil. *Biochemistry,* 2002, *41*(8), 2712-2718.

Chapter 4

Cytochrome P450 Dependent Catabolism of Vitamin K: ω-Hydroxylation Catalyzed by Human CYP4F2 and CYP4F11

4.1 Introduction

Vitamin K (VK) is a collective term for a series of naphthoquinone derivatives with important biological activities (Figure 1.4). The menaquinone, MK4, is currently approved for prevention and treatment of osteoporosis for women in Japan at a dose of 45 mg/day. Phylloquinone (PK) is routinely dosed to newborns at birth in the United States to prevent vitamin K deficiency bleeding. It is also used to rescue patients from serious bleeding events caused by a warfarin overdose. VK supplementation is being investigated for prevention or treatment of vascular calcification related to cardiovascular disease and chronic kidney disease [1] as well as for warfarin dose stabilization therapy [2], as reviewed in Chapter 1 of this thesis.

Given the plethora of biological functions now attributed to vitamin K and the increased interest in its use as a therapeutic agent, it is important to understand how the body regulates tissue concentrations of the various vitamin K vitamers. Metabolic processes can be expected to play an important role in vitamin K homeostasis, but surprisingly little is known about the enzymes that control catabolism of K vitamers. It has been established that the major urinary metabolites of PK and MK4 are K acid 1 and K acid 2 (Figure 4.1 A). This catabolic pathway presumably involves an initial ω-hydroxylation event followed by two additional oxidations to generate aldehyde and carboxylic acid products (Figure 4.1 B). The carboxylic acids can then be esterified to their CoA derivatives and transferred from the endoplasmic reticulum to either the mitochondria or peroxisomes for β-oxidation to the chain shortened metabolites that have been found in the urine as glucuronide conjugates. Analogous pathways exist for the structurally similar compounds, vitamin E and coenzyme Q [3-5].

Previously, we reported that CYP4F2 catalyzes side chain oxidation of phylloquinone [6], although the absence of an authentic chemical standard precluded unambiguous assignment of the metabolite as the ω-hydroxy phylloquinone. Here, we demonstrate unequivocally that CYP4F2 is an ω-hydroxylase of MK4, characterize formyl and carboxylic acid metabolites that results from further oxidation of the primary metabolic product, establish an ‘orphan’ P450, CYP4F11, as a new vitamin K ω-hydroxylase, and quantitate CYP4F2 and CYP4F11

in human liver microsomes by LC-MS/MS in order to scale the relative contributions of these two P450 enzymes to initiation of vitamin K catabolism.

4.2 Materials and Methods

Materials. Human liver microsomes (a pool of 50 donors) were obtained from Xenotech LLC (Lenexa, KS). Additional human liver microsomes were prepared from the University of Washington Department of Medicinal Chemistry Human Liver Bank, as described previously [6]. $^{13}C^{15}N$ isotopically- labeled peptides were from Pierce Thermo custom peptide services. The C-terminal lysine contained 6 heavy carbon atoms and 2 heavy nitrogen atoms. The peptides were >99% isotopically-enriched, >97% pure, and concentration precision was ±25%. DLPC (1,2-dilauroyl-*sn*-glycero-3-phosphocholine) was from Avanti Polar Lipids. Alcohol dehydrogenase (ADH) from equine liver, lapachol, and methyl-β-cyclodextrin were purchased from Sigma Aldrich. ω-Hydroxy MK4 was synthesized and characterized as described previously [7]. CYP4F11 was expressed with a C-terminal histidine tag in *Escherichia coli* and purified as described previously [8]. CYP4F2 was expressed with C-terminal histidine tag in insect cells (using baculovirus) and purified as described previously [9]. Supersomes preparations of human P450 enzymes expressed in insect cells were obtained from BD Gentest, rat P450 oxidoreductase and rat cytochrome b_5 were expressed in *E. coli* and purified as previously described [10, 11]. The CYP4F11 antibodies used were 20012-1-AP (Proteintech, Chicago, IL), MAB10111 (Millipore, Billerica, MA), and PA5-30784 (Thermo Scientific Pierce Antibodies, Rockford, IL).

Metabolic Reactions with Vitamin K. Supersomes or reconstituted P450s were incubated with MK4 or PK in a total volume of 500 µl in an amber Eppendorf microcentrifuge tube. P450 (10 or 30 pmol) was typically used per metabolic incubation. Purified P450 enzymes, P450 oxidoreductase, cytochrome b_5, and DLPC were reconstituted at a molar ratio of 1:2:1:160 on ice for 5 min. A stock solution of DLPC was prepared by extrusion into water using a 0.05 µm filter to yield uniformly-sized liposomes. Vitamin K substrate was added in 2-propanol ensuring that the organic concentration did not exceed 0.4% v/v in the final reaction volume. Due to the insolubility of the substrates in buffer the order of addition of the incubation components was as follows: P450 enzyme preparation, 85 µl 0.1M potassium phosphate buffer, pH 7.4 (KPi), methyl-β-cyclodextrin (if included; the solubilizing agent was omitted from metabolic incubations designed to measure kinetic constants), substrate.

When included, methyl-β-cyclodextrin was added to a final concentration of 1 mM. Reactions were preincubated at 37 °C for 3 min, initiated by addition of 1 mM NADPH, and allowed to proceed at 37 °C for 20 min.

Incubations of pooled human liver microsomes (0.25 mg/mL) using ω-hydroxy MK4 as the substrate were performed similarly, using either NAD+ or NADPH to initiate the reaction. Reactions were quenched with 50 µl 2-propanol containing 0.1 µM lapachol (2-hydroxy-3-(3-methylbut-2-enyl)naphthalene-1,4-dione) as internal standard. Metabolic incubations were extracted (2 × 700 µl hexanes) into silanized glass test tubes and spun for 90 s in a tabletop centrifuge. The hexanes layer was removed, evaporated with N_2 at room temperature and the residue was dissolved in 100 µl of 2-propanol. Samples were immediately transferred to amber vials and analyzed by LC-MS/MS, typically injecting 4 µl on the column. Standard curves for quantitation of ω-hydroxy MK4 production contained the appropriate amount of human liver microsomal protein, control Supersomes™ (containing P450 oxidoreductase and cytochrome b_5 only), DLPC liposomes, and/or MβCDX.

To biosynthesize the ω-formyl MK4 standard, 2 units of equine ADH was added to 450 µl KPi. ω-hydroxy MK4 was added in 2-propanol to a final concentration of 100 µM. The reaction was initiated with 1 mM NAD^+ and allowed to proceed at 37 °C for 60 min. The incubation was extracted as described above before analysis by LC-MS/MS.

LC-MS/MS Analysis. The LC system consisted of a triple quadrupole mass spectrometer (SCIEX API4000; Applied Biosystems, Foster City, CA) coupled to a UPLC (Waters, Milford, MA). Analytes were separated on an Acquity UPLC C18 1.7 µm, 50 × 2.0 mm column (Waters) with water (A) and methanol (B) mobile phases. The concentration of B was held at 45% from 0-1.5 minutes, increased and held at 85% (for MK4 analysis) or 90% (for PK analysis) from 1.5-6 minutes, held at 100% from 6-7 min, and decreased and held at 45% again from 7-8.5 min at a flow rate of 0.6 ml/min. At 6.1 min 100% of the flow was diverted to waste. Vitamin K metabolite retention times under these conditions were as follows (min): ω-hydroxy MK4 (4.2), ω-formyl MK4 (4.5), ω-carboxy MK4 (4.1), and lapachol IS (2.0), ω-OH PK (3.6), ω-carboxy PK (3.9). The mass spectrometer was operated in APCI negative ion mode with a heated nebulizer source at the following settings: temperature 450 °C, nebulizer current (NC) 5 V, curtain gas (CUR) 35 psi, ion source gas 1 (GS1) 45 psi, ion source gas 2 (GS2) 45 psi, collision gas (CAD) 7 psi, entrance potential (EP) 10 V, collision cell exit potential (CXP) 15 V. The following MRM mass transitions and instrument settings for incubations containing MK4 and PK were as

follows: ω-hydroxy MK4 (460.3>185.0, DP 90 V, CE 42 V), ω-formyl MK4 (458.4>185.0, DP 90 V, CE 40 V), ω-carboxy MK4 (474.4>185.0, DP 90 V, CE 40 V), and lapachol (internal standard) (241.0>186.1, DP 75 V, CE 28 V), ωOH PK (466.3>185.0, DP 90 V, CE 42 V), ω-carboxy PK (480.4>185.0, DP 90 V, CE 40 V).

Microsomal CYP4F Quantitation by Peptide LC-MS/MS. The P450 digestion protocol was adapted from previously described methods [12, 13]. Human liver microsomes (40 µl, 2 mg protein/ml) were incubated with 4 µl dithiothreitol (100 mM) and 40 µl ammonium bicarbonate buffer (100 mM, pH 7.8) for 5 min at 95 °C (denaturation). The samples were cooled to room temperature and alkylated by adding 4 µl iodoacetamide (200 mM) for 20 min at room temperature in the dark. Ten µl trypsin solution was added (0.16 mg/ml) and samples were digested at 37 °C for 24 h. At the end of digestion period, the reaction was quenched by adding 30 µl of stable-isotope labeled (SIL) internal standard solution (50% acetonitrile, 0.1% formic acid) and centrifuged at 5000 x g for 5 min at 4 °C and stored at -80 °C until analysis. The LC-MS/MS instrument, which consisted of an Agilent 6460A triple-quadrupole mass spectrometer coupled to an Agilent 1290 Infinity LC system (Agilent Technologies, Santa Clara, California), was operated in electrospray ionization positive ion mode. Five µl of sample were injected onto an Acquity UPLC C18 1.7 µm, 50 mm × 2.0 mm column (Waters). The mobile phases were 0.1% formic acid (v/v) in water (A) and acetonitrile (B), and the flow rate was 0.4 ml/min. The mobile phase gradient was as follows: 0-2.5 min (hold 3% B, v/v), 2.5-5 min (3-12% B, v/v), 5-11 min (hold 12% B, v/v), 11-13.9 min (12-28% B, v/v), 13.9-14 min (28-80% B, v/v), 14-14.9 min (hold 80% B, v/v), 14.9-15 min (80-3% B, v/v), 15-17 min (hold 3% B, v/v). The multiple reaction monitoring (MRM) transitions monitored and the peptide retention times are listed in Table 1. Data collection was compartmentalized so that the relevant MRM channels were only open over the window of time that the target peptide was eluting. The instrument settings were (for CYP4F2 or CYP4F11 peptides, respectively): dwell time, 100 ms; fragmentor, 125 or 150 V; collision energy, 16 or 22 eV; and cell accelerator voltage, 7 V. Other system parameters were as follows: gas temperature, 350 °C; gas flow, 5 l/min; nebulizer, 45 psi; sheath gas temperature, 350 °C; sheath gas flow, 9 l/min; capillary voltage, 3500 V; nozzle voltage, 500 V; cell RF (radio frequency), 400; EMV (electron multiplier voltage), 1280 V; and delta EMV, 500. The data were processed by integrating the peak areas generated from the ion chromatograms for the analyte peptide and the SIL internal standard using MassHunter software (Agilent Technologies).

4.3 Results

Assay Development. Isoprenyl quinones are efficiently ionized using atmospheric pressure chemical ionization (APCI) [14, 15]. In the MRM assay developed here for incubations using MK4 as the substrate, there were fewer background peaks in negative ion mode compared to positive ion mode, therefore, negative APCI mode was selected to ionize vitamin K metabolites. At low collision energies (~10-20 V) the molecular ions of MK4 and ω-hydroxy MK4 produced similar fragment ions due to cleavage on the phytyl chain at *m/z* 375, 360, 307, 292, 239, 224, and 185 (Figure 4.2C). At higher collision energies (~40-50 V) the transition from M-· radical parent ion to the menadione fragment ion at *m/z* 185.0 was optimal, and this transition was used for the MRM-based quantitation of all metabolites described below.

ω-Hydroxylation of MK4 by CYP4F2. In the presence of NADPH, CYP4F2 Supersomes oxidized MK4 to a major product that eluted at 4.2 min with detection in the 460.3>185.0 MRM channel (Figure 4.2A). Assignment of this product as ω-OH MK4 was made by comparison of its retention time and daughter ion spectrum to the authentic synthesized chemical standard (Figure 4.2B).

Sequential Metabolism of MK4 by CYP4F2 to ω-carboxy MK4. CYP4F2 Supersomes formed a second NADPH-dependent MK4 metabolite that was detected in the 474.3>185.0 MRM channel, eluting at 4.1 min (Figure 4.2A). At low collision energies, the spectra for this metabolite showed diagnostic fragments of *m/z* 457, 430, and 375. Loss of 44 Da from the molecular ion suggests strongly that this metabolite is the terminal carboxylic acid, ω-carboxy MK4 (Figure 4.3B). It has previously been shown that, for very long chain fatty acids (VLCFAs) such as C22:0 and C26:0, a microsomal alcohol dehydrogenase (ADH) and fatty aldehyde dehydrogenase (fALDH, encoded by the *ALDH3A2* gene) catalyze the two oxidative transformations from the ω-OH-VLCFA to the corresponding aldehyde and subsequently to the dicarboxylic acid, using NAD^+ as the cofactor [16]. Analogously, we found that ω-carboxy MK4 was formed in both an NAD^+ or NADPH dependent manner when ω-OH MK4 was used as a substrate with HLM as the enzyme source. This result demonstrates that microsomal ADH/ALDH and P450 enzymes, respectively, are able to form the ω-carboxy MK4 (Figure 4.3A). Similar catalytic efficiencies for the formation of ω-carboxy MK4 from ω-OH MK4 were measured for both the NAD^+

and NADPH dependent reactions in human liver microsomes (K_m 28 μM, V_{max} 18.3 pmol/min/mg protein, V_{max}/K_m 0.65 ± 0.22 for NAD^+ and K_m 23 μM, V_{max} 8.3 pmol/min/mg protein, V_{max}/K_m 0.35 ± 0.13 for NADPH) (Figure 4.4).

Sequential Metabolism of MK4 to ω-Carboxy MK4 by CYP4F2 Supersomes and Reconstituted Enzyme. CYP4F2 Supersomes and reconstituted enzyme form ω-carboxy MK4 from MK4. This requires the following series of oxidations: MK4 → ω-hydroxy MK4 → ω-formyl MK4 → ω-carboxy MK4. Figure 4.6 shows formation kinetics of ω-hydroxy MK4 and ω-carboxy MK4 derived from CYP4F2-mediated metabolism of MK4 with and without methyl-β-cyclodextrin (MβCDX) (1mM). Previous reports have demonstrated increases in enzyme activity and substrate solubility by using various cyclodextrins to aid in delivery of very water insoluble substrates [16-20]. Using CYP4F2 Supersomes without MβCDX (Figure 4.6A), ω-carboxy MK4 formation from MK4 exhibits a hyperbolic curve suggesting there is at least some element of sequential metabolism from MK4 all the way to the ω-carboxy product without release of substrate [21, 22]. The addition of MβCDX to these incubations increases both the K_m and V_{max} for the MK4 → ω-OH MK4 step (K_m from 3.2 μM to 18 μM and V_{max} from 0.21 min^{-1} to 2.5 min^{-1}). Using reconstituted CYP4F2, however, the K_m is slightly decreased while the V_{max} is still increased upon MβCDX addition (K_m from 1.6 μM to 0.78 μM and V_{max} from 0.085 min^{-1} to 0.39 min^{-1}). In the plots for ω-carboxy MK4 formation there is substantially more substrate inhibition by MK4 when MβCDX is present, presumably because the enzyme is exposed to higher MK4 levels which compete with the processive reaction of ω-carboxy MK4 formation. It is clear that the reaction under all of these conditions is not completely processive because ω-hydroxy MK4 is a readily detectable primary metabolite of MK4.

ω-Formyl MK4 Synthesis by Horse Liver ADH. We next looked for evidence of formation of the presumptive ω-formyl intermediate in the CYP4F2-mediated conversion of the MK4 terminal alcohol to the carboxylic acid. Preliminary screening of metabolic incubations for the ω-aldehyde in the expected 458.3>185.0 MRM channel did not detect this product. However, to improve confidence that it is not released along the P450 pathway from ω-alcohol to ω-carboxy, we supplemented equine liver ADH with NAD^+ to biosynthesize the ω-aldehyde from authentic ω-OH MK4. The resulting ω-aldehyde of MK4 eluted slightly later (t_R 4.5 min) than the corresponding ω-carboxy and ω-hydroxy metabolites (Figure 4.5). The MS^2 spectra of the ω-formyl MK4 parent ion at low

collision energies resulted in a fragmentation pattern consistent with the assigned structure. These data demonstrate that the ω-aldehyde intermediate is not released during either the ADH/fALDH- or P450-dependent metabolism of ω-hydroxy MK4 and so both oxidations are highly sequential. This also appears to be the case for metabolism of ω-hydroxy-VLCFA metabolism by microsomal ADH/fALDH [16].

CYP4F11 is Also a Vitamin K ω-Hydroxylase. The CYP4 gene cluster on human chromosome 19 encodes several P450 enzymes that are not commercially available, *viz* CYP4F8, CYP4F22, and CYP4F11. CYP4F11 is of particular interest because the gene is located only 16 kb away from *CYP4F2* and the two may be co-regulated [23]. Additionally, CYP4F11 mRNA is present in the liver at higher levels than CYP4F2, whereas CYP4F8 mRNA is negligible in liver and hepatic CYP4F22 mRNA levels are unknown [24-26]. Recombinant CYP4F11, expressed in *E. coli* and purified as previously described [8], was reconstituted with DLPC, cytochrome b_5, and P450 oxidoreductase and its ability to oxidize MK4 and phylloquinone compared with that of purified, reconstituted CYP4F2. Both purified enzymes ω-hydroxylated MK4 (Figure 4.7), but CYP4F11 did not generate any ω-carboxy metabolite under the conditions used. The steady-state kinetics of ω-OH MK4 formation was measured for both reconstituted enzyme systems and for CYP4F2 Supersomes (Figure 4.8). CYP4F2 and CYP4F11 formed ω-hydroxy MK4 with similar catalytic efficiencies.

Absolute Quantitation of CYP4F11 in Human Liver Microsomes by Immunoblotting. The CYP4F11 C-terminus has a relatively unique sequence compared to other CYP4F enzymes in liver. Western blots using a commercially available primary peptide antibody raised against the CYP4F11 C-terminus (Millipore) showed an immunoreactive band around 55 kDa in pooled human liver microsomes but did not recognize the *E.coli* expressed CYP4F11 protein, making quantitative Western blot analysis with this antibody impossible. Another commercially available CYP4F11 peptide antibody (Proteintech) recognized the CYP4F11 *E.coli* expressed protein but did not detect a band in HLMs at 55 kDa. Finally, the third commercially available peptide antibody we selected (Thermo Scientific Pierce Antibodies) displayed immunoreactive bands with both pure protein and human liver microsomes (Figure 4.9). This antibody did not recognize CYP4F2 or CYP4F3B Supersomes, and it minimally recognized CYP4F12 Supersomes (Figure 4.9A). Strangely, there appeared to be two immunoreactive bands very close together around 55 kDa in human liver microsomes, while there was only a single band in lanes

with recombinant purified protein. There appeared to be a large degree of inter-individual variability in the lower band, but not the upper band (Figure 4.9B). The two bands might be due to a large post translational modification that does not occur in the *E.coli* expressed protein, or one of the bands might be a completely different protein that binds to the antibody. Regardless, these results were difficult to interpret; therefore we opted to quantify CYP4F11 in human liver microsomes by peptide LC-MS/MS.

Absolute Quantitation of CYP4F2 and CYP4F11 in Human Liver Microsomes by Tryptic Peptide LC-MS/MS. Stable isotope label (SIL) tryptic peptide LC-MS/MS [12, 13] was used to quantitate CYP4F2 and CYP4F11 in human liver microsomes. The tryptic peptides monitored for CYP4F2 and CYP4F11 and their MRM transitions are shown in Table 1. These peptides were chosen for their uniqueness, lack of known polymorphic SNPs, stability, solubility, and ionization ability. Fourteen individual human liver microsomal samples from the University of Washington Liver Bank, as well as a commercially available pool of human liver microsomes from 50 donors (Xenotech) were subjected to digestion by trypsin. A standard curve was constructed using the purified preparations of CYP4F2 and CYP4F11, which were digested in the same manner as the microsomal samples in order to control for digestion efficiency. The SIL synthetic peptide was spiked into each sample after digestion and the peptides were injected onto a C18 UPLC column and chromatographically dispersed over a 16 min gradient. In the 14 human liver microsomal samples from the University of Washington Liver Bank, the average protein expression levels of CYP4F2 and CYP4F11 were 14.3 ± 6.3 pmol/mg protein and 8.4 ± 1.5 pmol/mg protein , respectively (Figure 4.10). For comparison, we also measured these protein levels in a commercially available pool of 50 human liver microsomes, and found similar results (14.0 and 8.3 pmol/mg protein, respectively). The standard deviations between three triplicate digestions of the same liver sample were <7%. The 14 human liver samples were genotyped for the common *CYP4F2*3* allele (V433M) and, in agreement with earlier findings from western blotting experiments [6], the amount of CYP4F2 protein present in human liver microsomes decreased as a function of the number of **3* variant alleles (Figure 4.10). Collectively, these data suggest that CYP4F2 will be a more dominant contributor to initiation of vitamin K catabolism, except in *CYP4F2*3* homozygotes. MK4 ω-hydroxylation activity was measured in the 14 human liver microsomal samples, and activity was found to vary from ~6 to 60 pmol/min/mg protein (the MK4 substrate concentration was 20 μM, and 1 mM MβCDX was included). There was only a slight correlation between CYP4F2 content and

MK4 ω-hydroxylation activity and no correlation to CYP4F11 content (Figure 4.10). This may be due to the involvement of other human liver enzymes involved in MK4 metabolism reported in Chapter 5 of this thesis.

Formamidoxime Inhibition of CYP4F11 and CYP4F2. HET0016 derivatives, described in Chapter 2 of this thesis, were used to determine if inhibitor discrimination could be achieved between CYP4F11 and CYP4F2 (Figure 4.11). Unfortunately, HET0016 and all derivatives chosen (at 100 nM inhibitor concentration) inhibited both enzymes' ω-hydroxy MK4 activity to the same degree and so will not be useful to evaluate CYP4F isoform-mediated vitamin K metabolism in microsomes or cells. Compounds 10 and 11 did not inhibit CYP4F2 or CYP4F11, although these derivatives did inhibit CYP4F3B modestly (Figure 2.11). It may be worth investigating whether inhibitor selectivity can be gained within the CYP4F family by further modification of this series of compounds.

4.4 Discussion

As noted above, there is increasing interest in the use of menaquinones (and phylloquinone) as pharmacotherapeutic agents [1, 2, 27], although there appears to be wide inter-individual variability in response to supplementation with these agents [28]. Therefore, a major goal of this study was to identify P450 enzymes that catalyze metabolism of MK4, delineate their relative contributions to microsomal catabolism and evaluate pharmacogenetic factors that might contribute to variability in metabolism.

An important new finding from our studies is that CYP4F11 is a vitamin K ω-hydroxylase. CYP4F11 is known to be an efficient ω-hydroxylase of 3-hydroxy fatty acids, with relatively high catalytic efficiency (k_{cat}/K_m 0.37 ± 0.14 $min^{-1}\mu M^{-1}$) [8]. It has also been shown to oxidize some xenobiotics, e.g. erythromycin, with very low efficiencies (k_{cat}/K_m 0.0066 $min^{-1}\mu M^{-1}$) [23]. Here we demonstrate that CYP4F11 is an ω-hydroxylase of MK4, albeit with relatively low efficiency ($V_{max}/K_m = 0.067 \pm 0.2$ min^{-1} μM^{-1}). Low catalytic efficiency *in vitro* is likely exacerbated by poor solubility/delivery of the substrate to the enzyme active site because reaction velocities were increased more than 10-fold by inclusion of the solubilizing agent, methyl-β-cyclodextrin (MβCDX), in metabolic incubations.

CYP4F2, but not CYP4F11, metabolized MK4 in a partially non-dissociative manner to the ω-carboxy metabolite. Our data suggest further that, while CYP4F2 released some of the initially formed ω-hydroxy MK4,

the ω-formyl metabolite may remain bound to the enzyme such that some of the initially formed alcohol is sequentially metabolized to the acid. Alternatively, the ω-formyl metabolite may not have been detected because this α/β-unsaturated aldehyde is sufficiently reactive to bind irreversibly to components of metabolic reaction mixtures [29]. Regardless, released ω-hydroxy MK4 may take several paths to the ω-acid product; it could rebind to CYP4F2 and be further oxidized, it could be oxidized by CYP4F11 and/or other P450 enzymes in microsomes, or it could be oxidized by the microsomal ADH/fALDH complex. Insufficient quantities of the authentic ω-hydroxy metabolite precluded studies to differentiate between these possibilities. The opposite trend in K_m change upon MβCDX addition observed between CYP4F2 Supersomes system and reconstituted enzyme systems was unexpected, and perhaps more complicated binding models must be used to fit data when MβCDX is included due to the additional equilibria existing between the cyclodextrin, the substrate, and other constituents such as lipid or cholesterol (for Supersomes) [18].

Based on the catalytic efficiencies of formation of released ω-hydroxy MK4 we can predict which of the two CYP4F enzymes dominates metabolite formation if the relative microsomal concentrations of the two enzymes are known. CYP4F2 concentrations in human liver microsomes have been reported to average ~16 pmol/mg protein with large variability from 0-80 pmol/mg protein [30]. However, it was not known how much CYP4F11 protein is present in human liver microsomes. In human liver, CYP4F2, CYP4F3B, CYP4F11, and CYP4F12 are all readily detectable at the mRNA level [24-26]. The CYP4F11 C-terminus has a relatively unique sequence compared to other human CYP4F enzymes in liver, however, extensive attempts to immunoquantitate CYP4F11 with three different commercially available antibodies failed due to inadequate selectivity of detection in microsomal samples and/or failure of the antibody to detect recombinant CYP4F11. Therefore, we measured CYP4F11 (and CYP4F2) in HLMs by tryptic peptide LC-MS/MS, using isotopically-labeled peptide fragments and trypsin digests of purified CYP4F11 and CYP4F2 for robust quantitation. These data revealed that, on average, CYP4F11 was present at approximately half the concentration of CYP4F2 in human liver microsomes. Moreover, CYP4F2, but not CYP4F11, displayed evidence of partially sequential metabolism of MK4 to the ω-acid. Therefore, it would be expected that CYP4F2 would, in general, be a more dominant contributor to the initiation of MK4 catabolism than CYP4F11. However, both enzymes exhibit at least one common genetic variant, i.e. *CYP4F2 V433M* (*CYP4F2*3*) and *CYP4F11 D446N*. The *CYP4F2*3* allele correlates with warfarin maintenance dose in patients on this anticoagulant therapy [6]. It is also linked to altered 20-HETE biosynthesis

and hypertension risk [31]. Genetic polymorphisms in the *CYP4F11* gene have not been studied, however the common SNP, rs1060463 (which results in the D446N variant), occurs with minor allele frequency of 40% in Caucasians. We reported previously that human liver microsomal preparations from donors carrying the *CYP4F2*3* (V433M) allele possessed lower levels of immunoreactive CYP4F2 protein [6], and the current LC-MS quantitation efforts support this earlier finding. In contrast, CYP4F11 levels in HLMs did not vary with *CYP4F11 D446N* genotype, and microsomal MK4 ω-hydroxylation activities were independent of *CYP4F11* genotype. Therefore, the common *CYP4F11 D446N* variant does not appear to affect P450 enzyme activity or microsomal enzyme concentrations. Consequently, in *CYP4F2*3* homozygotes (5-10% of Caucasian populations), we predict that CYP4F11 enzyme activity would be a more important contributor to MK4 ω-hydroxylation, irrespective of *CYP4F11* genotype. Studies with the recombinantly expressed variants are needed to more fully evaluate the functional capabilities of CYP4F11 variants.

The foregoing findings may also be relevant to the metabolism of structurally similar vitamin E and coenzyme Q, which have degradation pathways analogous to that of vitamin K. Additionally, it is unknown whether MK7, another form of vitamin K2, is a CYP4F2 and CYP4F11 substrate. This is of interest because MK7 has been proposed as a better vitamin K supplement than PK or MK4 due to more optimal pharmacokinetic properties [32-34].

In summary, we have shown that both CYP4F2 and CYP4F11 are vitamin K1 and K2 ω-hydroxylases, and that CYP4F2, at least to some extent, sequentially metabolizes vitamin K to the ω-carboxy metabolite. However, microsomal ADH/fALDH or other P450 enzymes may also play a role in formation of this metabolite after initial ω-hydroxylation by these CYP4 enzymes. Depending on CYP4F2 genotype, either CYP4F2 or CYP4F11 is the more dominant contributor to initiation of vitamin K catabolism. These findings are important in our efforts to understand factors involved in vitamin K homeostasis and inter-individual variability in response to supplementation with these vitamins.

Figure 4.1: A) The elimination pathway of phylloquinone (PK) and menaquinone-4 (MK4). The major urinary metabolites are the β-oxidized, chain-shortened glucuronides of K acid 1 and K acid 2. B) Both PK and MK4 must undergo an initial ω-hydroxylation step before β-oxidation can commence.

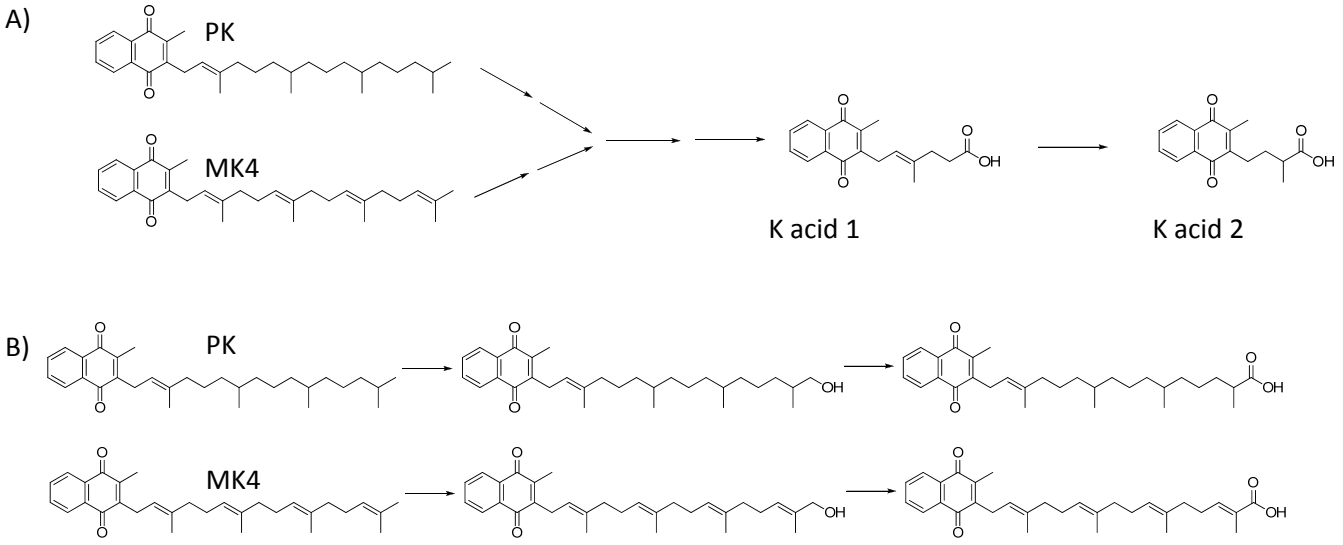

Figure 4.2 A) MRM chromatogram of an incubation with CYP4F2 supersomes, NADPH, and MK4. Dark gray: ω-hydroxy MK4, MRM transition 460.3>185.0, t_R 4.2 min; light gray: ω-acid MK4 MRM transition 474.4>185.0, t_R 4.1 min; Medium gray: lapachol internal standard, MRM transition 241.0>186.1, t_R 2.0 min. B) Synthetic standard of ω-hydroxy MK4 *C*, Q3 scan of parent ion 460.3 at 4.2 minutes from incubation with CYP4F2 Supersomes and MK4.

A)

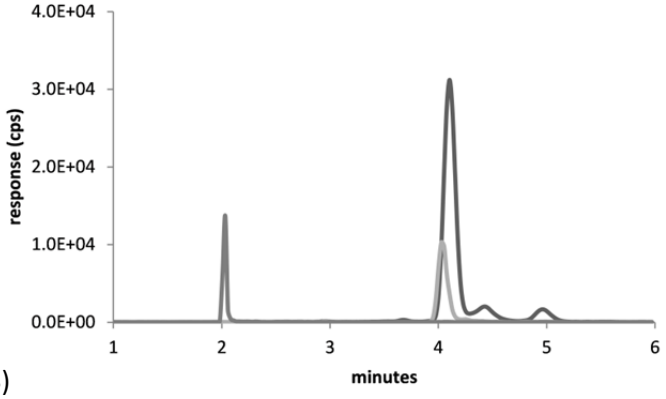

B)

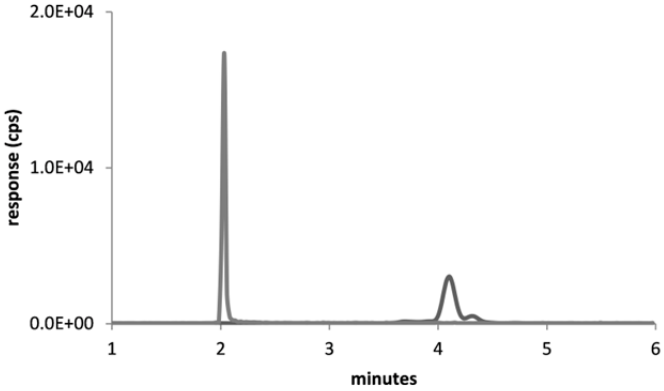

C)

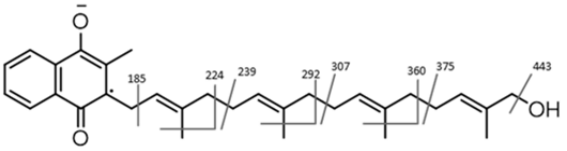

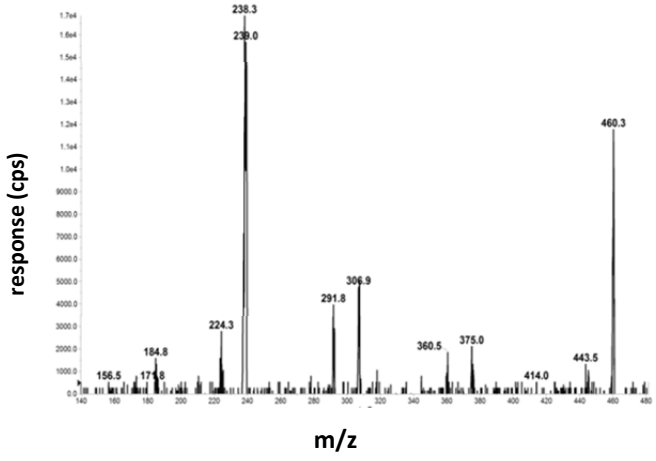

Figure 4.3: TOP: MRM chromatogram of an incubation with human liver microsomes, NAD^+, and ω-hydroxy MK4. Dark gray: ω-acid MK4 product, MRM transition 474.4>185.0, t_R 4.1 min; Light grey: lapachol internal standard, MRM transition 241.0>186.1, t_R 2.0 min. BOTTOM: A Q3 scan of parent ion 474.4 at 4.1 min.

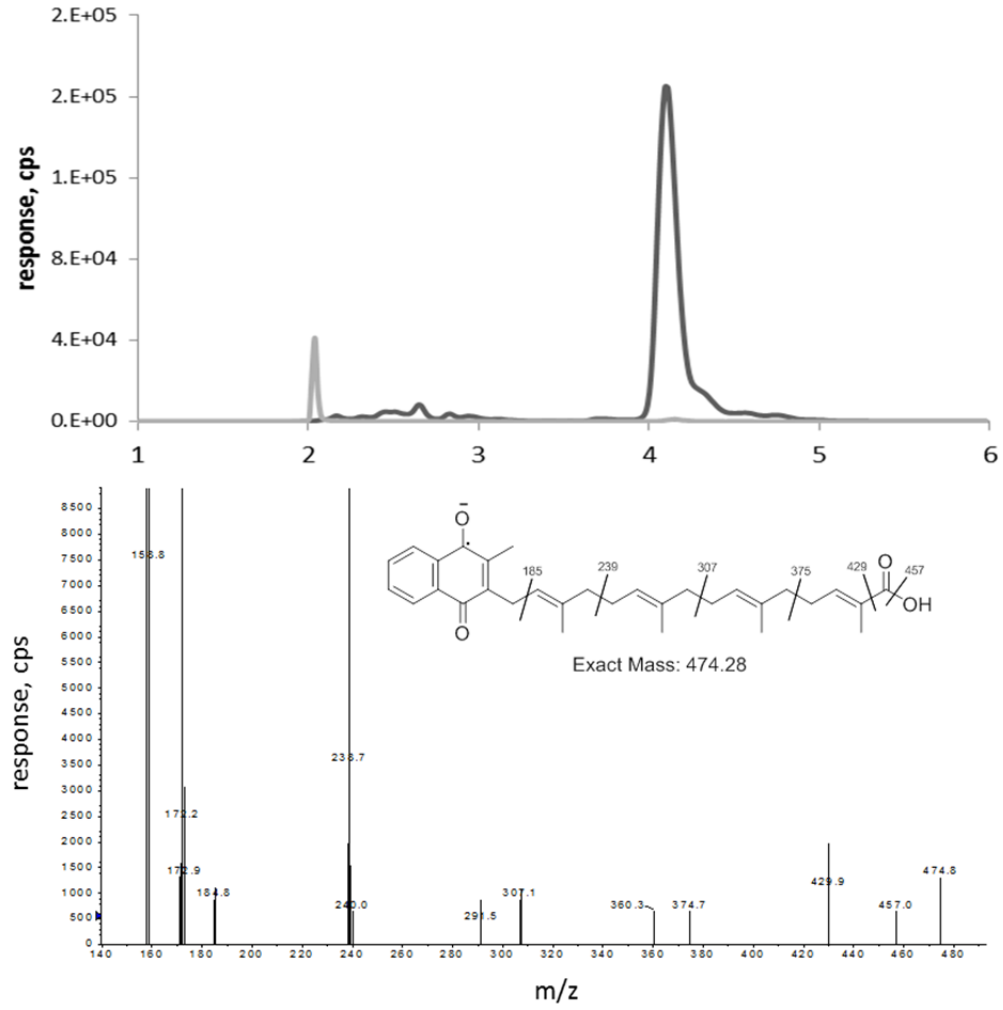

Figure 4.4: NAD^+ (left) and NADPH (right) dependent formation of ω-acid metabolite of MK4 in human liver microsomal incubations. $V_{max}/ K_m = 0.65 \pm 0.22$ and 0.35 ± 0.13, respectively.

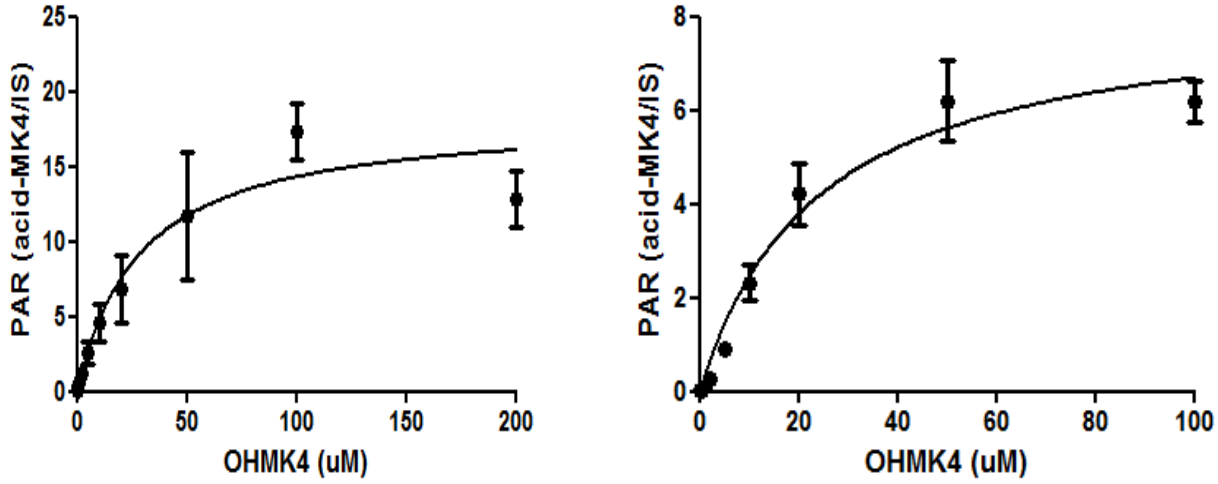

Figure 4.5: A) MRM chromatogram of an incubation with equine liver ADH, NAD^+, and ω-OH MK4. Dark gray: ω-aldehyde MK4, 458.3> 185.0, t_R 4.5 min; Light gray: lapachol internal standard, MRM transition 241.0>186.1, t_R 2.0 min. B) Q3 scan of parent ion 458.3 at 4.5 min.

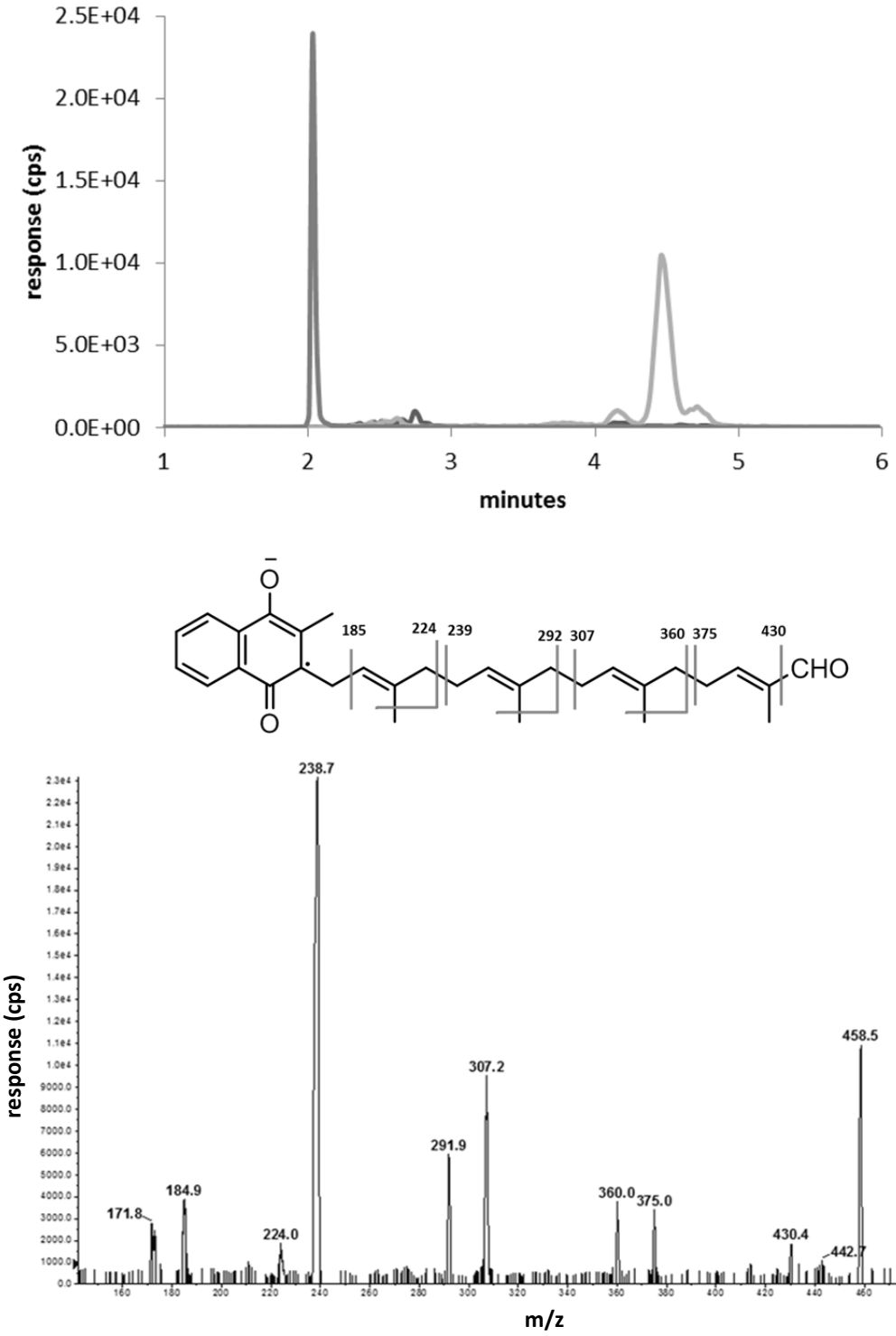

Figure 4.6: Sequential metabolism kinetics of MK4 to ω-hydroxy MK4 and ω-carboxy MK4 by CYP4F2 Supersomes and reconstituted enzyme with and without methyl-β-cyclodextrin. Kinetic constants were calculated for ω-OH MK4 formation. A) CYP4F2 Supersomes – mβcdx. K_m= 3.2 ± 0.5 μM, V_{max}= 0.21 ± 0.009 min^{-1}, V_{max}/K_m= 0.067 ± 0.02 $\mu M^{-1}min^{-1}$. B) CYP4F2 Supersomes + mβcdx. K_m = 18 ± 6 μM, V_{max}= 2.5 ± 0.3 min^{-1}, V_{max}/K_m= 0.14 ± 0.05 $\mu M^{-1}min^{-1}$. C) CYP4F2 reconstituted enzyme – mβcdx. K_m= 1.6 ± 0.4 μM, V_{max}= 0.085 ± 0.004 min^{-1}, V_{max}/K_m = 0.052 ± 0.01 $\mu M^{-1}min^{-1}$. D) CYP4F2 reconstituted enzyme +mβcdx. K_m= 0.78 ± 0.2 μM, V_{max}= 0.39 ± 0.01 min^{-1}, V_{max}/ K_m= 0.5 ± 0.05 $\mu M^{-1}min^{-1}$.

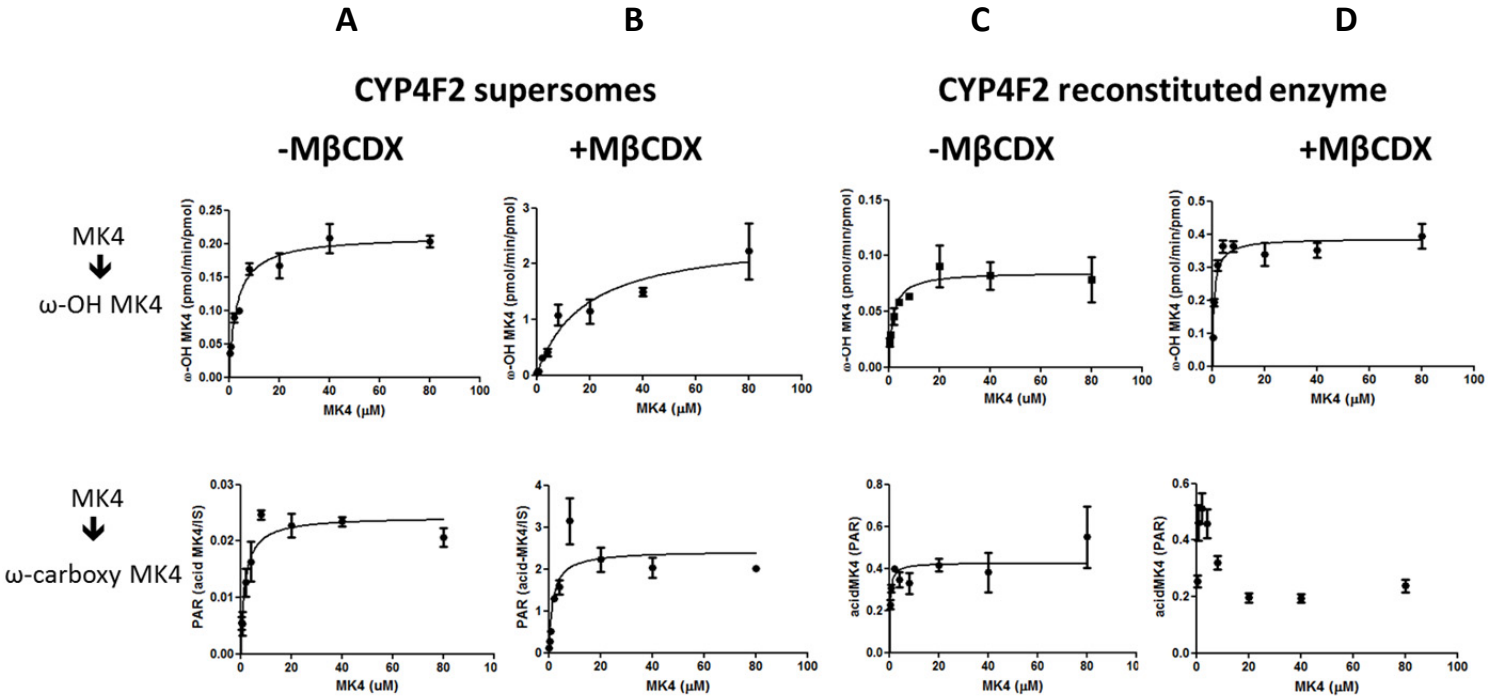

FIGURE 4.7: MRM chromatograms of incubations with purified reconstituted CYP4F2 (left) and CYP4F11 (right) with PK (top) and MK4 (bottom) substrates. Peaks that are starred are not NADPH dependent. TOP: Incubations with PK. Dark gray: ω-OH PK metabolite, MRM transition 466.3>185.0, t_R 3.9 min; Light gray: ω-acid PK metabolite, MRM transition 480.4>185.0, t_R 3.6 min; Medium gray: lapachol internal standard, MRM transition 241.0>186.1, t_R 2.0 min. BOTTOM: Incubations with MK4. Dark gray: ω-hydroxy MK4 product, MRM transition 460.3>185.0, t_R 4.2 min; Light gray: MK4 ω-acid product, MRM transition 474.4>185.0, t_R 4.1 min; Medium gray: lapachol internal standard, MRM transition 241.0>186.1, t_R 2.0 min.

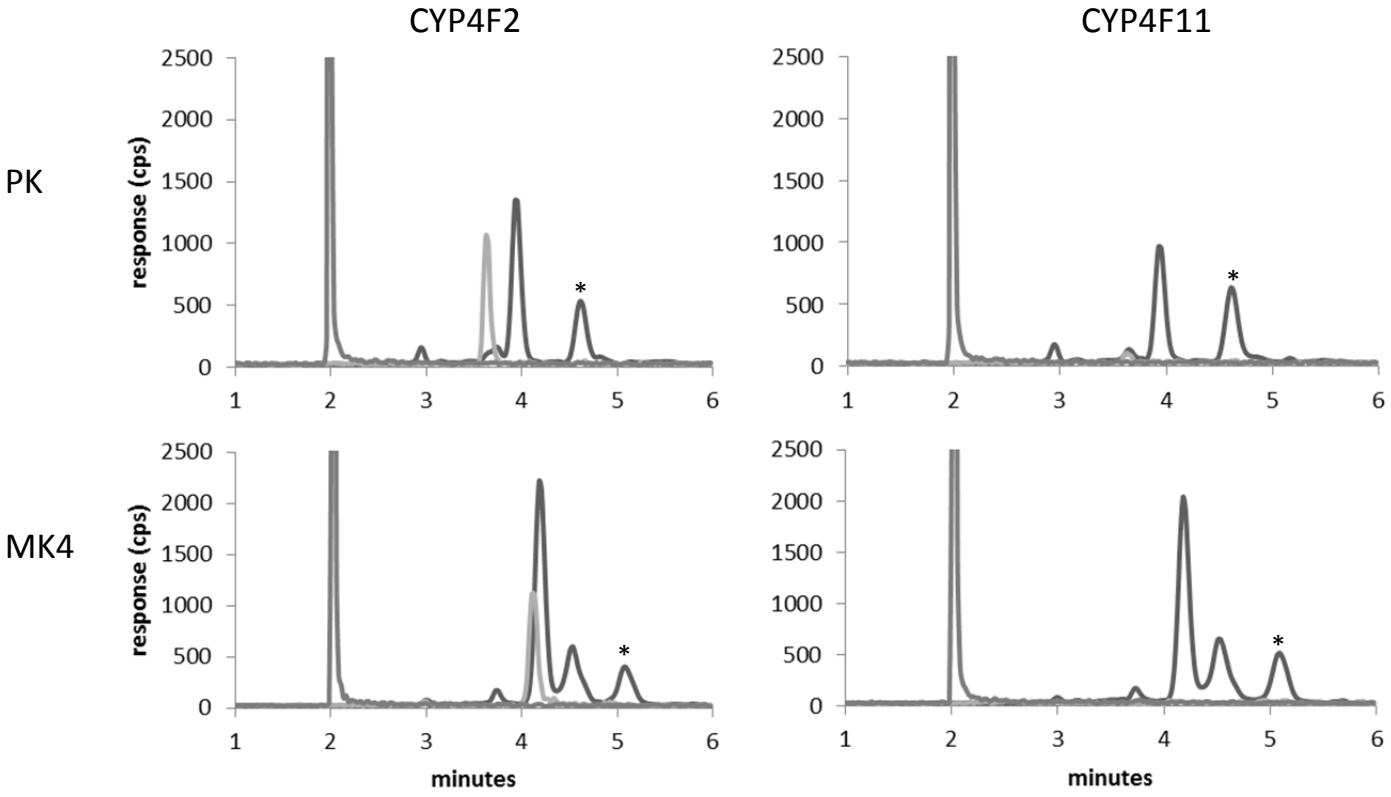

Figure 4.8: Kinetic plots for the formation of ω-hydroxy MK4 from: A) CYP4F2 Supersomes, B) reconstituted CYP4F2, C) reconstituted CYP4F11. A) K_m = 3.2 ± 0.5 μM, V_{max}= 0.21 ± 0.009 min^{-1}, V_{max}/K_m = 0.039 ± 0.01$min^{-1}\mu M^{-1}$ B) K_m = 1.7 ± 0.2 μM, V_{max}= 0.067 ± 0.002 min^{-1}, V_{max}/K_m = 0.037 ± 0.008 $min^{-1}\mu M^{-1}$ C) K_m= 2.4 ± 0.5 μM, V_{max}= 0.088 ± 0.004 min^{-1}, V_{max}/K_m = 0.067 ± 0.02 $min^{-1}\mu M^{-1}$.

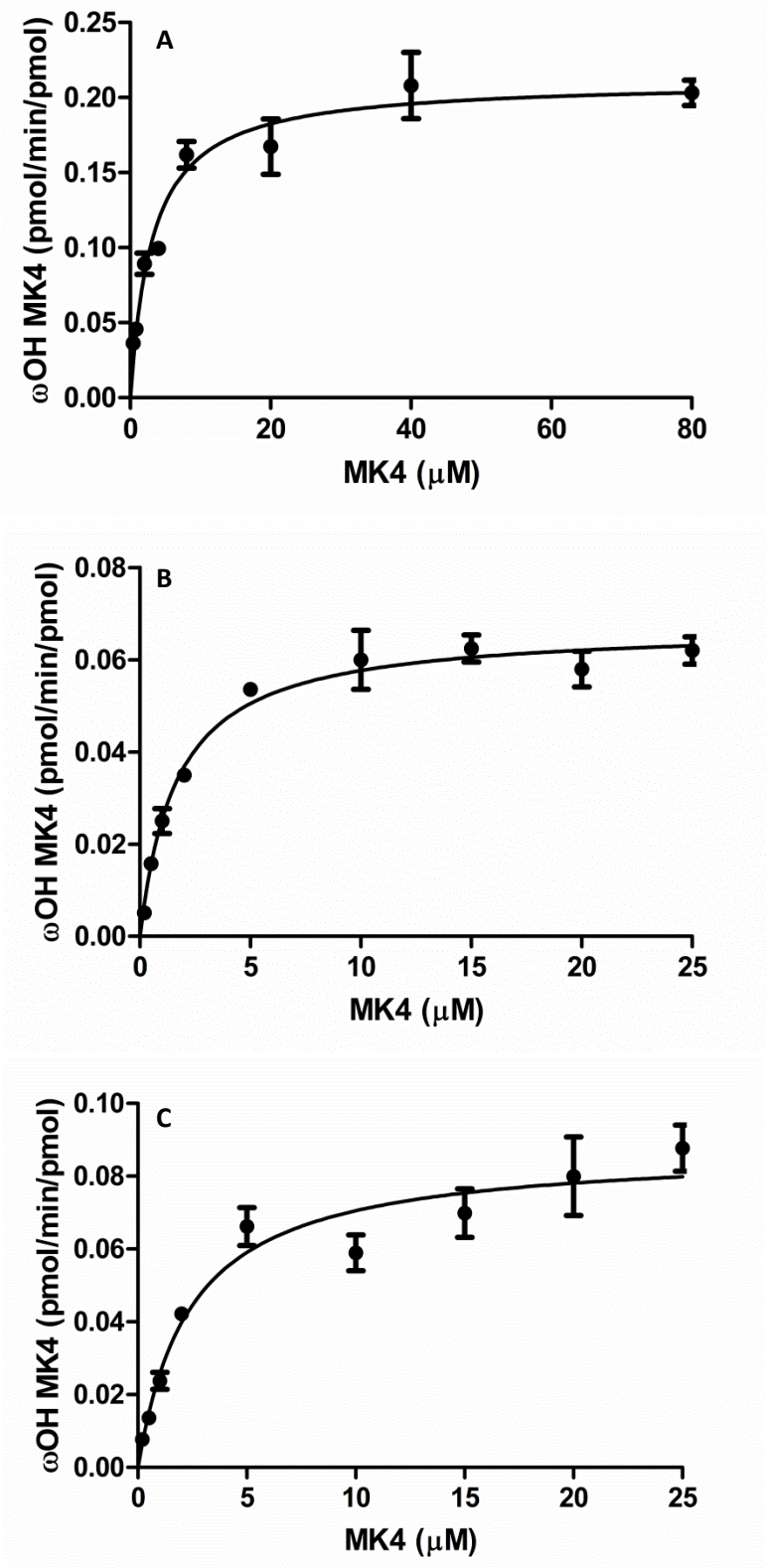

Figure 4.9: Quantitative western blotting of CYP4F11 with commercially available antiobody (PA5-30784, Thermo-Scientific Pierce). A) Cross reactivity of CYP4F11 antibody with other CYP4F enzymes present in liver and immunoreactivity with pooled human liver microsomes. B) Inter-individual variability between eight human livers. C) Immunoquantitation of CYP4F11 in pooled human liver microsomes and a standard curve of recombinantly expressed CYP4F11.

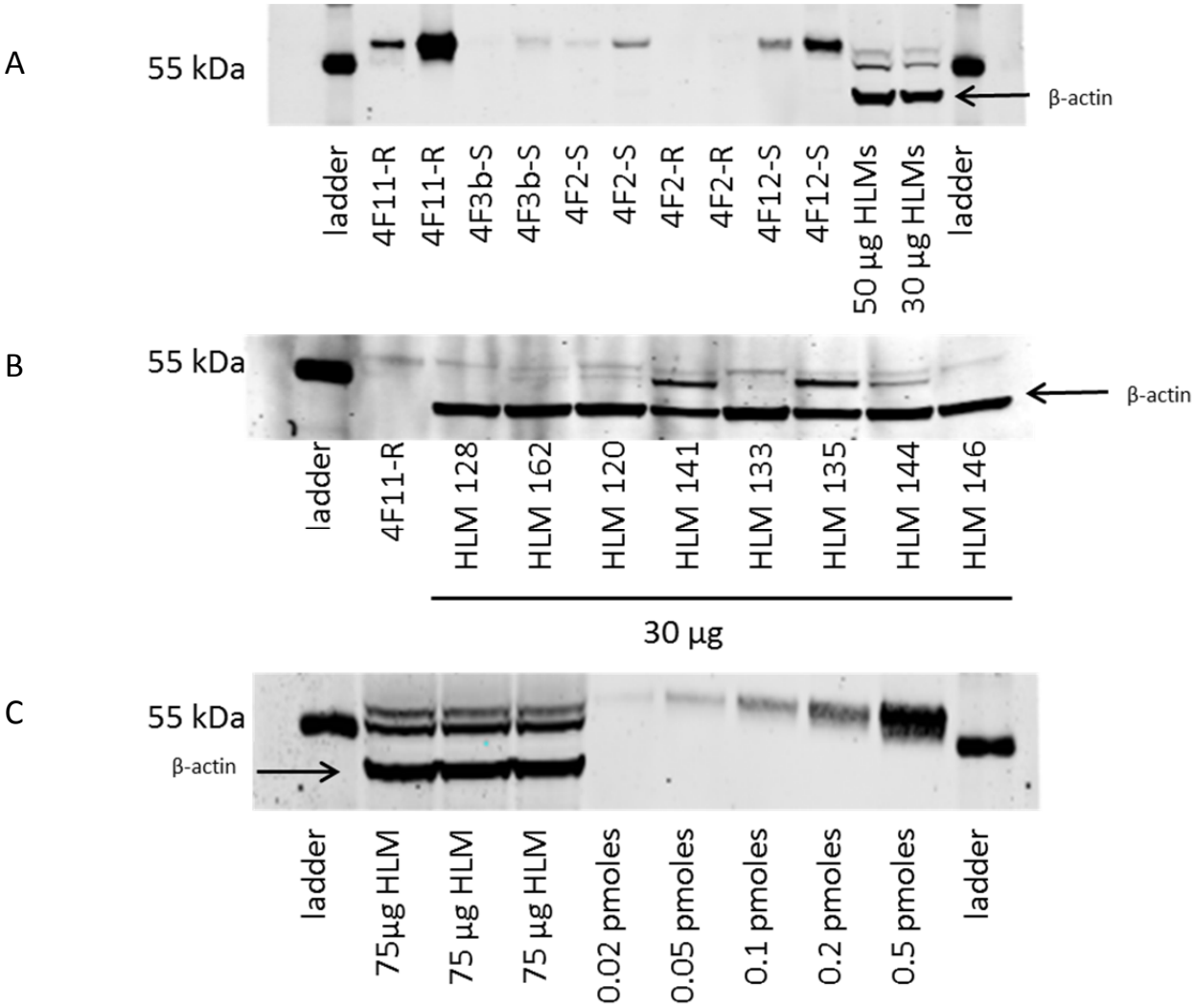

Figure 4.10: TOP: CYP4F2 and CYP4F11 protein levels in human liver microsomes measured by peptide LC-MS/MS. For CYP4F2, T genotype refers to rs2108622 and corresponds to the V433M variant (TT n=2, TC n=5, CC n=7). For CYP4F11, G genotype refers to rs1060463 and corresponds to the D446N variant. (GG n=3, AG n=6, AA n=5). BOTTOM: ω-hydroxy MK4 formation correlated weakly with CYP4F2 protein content and did not correlate with CYP4F11 protein content.

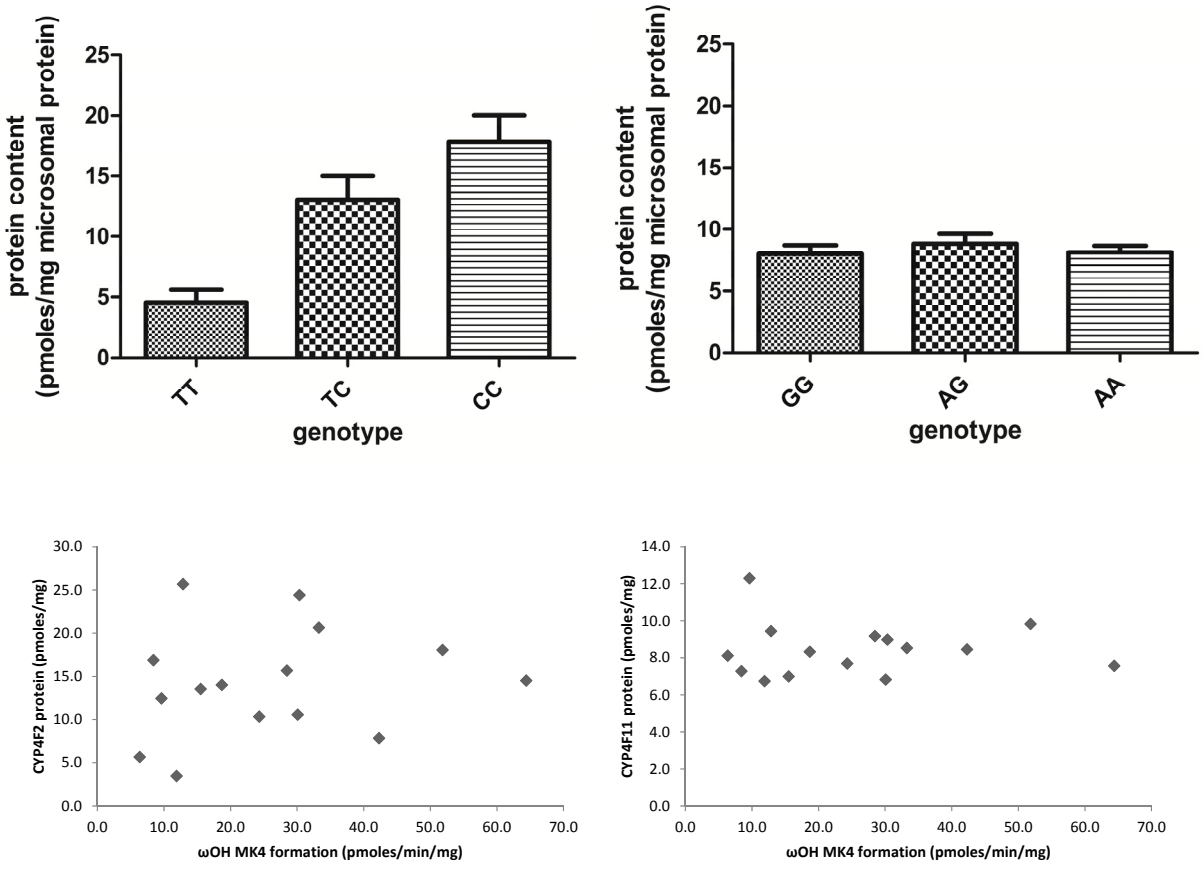

Figure 4.11: HET0016 and derivatives inhibition of recombinant A) CYP4F11 and B) CYP4F2. See Figure 2.9 for structures of inhibitors.

A)

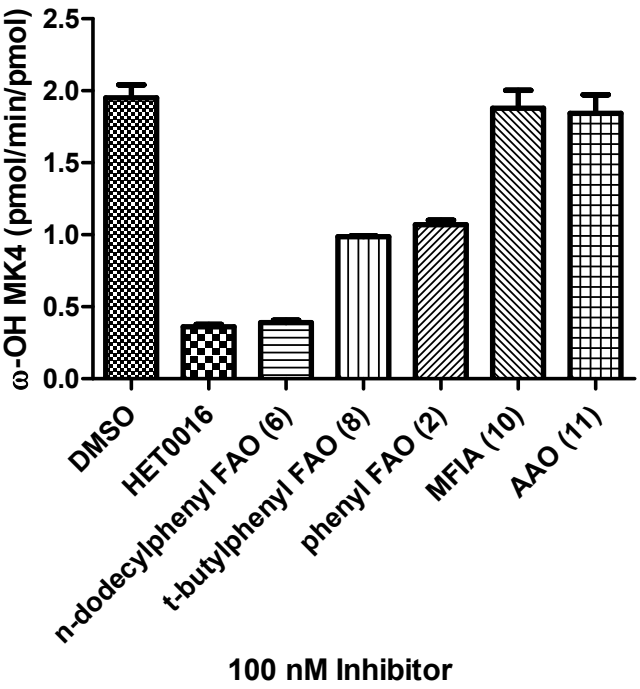

B)

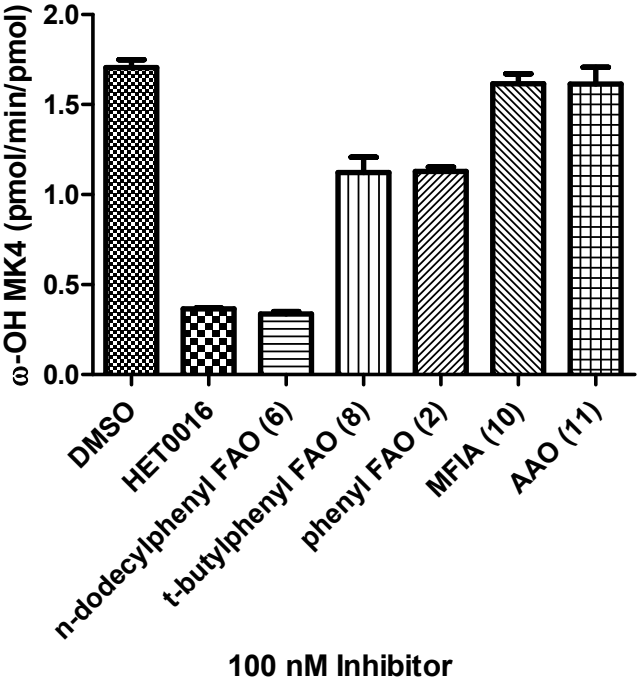

Table 4.1

Enzyme	Retention time	Peptide Sequence	Parent (m/z) z=2	Fragments (m/z) z=1
CYP4F2	9.4 min	SVINASAAIAPK	571.3	499.3
		AA 109-120		657.4
				728.4
		SVINASAAIAPK*	575.3	507.3
		internal standard		665.4
				736.4
CYP4F11	13.7 min	TLTQLVTTYPQGFK	798.9	576.4
		AA 76-89		941.6
				1040.6
		TLTQLVTTYPQGFK*	802.9	584.4
		internal standard		949.6
				1048.6

* Lysine residue is $^{15}N^{13}C$ labeled: 2 nitrogen atoms and 6 carbon atoms are heavy isotopes

4.5 References

[1] Dalmeijer, G.W.; van der Schouw, Y.T.; Vermeer, C.; Magdeleyns, E.J.; Schurgers, L.J.; Beulens, J.W., Circulating matrix Gla protein is associated with coronary artery calcification and vitamin K status in healthy women. *J Nutr Biochem,* 2013, *24*(4), 624-628.

[2] Sconce, E.; Avery, P.; Wynne, H.; Kamali, F., Vitamin K supplementation can improve stability of anticoagulation for patients with unexplained variability in response to warfarin. *Blood,* 2007, *109*(6), 2419-2423.

[3] Sontag, T.J.; Parker, R.S., Cytochrome P450 omega-hydroxylase pathway of tocopherol catabolism. Novel mechanism of regulation of vitamin E status. *J Biol Chem,* 2002, *277*(28), 25290-25296.

[4] Bhagavan, H.N.; Chopra, R.K., Coenzyme Q10: absorption, tissue uptake, metabolism and pharmacokinetics. *Free Radic Res,* 2006, *40*(5), 445-453.

[5] Nakamura, T.; Ohno, T.; Hamamura, K.; Sato, T., Metabolism of coenzyme Q10: biliary and urinary excretion study in guinea pigs. *Biofactors,* 1999, *9*(2-4), 111-119.

[6] McDonald, M.G.; Rieder, M.J.; Nakano, M.; Hsia, C.K.; Rettie, A.E., CYP4F2 is a vitamin K1 oxidase: An explanation for altered warfarin dose in carriers of the V433M variant. *Mol Pharmacol,* 2009, *75*(6), 1337-1346.

[7] Suhara, Y.; Watanabe, M.; Nakagawa, K.; Wada, A.; Ito, Y.; Takeda, K.; Takahashi, K.; Okano, T., Synthesis of novel vitamin K2 analogues with modification at the omega-terminal position and their biological evaluation as potent steroid and xenobiotic receptor (SXR) agonists. *J Med Chem,* 2011, *54*(12), 4269-4273.

[8] Tang, Z.; Salamanca-Pinzon, S.G.; Wu, Z.L.; Xiao, Y.; Guengerich, F.P., Human cytochrome P450 4F11: heterologous expression in bacteria, purification, and characterization of catalytic function. *Arch Biochem Biophys,* 2010, *494*(1), 86-93.

[9] Nakano, M.; Kelly, E.J.; Wiek, C.; Hanenberg, H.; Rettie, A.E., CYP4V2 in Bietti's crystalline dystrophy: ocular localization, metabolism of omega-3-polyunsaturated fatty acids, and functional deficit of the p.H331P variant. *Mol Pharmacol,* 2012, *82*(4), 679-686.

[10] Mulrooney, S.B.; Waskell, L., High-level expression in Escherichia coli and purification of the membrane-bound form of cytochrome b(5). *Protein Expr Purif,* 2000, *19*(1), 173-178.

[11] Shen, A.L.; Porter, T.D.; Wilson, T.E.; Kasper, C.B., Structural analysis of the FMN binding domain of NADPH-cytochrome P-450 oxidoreductase by site-directed mutagenesis. *J Biol Chem,* 1989, *264*(13), 7584-7589.

[12] Prasad, B.; Lai, Y.; Lin, Y.; Unadkat, J.D., Interindividual variability in the hepatic expression of the human breast cancer resistance protein (BCRP/ABCG2): effect of age, sex, and genotype. *J Pharm Sci,* 2013, *102*(3), 787-793.

[13] Deo, A.K.; Prasad, B.; Balogh, L.; Lai, Y.; Unadkat, J.D., Interindividual variability in hepatic expression of the multidrug resistance-associated protein 2 (MRP2/ABCC2): quantification by liquid chromatography/tandem mass spectrometry. *Drug Metab Dispos,* 2012, *40*(5), 852-855.

[14] Hansen, G.; Christensen, P.; Tuchsen, E.; Lund, T., Sensitive and selective analysis of coenzyme Q10 in human serum by negative APCI LC-MS. *Analyst,* 2004, *129*(1), 45-50.

[15] Suhara, Y.; Kamao, M.; Tsugawa, N.; Okano, T., Method for the determination of vitamin K homologues in human plasma using high-performance liquid chromatography-tandem mass spectrometry. *Anal Chem,* 2005, *77*(3), 757-763.

[16] Sanders, R.J.; Ofman, R.; Dacremont, G.; Wanders, R.J.; Kemp, S., Characterization of the human omega-oxidation pathway for omega-hydroxy-very-long-chain fatty acids. *FASEB J,* 2008, *22*(6), 2064-2071.

[17] Shinkyo, R.; Xu, L.; Tallman, K.A.; Cheng, Q.; Porter, N.A.; Guengerich, F.P., Conversion of 7-dehydrocholesterol to 7-ketocholesterol is catalyzed by human cytochrome P450 7A1 and occurs by direct oxidation without an epoxide intermediate. *J Biol Chem,* 2011, *286*(38), 33021-33028.

[18] Shinkyo, R.; Guengerich, F.P., Cytochrome P450 7A1 cholesterol 7alpha-hydroxylation: individual reaction steps in the catalytic cycle and rate-limiting ferric iron reduction. *J Biol Chem,* 2011, *286*(6), 4632-4643.

[19] Komen, J.C.; Wanders, R.J., Identification of the cytochrome P450 enzymes responsible for the omega-hydroxylation of phytanic acid. *FEBS Lett,* 2006, *580*(16), 3794-3798.

[20] Huang, D.; Ou, B.; Hampsch-Woodill, M.; Flanagan, J.A.; Deemer, E.K., Development and validation of oxygen radical absorbance capacity assay for lipophilic antioxidants using randomly methylated beta-cyclodextrin as the solubility enhancer. *J Agric Food Chem,* 2002, *50*(7), 1815-1821.

[21] Woods, C.M.; Fernandez, C.; Kunze, K.L.; Atkins, W.M., Allosteric activation of cytochrome P450 3A4 by alpha-naphthoflavone: branch point regulation revealed by isotope dilution analysis. *Biochemistry,* 2011, *50*(46), 10041-10051.

[22] Bell-Parikh, L.C.; Guengerich, F.P., Kinetics of cytochrome P450 2E1-catalyzed oxidation of ethanol to acetic acid via acetaldehyde. *J Biol Chem,* 1999, *274*(34), 23833-23840.
[23] Kalsotra, A.; Turman, C.M.; Kikuta, Y.; Strobel, H.W., Expression and characterization of human cytochrome P450 4F11: Putative role in the metabolism of therapeutic drugs and eicosanoids. *Toxicol Appl Pharmacol,* 2004, *199*(3), 295-304.
[24] Cui, X.; Nelson, D.R.; Strobel, H.W., A novel human cytochrome P450 4F isoform (CYP4F11): cDNA cloning, expression, and genomic structural characterization. *Genomics,* 2000, *68*(2), 161-166.
[25] Nishimura, M.; Yaguti, H.; Yoshitsugu, H.; Naito, S.; Satoh, T., Tissue distribution of mRNA expression of human cytochrome P450 isoforms assessed by high-sensitivity real-time reverse transcription PCR. *Yakugaku Zasshi,* 2003, *123*(5), 369-375.
[26] Hashizume, T.; Imaoka, S.; Hiroi, T.; Terauchi, Y.; Fujii, T.; Miyazaki, H.; Kamataki, T.; Funae, Y., cDNA cloning and expression of a novel cytochrome p450 (cyp4f12) from human small intestine. *Biochem Biophys Res Commun,* 2001, *280*(4), 1135-1141.
[27] Vermeer, C., Vitamin K: the effect on health beyond coagulation - an overview. *Food Nutr Res,* 2012, *56*.
[28] Booth, S.L., Roles for vitamin K beyond coagulation. *Annu Rev Nutr,* 2009, *29*, 89-110.
[29] Lonkar, P.; Dedon, P.C., Reactive species and DNA damage in chronic inflammation: reconciling chemical mechanisms and biological fates. *Int J Cancer,* 2011, *128*(9), 1999-2009.
[30] Hirani, V.; Yarovoy, A.; Kozeska, A.; Magnusson, R.P.; Lasker, J.M., Expression of CYP4F2 in human liver and kidney: assessment using targeted peptide antibodies. *Arch Biochem Biophys,* 2008, *478*(1), 59-68.
[31] Stec, D.E.; Roman, R.J.; Flasch, A.; Rieder, M.J., Functional polymorphism in human CYP4F2 decreases 20-HETE production. *Physiol Genomics,* 2007, *30*(1), 74-81.
[32] Schurgers, L.J.; Teunissen, K.J.; Hamulyak, K.; Knapen, M.H.; Vik, H.; Vermeer, C., Vitamin K-containing dietary supplements: comparison of synthetic vitamin K1 and natto-derived menaquinone-7. *Blood,* 2007, *109*(8), 3279-3283.
[33] Sato, T.; Schurgers, L.J.; Uenishi, K., Comparison of menaquinone-4 and menaquinone-7 bioavailability in healthy women. *Nutr J,* 2012, *11*, 93.
[34] Knapen, M.H.; Drummen, N.E.; Smit, E.; Vermeer, C.; Theuwissen, E., Three-year low-dose menaquinone-7 supplementation helps decrease bone loss in healthy postmenopausal women. *Osteoporos Int,* 2013.

Chapter 5

Menaquinone-4 Metabolism: New P450 Enzymes Involved in ω-Hydroxylation and New Metabolites Formed in Human Liver Microsomes

5.1 Introduction

As noted in earlier Chapters, the major route of vitamin K elimination involves initial ω-hydroxylation followed by β-oxidation to chain shortened acidic metabolites that are conjugated and excreted in the urine and bile. The large majority of the studies describing this pathway focus on phylloquinone (PK). However, menaquinone-4 (MK4), and longer-chain menaquinones are transported and eliminated differently, as is evident from early studies with radioactive compounds administered to rat and human, as well as more recent pharmacokinetic studies [1, 2]. In the rat, after an intravenous dose of MK4 and PK, 74% and 8.5% of the radioactivity, respectively, was recovered in bile over 12 hours [3]. Thus, it seems that MK4 is eliminated more rapidly from both plasma and liver than PK. Tadano *et al*. [4] found that following either intravenous or oral administration of MK4 to rats, only 6.0% and 10.3%, respectively, of the radioactive dose was found in urine as the chain shortened metabolites, with a further 63% of the intravenous administered dose found in the feces via bile within 24 hours. Of the latter amount, only ~30% was unchanged MK4, the ω-carboxylic acid glucuronide or the glucuronides of the chain-shortened metabolites (K-acid 1 and 2), according to GCMS analysis. Thus, approximately 40% of an intravenous dose of radioactive MK4 given to a rat is cleared as unidentified metabolites in the feces [5].

In Chapter 4 of this thesis, we reported ten-fold range in ω-hydroxy MK4 formation in human liver microsomes (HLMs), and only a weak correlation (r^2= 0.13, P = 0.05) between CYP4F2 enzyme levels and ω-hydroxy MK4 activity among 29 human liver microsomal samples (Figure 4.10). There was no correlation between CYP4F11 levels and MK4 hydroxylase activity. These findings, along with historical *in vivo* radioactivity experiments, led us to hypothesize that other enzymes may be involved in MK4 metabolism. This chapter reports that additional P450 enzymes in the CYP2 family are MK4 ω-hydroxylases and identifies novel MK4 metabolites formed by HLMs.

5.2 Materials and Methods

Materials- Human liver microsomes (HLMs) (pool of 50 donors) and human liver mitochondria (pool of 5 donors) were purchased from Xenotech, LLC (Lenexa, Kansas). All other HLMs were prepared from the UW Department of Medicinal Chemistry human liver bank as reported previously [6]. HLMs from St. Jude's Childrens Hospital Liver Bank were prepared using a tissue homogenization method that utilized cell disruptor beads (2.8 mm) and stored in storage buffer (50 mM KPi, 0.25 M sucrose, 10 mM EDTA, pH 7.4). Supersomes preparations of recombinant human P450s were purchased from BD Biosciences (San Jose, California). Bacterial CYP102 was a gift from Dr. Rheem Totah (University of Washington), expressed and purified as described previously [7]. 3-Chloroperbenzoic acid (mCPBA), methyl-β-cyclodextrin, menaquinones-4, lapachol, phylloquinone, 3-(+)-N-3-benzylnirvanol, and sulfaphenazole were purchased from Sigma-Aldrich. HET0016 was synthesized in house (see Chapter 2), and danazol was a gift from Dr. Rheem Totah.

Metabolic Reactions with Vitamin K - See Materials and Methods section of Chapter 4. Chemical inhibitors were added in methanol, which did not exceed a final concentration of 0.4 % v/v. Q3 scans of novel metabolites were obtained on the same triple quadrupole mass spectrometer (SCIEX API4000; Applied Biosystems, Foster City, CA) used for the MRM assay. The mass spectrometer was operated in product ion (MS2) mode and scanned from 50-500 Da with a collision energy ramp from 10-50 V and a declustering potential ramp from 30-100 V. All other settings were the same as reported in the MRM assay.

Bioreactor production of MK4 metabolites - CYP102 was used as a bioreactor for production of MK4 metabolites. Reactions contained CYP102 (0.8 μM), and were incubated in a total volume of 500 uL in KPi for 60 minutes at 37^{o}C. Liposomes were prepared by extrusion from DLPC (1:160 P450:DLPC molar ratio), 1 mM MβCDX was included, and the MK4 concentration was 80 μM.

Synthesis of 14,15-epoxy MK4 standard - MK4 (20 mg) was stirred on ice with 4 mL CH_2Cl_2. One molar equivalent of *m*CPBA was added and stirred for 30 minutes. The organic phase was extracted with water/NaOH

and evaporated under vacuum. The product was diluted into IPA and injected as the crude product onto the LC-MS for identification purposes.

5.3 Results

Effect of methyl-β-cyclodextrin (MβCDX) on MK ω-hydroxylase activity - Figure 5.1A is an MRM trace from a metabolic incubation with MK4 and human liver microsomes (HLMs). The three MRM channels shown are; *m/z* 460.3 (MK4+16) →185.0 (black trace), 474.4 (MK4+30)→185.0 (dark grey trace), and 241.0→186.1 for the internal standard (light grey trace). Chromatographic peaks that eluted between 3 min and 6 min were formed in an NADPH dependent fashion, with the exception of the peak labeled with a star (t_R= 5.0 minutes). The authentic synthetic standard of ω-hydroxy MK4 co-eluted with the peak labeled M1 (t_R = 4.2 minutes). A substantial increase in metabolite formation was observed in incubations containing 1 mM MβCDX (Figure 5.1B). Similar increases were not observed by adding α-cyclodextrin or bovine serum albumin to the incubations (not shown). MβCDX increased metabolite formation of MK4 and PK in HLMs, Supersomes and purified reconstituted enzyme preparations. This phenomenon has been well documented with other fatty acid substrates [8], and may reflect the lack of solubility of vitamin K in water. The catalytic efficiency for ω-hydroxy MK4 formation (M1) in HLMs in the absence of MβCDX was 0.55 μl/min/mg protein (V_{max}= 4.7 pmoles/min/mg, K_m= 8.6 μM) (Figure 5.2). MβCDX was not included in metabolic incubations measuring kinetic constants.

ω-Hydroxylation of MK4 by Cytochrome P450 Family 2 (CYP2) Enzymes - In a screen of commercially available human P450 enzymes incubated with NADPH and 20 μM MK4, CYP2C19, CYP4F2, CYP2C9, and CYP2J2 produced similar amounts of the ω-hydroxy metabolite (Figure 5.4). This is in contrast to the human P450 mediated ω-hydroxylation of PK, which is only catalyzed by CYP4F2 and CYP4F11 enzymes. CYP4F11 was not included in the current screen for MK4 ω-hydroxylation because it is not available as a Supersomes preparation; however, the enzyme does produce this MK4 metabolite, as shown in Chapter 4 of this thesis. To determine which P450 was most important for MK4 metabolism in the liver, we measured kinetic efficiencies for each enzyme (Figure 5.5). The order of catalytic efficiency was CYP2C19 >> CYP2J2 > CYP4F2 > CYP2C9.
Next, we investigated the inhibition of HLM-catalyzed MK4 ω-hydroxylation by diagnostic chemical inhibitors to determine which P450 enzymes dominate MK4 metabolism in human liver. Surprisingly, HET0016 was the only

inhibitor able to decrease activity in HLMs (Figure 5.6A). (+)-*N*-3-benzyl-nirvanol (3-BN) is a potent and selective inhibitor of CYP2C19-catalyzed S-mephenytoin hydroxylation [9]. However, 3-BN did not inhibit ω-hydroxy MK4 formation in HLMs at a concentration of 2 μM MK4 with MβCDX. Very interestingly, under the same conditions, CYP2C19 Supersomes-catalyzed MK4 ω-hydroxylation was inhibited by only 23% using 3-BN (1 μM) (Figure 5.6B), indicating either the substrate conditions used in these experiments were inadequate to achieve the expected degree of inhibition or CYP2C19 is inhibited in a substrate specific manner by 3-BN. Additionally, the IC50 reported for HET0016-mediated inhibition of CYP2C19 is 272 nM [10]. Thus, HET0016 might be inhibiting CYP2C19 under these conditions. As a control, it was confirmed that 3-BN inhibited S-mephenytoin 4-hydroxylase activity by CYP2C19 Supersomes to > 50% at a concentration of 1 μM inhibitor and 20 μM S-mephenytoin substrate using a previously described LC-MS/MS analytical method [11] (data not shown). Another potential complication of these inhibition experiments is that MβCDX was included in metabolic reactions. When MβCDX was omitted, the lowest substrate concentration at which reliable and quantifiable inhibition data could be obtained in HLMs was 10 μM. In this case, 3-BN actually slightly *increased* ω-hydroxy MK4 formation as compared to the control (Figure 5.6B). This finding, together with the lack of inhibition by 3-BN in CYP2C19 Supersomes, led us to investigate the contribution of CYP2C19 through a different - pharmacogenetic - approach.

To determine if ω-hydroxy MK4 formation correlated with *CYP2C19* genotype, we compared metabolism catalyzed by HLMs that had been genotyped as either wild type homozygotes (**1/*1*), **1/*2* heterozygotes or **2/*2* poor metabolizers. Due to the large variability in CYP2C19 activity for any genotype other than **2/*2*, we only analyzed differences between liver samples carrying the wild type (ancestral) alleles and those that were heterozygous or homozygous for the **2* allele. For this group of 14 human livers, n=1 for the **2/*2* genotype, n=7 for the **1/*2* genotype, and n=6 for the **1/*1* genotype (Figure 5.7A). The single CYP2C19**2/*2* sample in this cohort was also a CYP4F2**3/*3* genotype, which is the CYP4F2 V433M variant studied in Chapter 4 of this thesis that leads to decreased protein levels and reduced enzyme activity. Due to this confounding factor, we also analyzed HLMs prepared from the St. Jude's Childrens Hospital Liver Bank (n= 3 **2/*2*, n= 6 **1/*2*, n= 6 **1/*1*), which were gifted to us by Dr. Erin Scheutz. All three CYP2C19 **2/*2* samples in this cohort were CYP4F2 **1/*1* (wild type), and still exhibited low ω-hydroxy MK4 activity (Figure 5.7B). On average, the HLMs from the St. Jude's Liver Bank had lower activity than those prepared from the University of

Washington Liver Bank (10.2 ± 7 pmoles/min/mg versus 24.0 ± 15 pmoles/min/mg, respectively). There were not enough samples in either cohort to gain statistical significance, but the trend is clear enough in both cohorts to support a role for CYP2C19 involvement in MK4 ω-hydroxylation catalyzed by HLMs.

Characterization of novel MK4 metabolites in microsomes: 14,15-epoxy MK4 and ω-3 hydroxy-MK4 - Figure 5.8A shows an MRM trace from a metabolic incubation with MK4 and HLMs. The three channels shown represent the MK4+16 metabolites (black race), MK4+30 metabolites (dark grey trace), and the internal standard (light grey trace). M1 (RT= 4.2 minutes) is the ω-hydroxy MK4 metabolite, since it co-chromatographed with the synthetic standard and showed similar fragmentation of the m/z 460.3 Da parent ion. M2 is also NADPH dependent, and although there was no diagnostic fragmentation of the parent 460.3 ion, this peak co-chromatographed with a sample of MK4 that had been subjected to epoxidation by mCPBA in CH_2Cl_2 (Figure 5.8B). This chemical reaction was performed on ice for only 20 minutes to ensure that the major product would be the least sterically hindered product, i.e. the 14,15-epoxide, although trace quantities of the other isomeric epoxides were also formed (not shown). The MS2 spectra of the mCPBA product (Figure 5.8C) showed a fragment ion at *m/z* 376 consistent with the oxygen residing at the end of the phytyl chain. In some cases, the fragment ions observed for the MK4 phytyl chain would differ from expectations by 1 mass unit. This is likely due to fragmentation of a radical M-· parent ion and subsequent rearrangements (loss or gain of a proton) in the mass spectrometer. Thus, we have only tentatively identified this peak as the 14,15-epoxy MK4. In a Supersomes screen for enzymes responsible for formation of the epoxide, each P450 enzyme formed a similar amount of this metabolite, and adding superoxide dismutase or catalase to the HLM reaction did not decrease the peak intensity (data not shown). Additionally, neither HET0016 (0.5 μM), sulfaphenazole (1 μM), benzylnirvanol (1 μM), danazol (1 μM) nor troleandomycin (1 μM) inhibited formation of this peak in the pooled HLMs. We are currently determining if this metabolite is formed in cells and which P450 might be the major contributor to its production in HLMs. The possibility of a new MK4 elimination pathway via epoxide → epoxide hydrolase → glucuronide or sulfate conjugation → excretion in bile is now under consideration.

Similarly, M3 (RT= 3.8 minutes) (Figure 5.9) was also formed in HLMs and was NADPH dependent. Recombinant CYP102, a soluble, bacterial, fatty acid ω-1, ω-2 and ω -3 hydroxylase [12, 13], formed a relatively large amount of M2 and M3. The *m/z* 460.3 parent ion fragmented in a Q3 scan to produce a major fragment of

m/z 375, indicating that the hydroxylation was on the ω-3 carbon as opposed to the ω-4 or any other more internal carbon. Thus, we have tentatively identified two new metabolites of MK4 that are made in an NADPH dependent fashion in HLMs: 14,15-epoxy MK4 and ω-3 hydroxy MK4.

PK and MK4 omega-hydroxylase activity in human liver mitochondrial preparations - MK4 is an electron carrier in the mitochondria of the fruit fly [14]. Since MK4 is clearly present in the mitochondria of eukaryotic cells, it seems logical that mitochondria should be capable of both ω-hydroxylation and β-oxidation of MK4. Human liver mitochondrial preparations showed NADPH-dependent PK and MK4 ω-hydroxylase activity, that was slightly lower than that observed in HLMs (Figure 5.10). The activity was inhibited by only 12% upon addition of 30 μM vitamin D3 (cholecalciferol). This concentration is about 10x the K_m for CYP27A1 and vitamin D3 [15]. This is the first report that mitochondrial P450 enzymes ω-hydroxylate vitamin K.

5.4 Discussion

This work shows that MK4 is more susceptible than PK to oxidation by P450 enzymes. In the context of CYP4 enzyme activity, ω-hydroxylation is the terminal hydroxylation of a saturated alkyl chain. The bond dissociation energy (BDE) for a primary C-H bond is 104 kcals/mol, whereas the BDEs of secondary and tertiary C-H bonds of a saturated alkyl chain are approximately 95 and 92 kcals/mol, respectively [16]. In contrast to PK, MK4, and all menaquinones, have a double bond between carbon 14 and 15 at the end of the phytyl chain that substantially lowers the BDE of the terminal C-H bond to around 88 kcals/mol. This allylic hydrogen is much more metabolically labile (to P450 chemistry) than that of PK, therefore, it is not surprising that we have found P450 enzymes other than those belonging to the CYP4 enzyme family that are able to ω-hydroxylate MK4. Similar to the ω C-H bond of MK4, the ω-3 C-H bond is also allylic and should be more susceptible to hydroxylation by P450s than the ω-3 C-H bond of PK.

MβCDX in these experiments is most likely increasing the solubility of MK4, however, it is also widely used in cell and molecular biology to deplete cell membranes of cholesterol. In order to gain a better understanding of the mechanism by which MβCDX affects P450 activity, we compared the kinetic effects of MβCDX addition on CYP4F2 Supersomes and CYP4F2 reconstituted enzyme, the latter being devoid of cholesterol (Figure 5.3). For CYP4F2 Supersomes formation of ω-hydroxy MK4, both K_m and V_{max} were

increased, such that efficiency was only increased 2-fold. V_{max} was increased and K_m was actually decreased with CYP4F2 reconstituted enzyme, such that efficiency was increased about 10-fold. The reasons behind the differential effects on K_m are unclear, but these observations support the exclusion of MβCDX from metabolic incubations measuring kinetic constants, if at all possible. Interestingly, the product formation plot for the (sequentially formed) ω-carboxy MK4 metabolite showed more substrate inhibition when reactions were catalyzed by both Supersomes and reconstituted enzyme in the presence of MβCDX. This is presumably due to more competition for the active site between the higher concentrations of available MK4 substrate and the ω-hydroxy MK4 already in the active site.

CYP4F2, CYP2C19, and CYP2C9 are all highly polymorphic enzymes. They are present in the liver at approximately 16 pmoles/mg, 4 pmoles/mg, and 80 pmoles/mg of microsomal protein on average, respectively [17, 18]. Relative amounts of each protein in the liver, as well as the intrinsic activity of the enzymes for the substrate, determine the contribution that an enzyme will have to metabolism *in vivo*. CYP4F2 and CYP2C19 are not very highly expressed in the liver compared to CYP2C9, and the CYP4F2 catalytic efficiency for MK4 ω-hydroxylation was much lower than CYP2C19. Thus, it might be expected that CYP4F2 would only play a minor role in this metabolites overall formation in microsomes, and that CYP2C9 or CYP2C19 might dominate. Curiously, the CYP4F2 and CYP4F11 inhibitor, HET0016, was the only inhibitor able to effectively reduce ω-hydroxylation of MK4 in microsomes. However, HET0016 may also inhibit CYP2C19 at nanomolar concentrations, as the published IC_{50} value for a fluorescent probe substrate is 0.272 μM [10]. We found that 3-BN did not inhibit microsomal MK4 hydroxylation at a concentration of 5 μM, with 2 μM MK4 and 1mM MβCDX. The measured K_m for formation of ω-hydroxy MK4 without MβCDX in CYP2C19 Supersomes is 1.7 μM (Figure 5.5). However, due to the detection limits of the assay, activity measurements in HLMs lower than 2 μM without MβCDX are unobtainable. Thus, the MK4 concentration may be too high to achieve adequate inhibition of CYP2C19 in HLMs with 3-BN. It would be valuable to known the K_m of CYP2C19 ω-hydroxy MK4 formation *with* MβCDX. Alternatively, CYP2C19 may be inhibited in a substrate-dependent manner by 3-BN. This has previously been demonstrated for other drug metabolizing P450 enzymes, such as CYP3A4 and CYP2C9 [19, 20]. However, this has not been observed previously with CYP2C19. Indeed, 3-BN has been shown to inhibit a variety of xenobiotic substrates effectively [11]. CYP2C19 also hydroxylates farnesol, a structurally similar phytyl alcohol, at the ω position [21]. It would be interesting to analyze CYP2C19-dependent

inhibition of farnesol ω-hydroxylation by 3-BN, as it is conceivable that a fatty acid binding site in CYP2C19 is distinct from a drug binding site which may help explain the observed lack of inhibition of MK4 hydroxylase activity. The peculiar observation of metabolic activation in HLMs upon addition of 3-BN (with 10 μM MK4 and no MβCDX) might also be explained by two distinct binding sites for a drug and a fatty acid in CYP2C19.

Extreme variability in enzyme activity has been documented with CYP2C19 for samples with the same genotype. Thus, a large number of samples are required to achieve statistical significance in genotype-phenotype correlations. CYP2C19**2/*2* homozygotes, or poor metabolizers, have the least amount of activity and the least amount of inter-individual variability. Due to the overall lower activity in the St. Jude's Liver Bank samples compared to the University of Washington Liver Bank samples, it may not be appropriate to combine these data sets. The differential method of microsomes preparation might explain the average differences in activity. However, when combined, CYP2C19 **2/*2* and **1/*1* genotypes were significantly different ($P = 0.02$). This work has generated interesting hypotheses regarding the role of CYP2C19 in MK4 ω-hydroxylation, and future directions in this aspect of MK4 metabolism include inhibition of CYP2C19-mediated ω-hydroxy MK4 activity by alternative chemical inhibitors and antibodies. Additionally, phenotyping the HLM samples for S-mephenytoin activity and performing a correlation analysis between ω-hydroxy MK4 activity will provide more information on the role of CYP2C19 in MK4 metabolism. This is important because CYP2C19, an extremely polymorphic P450, could explain some of the observed inter-individual response to MK4 supplementation [22, 23].

We have discovered and tentatively identified two new MK4 metabolites in HLMs; 14,15-epoxy MK4 and ω-3 hydroxy MK4. The chain shortened vitamin K urinary metabolites have been long known, however, it is clear from studies with radioactive substrates that much less than 100% of an oral or intravenous dose of MK4 is cleared via this pathway [5]. It is possible that the 14,15-epoxy MK4 characterized here is formed by numerous P450 enzymes, hydrolyzed and excreted as glucuronides or sulfides in bile. Similarly, the ω-3 hydroxy MK4 metabolite may also be conjugated and cleared via the bile, but these are speculative scenarios in the absence of additional data. Vitamin E has a similarly well-characterized excretion pathway via ω-oxidation followed by β-oxidation. Tocotrienols are vitamin E forms with unsaturated phytyl chains analogous to MK4, and it is possible that other P450 enzymes are involved in tocotrienol elimination as well.

The finding that human liver mitochondria have vitamin K hydroxylase activity is intriguing because there may be an unknown mitochondrial P450 contributing to vitamin K homeostasis and inter-individual variability in response to supplementation with vitamin K. CYP27A1 metabolizes cholesterol at the C-27 position in the liver during biosynthesis of bile acids. This oxidation is technically an ω-hydroxylation, producing the 27-hydroxy cholesterol product almost exclusively and making no 25-hydroxy cholesterol [16]. This suggests that CYP27A1 might be inclined towards PK ω-hydroxylation. However, this enzyme also metabolizes vitamin D3 (chocaleciferol) at the C-25 position, which is the more chemically labile tertiary C-H bond. CYP27C1 is an orphan P450 localized to the mitochondria [24, 25], and its function is unknown. Either of these P450 enzymes might be responsible for the vitamin K ω-hydroxylase activity in mitochondria.

In conclusion, we have characterized two novel metabolites of MK4 produced in human liver microsomes and established a role for human CYP2C enzymes in the ω-hydroxylation of MK4. Future directions include a thorough characterization of the P450 enzymes responsible for the production of these new metabolites, and evaluation of their formation in cell systems and *in vivo*. Metabolism of other pharmacologically relevant vitamin K forms, such as MK7, also warrants investigation at this stage.

Figure 5.1: Menaquinone-4 metabolism in human liver microsomes and the effect of 1 mM methyl-β-cyclodextrin (MβCDX) on MK4 (20 μM) metabolite formation. Black trace, *m/z* 460.3>185.0; grey trace, 474.3>185.0; light grey trace 240.3>186.1.

A) Human liver microsomes +MK4 - MβCDX

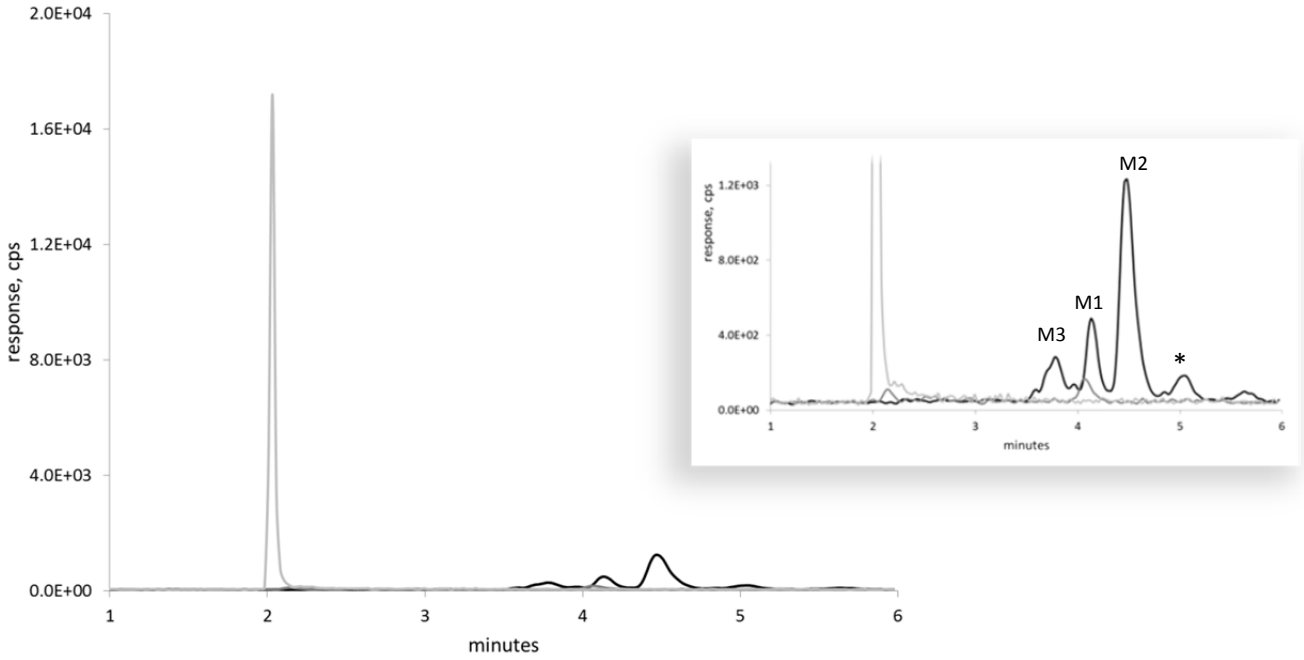

B) Human liver microsomes +MK4 + MβCDX

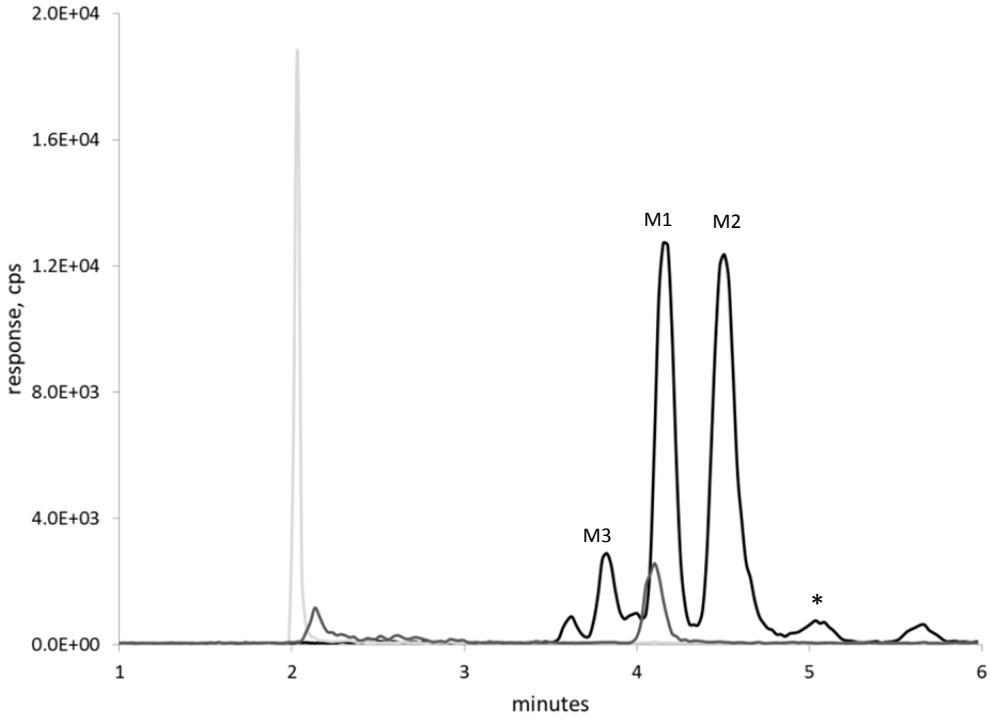

Figure 5.2: Direct plot of ω-hydroxy MK4 formation in human liver microsomes. V_{max} = 4.7 pmoles/min/mg protein, K_m = 8.6 μM. MβCDX was omitted from this experiment.

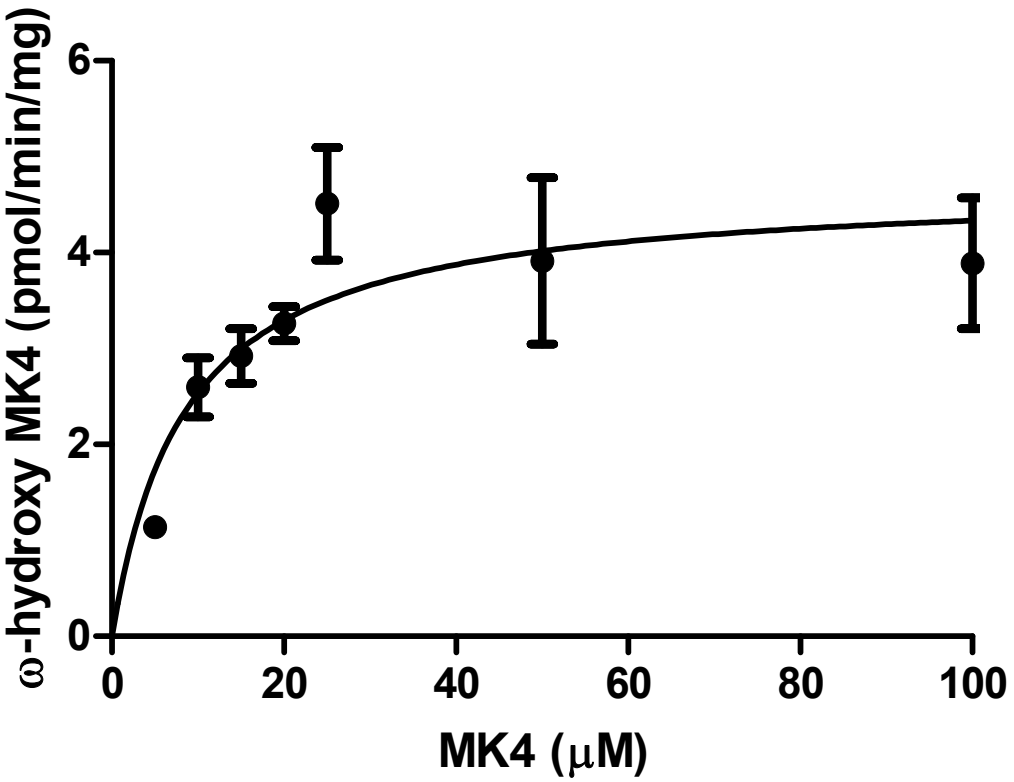

Figure 5.3: Methyl-β-cyclodextrin (MβCDX) effects on ω-hydroxy MK4 and ω-carboxy MK4 formation by CYP4F2 Supersomes and reconstituted enzyme. A) V_{max} (min^{-1})= 0.21 +/- 0.009, K_m (μM)= 3.2 +/- 0.5, V_{max}/K_m = 0.067 +/- 0.02. B) V_{max} (min^{-1})= 2.5 +/- 0.3, K_m (μM)= 18 +/- 6, V_{max}/K_m = 0.14 +/- 0.05. C) V_{max} (min^{-1})= 0.085 +/- 0.004, K_m (μM)= 1.62 +/- 0.4, V_{max}/K_m = 0.052 +/- 0.01. D) V_{max} (min^{-1}) = 0.39 +/- 0.01, K_m (μM)= 0.78 +/- 0.2, V_{max}/K_m = 0.5 +/- 0.05

MK4 → ω-hydroxy MK4 | MK4 → ω-carboxy MK4 V_{max}

A) CYP4F2 Supersomes - MβCDX

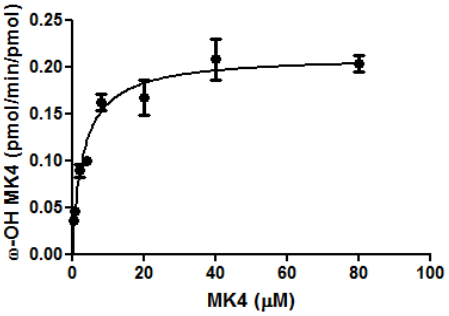

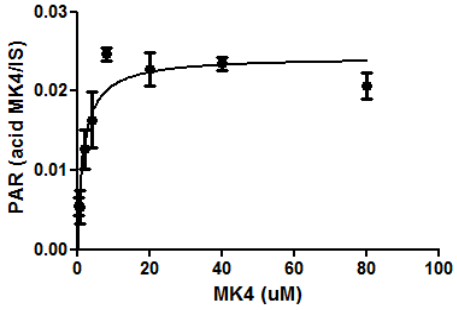

B) CYP4F2 Supersomes + MβCDX

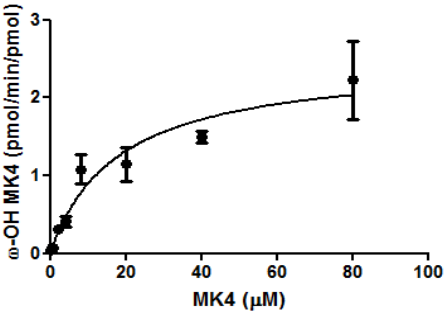

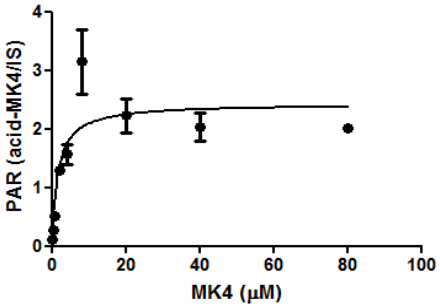

C) CYP4F2 reconstituted enzyme - MβCDX

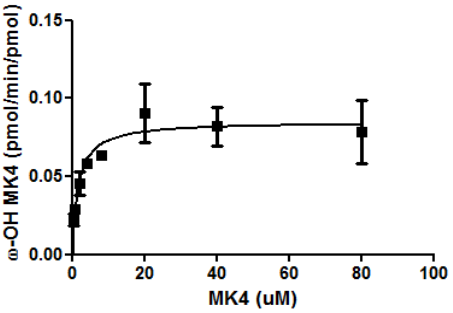

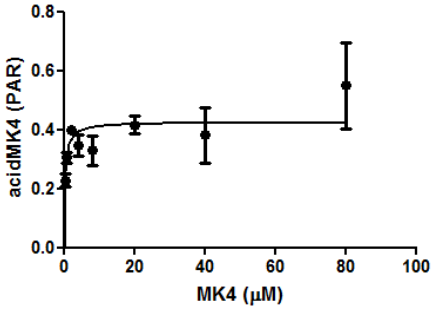

D) CYP4F2 reconstituted enzyme + MβCDX

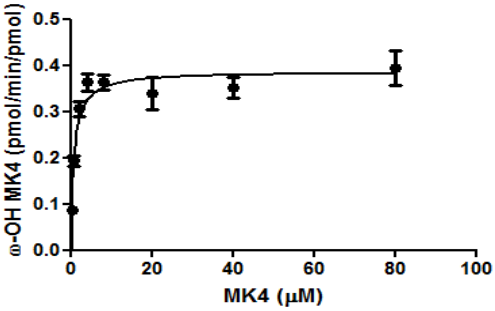

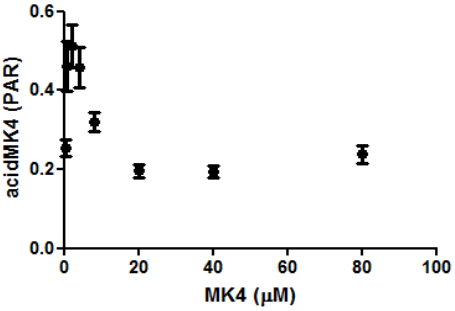

Figure 5.4: Screen of P450 enzymes able to convert MK4 to ω-hydroxy MK4

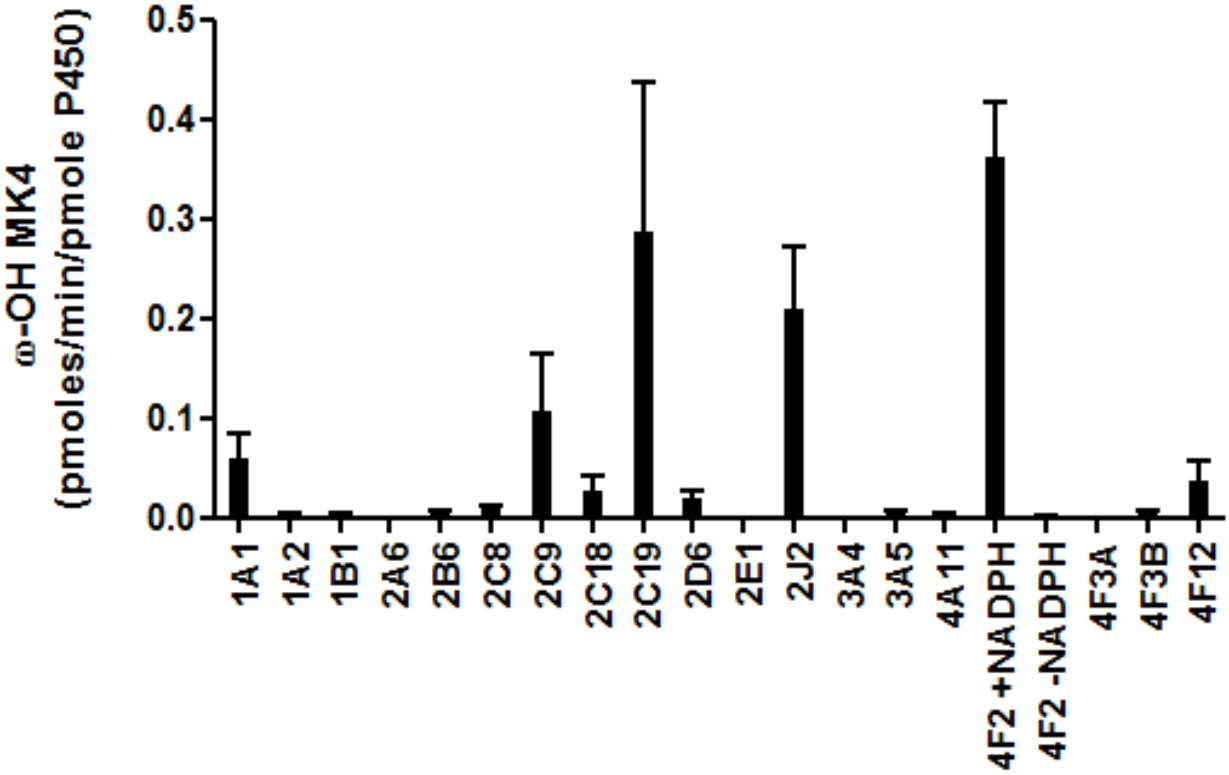

Figure 5.5: Direct plots for ω-hydroxy and ω-carboxy MK4 formation by CYP2C19, CYP2J2, CYP4F2, and CYP2C9 Supersomes. A) CYP2C19, V_{max} (min^{-1})= 1.7 +/- 0.1, K_m (μM)= 1.7 +/- 0.5, V_{max} / K_m = 1.0 +/- 0.2; B) CYP2J2, V_{max} (min^{-1})= 0.25 +/- 0.02, K_m (μM)= 1.8 +/- 0.7, V_{max}/ K_m = 0.14 +/- 0.03; C) CYP4F2, V_{max} (min^{-1})= 0.21 +/- 0.009, K_m (μM)= 3.2 +/- 0.5, V_{max}/ K_m = 0.067 +/- 0.02; D) CYP2C9, V_{max} (min^{-1})= 0.11 +/- 0.007, K_m (μM)= 3.5 +/- 0.9, V_{max}/ K_m = 0.03 +/- 0.008.

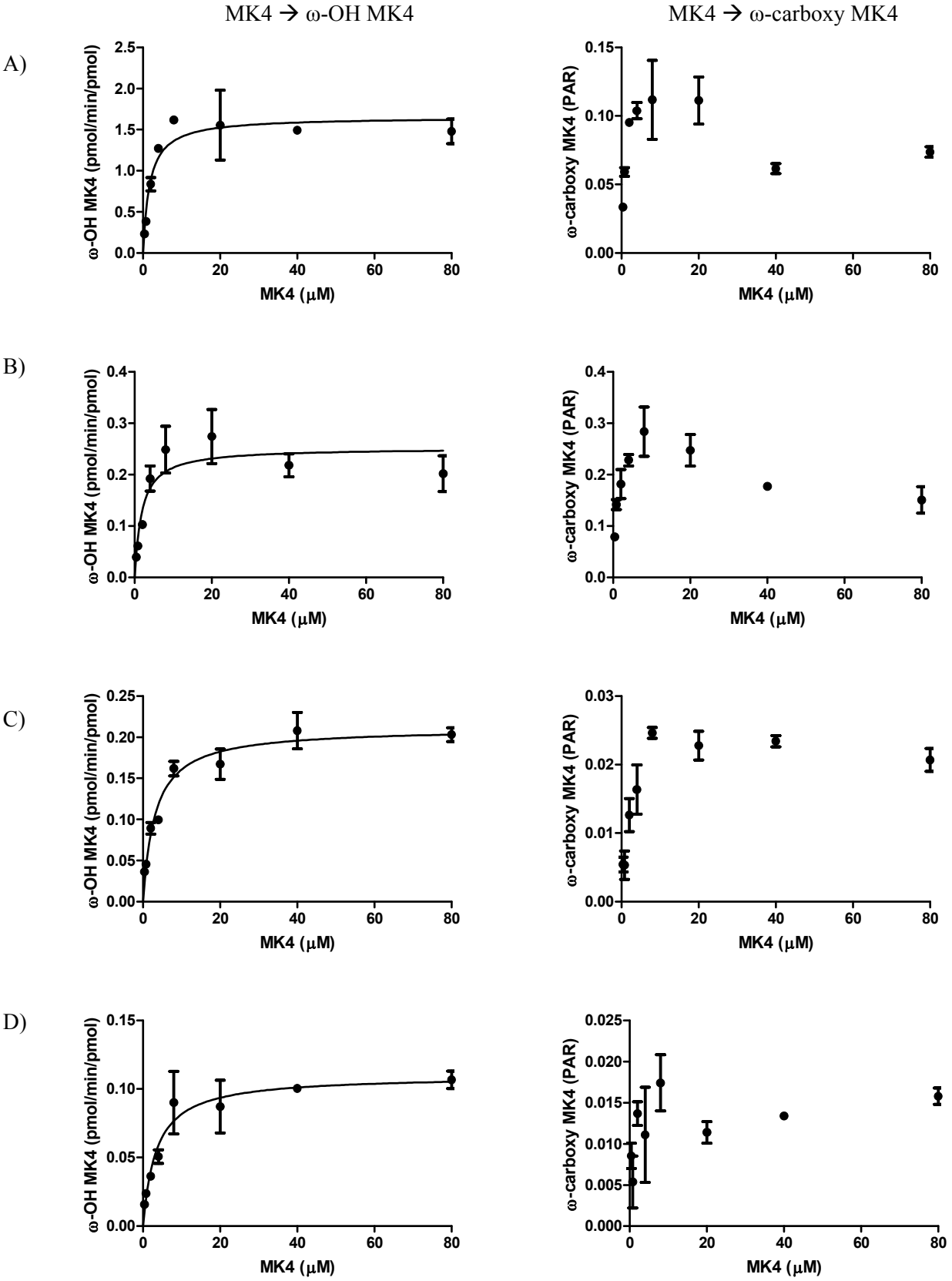

Figure 5.6: Inhibition of ω-hydroxy MK4 formation with P450 specific inhibitors. HET0016 (CYP4 inhibitor), 3-BN = (+)-*N*-3-benzyl-nirvanol (CYP2C19 inhibitor), SFZ = sulfaphenazole (CYP2C9 inhibitor), DNZ = danazol (CYP2J2 inhibitor). A) Inhibition of HLMs. MK4 concentration was 2 μM. MβCDX (1mM) was included. B) Inhibition of CYP2C19 Supersomes. MK4 concentration was 2 μM. MβCDX (1mM) was included. C) Inhibition of HLMs. MK4 concentration was 10 μM. MβCDX was omitted.

A)

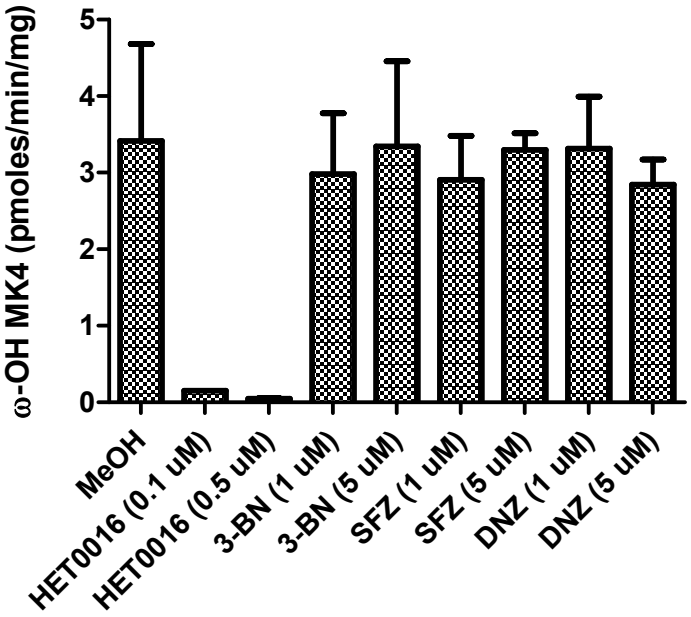

B)

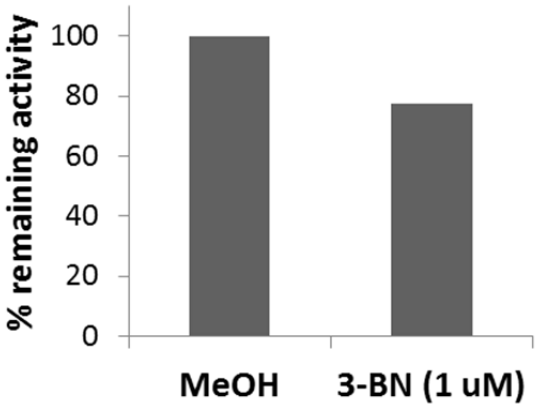

C)

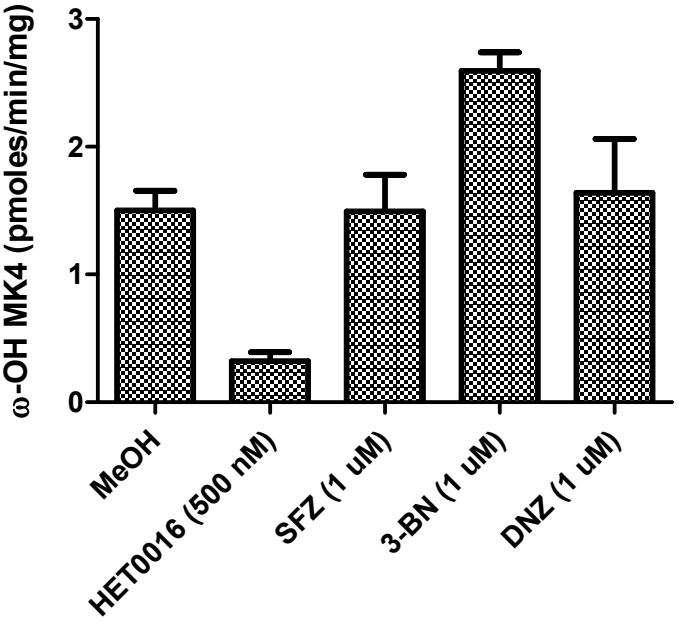

Figure 5.7: ω-Hydroxy MK4 formation by human liver microsomes genotyped for the *CYP2C19*2* allele. A) University of Washington Liver Bank. No statistical significance. B) St. Jude's Children's Hospital Liver Bank. **1/*1* and **2*2* were not significantly different (P = 0.13). C) Cohorts in A and B combined. **1/*1* and **2/*2* were significantly different (P = 0.02). Dots are University of Washington Liver Bank samples. Stars are St. Jude's Liver Bank samples.

A)

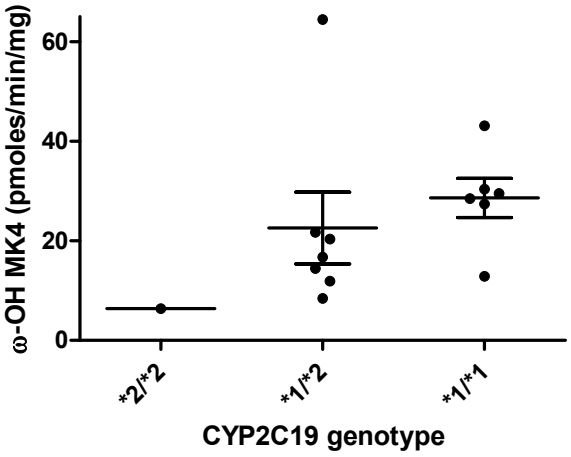

B)

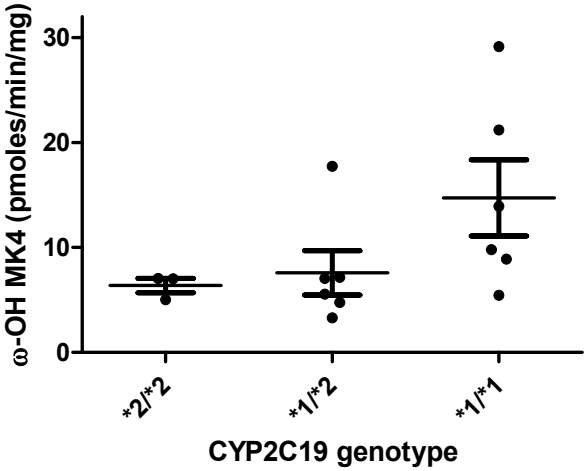

C)

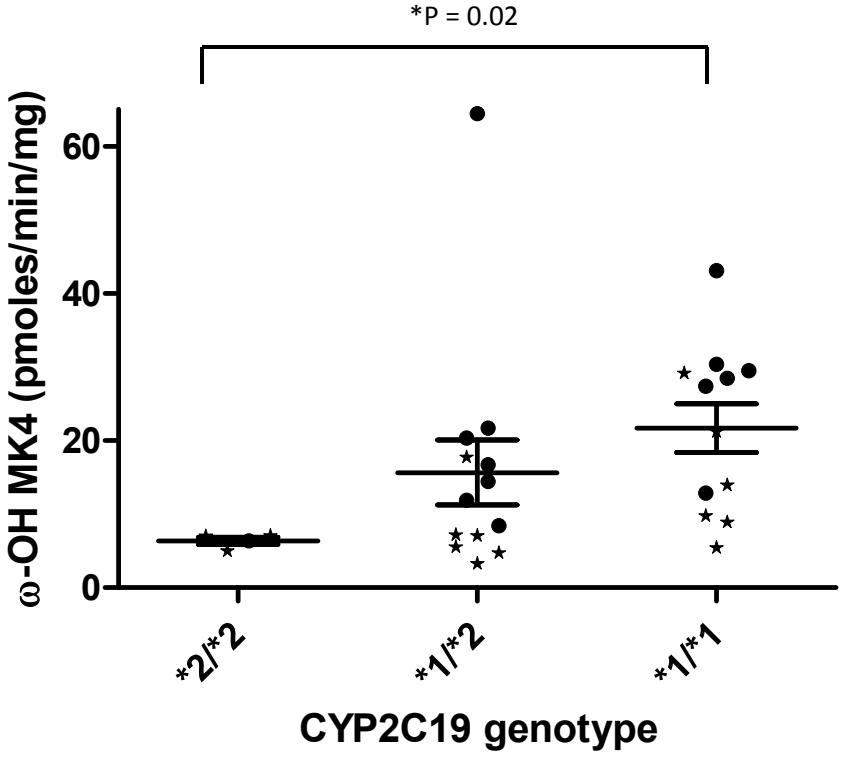

Figure 5.8: 14,15-epoxy MK4 characterization using mCPBA. Black trace, *m/z* 460.3>185.0; grey trace, 474.3>185.0; light grey trace 240.3>186.1. A) Metabolic incubation of HLMs with MK4. B) Synthetic standard of MK4 from mCPBA. Retention time was 4.6 minutes. C) Q3 scan of *m/z* 460.3 at retention time 4.6 minutes.

A)

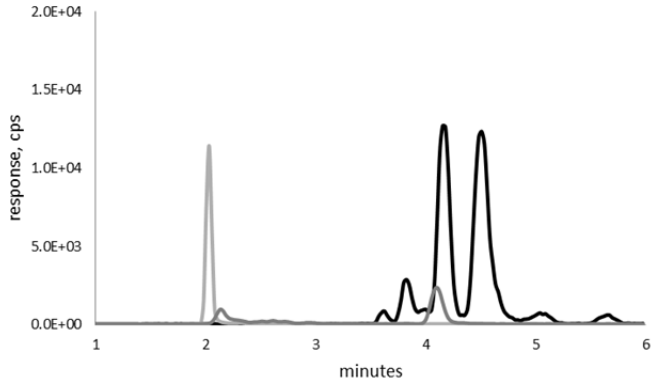

B)

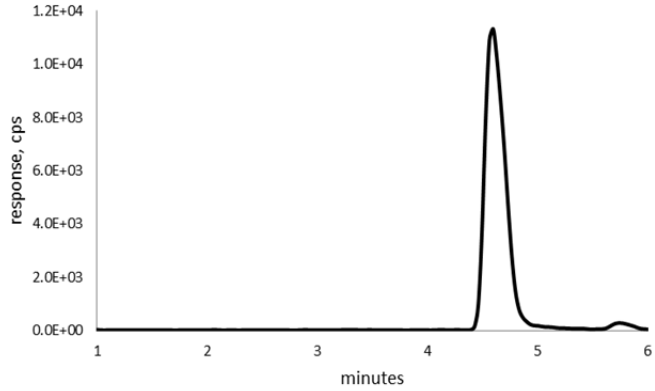

C)

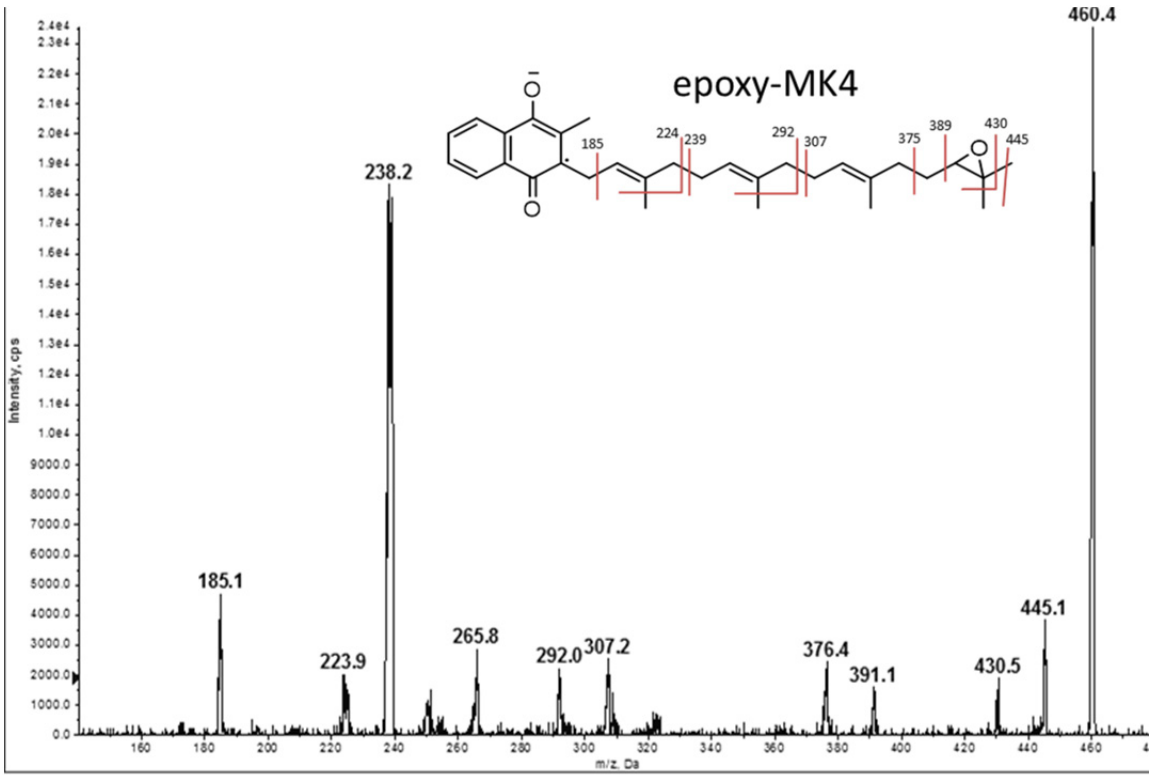

Figure 5.9: ω-3 Hydroxy MK4 characterization using CYP102. Black trace, *m/z* 460.3>185.0; grey trace, 474.3>185.0; light grey trace 241.0>186.1. A) Metabolic incubation of HLMs with MK4. B) Metabolic incubation of CYP102 with MK4. Retention time for the putative ω -3 metabolite was 3.8 minutes C) Q3 scan of *m/z* 460.3 at retention time 3.8 minutes.

A)

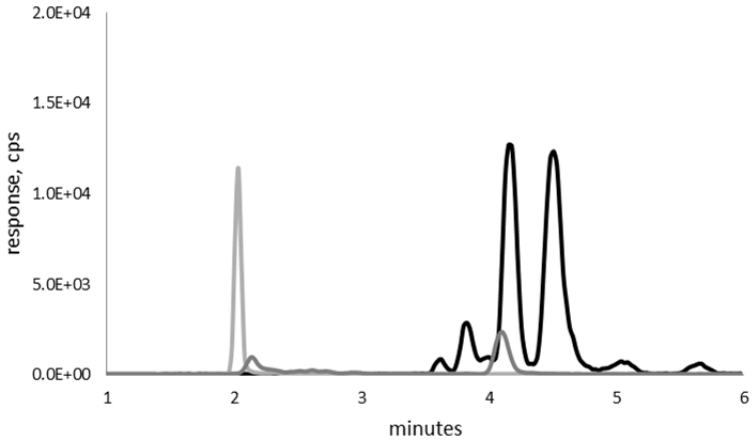

B)

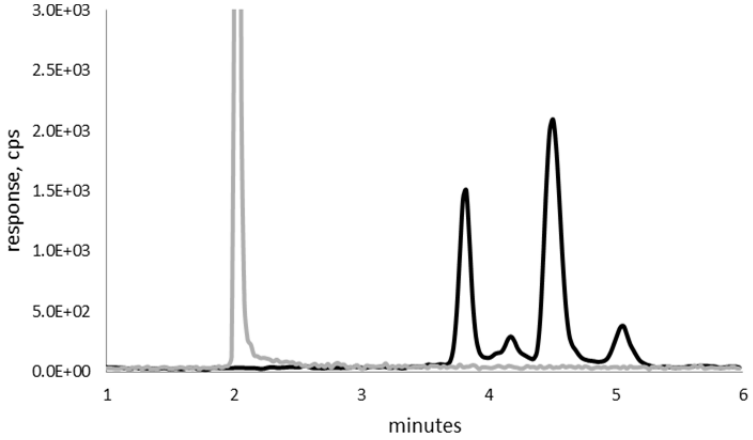

C)

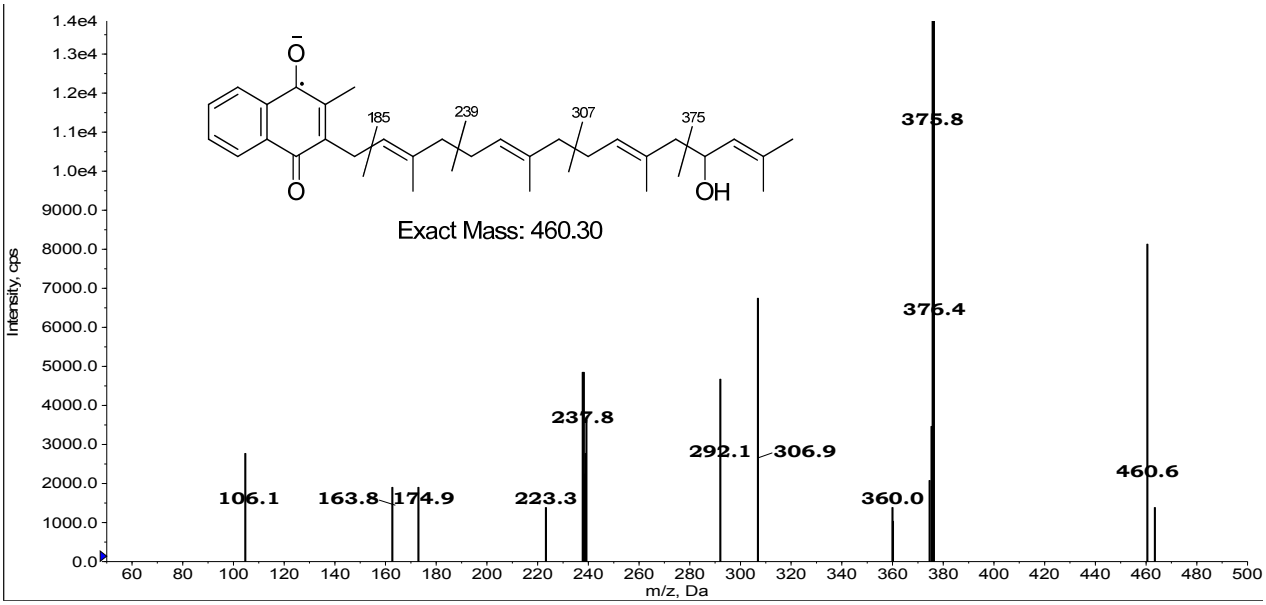

Figure 5.10: MK4 (A) and PK (B) hydroxylase activity catalyzed by human liver mitochondrial preparations. Substrate concentrations were 20 μM and MβCDX (1 mM) was included. Black trace, *m/z* 460.3> 185.0, Grey trace, 241.0>186.0. Peaks with stars were not NADPH dependent. Peaks in panel A correspond to the previously characterized metabolites, ω-hydroxy MK4 (M1) and 14, 15-epoxy MK4 (M2). Peaks with a star label are not NADPH dependent.

A)

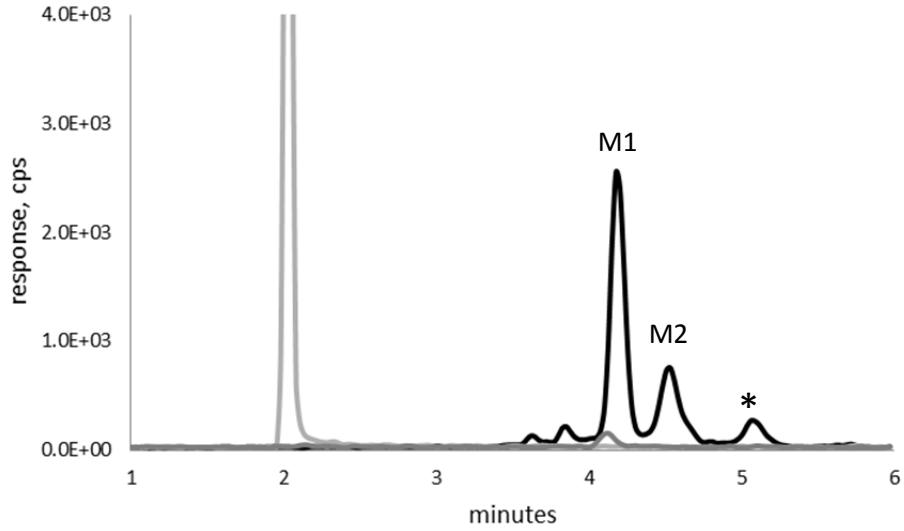

B)

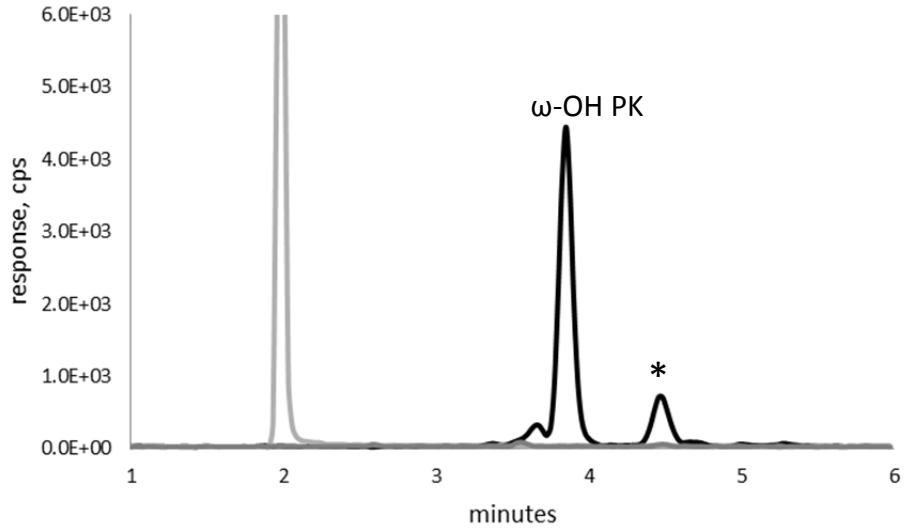

Figure 5.11: Summary of MK4 metabolism pathways in HLMs

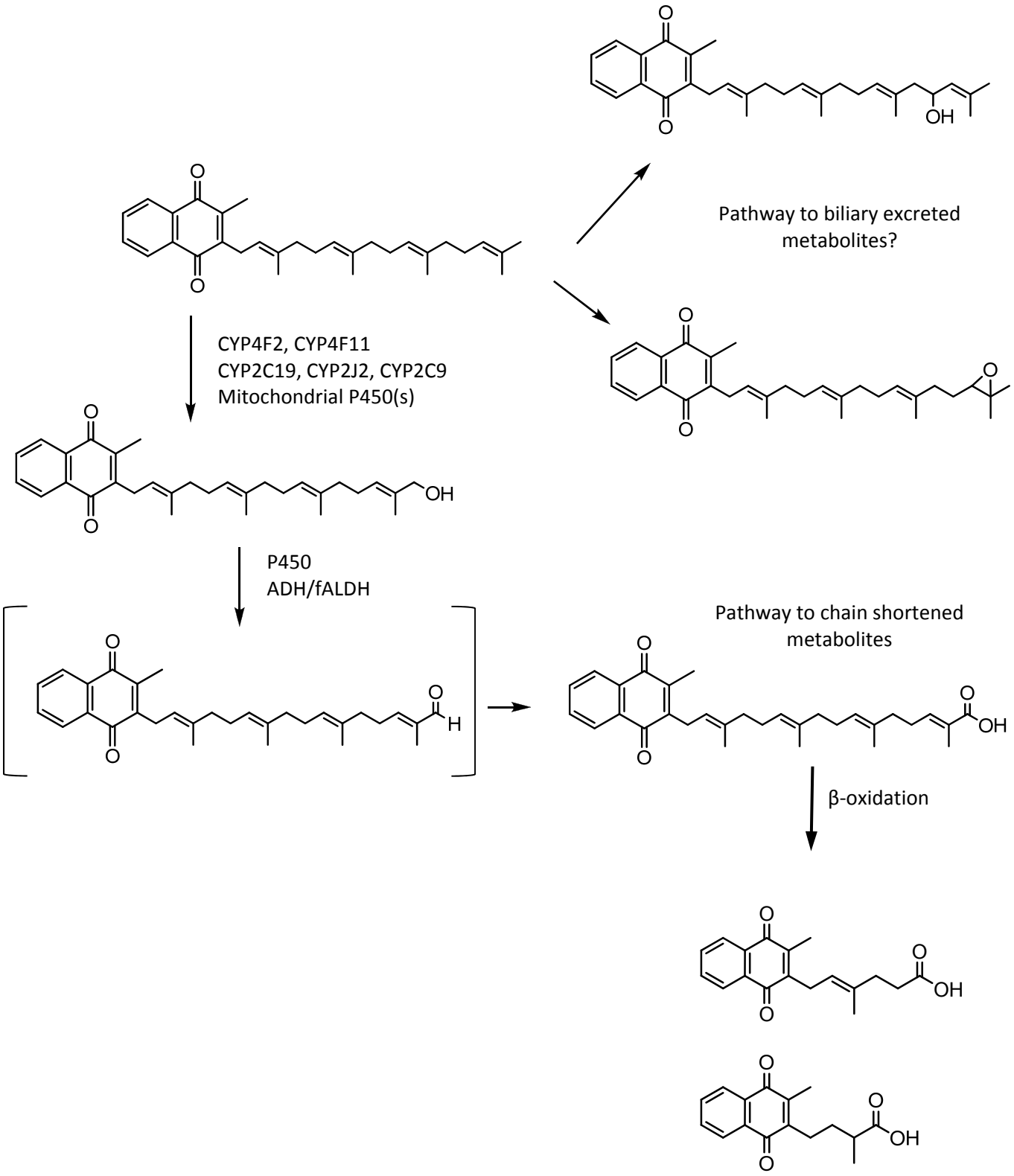

5.5 References

[1] Shearer, M.J.; Newman, P., Metabolism and cell biology of vitamin K. *Thromb Haemost,* 2008, *100*(4), 530-547.
[2] Schurgers, L.J.; Teunissen, K.J.; Hamulyak, K.; Knapen, M.H.; Vik, H.; Vermeer, C., Vitamin K-containing dietary supplements: comparison of synthetic vitamin K1 and natto-derived menaquinone-7. *Blood,* 2007, *109*(8), 3279-3283.
[3] Konishi, T.; Baba, S.; Sone, H., Whole-body autoradiographic study of vitamin K distribution in rat. *Chem Pharm Bull (Tokyo),* 1973, *21*(1), 220-224.
[4] Tadano, K.; Yuzuriha, T.; Sato, T.; Fujita, T.; Shimada, K.; Hashimoto, K.; Satoh, T., Identification of menaquinone-4 metabolites in the rat. *J Pharmacobiodyn,* 1989, *12*(10), 640-645.
[5] Tadano, K.; Yuzuriha, T.; Sato, T.; Fujita, T.; Shimada, K.; Hashimoto, K.; Satoh, T., Identification of Menaquinone-4 Metabolites in the Rat. *Journal of Pharmacobio-Dynamics,* 1989, *12*(10), 640-645.
[6] McDonald, M.G.; Rieder, M.J.; Nakano, M.; Hsia, C.K.; Rettie, A.E., CYP4F2 is a vitamin K1 oxidase: An explanation for altered warfarin dose in carriers of the V433M variant. *Mol Pharmacol,* 2009, *75*(6), 1337-1346.
[7] Kaspera, R.; Sahele, T.; Lakatos, K.; Totah, R.A., Cytochrome P450BM-3 reduces aldehydes to alcohols through a direct hydride transfer. *Biochem Biophys Res Commun,* 2012, *418*(3), 464-468.
[8] Komen, J.C.; Wanders, R.J., Identification of the cytochrome P450 enzymes responsible for the omega-hydroxylation of phytanic acid. *FEBS Lett,* 2006, *580*(16), 3794-3798.
[9] Suzuki, H.; Kneller, M.B.; Haining, R.L.; Trager, W.F.; Rettie, A.E., (+)-N-3-Benzyl-nirvanol and (-)-N-3-benzyl-phenobarbital: new potent and selective in vitro inhibitors of CYP2C19. *Drug Metab Dispos,* 2002, *30*(3), 235-239.
[10] Nakamura, T.; Sato, M.; Kakinuma, H.; Miyata, N.; Taniguchi, K.; Bando, K.; Koda, A.; Kameo, K., Pyrazole and isoxazole derivatives as new, potent, and selective 20-hydroxy-5,8,11,14-eicosatetraenoic acid synthase inhibitors. *J Med Chem,* 2003, *46*(25), 5416-5427.
[11] Foti, R.S.; Rock, D.A.; Han, X.; Flowers, R.A.; Wienkers, L.C.; Wahlstrom, J.L., Ligand-based design of a potent and selective inhibitor of cytochrome P450 2C19. *J Med Chem,* 2012, *55*(3), 1205-1214.
[12] Li, H.; Poulos, T.L., Fatty acid metabolism, conformational change, and electron transfer in cytochrome P-450(BM-3). *Biochim Biophys Acta,* 1999, *1441*(2-3), 141-149.
[13] Li, H.Y.; Darwish, K.; Poulos, T.L., Characterization of recombinant Bacillus megaterium cytochrome P-450 BM-3 and its two functional domains. *J Biol Chem,* 1991, *266*(18), 11909-11914.
[14] Vos, M.; Esposito, G.; Edirisinghe, J.N.; Vilain, S.; Haddad, D.M.; Slabbaert, J.R.; Van Meensel, S.; Schaap, O.; De Strooper, B.; Meganathan, R.; Morais, V.A.; Verstreken, P., Vitamin K2 is a mitochondrial electron carrier that rescues pink1 deficiency. *Science,* 2012, *336*(6086), 1306-1310.
[15] Sawada, N.; Sakaki, T.; Ohta, M.; Inouye, K., Metabolism of vitamin D(3) by human CYP27A1. *Biochem Biophys Res Commun,* 2000, *273*(3), 977-984.
[16] Johnston, J.B.; Ouellet, H.; Podust, L.M.; Ortiz de Montellano, P.R., Structural control of cytochrome P450-catalyzed omega-hydroxylation. *Arch Biochem Biophys,* 2011, *507*(1), 86-94.
[17] Powell, P.K.; Wolf, I.; Jin, R.; Lasker, J.M., Metabolism of arachidonic acid to 20-hydroxy-5,8,11, 14-eicosatetraenoic acid by P450 enzymes in human liver: involvement of CYP4F2 and CYP4A11. *J Pharmacol Exp Ther,* 1998, *285*(3), 1327-1336.
[18] Kawakami, H.; Ohtsuki, S.; Kamiie, J.; Suzuki, T.; Abe, T.; Terasaki, T., Simultaneous absolute quantification of 11 cytochrome P450 isoforms in human liver microsomes by liquid chromatography tandem mass spectrometry with in silico target peptide selection. *J Pharm Sci,* 2011, *100*(1), 341-352.
[19] Stresser, D.M.; Blanchard, A.P.; Turner, S.D.; Erve, J.C.; Dandeneau, A.A.; Miller, V.P.; Crespi, C.L., Substrate-dependent modulation of CYP3A4 catalytic activity: analysis of 27 test compounds with four fluorometric substrates. *Drug Metab Dispos,* 2000, *28*(12), 1440-1448.
[20] Hutzler, J.M.; Balogh, L.M.; Zientek, M.; Kumar, V.; Tracy, T.S., Mechanism-based inactivation of cytochrome P450 2C9 by tienilic acid and (+/-)-suprofen: a comparison of kinetics and probe substrate selection. *Drug Metab Dispos,* 2009, *37*(1), 59-65.
[21] DeBarber, A.E.; Bleyle, L.A.; Roullet, J.B.; Koop, D.R., Omega-hydroxylation of farnesol by mammalian cytochromes p450. *Biochim Biophys Acta,* 2004, *1682*(1-3), 18-27.
[22] Shea, M.K.; Benjamin, E.J.; Dupuis, J.; Massaro, J.M.; Jacques, P.F.; D'Agostino, R.B., Sr.; Ordovas, J.M.; O'Donnell, C.J.; Dawson-Hughes, B.; Vasan, R.S.; Booth, S.L., Genetic and non-genetic correlates of vitamins K and D. *Eur J Clin Nutr,* 2009, *63*(4), 458-464.

[23] Booth, S.L., Roles for vitamin K beyond coagulation. *Annu Rev Nutr,* 2009, *29*, 89-110.
[24] Nelson, D.R.; Zeldin, D.C.; Hoffman, S.M.; Maltais, L.J.; Wain, H.M.; Nebert, D.W., Comparison of cytochrome P450 (CYP) genes from the mouse and human genomes, including nomenclature recommendations for genes, pseudogenes and alternative-splice variants. *Pharmacogenetics,* 2004, *14*(1), 1-18.
[25] Omura, T., Mitochondrial P450s. *Chem Biol Interact,* 2006, *163*(1-2), 86-93.

Chapter 6

General Conclusions and Future Directions

The studies presented in this dissertation demonstrate that HET0016 is a potent, competitive Type II inhibitor of several human CYP4 enzymes. Inhibition of CYP4A11, but not CYP4F2 or CYP4F3B, by HET0016 analogs is greatly reduced by removal or elongation of n-alkyl groups from the HET0016 nucleus, resulting in the development of novel CYP4F-selective inhibitors.

None of the synthesized HET0016 analogs were selective inhibitors of individual human CYP4 sub-families. Success in this area would be useful for the development of more targeted 20-HETE synthase inhibiting drug candidates and for determining specific CYP4F sub-family enzyme contributions to metabolism of endogenous (and exogenous) substrates. The introduction of a phytyl alkyl chain to the HET0016 template might yield a CYP4F2/CYP4F11 inhibitor that does not inhibit other CYP4F enzymes, since these are the only two CYP4 enzymes that metabolize vitamin K. However, it is unlikely that selective inhibitors for each of the four CYP4F enzymes present in the liver and kidney, namely CYP4F2, CYP4F3B, CYP4F11, and CYP4F12, will be attained without a larger screen of compounds that explore more diverse chemical space at various positions on the phenyl ring of the HET0016 template. A number of structurally diverse HET0016 derivatives have previously been synthesized by Nakamura *et al*. at Taisho Pharmaceutical Company [1-4], and it might be fruitful to use this series of compounds as a starting point to develop CYP4F specific inhibitors.

This work has also revealed that HET0016 is an efficient mechanism-based inhibitor of CYP4A11, a principal 20-HETE synthase. The mechanism of inactivation did not appear to involve formation of a metabolite-intermediate complex or heme adduction/destruction. A carbodiimide or isocyanate that could conceivably bind to CYP4A11 apo-protein has been proposed, however more studies are required to prove this mechanism. It may be informative to determine if M3 and M5, two HET0016 metabolites on path to either of the proposed reactive species, are mechanism based inhibitors of CYP4A11. Regardless, additional efforts involving protein or peptide mass spectrometry would need to be pursued to provide evidence of a protein adduct.

The latter portion of this dissertation explored CYP4 enzyme involvement in vitamin K metabolism. After optimization of a new UPLC-APCI-MS/MS method to analyze vitamin K and metabolites, it was demonstrated that CYP4F2 and CYP4F11 are vitamin K1 and K2 ω-hydroxylases, and that CYP4F2, at least to some extent, sequentially metabolizes vitamin K to the ω-carboxy metabolite. Additionally, it was found that

microsomal ADH/fALDH is also likely to be involved in the formation of the ω-carboxy vitamin K metabolite. A novel LC/MS-MS assay was developed to measure the CYP4F11 specific content in human liver microsomes, which was about half that of CYP4F2, on average. It was further confirmed that human hepatic CYP4F2 protein levels correlated with the presence of the common *CYP4F2*3* (V433M) allelic variant. It was concluded that, depending on the CYP4F2 genotype, either CYP4F2 or CYP4F11 can be the more dominant contributor to initiation of vitamin K catabolism. Additionally, the novel menaquinone-4 (MK4) metabolites, 14,15-epoxy MK4 and ω-3 hydroxy MK4, were characterized as human liver microsomal metabolities. A role for CYP2C19 in ω-hydroxy MK4 formation was proposed based on formation of this metabolite in genotyped human liver microsomes. However, 3-BN, a specific CYP2C19 inhibitor, did not reduce ω-hydroxy MK4 formation in human liver microsomes, and an explanation for this finding requires further investigation.

Future directions include characterizing the formation of ω-hydroxy vitamin K, ω-carboxy vitamin K, and the numerous chain shortened downstream metabolites in whole cell systems, such as hepatocytes, as well as in urine and bile of animal models dosed with vitamin K. A comprehensive characterization of the P450 enzymes responsible for the production of the new MK4 metabolites is now warranted. It will also be important to establish P450 enzyme involvement in ω-hydroxylation of menaquinone-7, since this form of vitamin K is also under consideration for use as a pharmacotherapeutic agent.

6.2 References

[1] Nakamura, T.; Sato, M.; Kakinuma, H.; Miyata, N.; Taniguchi, K.; Bando, K.; Koda, A.; Kameo, K., Pyrazole and isoxazole derivatives as new, potent, and selective 20-hydroxy-5,8,11,14-eicosatetraenoic acid synthase inhibitors. *J Med Chem,* 2003, *46*(25), 5416-5427.

[2] Nakamura, T.; Ishii, T.; Miyata, N.; Taniguchi, K.; Tomishima, Y.; Ueki, T.; Sato, M., Design and synthesis of 1-(4-benzoylphenyl)imidazole derivatives as new potent 20-HETE synthase inhibitors. *Bioorg Med Chem Lett,* 2004, *14*(21), 5305-5308.

[3] Nakamura, T.; Kakinuma, H.; Umemiya, H.; Amada, H.; Miyata, N.; Taniguchi, K.; Bando, K.; Sato, M., Imidazole derivatives as new potent and selective 20-HETE synthase inhibitors. *Bioorg Med Chem Lett,* 2004, *14*(2), 333-336.

[4] Nakamura, T.; Kakinuma, H.; Amada, H.; Miyata, N.; Taniguchi, K.; Koda, A.; Sato, M., Pyrazole derivatives as new potent and selective 20-hydroxy-5,8,11,14-eicosatetraenoic acid synthase inhibitors. *Bioorg Med Chem,* 2004, *12*(23), 6209-6219.